ELECTRO-OPTIC AND SCATTERING STUDIES OF CONCENTRATED POLYMER SOLUTIONS

by

Okeke Paulinus Nwammuo *B.Sc.(Chem. Eng.) Ife, Dipl.(Pet.Eng.) Ibadan, M.Sc. London, D.I C.*

A thesis submitted for the Degree of Doctor of Philosophy of the University of London.

Department of Chemical Engineering and Chemical Technology,
Imperial College of Science and Technology, London S.W.7.

March 1982

ABSTRACT

The work described in this thesis is concerned with the experimental study of the dynamics of polymer chains in concentrated solution. The objectives were three fold: to study the effects of molecular structure, molecular weight (and its distribution), concentration, temperature and solvent on the chain dynamics: to use the data obtained to quantitatively test presently available theoretical models: and to quantify the effect of chain flexibility on the dynamic polymer behaviour.

The experimental techniques employed were the dynamic Kerr effect, which gives relaxation times, τ, characteristic of rotational motion and the photon correlation spectroscopy(PCS) which gives information on the translational motion of polymer chains and their constituent segments. The polymers studied, chosen to cover as wide a range of molecular flexibility as possible were poly-γ-benzyl-L-glutamate, poly(n-butyl isocyanate), polysulphone, polypropylene glycol/oxide and ethyl cellulose.

Two types of relaxation process were identified in the Kerr experiments. The first, associated with whole molecule rotation displayed qualitatively the same behaviour for all the systems. The results were well described by the expression of the form $\tau \propto C^{\zeta c} M^{\zeta m}$ where the exponents ζ_c and ζ_m changed dramatically at some characteristic concentration, C_r. The second type, corresponding to segmental motions showed much weaker molecular weight and concentration dependences. In the PCS experiments, marked changes in the shape of the correlation functions were observed at the same critical concentration. Results have been also obtained for the dependence of the Kerr constant, effective dipole moments, and polarisability anisotropies on concentration.

A number of quantitative criteria for assessing the flexibility of polymer chains are proposed and applied to the results of this work. The experimental exponents ζ_c and ζ_m are compared with various theoretical models for concentrated polymer chain dynamics, including a modification of the de Gennes-Doi-Edwards reptation model for semi-flexible chain developed in this work. The experimental exponents are in general lower than those predicted by the Doi-Edwards rigid rod model. Although the results can in some cases be explained semi-quantitatively by other models, a number of significant discrepancies remain.

ACKNOWLEDGEMENTS

I wish to express my gratitude to my Supervisor, Dr. Geoff Maitland for his devoted attention, encouragement and untiring guidance throughout the entire period of this research.

My thanks also to Drs. M. Letherby and D. Young for their interest and assistance at various stages during the experimentation, especially for allowing me use the photon correlation spectroscopy equipment and the low temperature refrigerator. Constructive critism of the thesis draft by Dr Letherby is immensely appreciated.

Thanks also go to members of staff of the Departmental Mechanical and Electronic workshops especially Messrs Malcolm Dix and Bob King and to the glass blowers for their contribution in putting various components of the Kerr equipment together. The valuable help of the librarians Miss Peggy Browett and Mrs Caroline Fletcher on reference matters is thankfully appreciated.

My colleagues Dr. C.L. Chong, D. Bosworth and P. Musonge who shared my anxious moments and company during this programme are fondly remembered.

Finally my leave of absence from the Nigerian National Petroleum Corporation; an equipment grant from the Science Research Council, financial assistance from the British Council, and the Federal Republic of Nigeria are all gratefully acknowledged.

Dedicated to
my wife ANGY
& daughter CHIBUZO

CONTENTS

LIST OF TABLES

LIST OF FIGURES

LIST OF PRINCIPAL SYMBOLS

Roman Capitals

B Experimental Kerr constant of solution in $V^{-2}m$

C Mass concentration in kg m^{-3}

C_n Number concentration

C_r Experimental critical concentration

C_v Volume fraction of solute

C* Onset of overlap concentration kg m^{-3}

C** Onset of isotropic nematic transition kg m^{-3}

C^*_{rc} Overlap concentration based on random coil model kg m^{-3}

C^*_{rr} Overlap concentration based on rigid rod model ,,

C(τ) Correlation function

D Diffusional coefficient

D_c Cooperative diffusional coefficient m^2s^{-1}

D_i Translational diffusion obtained at shorter times

D_ℓ Long time translational diffusion coefficient in m^2s^{-1}

D_m Translational diffusion ascribed to individual chains through highly interacting systems m^2s^{-1}

D_r Rotational diffusion coefficient in dilute solution in s^{-1}

D_{rc} Rotational diffusion coefficient in concentrated solution in s^{-1}

D_t Translational diffusion coefficient in dilute solution in $m^2\ s^{-1}$

E Field gradient in V m^{-1}

E_a Activation energy in J mol^{-1}

$G^{(1)}(t,t+\tau)$ = The field autocorrelation function.

$G^{(2)}(t,t+\tau)$ = The intensity autocorrelation function

I Intensity of light.

I_o Intensity of light when analyser and polariser are parallel

Roman Capital

K Kerr constant in $V^{-2}m^2$ ($= \Delta n/(nE^2)$)
The efficiency factor taking care of loss in light intensity due to reflection and absorption by optical components
Momentum transfer (function of wave vector) m^{-1}

K_m The molar Kerr constant $V^{-2}m^2\ mol^{-1}$

K_{sp} The specific Kerr constant $V^{-2}m^2$ ($= K/C_\nu$)

M Molecular mass (molecular weight)

N_A Avogadro's number ($6{,}02252 \times 10^{23}\ mol^{-1}$)

P Permanent dipole parameter ($= \mu^2/(kT)^2$) in $V^{-2}m^2$

Q Induced dipole parameter $\{=(\alpha_1 - \alpha_2)/kT\}$ in $V^{-2}m^2$

S(K,t) = The dynamical structure factor

T Absolute temperature in K

U Energy of interaction of the electric field with the macromolecules in Joules.

Roman Lower case

a_c The correlation or screening length(essentially the mean distance between chain contacts)

$f(\theta)$ The orientation distribution function

g_1-g_2 The optical anisotropy factor

$g^{(1)}(t,t+\tau)$ = Normalised field autocorrelation function

$g^{(2)}(t,t+\tau)$ = Normalised intensity autocorrelation function.

k Boltzmann's constant ($1.3805 \times 10^{-23}\ J\ K^{-1}$)

ℓ The length of cell in m
The statistical length of flexible macromolecule

ℓ_q Persistence length calculated from the critical concentration, in m

n The refractive index
The degree of polymerisation

$\Delta n = n_{//} - n_{\perp}$ Optical double refraction ,birefringence

Roman Lower Case

Δn_{oi} Birefringence at zero time for component i

$\Delta n(t)$ Birefringence at time t

q Persistence length for stiff molecule in m

r Ratio of the permanent term to induced dipole term

Greek Symbols

$\alpha_1-\alpha_2$ The polarisability anisotropy (F m^2)

The analyser angle away from the crossed position in degrees

Γ The reciprocal time constant (PCS measurements) ($\Gamma=D_t K^2$)

β The spread factor (a measure of deviation from single exponential behaviour)
The permanent dipole term($=\mu E/kT$)

γ Induced dipole interaction term $\{(\alpha_1-\alpha_2)E^2/2kT\}$

δ The retardation due to the birefringence in radians

δ_o Strain retardation from the windows , in radians.

ε The dielectric constant, ε' represents the real part and ε'', the imaginary part.

ζ_c The concentration exponent

ζ_m The molecular weight exponent

η The solution viscosity in centipoise

η_s The solvent viscosity in centipoise

$[\eta]$ The intrinsic viscosity $m^3\ kg^{-1}$

θ The orientation angle in radians

λ The wavelength of light *in vacuo* in m

μ The permanent dipole moment Cm

τ The relaxation time in s

τ_{def} Characteristic relaxation time of the defect diffusion

τ_e Relaxation time associated with $\Delta n/\Delta n_o = e^{-1}$ in s

τ_{in} Initial relaxation time in s

τ_p 'Peeled' relaxation time in s

Greek Symbols

τ_r Relaxation time associated with the rise transient in s

τ_{re} Relaxation time associated with the reptation wriggling motion in s

$\phi(\beta,\gamma)$ = The orientation factor

ω_o Angular frequency in radians s^{-1}

Chapter One

INTRODUCTION

Polymeric materials play a key role in present day technology. The application of high tonnage polymers such as polystyrene, polyethylene and polyvinyl chloride (PVC) is well established and emphasis is increasingly placed on producing speciality polymers, tailor-made to meet desired specifications. The successful development of such "molecular engineering" calls for a detailed understanding of the relationship between the bulk properties of materials and the structure, size and interactions of the molecules of which they are constituted.

The major characteristics of polymers which distinguish them from other materials are (i) a wide range of characteristics from high modulus brittle solids through weaker rubbery solids to elastic melts; (ii) properties which are time dependent - which characteristics they exhibit depends on the time scale of observation and / or the mechanical and thermal history of the material. This range of behaviour and its time dependence stems from the wide range of time scales of the molecular motions which the polymer chains can undergo. An understanding of the dynamic properties of polymer chains is therefore fumdamental to an understanding of the structure - bulk property relationships of polymeric materials.

The dynamics of polymer chains is determined in turn by the forces acting within the system, both intramolecular and intermolecular. One approach to understanding the properties of polymers is to examine how changes in these forces affect the chain dynamics, and hence the bulk properties. In the long term, such an approach via molecular dynamics simulations may indeed prove fruitful. Calculations of this type for model systems are beginning to be made [111]. However, our knowledge of such forces for real systems is severely limited at present and a more practical approach is to use experimental techniques to probe the chain dynamics directly. These

results can be used in two directions: to increase our understanding of how bulk properties are likely to change with varying conditions, or to give insight into the nature of the forces involved in polymer systems.

The obvious starting point to study isolated molecular dynamics is in the gaseous phase, but this is impracticable for macromolecules. For polymers we use very dilute solutions to characterise single chain dynamics. Here intramolecular effects dominate, although chain - solvent interactions also have an important role to play. Two techniques which have been widely used to probe such isolated chain dynamics are,

(a) The dynamic Kerr effect. Here the principle is to partially orientate the polymer molecules in solution by application of an electric field, and to monitor the orientation and the subsequent disorientation (or relaxatiom) of the molecules on the removal of the electric field by monitoring the changes in the birefringence of the sample. In particular the technique has been successfully employed in the study of size, shape and electrical properties of biopolymers, rigid rod polymers and viruses and some flexible synthetic macromolecules [1].

(b) Photon correlation spectroscopy. Here the time and angular dependence of the intensity fluctuations of light scattered from a polymer solution is used to obtain information about the motion of the scattering centres. These two techniques have been widely applied in dilute solutions to characterise molecular geometry and motions. In addition, the Kerr effect has been used to give information on the electrical characteristics of chains, such as dipole moment and polarisability anisotropy.

As polymer concentration increases, interactions between chains become significant and their motion becomes drastically modified. Since most processing and application of polymers occurs in concentrated systems, an understanding of the changes in molecular dynamical behaviour as chain concentration is increased from dilute to highly entangled systems is fundamental to a molecular understanding of the bulk properties of polymers under conditions in which they are normally used. Very little experimental work has been

carried out on the dynamics of concentrated polymer solutions, or on molecules of a wide range of flexibilities. One objective of this work has been to use the Kerr effect and PCS to characterise polymer chain dynamics over a sufficiently wide range of concentrations to be able to separate the effects of intramolecular forces (i.e. chain conformation or 'flexibility') and intermolecular forces (i.e. interactions or 'entanglements' as they are commonly described). The effects of changing chain structure, molecular weight and molecular weight distribution, concentration, temperature and environment have been systematically examined.

Most theoretical predictions of polymer dynamics and rheological behaviour based on molecular ideas has been restricted to isolated chains in a solvent. The ideas of Rouse[3] and Zimm [11] for flexible molecules and Perrin [65] and Broersma [14] for rigid bodies are the basis of work in this area. However, in the last few years there has been a great deal of interest in developing models for concentrated systems. In particular Doi and Edwards have developed theories for the chain dynamics and rheological behaviour of both rigid systems [4] and flexible chains [96] based on reptation ideas first introduced by de Gennes [17]. These predict dramatic changes in the rates of molecular motion with concentration and molecular weight as the concentration of the polymer is increased from the infinite dilution limit. Part of the impetus for the present experiments came from the theoretical advances made in this area in the late 1970's. To quantitatively test these theories for real systems and examine the extent to which they can be applied to systems of varying flexibility has been another of the objectives of this work.

Chapter 2 of this thesis, introduces the range of motions that polymer chains can undergo and describes the available theories of polymer chain dynamics. The theory underlying the experimental techniques used is also outlined here. The equipmemt used, the experimental procedure and the methods of data analysis employed are described in Chapter 3. Chapter 4 gives details of polymers used and the methods of

sample preparation. The experimental results are presented and discussed system by system in Chapter 5. This is in two parts: I) Dynamic studies and II) Static (electrical) properties. Finally in Chapter 6 the results for the different systems are compared with each other and with current theories for rigid and flexible molecules together with semi-flexible chains developed in this work.

Chapter Two

DYNAMICS OF POLYMERS

2.1 Significance of dynamic studies

A particular polymer sample can exhibit a wide range of mechanical and flow properties depending on the conditions (eg temperature, time scale, environment) in which it is being used. Such behaviour has considerable implications for polymers at all stages of their existence - in the manufacture of raw polymer, in its processing to finished articles and its eventual use. The properties observed under particular circumstances are determined to a large extent by the extent of molecular motion within the polymeric material i.e. by the chain dynamics (2).

Thermoplastic polymers, like metals, are solid at low temperatures and flow as viscous liquids at high temperatures. Although the precise nature of polymeric solids and liquids is very differnt from that of the metals in these two states, it is between these two extremes that the most characteristic differences between polymers and metals and other inorganic compounds is found (Fig 2.1). In changing from a solid glassy material to

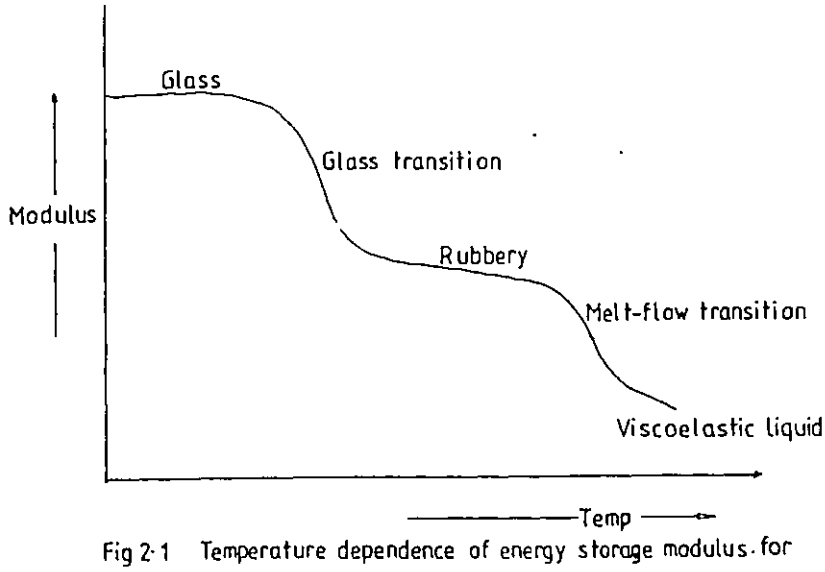

Fig 2·1 Temperature dependence of energy storage modulus for an amorphous polymer.

the viscous liquid state, polymers go through five distinquishable states - glass-like, the glass transition, rubber-like, the melt transition (rubbery liquid) and the viscoelastic liquid. Each change is characterised by an increasing degree of molecular motion in the material. In the glass state neither segmental rotation nor chain translational motion occur to any appreciable extent, but in the rubbery state considerable segmental rotation can occur alongside limited translational motion, so allowing molecular and hence bulk deformation without significant irreversible flow. In the viscous flow region both motions are significant.

The bulk mechanical properties and the flow behaviour of a polymeric system depend on those factors which influence molecular motion: molecular structure, molecular weight (and its distribution), the polymer environment (e.g. solvent, concentration),

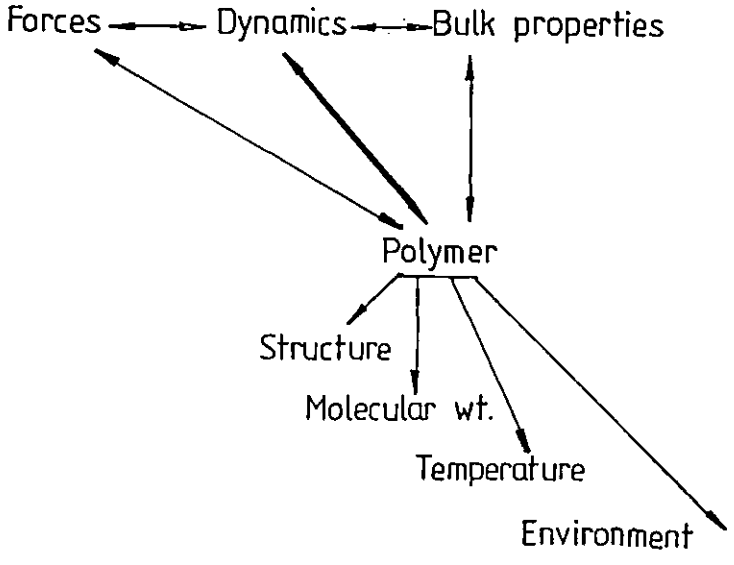

Fig 2.2 Factors determing polymeric behaviour

and temperature. The observed transitions in many physical properties are due to the changes in the segmental and/ or translational motions of the molecules. The motions involve

rotation about bonds in the backbone of the polymer chain and are affected by both intramolecular (or 'steric') and intermolecular ('chain entanglements') forces.

The various routes of studying polymer behaviour are shown schematically in Fig 2.2. Parameters such as polymer molecular weight, structure, environment and temperature influence the various forces within the polymer system and through the chain dynamics determine the bulk properties. Our current quantitative understanding of the inter and intramolecular forces in such complex systems is severely limited and a more fruitful approach is to study the chain dynamics directly by experiments. This polymer-dynamics route (thick line in Fig 2.2) is the one on which attention is focussed in this work. It involves determining and attempting to understand how the polymer chain dynamics are modified by the different parameters listed above. Thus, by understanding the polymer dynamics, and the mechanisms responsible for them, we should be better equipped to modify and improve polymer characteristics to meet desired end properties. By examining changes in microscopic properties, polymer dynamics studies should therefore ultimately enhance our understanding of the resulting mechanical and rheological behaviour.

2.1.1 Types of molecules

If we represent the end-to-end distance of a macromolecule by r, the contour length by L, the chain diameter d, the monomer unit length ℓ, and the persistence length, which is a measure of the extent to which the macromolecule sustains its initial displacement by q, polymer chains can be broadly classified into three major groups:

(i) Stiff rigid macromolecules, in which $\ell/d \gg 1$ and the end-to-end distance r equals the contour length L. The persistence length q is so large that $q=\infty$ implying that chain flexibility is negligible. The macromolecules can often be represented as long rigid rods (Fig 2.3 (a)) or sometimes by other rigid geometries such as ellipsoids of revolution or spherocylinders. The only possible rotational motion for this type of macromolecule involves the entire molecule, as rotation about backbone bonds is severely restricted. A time dependent definition of chain stiffness implies that the time required for such changes

in conformation by segmental rotation are far greater than the time required for the rotation of the whole molecule.
(ii) Highly flexible random coiled macromolecules, in which the average persistence length projection q, is similar to ℓ ($\therefore \ell \simeq q << L$). The macromolecule can coil and assume a wide range of overall conformations (see Fig 2.3 (b)). Each segment of the chain can undergo orientation and displacement largely independently of the motions of other segments in the same chain, apart from those to which it is directly attached. A whole range of motions is possible, from local segmental rotation to whole molecule rotation and/or translation (see section 2.2)

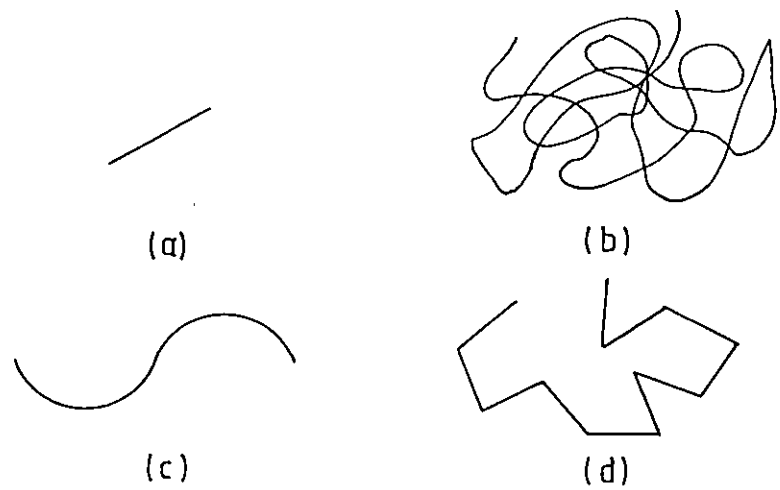

Fig 2·3 Schematic diagram of molecular types.
(a) Cómpletely stiff (rod-like) macromolecule (b) Random coiled macromolecule (c) Weakly-flexible persistent macromolecule (d) Semi-flexible freely jointed macromolecule.

(iii) Semi-flexible macromolecules, Between the two extremes of the rigid and random coil models there exists a broad spectrum of macromolecules which are referred to as semi-flexible. For this group $L/d \simeq 1$ and $\ell < q < L$. Here the degree of chain flexibilty as defined by q is important. With q close to L, the chain can be described as 'weakly bending' (Fig 2.3 (c)). For low values of q (q closer to ℓ) a model involving

freely jointed segments of length q (see Fig 2.3(d)) becomes more appropriate. Again segmental and whole molecular rotation are possible with the time scales of these motions, τ_s and τ_r respectively, getting closer together as the chain becomes stiffer. τ_s/τ_r hence ranges from values far less than one for $q \simeq L$ through unity to values far greater than one where q approaches L. Relative changes in these characteristic times and hence the 'chain flexibility' can be brought about by any of the parameters shown in Fig 2.2 and so the choice of am appropriate model for a polymer chain is not determined solely by the inherent chemical structure.

2.2 Modes of motion of macromolecules in solution

There are three main types of molecular motion of importance in polymers:

(a) Translational motion, involving movement of the centre of mass. The time scale of this motion is typically $\sim 10^{-6}$s (for an isolated chain to translate a distance equivalent to the radius of gyration, R_G).

(b) Rotational motion involving the entire molecule. Here all segments of the molecule move in unison and such motion involves a well defined intersegmental geometry. For rod like macromolecules the rotation can either be about the minor axis (Fig 2.4 (a)) or major axis (Fig 2.4 (b)) with fixed geometry.

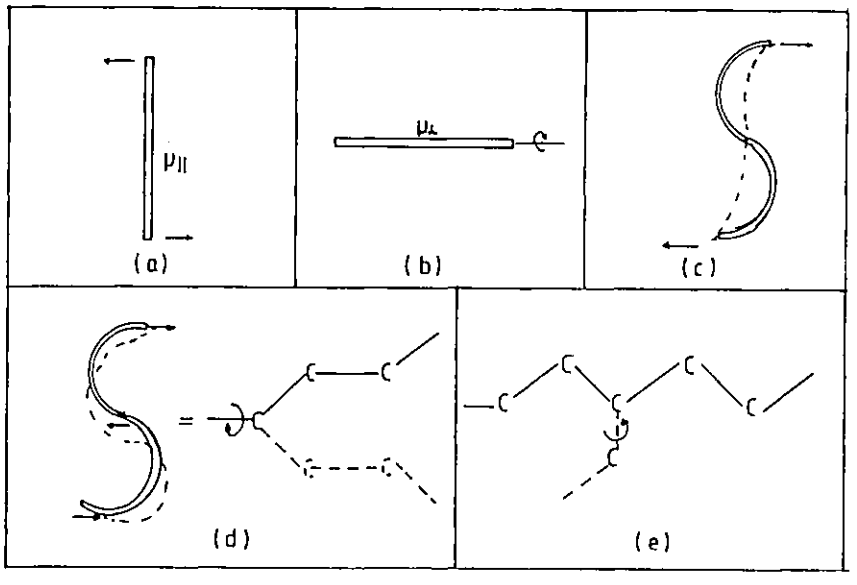

Fig 2.4 Modes of relaxation for macromolecules: (a) Rotation of rods about minor axis(end-over-end) (b) Rotation of rods about major axis (c) 1st mode relaxation of flexible macromolecules:(d) Rotation about backbone chain (e) Side chain rotation.

The time for whole molecule rotation depends on the macromolecular size and shape, ranging from $\sim 10^{-6}$s for isolated short chains to $\sim 10^{-4}$s for longer chains in typical low viscosity solvents. For flexible chains, the translational and end-over-end rotational motions of the entire molecule are associated with the zeroth and first normal modes [1] respectively (Fig 2.4(c) , see section 2.3.1).

(c) Segmental motion, which may involve parts of the main chain backbone or the substituent side groups. The backbone chain segmental motion involves changes in the local conformations of the chain and takes place only in flexible macromloecules. These motions which involve rotation about the backbone bonds (Fig 2.4(d)) can occur with increasing independence of the motion of other segments as the chain becomes more flexible. The times for segmental rearrangement are shorter than those for rotation of the entire chain ($\sim 10^{-8}$s). Side chain rotational motion (Fig 2.4(e)) is faster still and can take place independently of the backbone motion (typically 10^{-10} - 10^{-8}s), although in some molecules there is evidence of co-operative motion of side chains and local main chain segments (77) .

2.3 Theories of macromolecular dynamics.

The dynamics of chain molecules are expected to change dramatically as the extent of molecular interactions increases. It is convenient to distinquish three concentration regimes in which the degree of chain interaction is qualitatively different see Fig 2.5. At infinite dilution (Fig 2.5 (a)), the molecules are on average sufficiently far apart that chain interactions are negligible. As concentration increases, long range interactions will come into effect and small changes in dynamics will be observed. When the concentration is sufficiently high for the effective hydrodynamic volumes swept out by each molecule to overlap, then a significant increase in interactions occurs and marked changes in the dynamics are expected (semi-dilute region -Fig 2.5 b). On increasing concentrations still further, the chains increasingly restrict each other's motion. When the mean distance between the chains becomes comparable with the smallest dimension of the polymer molecules or with the length over which significant flexibility exists, then another qualitative change in the

nature of the dynamics is expected. In such a concentration or entangled regime (Fig 2.5 c) , the system is approaching a uniform segment density where the identity of specific segments with individual chains becomes increasingly less important.

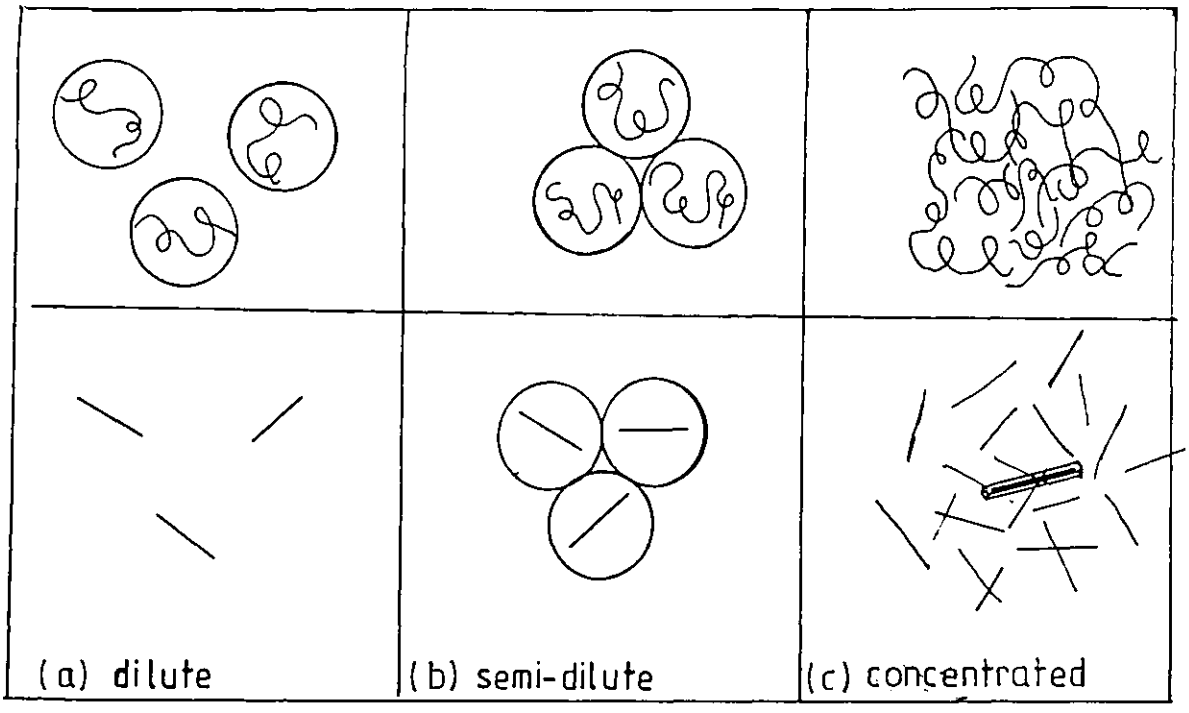

Fig 2·5 Concentration regimes for coils and rods.

Many theoretical models have been proposed, aimed at explaining the dynamics of dissolved macromolecules in solution. The theories for the dynamics of isolated chains in dilute solution are extensive and have been used to explain experimental observations and interpret them in terms of macromolecular dimensions. The dynamics in the semi-dilute and concentrated regimes are complex and relatively few theoretical (4,5,6) and experimental (7,8,9) investigations have been carried out. Each of the theories will be outlined briefly, classifying them on the basis of concentration regime and chain flexibility.

2.3.1 Dilute solution

The mean distance between polymer molecules in dilute solution is sufficiently large for polymer-polymer interactions to be negligible so that only solvent-polymer molecular interactions are of importance. Theoretical models of polymer dynamics in this regime have been devised for the random coil model, the rigid rod model and the semi-flexible coil model.

Random coil model

The most successful dynamical models for flexible chains are those associated with Rouse (3), Bueche (10) , and Zimm (11). The Rouse-Bueche-Zimm model or 'bead-spring' model as it is often referred to, is a device to avoid the complications of describing local chain motions and still obtain information on the large scale configurational relaxations which control the viscoelastic behaviour. The model replaces the real molecule of n main atoms by a mechanical chain of N+1 beads joined by N linear springs (see Fig 2.6 a, b). The frictional

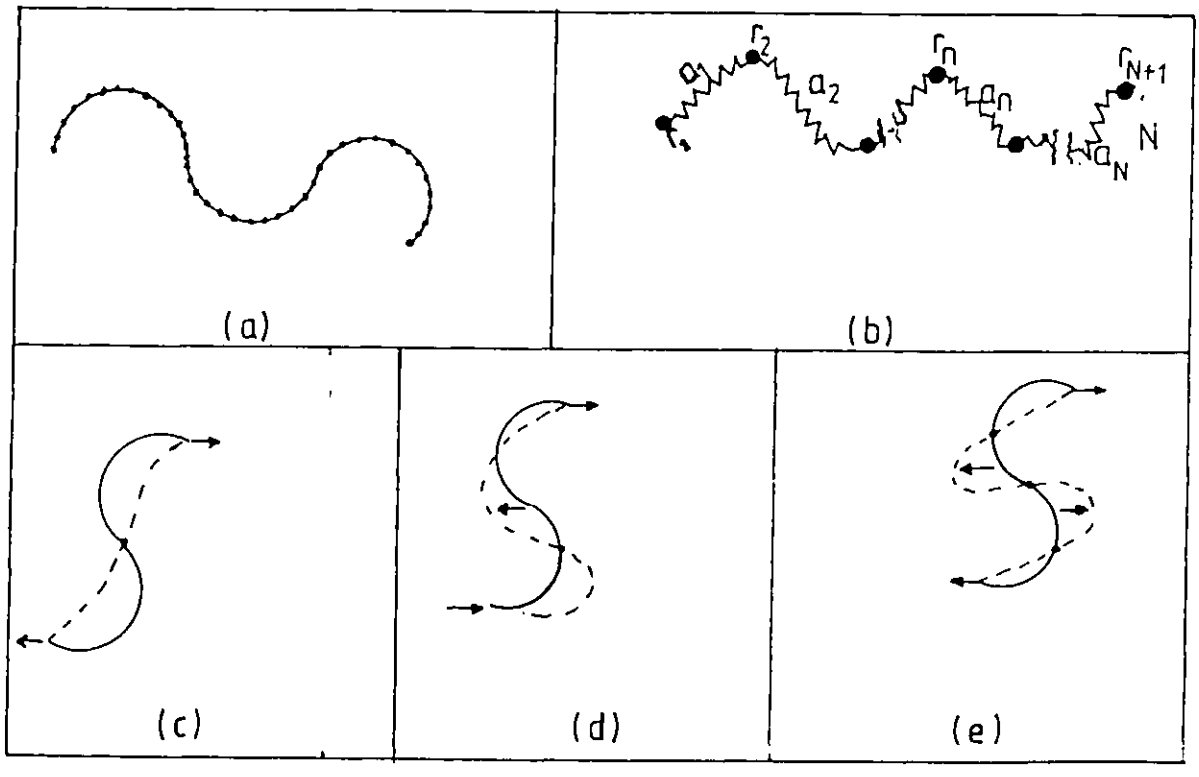

Fig 2·6 Spring-bead model and lower modes of motion.

interactions with the medium, distributed uniformly along the molecular length, are modelled by a frictional coefficient

concentrated on the beads, $\underline{r}_i$. Each segment contains sufficient monomer units to behave as a Gaussian subchain of mean end-to-end distance $\underline{r}_{i+1} - \underline{r}_i$. Deviations from this mean value are opposed by entropic forces which are the physical origin of the springs in the model. The ability of the molecule to undergo configurational changes lies in the polymer flexibility, which allows each part of it to move with the velocity of the surrounding medium. The Brownian motion is responsible for restoring the segments to an equilibrium distribution. The model describes the motion of individual beads in terms of a series of normal modes each of which involves a cooperative motion of the whole chain, characterised by a characteristic period or relaxation time. For the case in which perturbation of the solvent velocities by the chain is ignored ('free draining coil' or Rouse model), the relaxation times of these modes have been related to the molecular weight, the intrinsic viscosity , $[\eta]$, solvent viscosity, η_s, temperature T and the gas constant, R, according to the expression, (3, 11, 85)

$$\tau_p = \frac{1.21\, M[\eta]\eta_s}{R\, T\, p^2} \qquad 2.1$$

where p is the mode number. The first normal mode (p=1) is associated with whole molecular rotation, and higher modes with in-phase wriggling-type motions of shorter wavelength, involving increasingly smaller parts of the chain moving in phase with each other (see Fig 2.6 (c),(d),(e)).

The non-free draining approximation of Zimm considers the interaction between the beads and the solvent and the consequent perturbations in local solvent velocity. It merely leads to a modification of the constant in the equation 2.1, the first normal mode relaxation time being [3,11,85],

$$\tau_1 = \frac{0.85 M[\eta]\eta_s}{R\, T} \qquad 2.2$$

However the molecular weight dependence of the relaxation times according to the two models is different, since for a Rouse chain $[\eta] \propto M$ whereas for the Zimm case $[\eta] \propto M^{\frac{1}{2}}$.

Rigid rod model

Theoretical descriptions of the rotational and the translational dynamics of dilute systems of rods in solution have been formulated by several authors. The basic models are those of Kirkwood and Auer [12] and of Riseman and Kirkwood [13]. A rigid rod particle in a velocity gradient experiences forces trying to align it with its axis in the direction of the flow. This will be opposed by Brownian forces trying to disorientate the molecules, but unlike in the Rouse model, no molecular deformation will occur. The net result is that the molecule undergoes a forced translatory motion of its centre of mass and rotational motion arising from the rotational component of velocity. The relevant diffusion coefficients have been related to the molecular length, L, and diameter, d according to the expressions [12, 13, 65]

i) for translational diffusion parallel to rod axis,

$$D_t = \frac{kT}{2\pi\eta_s L} \ln L/d \qquad 2.3$$

ii) for translational diffusion perpendicular to rod axis

$$D_t = \frac{kT}{4\pi\eta_s L} \ln L/d \qquad 2.4$$

iii) for rotational diffusion of the rod,

$$D_r = \frac{3kT}{\pi\eta_s L^3} \ln L/d \qquad 2.5$$

where η_s is the solvent viscosity and k Boltzmann's constant.

Broersma [14] conducted a detailed study of the rotational dynamics of perfect rods. He obtained a similar expression for D_r as above, with an additional correction term γ which caters for end effects:

$$D_r = \frac{3kT}{\pi\eta_s L^3} \{ \ln 2L/d - \gamma \} \qquad 2.6$$

$$\gamma = 1.57 - 7\{(\ln 2L/d)^{-1} - 0.28\}^2 \qquad 2.6(a)$$

Semi-flexible model

The random coil and the rod models do not represent a large number of polymers which exhibit neither of these extreme types of behaviour. The available models that have been developed for molecules of intermediate flexibility are those of Hearst [15] for the 'worm-like' chain and the 'weakly bending' rod.

The 'worm-like' model starts from a polymer chain of the random coil (Rouse) type and introduces factors that inhibit coiling of the chain, thus introducing some persistence of segments in the direction of successive chain units. For such a molecule, the isolated rotational coefficient D_r is given by

$$D_r = \frac{k\,T\,\rho^2}{\eta_s\,q\,M^2}\left\{0.126\sqrt{M/q\rho} + 0.159 \ln \frac{2q}{b} - .387 + 0.16(b/a)\right\}$$

where L is the chain contour length, M the molecular mass, $\rho = M/L$ the mass per unit length, q the persistence length, a the Stokes diameter ($\simeq \zeta / 6\pi\eta_s$ where ζ is a segmental frictional coefficient) and b the spacing between frictional elements (segment length).

The 'weakly bending' rod model seeks to determine the deviation from the rotational diffusion properties of a perfectly rigid rod. The rigid rod macromolecule, is represented by an array of 2n+1 frictional groups, spread at equal distances b, on a linear axis of length, L. The 'weakly bending' rod model introduces the additional parameter q, the persistence length, and relates the rotational diffusion coefficient with the molecular parameters by:

$$D_r = \frac{kT\rho^3}{\pi\eta_s M^3}\left\{3 \ln \frac{M}{2\rho b} - 4.92 + 4\left(\frac{b}{a}\right) + \frac{M}{4\rho q}\left(4.5 \ln \frac{M}{2\rho b} - 10.2 + 4\left(\frac{b}{a}\right)\right)\right\} \qquad 2.8$$

The symbols are the same as for the 'worm-like' chain model. The rotational diffusion coefficients for the two models have different molecular weight dependences; ($D_r \propto M^{-1.5}$ for the 'worm-like' model and M^{-3} for the 'weakly bending' model).

2.3.2 Concentrated solution

Increasing the concentration brings macromolecules closer together on average and the molecular dynamics become considerably modified. The motions of individual chains become hindered by intermolecular effects. The dynamical behaviour in this regime is as fascinating as it is complex and shows a unique combination of viscous and elastic characteristics. However, relatively few theoretical models have been developed to describe such behaviour. Existing theories include those of de Gennes [17, 44], Doi and Edwards [4,96] , Edwards and Evans [19], Schaefer et al [97], Freed and Edwards [5] and Yamakawa [20].

Flexible coil

de Gennes [17] developed the concept of chain reptation for flexible chains in the semi-dilute regime. According to this idea a polymer chain in such an environment is constrained by its neighbours to move within a hypothetical tube (Fig 2.7 c ,e). The translational motion of the whole chain along the axis of this tube is achieved by local reptative (or repeated wriggling) motion of small segments (see Fig 2.7 d). The theory describes the wriggling motion along the chain by diffusion of defects which for a flexible chain is relatively rapid. The longest characteristic relaxation time associated with this wriggling defect diffusion is of the form,

$$\tau_{def} = \frac{(na_c)^2}{\pi^2 \Delta} \qquad \propto \qquad M^2 \qquad 2.9$$

where n is the degree of polymerisation of the real chain, M the molecular weight, Δ the defect diffusion coefficient and a_c the correlation or screening length(essentially the mean distance between chain contacts (see Fig 2.7 (a)).

On the time scale $t > \tau_{def}$ the wriggling motion merely represents a high frequency fluctuation, within the tube surrounding a specimen chain, about the overall curvilinear diffusion out of this tube (see Fig 2.7 e). The chain only changes its overall conformation by disengaging from the original tube followed by creation of another (see Fig 2.7 e). The characteristic relaxation time τ_{re} for such tube renewal (or 'disengagement time') is given by

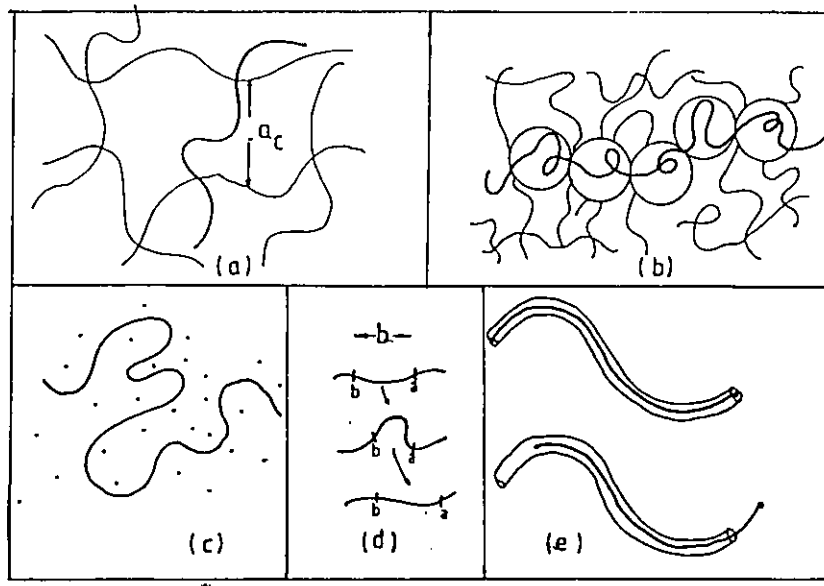

Fig 2·7 Diagramatic representations of chain reptation

$$\tau_{re} = \frac{(n\, a_c)^3}{\pi\, \rho\, b^2 \Delta} \propto M^3 \qquad 2.10$$

Unlike τ_{def}, τ_{re} is dependent on ρ, the density of defects, and b, the stored length. The model considers that the self diffusion of an entangled polymer coil in semi-dilute solution may be treated in terms of the motions of individual chains through a transient network formed by the overlapping coils. Each chain reptates in a tube of diameter a_c. The time taken for the chain to diffuse end-to-end along its curvilinear path, τ_{re}, gives a measure of the time taken for entanglement renewal.

Doi and Edwards [96] extended de Gennes theories and showed that for such a model the centre of mass diffusion coefficient is given by

$$D_G \propto \frac{a_c^2}{nb^2} D_c \propto M^{-2} c^{-2\alpha - \beta}$$

where D_c is the curvilinear diffusion coefficient ($\propto M^{-1} c^{-\beta}$). c is the mass concentration, and $a_c \propto c^{-\alpha}$. The characteristic diffusion time, τ_D, is hence proportional to M^2 in common with de Gennes defect time τ_{def}. They also predicted that the time of tube renewal, characterised by the longest relaxation τ_{re}, should depend on molecular weight and chain mass concentration c as

$$\tau_{re} \propto M^{3} c^{2\alpha+\beta} \qquad 2.12$$

For highly flexible chains, α was estimated to be 0.6 - 0.75 and β was estimated to be small and approximated to zero.

Semi-flexible chains

Schaefer et al [97] have made a detailed study of the static and dynamic properties of semi-flexible polymers in solvents of different quality. They showed that, for these chains, as concentration increases a number of different regions are encountered . The behaviour is illustrated on a temperature-concentration (T-C) diagram in Fig 2.8 . They distinguished five regions separated by a series of cross-over concentrations. These cross-over concentrations are determined by the limits of the correlation range of each regime. The regions are ;

(i) The dilute region ($c < c^{*}$) where the density of chains is low and interactions are negligible. c^{*} is the chain overlap concentration defined in section 2.3

(ii) Semi-flexible region - good solvent ($c^{*} > c > \tilde{c}$). The chains are here entangled and characterised by a correlation length a_c, which is essentially the mean distance between interchain contacts. At $c = c^{*}$ this length, a_c, is equal to the radius of gyration of independent chains, and decreases with increasing concentration. At $c = \tilde{c}$, it becomes equal to the length of the chain segment (or thermal 'blob') within which excluded volume effects can be neglected.

(iii) Semi-flexible - marginal solvent ($\tilde{c} < c \lesssim c^{+}$), This region extends from the concentration $\tilde{c}$, above which the chain dimensions become ideal, to a concentration c^{+}, at which the chain free energy becomes dominated by the third, rather than the second virial cofficient.

(iv) Semi-dilute - theta (Θ) solvent ($c^{+} < c < c^{**}$) where c^{**} is the concentration at which a_c becomes comparable with the chain persistence length, q.

(v) Concentrated region, $c > c^{**}$ where the chain dynamics are predicted to become independent of density.

They did not explicitly calculate rotational relaxation times or chain diffusion coefficients in these regions. However they did give the dependence of the correlation length

a_c on the reduced temperature, ϕ ,(= $(T-\Theta)/T$ where T and Θ are the solution temperature and the theta temperature respectively) and the chain concentration, c, as in terms of the expression

$$a_c \propto c^{-\alpha} \phi^{-\beta} \qquad 2.13$$

Table 2.1 below shows the values of the exponents α and β for the five different regions.

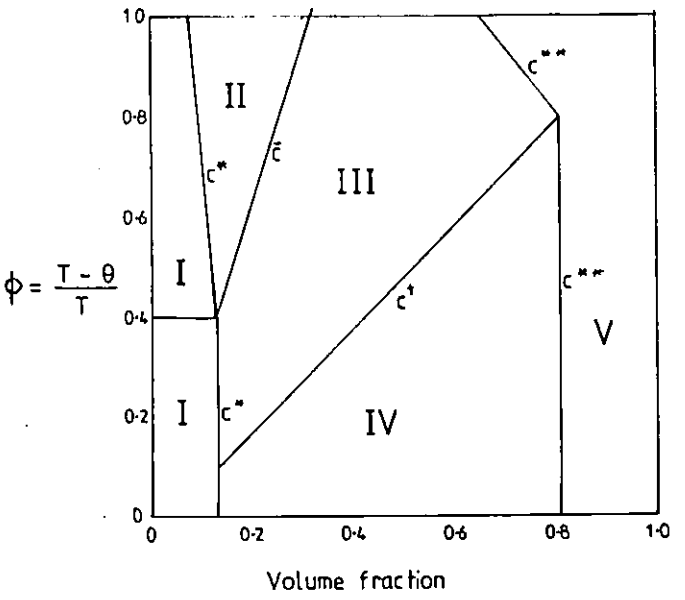

Fig 2·8 Temperature-concentration diagram for semi-flexible polymer solution (schematic)

Table 2.1 Predicted dependence of correlation length a_c on reduced temperature ϕ and chain concentration, c for semi-flexible chains {97}

$a_c \propto c^{-\alpha} \phi^{-\beta}$

Region	α	β
(i) Dilute theta		
(b) Dilute good		
(ii) Semi-dilute good	0.75	0.25
(iii) Semi-dilute marginal	0.5	0.5
(iv) Semi-dilute theta	1.0	
(v) Concentrated	0·0	

Rigid rods

In addition to the reptation model for flexible chains, Doi and Edwards have also studied the dynamics of rigid rod macromolecules in the concentrated regime defined by

$$\frac{M}{N_A L^3} = C^* < C < C^{**} = \frac{M}{N_A d L^2} \qquad 2.14$$

where M, L, d and N_A are the molecular weight, rod length, diameter and Avogadro's number respectively. C^* marks the onset of rod entanglement and C^{**} marks the upper limit beyond which there is local molecular ordering of the rod-like molecules - the critical concentration of the isotropic-nematic transition (see Fig 2.9).

In this regime the distribution function $\underline{F}(\underline{r},\underline{u},t)$ which specifies the configuration of the rod in terms of the position vector of the centre of mass, $\underline{r}$, and the unit vector parallel to the rod axis, $\underline{u}$, is normalised as

$$\int d^3r \int d^2u \, \underline{F}(\underline{r},\underline{u},t) = 1 \qquad 2.15$$

and satisfies the kinetic equation describing the Brownian motion

$$\frac{\partial \underline{F}(\underline{r},\underline{u}\ t)}{\partial t} = \mathcal{L}_{\underline{r}}[F] + \mathcal{L}_{\underline{u}}[F] \qquad 2.16$$

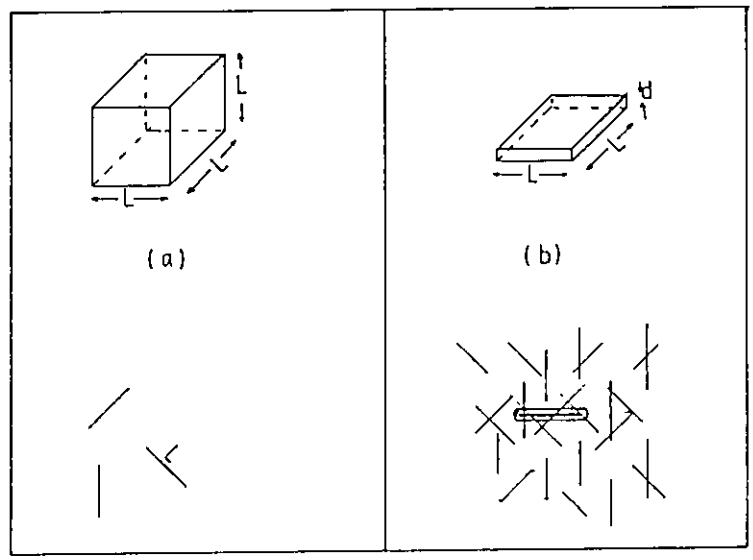

Fig 2·9 Schematic representations of the critical concentrations for (a) the dilute-semi-dilute and (b) semi-dilute concentrated transitions.

where the terms $\mathcal{L}_r[F]$ and $\mathcal{L}_u[F]$ represent the translational and the rotational motion respectively.

In dilute solution these terms are:

$$\mathcal{L}_r[F] = D_{t\parallel}(\underline{u}.\frac{\partial}{\partial \underline{r}})F + D_{t\perp}\{\frac{\partial^2}{\partial \underline{r}^2} - (\underline{u}.\frac{\partial}{\partial \underline{r}})^2\}F \qquad 2.17$$

$$\mathcal{L}_u[F] = D_r \nabla_u^2 F = D_r\left[\frac{1}{\sin\theta}\frac{\partial}{\partial\theta}\sin\theta\frac{\partial}{\partial\theta} + \frac{1}{\sin^2\theta}\frac{\partial^2}{\partial\phi^2}\right]F \qquad 2.18$$

where (θ,ϕ) are polar co-ordinates specifying the unit vector $\underline{u}$, $D_{t\parallel}$ and $D_{t\perp}$ are translational diffusion coefficients parallel and perpendicular to the rod axis respectively and D_r the rotational diffusion coefficient. These coefficients are given by equations 2.3 to 2.5.

The Brownian motion in the concentrated regime is complex due to entanglement interactions between the rods. Doi and Edwards modelled this situation by making the following assumptions:

(i) Modelling was restricted to long time scale motions only

(ii) The rod diameter was assumed to be so small, so that diffusion along the axis was essentially unhindered i.e. $D_{t\parallel c} = D_{t\perp 0} \equiv D_t$

(iii) Motion perpendicular to the rod was restricted to the mean distance between rods, a_c.

The rotational motion is severely restricted by rods surrounding a specimen rod, so that if a rod preventing the rotation of the specimen rod diffuses a distance of order, L, the constraint on the motion of the test rod is released allowing it to rotate by an amount of order a_c/L. The time for such linear axial diffusion is

$$\tau_o \simeq L^2/D_t \qquad 2.19$$

The Brownian motion then becomes a random walk on a unit sphere with jump frequency τ_o^{-1} and mean square displacement $(a_c/L)^2$. The rotational diffusion constant in this region D_{rc} is therefore

$$D_{rc} \sim (a_c/L)^2 / \tau_o \qquad 2.20$$

They show that for random rods where c_n is the number density of rods,

$$a_c = \left(\tfrac{1}{2} \pi c_n L^2 \right)^{-1} \qquad 2.21$$

and so substituting equations 2.9 and 2.21 into equation 2.20 yields

$$D_{rc} = \frac{4 D_t}{\pi^2 c_n^2 L^3} \qquad 2.22$$

Noting from equation 2.3 and 2.5 that

$$D_t = \frac{3}{2} D_r L^2 \qquad 2.23$$

gives

$$D_{rc} = \frac{6 D_r}{\pi^2 c_n^2 L^6} \sim D_r (c_n L^3)^{-2} \qquad 2.24$$

Since $D_r \propto L^{-3}$ and $c_n \propto cM^{-1}$ $(\propto cL^{-1})$ where c is the mass concentration

$$D_{rc} \propto c^{-2} L^{-7} \propto c^{-2} M^{-7} \qquad 2.25$$

This theory then predicts a marked concentration and molecular weight dependence of the rotational diffusion coefficient, D_{rc}. Photon correlation spectroscopy and the dynamic Kerr effect are appropriate experimental techniques with which to study such rod motions.

2.4 Experimental techniques

Polymer molecular motion can be studied using a variety of relaxation and scattering techniques. In a relaxation method we perturb the system from equilibrium and then follow its return to equilibrium. Such a perturbation is employed in mechanical, dielectric, Kerr effect, acoustical and pulsed NMR relaxation measurements. In a scattering technique we use radiation to probe the fluctuations occurring in a system at equilibrium. The time scale of such fluctuations is a measure of the rate of polymer motion in the system. Light and neutron scattering techniques have been employed in such fluctuation studies. Relaxation and scattering techniques give complementary information about the system and together enable the rotational and translational

motion of the chains to be characterised, together with characteristics such as dipole moments and polarisability anisotropy.

2.4.1 Dielectric and Kerr electro-optic experiments

In dielectric and Kerr effect studies, the polymer solution is subjected to an external electric torque which causes some alignment of the molecules. The opposite charges in the molecular dipole attempt to migrate in the field, hence orienting the molecule in the field direction. Macromolecules without permanent dipoles can orient in the field due to induced dipole effects since in general the chain polarisability is anisotropic. Kerr effect experiments measure the birefringence resulting from such alignment. Dielectric experiments measure the total electrical polarisation of such a system as reflected by the capacitance of the cell containing the sample. Measurement of the extent of either of these effects at equilibrium can give information about the electrical characteristics of the molecule such as dipole moments, μ, and electric polarisability α.

Studies of the time dependence of the effect can be made in two ways. By using an alternating field, the molecules are compelled to rotate with the frequency of the applied field until a frequency is reached at which the particular dipole of interest can no longer follow the field. The dipole can then no longer contribute to the polarisation of the system and the measured dielectric constant, ε', decreases over a frequency range characteristic of the motion of the particular dipole concerned. This results in the characteristic dielectric relaxation curve illustrated in Fig 2.10, where an inflection occurs at the characteristic frequency ω , of the molecular dipole.

In a simple case where there is only a single mode of rotation characterised by a single relaxation time ,τ, the change in dielectric constant with frequency may be described by the Debye relation

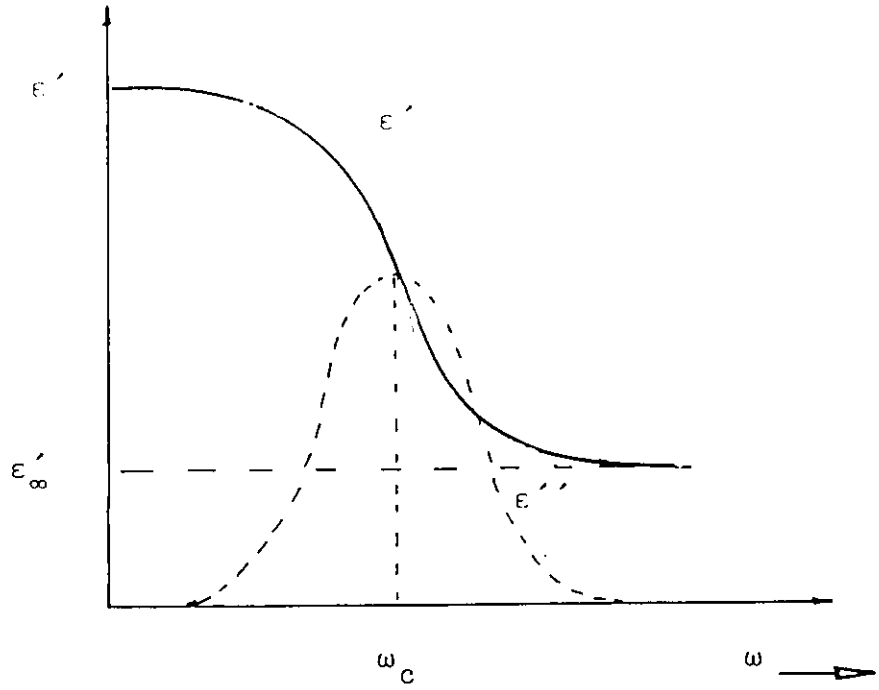

Fig 2.10 The frequency dependence of the real part of the dielectric constant ε´ (capacitance - solid line) and the imaginary part ε´´(resistance - broken line) of a polymer solution subjected to an alternating field.

$$\frac{\varepsilon'_\omega - \varepsilon'_\infty}{\varepsilon'_0 - \varepsilon'_\infty} = \{1 + 4\pi^2\omega^2\tau^2\}^{-1} \qquad 2.26$$

where ε'_ω is the dielectric permittivity at a frequency ω and ε'_0 and ε'_∞ the limiting values at low and high frequencies respectively. The characteristic relaxation time τ can be calculated from the critical frequency ω_c using

$$\tau = \{2\pi\omega_c\}^{-1} \qquad 2.27$$

A similar effect can be observed in the birefringence Δn. For a system obeying the Kerr law

$$\Delta n = K E^2 \qquad 2.28$$

where K is the Kerr constant and E is the applied field gradient, then for a single Debye relaxation, for the case of permanent dipole moment,

$$K_\omega = K_0\{1 + 4\pi^2\omega^2\tau^2\}^{-1} \qquad 2.29$$

where K_ω is the Kerr constant at frequency ω and K_o the value at zero frequency.

Alternatively, experiments can be performed in the time domain by making a step change in the electric field and following the build up or decay of either the polarisation or birefringence of the system to the steady state value. Such a method is used in the current work and is described in more detail in section 2.5. For a single Debye process, the time domain response is of the form

$$P(t) \text{ or } \Delta n(t) = A \exp -t/\tau \qquad 2.30$$

Experimentally the two methods have been widely employed in the study of dilute polymer systems. Dielectric experiments have been conducted on rigid rod like macromolecules such as poly-γ-benzyl-L-glutamate (PBLG) (21, 22,23) and poly(n-butyl isocyanate), PBIC (24,25,26,27),and flexible coil polymers such as polypropylene glycol/oxide (PPG/PPO) (28,29) and polyethylene oxide (PEO) (30,31) . Parallel Kerr effect studies on these macromolecules PBLG (32,33,34,35) , PBIC (36,37,38) , PPG/PPO (29) polystyrene (PS) [39] have also been undertaken. These studies have been relatively successful in giving information about the single chain dynamics of these polymers, their molecular size, shape and their electric properties.

2.4.2 Nuclear Magnetic Resonance (NMR)

Both proton (^1H) NMR and carbon-13 (^{13}C) NMR have been successfully employed for the quantitative examination of the structure and the dynamics of macromolecules. The technique utilizes the property of spin possessed by atomic nuclei with odd atomic mass and number. Application of a strong magnetic field to nuclei of spin quantum number $\frac{1}{2}$ splits the energy levels into two, representing states with spin parallel and antiparallel to the field. Transitions between the states lead to absorption or emission of radiation of energy, E, which is related to the magnetic field strength H_o and the magnetic moment of the nucleus, μ_m, according to the equation

$$E = 2\mu_m H_o$$

Having perturbed the system, one process that re-establishes the equilibrium is known as spin lattice relaxation. This return to equilibrium of the population of the nuclear magnetization is exponential, ($\exp -t/T_1$), and is governed by the characteristic time known as the spin lattice relaxation time, T_1. There is similarly a transverse relaxation time, T_2, which characterises the decay of the magnetic field to zero via spin-spin relaxation. Contributions to T_1 arise from rapid fluctuations of the magnetic field at the nucleus due to relative motions of the molecules, in which it is embedded. T_2 is a measure of nuclear coupling interactions, involving spin flips by electron coupling with other nuclei, which themselves are undergoing relaxation. The spin lattice and the spin-spin relaxation times provide dynamic information about the polymer chains, although much less directly than the other techniques (e.g. from their temperature dependence). The major advantage over other methods is that information is obtained about the motion of particular atoms in a polymer chain which can be distinguished by their individual chemical environment. The wide range of NMR studies of polymer dynamics has been reviewed by Schaefer [113] a recent study of relevance to the present work is that on the stiff rod molecule PBLG [114,115,116] and by Heatley and coworkers [117].

2.4.3 Dynamic light scattering

A polarised laser beam incident on a fluid exerts a force on the charges in the dielectric medium. As the Brownian forces perpetually bombard the fluid molecules, causing them to execute both translational and rotational motions, they cause fluctuations in the instantaneous dielectric constant of the medium. The optical inhomogeneities caused by such fluctuations cause scattering of the incident beam by the medium. Light scattering techniques have traditionally been used to measure the molecular weight and size of polymer chains by monitoring the angular dependence of the intensity of light scattered from dilute solution of the polymer. Recently, there has been increased use of dynamic light scattering techniques whereby the angular and time

dependence of the frequency of the scattered light is monitored to give information about the motions of polymer molecules in solution. Interaction of the light with the moving molecules causes a Doppler broadening of the scattered beam and a frequency domain analysis of the broadening has been used to study translational diffusion of macromolecules in solution[7,100]. Just as with relaxation methods, experiments can also be made in the time domain where the technique is usually termed photon correlation spectroscopy (PCS). Here the time dependence of the light intensity is measured as a function of angle to give information about translational, rotational and intramolecular modes of motion This technique, which is the one employed in this work, is described in detail in section 2.6. It has been applied to many polymers of varying flexibility in dilute solution and a few isolated studies have been made of more concentrated systems [97,99,100]

If radiation of wavelength, λ, is scattered in a medium of refractive index, n, at an angle θ, then we can define a scattering vector $\underline{K}$ whose magnitude is given by

$$|\underline{K}| = K = \frac{4\pi n}{\lambda} \sin \tfrac{1}{2}\theta \qquad 2.32$$

The length scale over which the radiation probes molecular motion is of order K^{-1}. For light of wavelength 400 - 700 nm at angles 10 - 150°, this range corresponds to 30 - 600 nm . Hence dynamic light scattering probes motions over distances corresponding to the large segments of a polymer chain upwards and therefore gives information about large scale intramolecular motions (the first few Rouse-type modes for flexible molecules) and translational and rotational diffusion in dilute polymer solutions. Using neutrons of wavelength $\sim$0.1 nm , at $\theta = 10^{o}$ $K^{-1} \simeq 0.1$ nm. Neutron scattering can therefore be used to give information about much shorter segments of polymer chains and substituted side groups. Many studies of polymers in conditions ranging from dilute solution to the melt state have been made using this technique [94,105,107,108]

2.5 The Kerr electro-optic technique.

2.5.1 The Kerr effect.

The Kerr electro-optic effect (electric birefringence) arises when molecules are aligned in an electric field and hence induce anisotropy in the refractive index (double refraction or birefringence) in the sample. The observation of the time dependence of the birefringence response to the application or removal of the electric field is termed the 'dynamic Kerr effect'.

The Kerr effect is exhibited by polar molecules of many kinds. In this work we are interested only in polymer systems. Polymer molecules dissolved in a solvent (at concentrations below any liquid crystalline transition) are randomly oriented and the solution is isotropic, with equal refractive indices in the x-y-z directions i.e. $n_x = n_y = n_z$ (see Fig 2.11 a). However under an applied electric field gradient E, the molecules will become oriented to some extent in the direction of the field, causing changes in the refractive indices parallel and perpendicular to the field direction. With $n_x \neq n_y = n_z$ (Fig 2.11 b) the solution becomes anisotropic and the phenomenon of double refraction results. The orientation of the macromolecules arises because of the interaction energy between the applied field and the permanent molecular dipole moment, μ and/ or the induced dipole, μ_{ind} which results from the difference $(\alpha_1 - \alpha_2)$ in

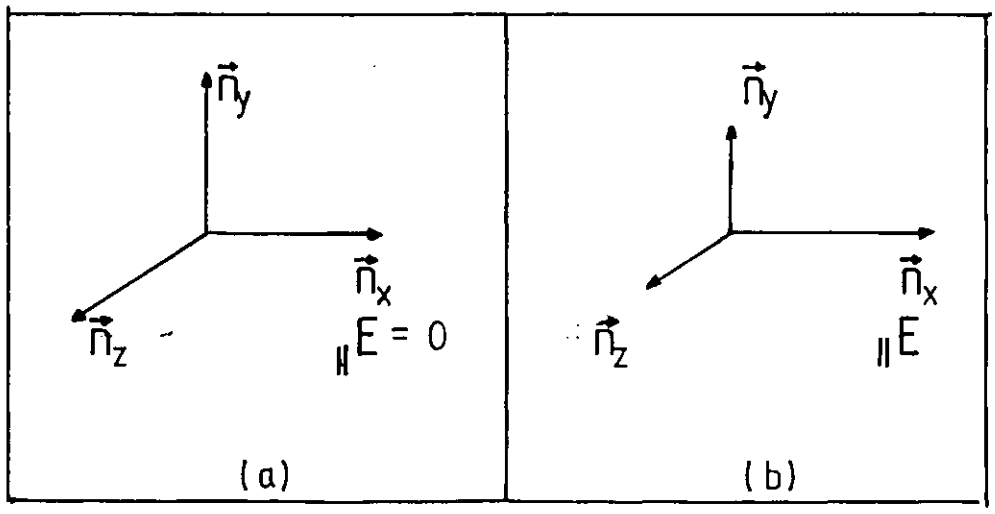

Fig 2·11 Birefringence (a) at zero field and (b) under field gradient, E .

the volume electric polarisabilities along the field direction (α_1) and perpendicular to it (α_2). The birefringence Δn is simply defined as

$$\Delta n = n_{\parallel} - n_1 = n_x - n_y \qquad 2.33$$

where $n_{\parallel} = n_x$ is the refractive index in the direction parallel, and $n_1 = n_y = n_z$ is the refractive index perpendicular, to the field.

2.5.2 Measurement of electric birefringence.

A schematic diagram of the experimental technique used to study the Kerr effect is given in Fig 2.12. Consider a monochromatic plane polarised beam of light incident on an isotropic solution situated between crossed polarisers. Since the refractive index of the sample is the same in all directions then the light beam traverses the medium with its polarisation characteristics unchanged and no light reaches the detector. If an electric field is applied to the sample at an angle ψ, to the axis of vibration of the polariser, P see Fig 2.13), the incident light beam of frequency, υ,

$$\mathcal{E}_o = A \cos 2\pi\upsilon t \qquad 2.34$$

can be resolved into two components, $\mathcal{E}_o \cos\psi$ along the field direction and $\mathcal{E}_o \sin\psi$ perpendicular to this direction.

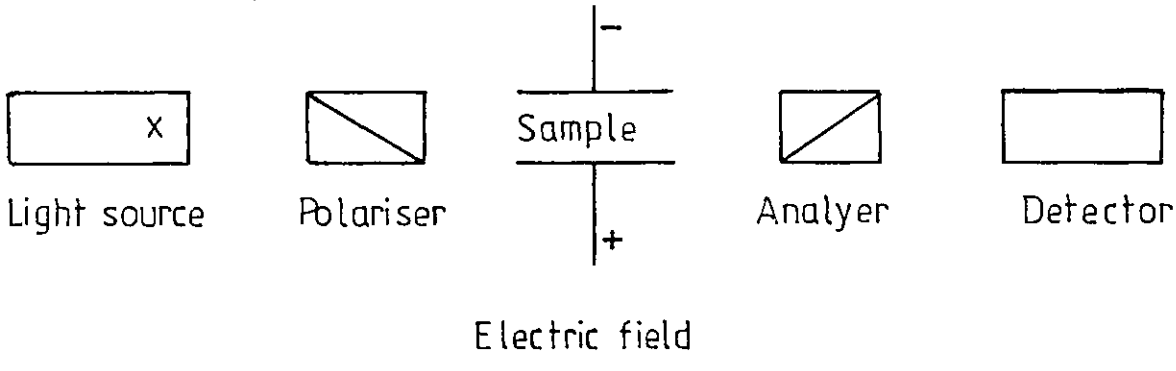

Fig 2.12 Kerr effect - Schematic diagram of experiments.

If the sample becomes anisotropic, $n_x \neq n_y$ and the components along these directions will travel at different velocities. If c represents the velocity of the light wave in air, the velocities along y and x directions in the solution will be c/n_y and c/n_x respectively, and if the solution has an optical path ℓ, the time necessary for the waves to emerge will be $n_y\ell/c$ and $n_x\ell/c$ respectively. The optical vectors of the waves will therefore have magnitudes;

$$\mathcal{E}_x = A\cos\psi\cos 2\pi\upsilon\left(t-\frac{n_x\ell}{c}\right) = A\cos\psi\cos 2\pi\left(\upsilon t-\frac{n_x\ell}{\lambda}\right) \qquad 2.35$$

$$\mathcal{E}_y = A\sin\psi\cos 2\pi\upsilon\left(t-\frac{n_y\ell}{c}\right) = A\sin\psi\cos 2\pi\left(\upsilon t-\frac{n_y\ell}{\lambda}\right) \qquad 2.36$$

where λ is the wavelength *in vacuo*. The waves will emerge out of phase by an amount called the optical retardation, (or phase shift) δ.

$$\delta = \frac{2\pi\ell}{\lambda}(n_x - n_y) = \frac{2\pi\ell}{\lambda}\Delta n \qquad 2.37$$

The magnitude of the phase shift depends on the degree of orientation induced and on the number of orienting macromolecules in solution . This phase shift converts the incident plane polarised light to an elliptical polarised beam. The intensity of the light reaching the detector will be proportional to the magnitude of the induced retardation. For the simple optical arrangement of Fig 2.12 this light intensity I is related to the retardation according to the equation

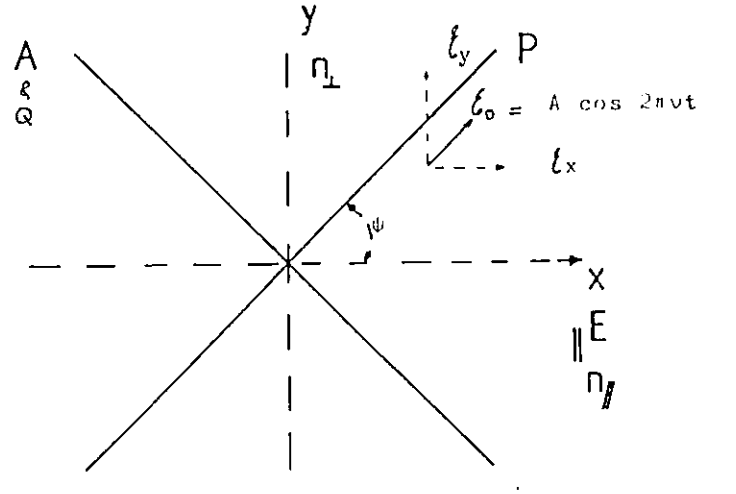

Fig 2.13 The incident beam direction and positioning of the analyser and the polariser.

$$I = \tfrac{1}{2}\sigma I_o \sin^2\delta \qquad 2.38$$

where I_o is the intensity of the incident beam and σ is a correction factor for absorption and reflection by the optical components. The detected intensity is then related to the birefringence Δn through equations 2.37 and 2.38. This expression is derived, along with others relating to alternative optical arrangements, in Chapter 3.

At sufficiently low field strengths, the observed birefringence is proportional to the square of the applied field gradient E - the Kerr law {1,57}.

$$\Delta n = B\lambda E^2 \qquad 2.39$$

where B is the Kerr constant.

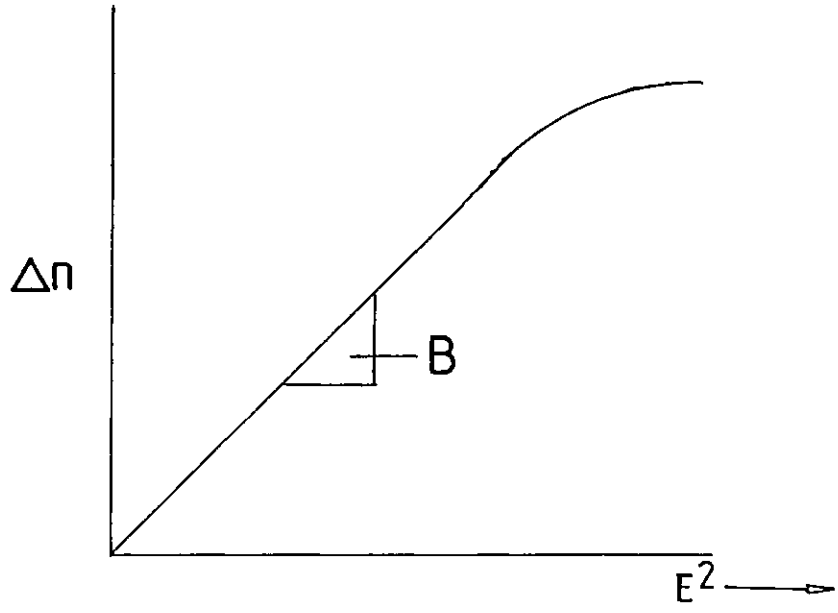

Fig 2.14 The field dependence of electric birefringence.

Combining equations 2.37 and 2.39 yields

$$\delta = 2\pi B L E^2 \qquad 2.40$$

The Kerr constant B, depends on the number of molecules present as well as such molecular electrical parameters as dipole moments the anisotropies of electric and optical polarisabilities and hyperpolarisabilities [1]. It is therefore a potential source of information about these molecular

properties. In non-dilute systems it also depends on the orientation correlations and therefore for polymers information on chain conformation and chain interactions can be obtained [56] .

Deviations from the Kerr law occur at high fields (Fig 2.14) because, as macromolecules approach complete orientation ('saturation'), further increases in the field strength gradient no longer lead to an increase in the birefringence. However changes in the birefringence due to deformation of the molecules can continue to occur.

2.5.3 Theory of the Kerr effect for rigid rod-like polymers:

The fundamental equation for the static birefringence of a solution of rod-like molecules was formulated by Stuart and Peterlin (59). They considered rigid symmetric particles which can be oriented by virture of either a permanent dipole moment and /or an induced dipole moment along the long axis Fig 2.15

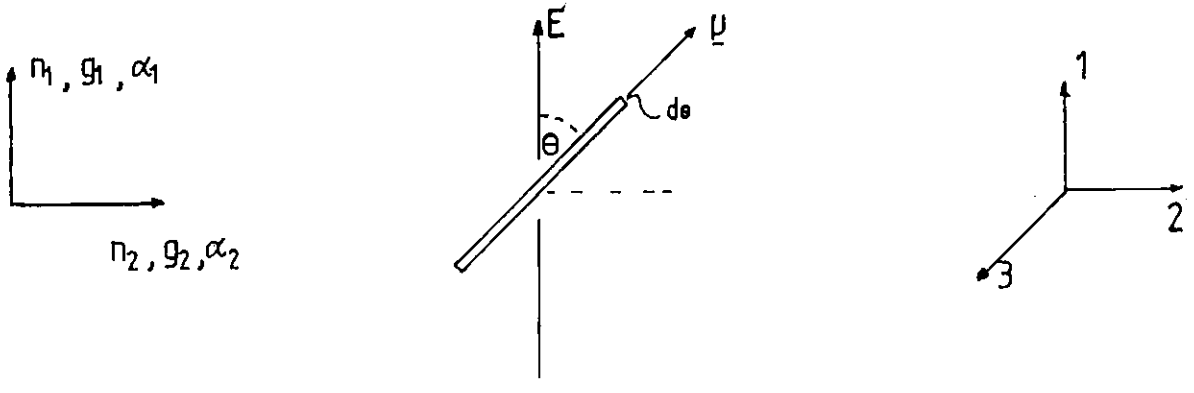

Fig 2.15 Diagrammatic representation of a rigid rod particle in an electric field; n=refractive index, g=optical polarisability and α=the electric polarisabilty.

In solution , particles will be distributed at various orientation angles θ to the electric field according to an angular distribution function $f(\theta)$, which describes the probability of finding the molecular axis at an angle between θ and $\theta + d\theta$ in a space element $d\theta$. The number of particles having the orientation at a given field is proportional to $f(\theta)$ and to the surface of the solid angle, which is

equal to $2\pi\sin\theta d\theta$. The solution birefringence is obtained by integrating the contribution of all categories of particles over all possible values of θ (60). This leads to

$$\Delta n = \frac{2\pi C_\nu n}{n}(g_1-g_2)\int_0^\pi f(\theta)\{\frac{3\cos^2\theta - 1}{2}\}2\pi\sin\theta d\theta \qquad 2.41$$

or

$$\frac{\Delta n}{C_\nu n} = \frac{2\pi}{n^2}(g_1 - g_2)\Phi(\beta,\gamma) \qquad 2.42$$

where C_ν is the volume fraction of macromolecules (= $\bar{\nu}c$ where $\bar{\nu}$ is the partial specific volume and c the concentration of macromolecules in kg m^{-3}), n the static refractive index of the solution and $g_1 - g_2$ the optical anisotropy factor $\Phi(\beta,\gamma)$ is the orientation factor given by [60,61]

$$\Phi(\beta,\gamma) = \int_0^\pi f(\theta)\left[\frac{3\cos^2\theta - 1}{2}\right]2\pi\sin\theta d\theta \qquad 2.43$$

Here β and γ represent the permanent and induced dipole terms respectively :

$$\beta = \frac{\mu E}{kT} \quad , P = \frac{\beta^2}{E^2} = \frac{(\mu)^2}{(kT)^2} \qquad 2.44$$

$$\gamma = \frac{(\alpha_1 - \alpha_2)E^2}{2kT} \quad , Q = \frac{2\gamma}{E^2} = \frac{\alpha_1 - \alpha_2}{kT} \qquad 2.45$$

The complete $\Phi(\beta,\gamma)$ function is rather complicated to compute in general but simplifications can be made for different limiting cases of interest.

a) Low field strengths ($\beta,\gamma < 1$) .

Expansion of $\Phi(\beta,\gamma)$ at low field strength leads to (60,62)

$$\Phi(\beta,\gamma) = \frac{2}{15}\gamma + \frac{1}{15}\beta + \frac{4}{315}\gamma^2 + \frac{4}{315}\beta^2\gamma - \frac{2}{315}\beta^2 \ldots\ldots \qquad 2.46$$

substitution into eqn 2.41 making use of eqns 44 and 45 gives

$$\Delta n = \frac{2\pi C_\nu}{15n}(g_1-g_2)\left(QE + PE + \frac{Q^2E^2}{21} + \frac{2PQE^2}{21} - \frac{2P^2E^2}{21}\right) \qquad 2.47$$

This equation is valid for rigid molecules having an axis of symmetry for their electric, optical and hydrodynamic properties. It also assumes that the solution is so dilute that interaction effects can be neglected. At very low field strengths for which $\beta,\gamma << 1.0$, the higher order terms in P and Q of eqn 2.47 can be neglected leading to

$$\Delta n = \frac{2\pi C}{15n}\nu\,(g_1-g_2)\,E^2\,(P+Q) \qquad 2.48$$

$$\lim_{E\to 0}\left(\frac{\Delta n}{E^2}\right) = \frac{2\pi C}{15\,n}\nu\,(g_1-g_2)\,(P+Q) = K_{sp}C_{\nu}n$$

where K_{sp} is the specific Kerr constant:

$$K_{sp} = \frac{2\pi\,(g_1-g_2)\,(P+Q)}{15\,n^2}$$

Therefore the specific Kerr constant is related to macromolecular parameters through the dipole moment μ, and the electrical and optical polarisability anisotropies $\alpha_1-\alpha_2$ and g_1-g_2. These properties are of interest in the elucidation of the macromolecular structure.

2.5.4 Flexible chain polymers

A number of models, due to Stuart and Peterlin (59), Dows (63) and Nagai et al (64), have been used to describe the Kerr effect in the flexible polymer. The Stuart and Peterlin model examined the random chain and describes them as a sequence of freely jointed segments having segmental dipolarity and polarisability anisotropy. These are conformational averages of bond polarisability anisotropies and dipole moments over the number of bonds contained in the segment. The specific Kerr constant is of the form,

$$K_{sp} = \frac{2\pi N_A(n^2+2)^2(\varepsilon+2)}{n\,m}\left(\frac{\alpha_1-\alpha_2}{45kT} + \frac{\mu^2(\alpha_1-\alpha_2)}{45\,k^2T^2}\right) \qquad 2.51$$

where N_A is Avogadro's number, m the monomer molecular weight, ε the solution relative permittivity, μ the segmental dipole moment, k Boltzmann's constant and T the absolute temperature.

Dows (63) treated flexible polymer chains as a sequence of dipolar and anisotropical polarisable chemical bonds and evaluated the appropriate averages from the conformation and orientation of the chain in the applied field. His theory was based on a dilute gas model and arrived at the same formula as Stuart and Peterlin (eqn 2.51). He concluded that the Kerr constant for non-correlated flexible polymer molecules, depends on the segment properties and as eqn. 2.51 shows, should be independent of concentration and molecular

weight .. Nagai et al (64,64a) however based their analysis on the additivity of bond dipole moments and of bond polarisabilities in a rotational isomeric state model and arrived at a rather complex expression for the molar Kerr constant :

$$K_m = \frac{2\pi N}{45kT} A\{(3\langle \underline{\mu}^{tr} \underline{\gamma} \underline{\mu} \rangle - Tr\langle \mu^2 \gamma \rangle)(kT)^{-1} + 3Tr\langle \gamma\gamma' \rangle - \langle (Tr\,\gamma)(Tr\,\gamma') \rangle\} \qquad 2.52$$

where $\underline{\mu}$, $\underline{\gamma}$ and γ are the dipole moment vector and the optical and static polarisability tensor of the polymer molecule respectively; $\underline{\mu}^{tr}$ is the transpose of, and Tr the trace of, the matrix.

2.5.5 Dynamic electric birefringence.

In order to study the dynamics of the electric birefringence, the polymer solution can be perturbed using either sinusoidal or rectangular pulsed fields. In the time domain when the electric field is applied,, the response of the polymer molecules is not instantaneous but lags behind the field, due to the finite time required for molecular orientation or disorientation. Studies of the birefringence response therefore give information on the macromolecules and how the angular distribution function $f(\theta,t)$, changes with time. In the absence of the field, the angle θ, takes all possible values with equal probability. However under the application of a field, angles near $\theta = 0$ become increasingly favoured and an equilibrium state is eventually reached, reflecting the balance between the electrical orienting torque and the random Brownian forces due to the solvent. On removal of the field, the macromolecules return to the random state in a way described by the distribution function $f(\theta,t)$. The time evolution of the function in the presence of an electric field gradient E is given by the following expression, due to Perrin (65).

$$\frac{1}{D_r}\frac{\partial f}{\partial t} = \frac{1}{\sin\theta}\frac{\partial}{\partial\theta}\left[\sin\theta\left(\frac{\partial f}{\partial\theta} - \frac{Zf}{kT}\right)\right] \qquad 2.53$$

where Z is the torque on the molecule

$$Z = E\mu\sin\theta - (\alpha_1 - \alpha_2)E^2\sin\theta\cos\theta. \qquad 2.54$$

D_r is the rotational diffusion coefficient and θ, μ, $\alpha_1-\alpha_2$, E, k and T are as previously defined.

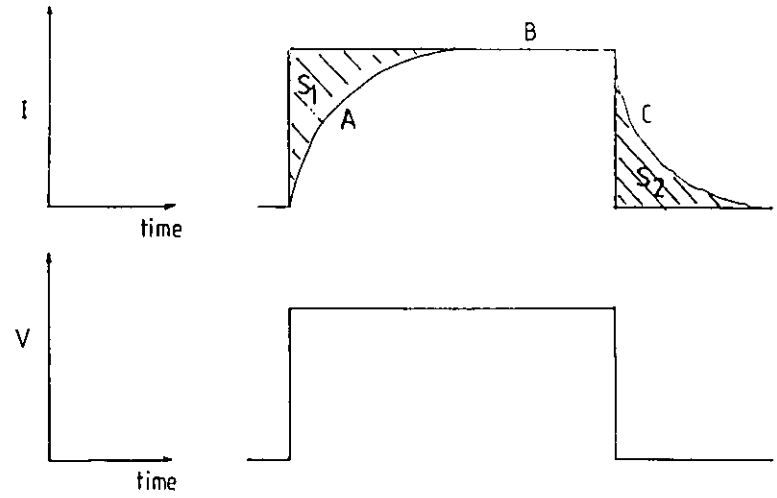

Fig 2·16 Macromolecular response to the rectangular applied field· A the rise, B the steady state and C the decay; S_1 and S_2 the areas above and below the rise and decay transients·

The macromolecular response to the rectangular applied field can be characterised by three distinct regions (Fig 2.16).

2.5.5(a) The rise curve A

Benoit (69) solved eqn 2.53 for axially symmetric rigid macromolecules and obtained an equation for the rise of the birefringence under the action of a rectangular pulse for the limiting case of low field strengths. His equation for the birefringence at any time t after the field is

$$\Delta n(t) = \frac{2\pi C_\nu E^2}{15\, n}(g_1-g_2)\left\{\frac{\mu^2}{k^2T^2}+\frac{(\alpha_1-\alpha_2)}{kT}-\frac{3}{2}\frac{\mu^2}{k^2T^2}\exp -2D_r t + \left(\frac{1}{2}\frac{\mu^2}{k^2T^2}-\frac{\alpha_1-\alpha_2}{kT}\right)\exp -6D_r t + \cdots\right\} \quad 2.55$$

The normalised birefringence rise transient is therefore

$$\frac{\Delta n(t)}{\Delta n_\infty} = 1 - \frac{3}{2}\frac{P/Q}{(P/Q+1)}\exp -2D_r t + \frac{P/Q-2}{2(P/Q+1)}\exp -6D_r t \quad 2.56$$

where P and Q are as defined in eqns 2.44 and 2.45 and the steady state value is given by

$$\Delta n_{\infty} = \frac{2\pi C_v (g_1 - g_2)}{15n} E^2 \left[\frac{\mu^2}{k^2 T^2} + \frac{\alpha_1 - \alpha_2}{kT} \right] \qquad 2.57$$

which is identical with eqn. 2.50. The time dependence of the rise transient is therefore determined by both the rotational diffusion coefficient and the nature of the orientation mechanism i.e. P/Q.

2.5.5(b) The steady state curve B - pulse reversal.

The theoretical equations for the static birefringence of sections 2.5.3 and 2.5.4 apply to the steady state birefringence. However information on the dynamics of polymer chains and the orientation mechanism can be deduced by observing changes in the birefringence as the polarity of the field is changed in this steady state region. The reversed rectangular pulse method offers a convenient and more accurate way of investigating the mechanism of orientation in particular the relative contributions of the permanent and induced dipole moments. When a rectangular field is applied to a solution, the macromolecules are aligned in the field, until a steady state is reached. If the field is suddenly reversed, the macromolecules aligned by virture of their permanent dipole will attempt to follow this sudden field reversal. It takes the macromolecules some definite time to do so, thus resulting in changes in the observed birefringence. The observed birefringence change depends on the macromolecular size and the solvent viscosity, and the rotational coefficient associated with this movement can be estimated. For induced dipole moments the field reversal is followed by a very rapid change in the polarity of the induced dipole which causes an insignificant change in the orientation of the molecules and hence the birefringence observed. However, when both mechanisms are present, the relative contribution of each mechanism is reflected by the depth of the birefringence minimum at the field reversal (see Fig 2.17).

For rigid rod systems, Matsumoto et al [62] and Tinoco et al [67] have related the changes in the birefringence and the time Δt_m (see Fig 2.17) for such a change to the

macromolecular parameters, the rotational diffusion coefficient D_r, the permanent dipole term P and the induced dipole term Q. They show that

$$\Delta t_m = \frac{\frac{1}{4}\ln 3}{D_r} = \frac{0.2747}{D_r} \qquad 2.58$$

and

$$\frac{P}{Q} = r = \frac{1 - \Delta}{0.1547 + \Delta}, \quad \Delta = \frac{\Delta n_{min}}{\Delta n_o} \qquad 2.59$$

The technique has the advantage that both P/Q and D_r can be determined fairly quickly and simultaneously.

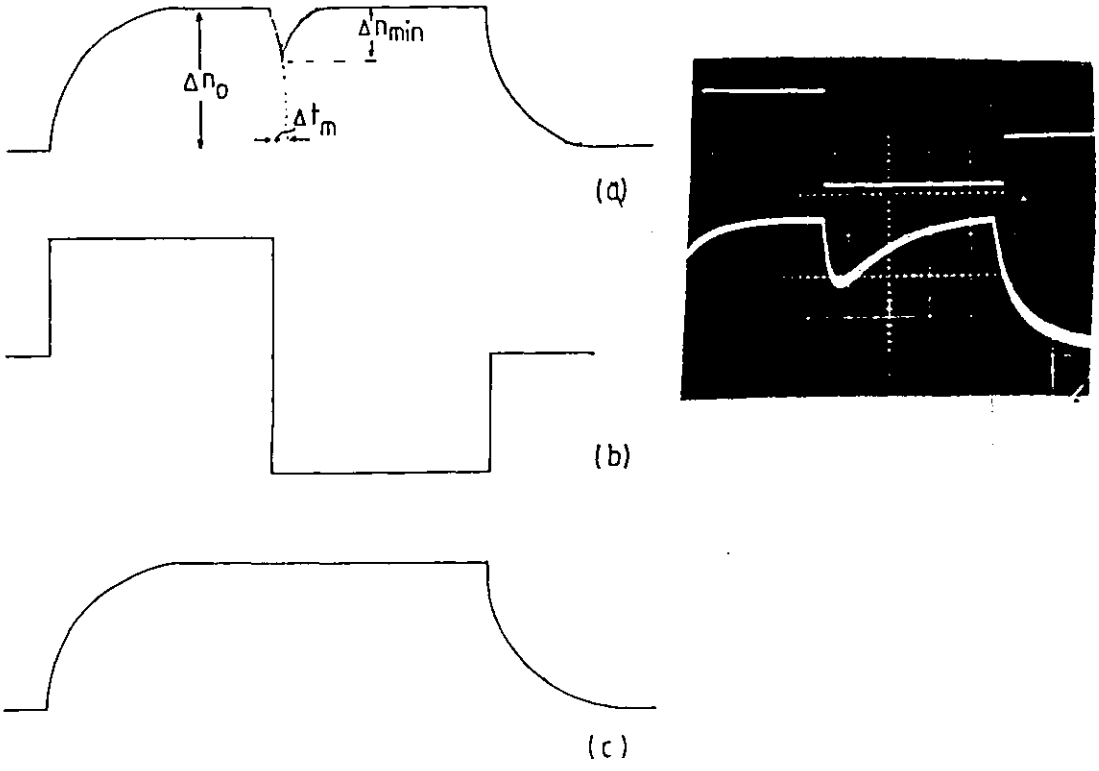

Fig 2·17 Birefringence at field reversal (a) permanent and induced dipole orientation (b) the reversed field (c) the induced orientation

2.5.5(c) <u>The decay, C</u>

When the field applied to the molecular solution is cut off, the orienting torque is released and Brownian forces return the molecules to the random state. The birefringence therefore falls asympotically to zero at a rate which reflects the free rotational motion of the polymer molecules. Benoit (66) and O'Konski and Zimm (55) ,have shown that the field -free decay birefringence of a monodisperse, dilute solution of rigid axially symmetric macromolecules is given

by

$$\Delta n(t) = \Delta n_o \exp^{-6D_r t} = \Delta n_o \exp^{-t/\tau} \qquad 2.60$$

here $\Delta n(t)$ is the birefringence at any time, Δn_o is the birefringence at the point when the field is first removed and τ the relaxation time, related to the rotational diffusion coefficient D_r, by

$$D_r = (6\tau)^{-1} \qquad 2.61$$

The rotational diffusion coefficient D_r, can be related to the macromolecular length and shape by eqns 2.5 and 2.6.

Deviations from exponetial decay do occur if
(a) the solution is not dilute so that chain interactions influence the decay rate;
(b) the macromolecules are not rigid, and hence relaxations corresponding to independent rotation of parts of the chain may contribute in addition to whole molecule rotation;
c) the sample is polydisperse so that even for rigid systems a range of molecular rotation rates is expected.

These cases are encountered in this work which has involved a study of concentrated solutions of polymers of varying flexibility and polydispersity.

For a polydisperse, dilute rod-like system the field free decay birefringence can be written as (4, 69)

$$\Delta n(t) = \sum_{i=1}^{N} \Delta n_{oi} \exp^{-6D_{ri} t} \qquad 2.62$$

where Δn_{oi} represents the contribution to the steady state birefringence from the ith species and τ_i (D_{ri}) is its characteristic relaxation time (rotational diffusion coefficient). Here the range of D_{ri} values give an indication of the degree of polydispersity and the extreme sizes of the macromolecules present in solution. For flexible polymers the above expressions are far from satisfactory, as non-exponential decay cannot be attributed entirely to the existence of different chain lengths. The polydisperse expression (eqn 2.62) can be applied to flexible particles, but the physical significance of the extracted parameters is uncertain.

The search for the analytic representation of experimentally observed non-exponential relaxation decays has lead to empirical decay functions such as that of Williams and

Watts [70]

$$\phi(t) = \exp^{-(t/\tau)\beta}, \quad 0 < \beta < 1 \qquad 2.63$$

where β, is the deviation parameter and is a measure of the deviation from single exponetial behaviour and τ is an effective relaxation time.

In the concentrated regime, a theoretical analysis of the decay transient is again available for rigid rod systems. Doi and Edwards (DE) have predicted that the birefringence decay in semi-dilute solutions should consist of two distinct regions - a fast inital decay followed by a slow long time relaxation. For the long time decay, close to the equilibrium state, they predict that

$$\Delta n(t) \simeq \Delta n_o \exp^{-6D_{rc}t} \qquad 2.64$$

where D_{rc} is the concentrated solution rotational diffusion coefficient ($D_{rc}=1/6\tau_r$). They relate the relaxation time τ_{rc}, to the molecular length,L, number and mass concentration,c_n and c as follows:

$$\tau_{rc} = \frac{1}{6D_{rc}} = \{D_r(c^2L^2)\}^{-1} \propto c_n^2L^2 \propto c^2M^7 \qquad 2.25$$

where M is the molecular weight and D_r the dilute solution rotational diffusion coefficient. Such high molecular weight and concentration exponents have aroused considerable interest and the extent of the applicability of this theory is one objective of this study.

The faster initial birefringence decay was predicted in the DE theory to be of the form

$$\Delta n(t) = \Delta n_o \exp^{-\frac{3}{2}\sqrt{2\alpha D_{rc}t + g(0)}} \qquad 2.65$$

where α is a numerical factor (=0.33) and

$$g(0) = \frac{kT}{\mu E} + \frac{kT}{(\alpha_1 - \alpha_2)E^2} \equiv \frac{1}{\beta} + \frac{1}{2\gamma} \qquad 2.66$$

The experimental realization of initial non-exponential behaviour requires a low value of g(0) i.e. a high field, E. For a polymer with a typical permanent dipole of $\sim 10^3$D, the field required to observe this is 10^2kV m^{-1} which is readily accessible experimentally, although the strength of dipole-dipole interactions in a real system (neglected in the DE theory) may influence the form of the relaxation considerably. On the other hand , induced dipole orientation alone would

require 10^5kV m^{-1} to observe this phenomenon and this is not easily accessible experimentally.

2.5.5(d) Influence of permanent and induced dipole moments on shape of transients.

As seen from section 2.5.5(b) the reversing pulse technique is a quick and accurate method of determining the relative contributions of permanent and induced dipole effects to the orientation process. However analysis of the rise birefringence curve offers another method as it depends on the field strength and the parameter P and Q by eqn. 2.56

$$\frac{\Delta n(t)}{\Delta n_\infty} = 1 - \frac{3^{P/Q}}{2(P/Q+1)} \exp -2D_r t + \frac{(P/Q-2)}{2(P/Q+1)} \exp -6D_r t \qquad 2.56$$

(a) If $\frac{P}{Q}$ =0 (i.e. no permanent dipole), this equation reduces to

$$\frac{\Delta n(t)}{\Delta n_\infty} = 1 - \exp -6D_r t \qquad 2.67$$

In this case the rise curve is symmetrical to the decay curve given by eqn 2.60

(b) If $\frac{P}{Q}$ is large the birefringence rise takes significantly longer time to reach the steady state and the overall birefringence transient is unsymmetrical.

Interestingly, comparing the area [68] above the rise curve, S_1 , and the area S_2 below the decay curve of the birefringence transients (see Fig 2.16) helps in estimating P and Q. Area S_2 below the decay transients is obtained by integrating eqn. 2.60.

$$S_2 = \int_0^\infty \frac{\Delta n(t)}{\Delta n_o} dt = \int_0^\infty \exp -6D_r t \, dt = \frac{1}{6D_r} (=\langle\tau\rangle) \qquad 2.68$$

Similarly the area above the rise S_1 can be obtained by integrating eqn. 2.56 to give

$$S_1 = \frac{4(P/Q+1)}{6D_r(P/Q+1)} \qquad 2.69$$

Therefore the ratio of the two areas S_1/S_2 is given by

$$S_1/S_2 = \frac{(4^{P/Q}+1)}{(^{P/Q}+1)} \qquad 2.70$$

This reaches a maximum value of 4 as $^{P}/_{Q} \rightarrow \infty$ (that is for pure permanent dipole moment orientation). and a minimum of 1 when P=0 (pure induced dipole orientation). For the usual situation of both permanent and induced dipole contributions, the ratio lies between these two extremes.

2.5.6 The relationship between Kerr effect and dielectric relaxations.

As discussed in section 2.4.1 both effects monitor the response of dipolar species to an electric field. Dielectric relaxation relates to the function , $\psi_1(t) = \langle \cos\theta(t) \rangle = P_1(\cos\theta(t))$ while Kerr effect relaxation relates to the function $\psi_2(t) = \{ \frac{1}{2} \langle 3\cos^2\theta - 1 \rangle \} = \langle P_2(\cos\theta(t)) \rangle$, where θ is the orientation angle of the dipole axis relative to the field and P_n is the Legendre polynomial of order n. For rotational diffusion by small angle steps {90}

$$\langle P_n(\cos\theta(t)) \rangle = \exp^{-n(n+1)D_r t} = \exp^{-t/\tau_n} \quad 2.71$$

$$1/\tau_n = n(n+1)D_r \quad 2.72$$

where D_r is the rotational diffusion coefficient and τ_n the relaxation time. Therefore the dielectric and the Kerr effect relaxation times for small angular rotational diffusion will yield $\tau_D\ (=\tau_1) = 1/2D_r$ and $\tau_K(\tau_2) = 1/6D_r$ respectively. The ratio of the relaxation times, τ_D/τ_K is therefore 3.

However Beevers and coworkers {90, 90(a)} have considered a 'fluctuation (jump) relaxation' model, in which the particle randomizes instantly and completely when it suffers a fluctuation in its environment. The diffusion here is by large angle jumps. The model predicts that the birefringence rise function ,$\psi_{2r}(t)$, is same as the birefringence decay function $\psi_{2d}(t)$ and that furthermore both functions are of the same form as the time function of the dielectric relaxation $\psi_1(t)$. Hence the dielectric relaxation time, τ_D, is equal to the Kerr effect relaxation time $\tau_{K,d}$ which is also equal to the Kerr effect rise time $\tau_{k,r}$. Table 2.1 below summarises the various reorientation models.

Table 2.2 Properties of reorientation models.

	Small angle rotational diffusion	Jump mechanism 'fluctuation jump mechanism'
Relation between rise and decay relaxation times τ_r and τ_d	$\tau_r > \tau_d \quad \frac{P}{Q} > 0$ $\tau_r = \tau_d \quad \frac{P}{Q} = 0$	$\tau_r = \tau_d$
Relation between Kerr and dielectric relaxation times τ_D and τ_k	$\tau_D = 3\tau_{K,d}$	$\tau_D = \tau_K$

2.6 Theory of Photon correlation spectroscopy.

An incident beam of polarised light exerts a force on the charges within any dielectric medium. These accelerating charges then radiate light in all directions. Scattering occurs because of the optical inhomogeneities in the medium. In a liquid these arise because of the translational and rotational motions of the molecules which cause fluctuations in the instantaneous dielectric constant.

The electric field associated with a plane monochromatic wave is of form

$$\underline{E}(\underline{r},t) = \underline{E}_o \exp\ i(\underline{k}.\underline{r} - \omega_o t) \qquad 2.73$$

where E_o is the amplitude, ω_o the angular frequency, $|\underline{k}|$ the wave vector $= 2\pi n/\lambda$, n the medium refractive index and λ the wavelength *in vacuo*.

With reference to Fig 2.18, the scattered light is detected at a point P, a distance R from the scatterer, at an angle θ to the incident beam. The incident field will induce an instantaneous dipole moment,

$$\underline{\mu}(\underline{r},t)dV = \underline{\alpha}(\underline{r},t).\underline{E}_o(\underline{r},t)dV \qquad 2.74$$

where $\underline{\alpha}(\underline{r},t)$ is the polarisability tensor and dV an elemental

volume, small compared with λ^3 at a point $\underline{r}$ in the illuminated region. The induced dipole will oscillate at the optical frequency and therefore radiate light in various directions. In the far field limit, $R \equiv |\underline{R}| >> \ell >> \lambda$, the instantaneous scattered field is given by

$$\underline{E}(\underline{R},t) = \frac{E_o \omega_o^2}{c^2 R} \exp\, i(\underline{k}_s.\underline{R} - \omega_o) \int dV.\alpha(\underline{r},t) \exp\,(i\underline{k}_i.\underline{r}) \qquad 2.75$$

where $\underline{k}_s$ is the scattering vector of magnitude $|\underline{k}_s|$ in the direction $\underline{R}$. The wavevector $\underline{K} = \underline{k}_i - k_s$ is equal to the momentum transfer which, since $|k_i| \simeq |k_s| = 2\pi n/\lambda$, is related to the scattering angle by the relation referred to in section 2.4.3

$$K = |\underline{K}| = \frac{4\pi n}{\lambda} \sin \tfrac{1}{2}\theta \qquad 2.32$$

in general $\alpha(\underline{r},t)$ is a fluctuating quantity which in the case of a pure liquid will be proportional to the thermally induced density fluctuations. In the case of macromolecules in solution (with polarisabilty tensor different from the solvent) $\alpha(\underline{r},t)$ will be related to the local concentration fluctuations. By writing α in terms of its average and fluctuating parts,

$$\alpha(\underline{r},t) = \langle\alpha\rangle + \delta\alpha(\underline{r},t) \qquad 2.76$$

we obtain

$$dV.\alpha(\underline{r},t) \exp i\underline{K}.\underline{r} = \langle\alpha\rangle V\, \delta(K) + dV\, \delta\alpha(\underline{r},t) \exp(i\underline{K}.\underline{r}) \qquad 2.77$$

where $\delta(K)$ is the Dirac delta function. This expresses the well known result that no light is scattered away from the incident direction by a wholly uniform scatterer and that it is fluctuations in the polarisabilty which cause the scattering. In the presence of fluctuations, no total cancellation will occur between the field scattered by two volume element The scattering equation becomes,

$$\underline{E}(R,t) = \frac{E_o \omega_o}{c^2 R} \exp\{i(\underline{k}.\underline{R} - \omega_o t) \int \delta\alpha(\underline{r},t) \exp\, i\underline{K}.\underline{r}\, dV \qquad 2.78$$

or for $\theta \neq 0$

$$\underline{E}(R,t) = \frac{E_o \omega_o^2 \exp}{c^2 R}\, i(\underline{k}.\underline{R} - \omega_o t)\, \delta\alpha(\underline{K},t) \qquad 2.79$$

where $\delta\alpha(\underline{r},t)$ and $\delta\alpha(\underline{K},t)$ are a Fourier transform pair.

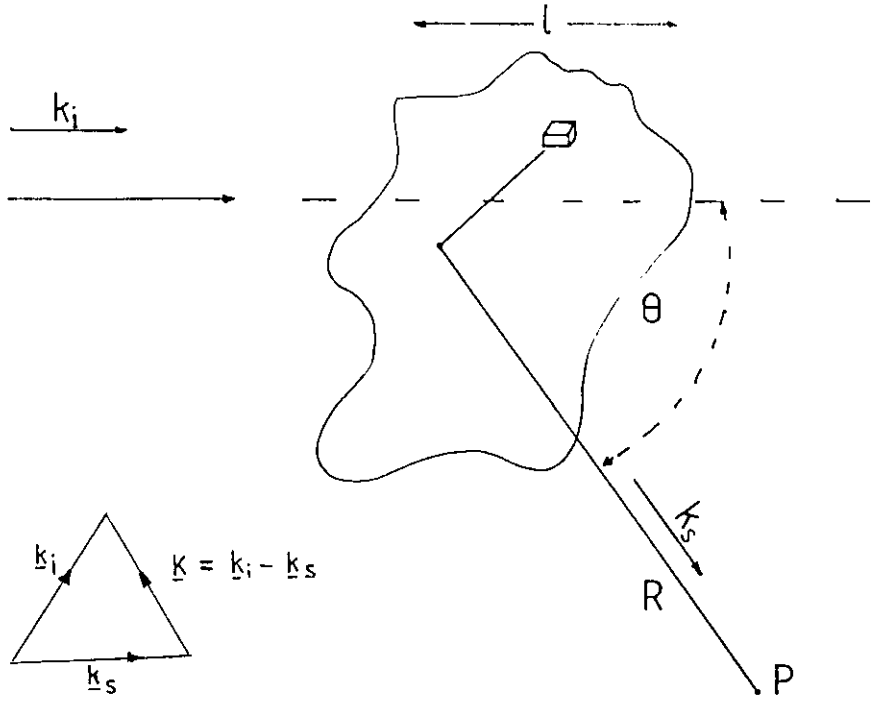

Fig 2.18 Scattering of an incident light beam by a dielectric medium.

The perpetual motion of the molecules within the medium causes the total scattered electric field at the detector to fluctuate in time. These fluctuations, therefore, may yield important structural and dynamic information about the positions and orientation of the molecules.

When solute particles are dissolved in solvents, the solution becomes more inhomogeneous, thereby increasing the scattered intensity. The increase in intensity may be used to evaluate the number of solute particles per volume, and in appropriate cases conclusions about the size and shape of these particles can be drawn from observation of the angular distribution of the scattered light (101)

2.6.1 Fluctuations and correlation functions

Time dependent correlation functions provide a concise method of expressing the degree to which two dynamic properties are correlated over a period of time. The correlation function $C(\tau)$ defined as

$$C(\tau) = \langle A_i(t)\, A_j(t+\tau) \rangle \qquad 2.80$$

measures the persistence of fluctuations in the property A, and shows how the value at a time $t+\tau$ relates to that at a previous time t. The subscripts i and j can refer either to a different particle or to a different property. In the case of an autocorrelation function, i=j and we are concerned with the time dependence of a single property associated with a given scattering centre i , as against the cross correlation which also accounts for terms $i \neq j$.

Photon correlation spectroscopy measures the field autocorrelation function defined as

$$G^{(1)}(t,t+\tau) = \langle \underline{E}(t)\, \underline{E}^{*}(t+\tau) \rangle \qquad 2.81$$

The corresponding intensity correlation function is defined as

$$G^{(2)}(t,t+\tau) = \langle I(t)\, I\,(t+\tau) \rangle \qquad 2.82$$

and is related to the field autocorrelation function by

$$I(\underline{R},t) = \underline{E}\, E^{*} = |E|^{2} \qquad 2.83$$

The normalised forms of these functions can be written as

$$g^{(1)}(t,t+\tau) = \frac{\langle E(t)E^{*}(t+\tau) \rangle}{\langle I \rangle} \qquad 2.84$$

$$g^{(2)}(t,t+\tau) = \frac{\langle I(t)I(t,t+\tau) \rangle}{\langle I \rangle^{2}} \qquad 2.85$$

These normalised field and intensity autocorrelation functions are related via the Siegert equation for a field that obeys Gaussian statistics:

$$g^{(2)}(t,t+\tau) = 1 + |\, g^{(1)}(t,t+\tau)|^{2} \qquad 2.86$$

By measuring the intensity as a function of time , we can construct the intensity correlation function and so determine the field correlation, $g^{(1)}$. $g^{(1)}$ is sometimes called the dynamic structure factor and is itself a Fourier transform of the frequency spectrum $S(\omega)$ which is given by the Wiener-Khinchin theorem.

$$S(\omega) = \frac{1}{2\pi} \int_{-\infty}^{\infty} |\langle \underline{E}(t).E^{*}(t+\tau) \rangle| \exp^{i(\omega-\omega_{o})} d\tau \qquad 2.87$$

For a dilute non-interacting polymer solution the time averaged scattered intensity may be written,

$$\langle I_{s} \rangle \propto MP(K) \qquad 2.88$$

where M is the molecular weight of the polymer chain and P(K) is the single particle scattering factor. For more concentrated solutions the angular variation of the scattered intensity also contains information concerning the interactions between solute particles.

$$\langle I_s \rangle \propto M P(K) S(K) \qquad 2.89$$

where S(K) is termed the structure factor.

Experimentally the scattered field $\underline{E}(K,t)$, corresponding to a momentum transfer $|\underline{K}|$, falls on the photocathode of a photomultiplier detector (PM). The output signal is proportional to the instantaneous optical intensity $|\underline{I}(K,t)| = |\underline{E}(K,t)|^2$. The autocorrelation of the output of the PM is built up by a correlator [102] . In practice the scattered intensity is obtained by measuring the number of photons $n(t,T)$ scattered at an angle θ in a time interval T, centred on time t. The correlator therefore constructs the photon count correlation function, $n(t)n(t+\tau)$ which is directly related to the field autocorrelation function by

$$g^{(2)}(\tau) = \frac{\langle I(t)\, n(t+\tau)\rangle}{\langle n\rangle^2} = 1 + \gamma |g^{(1)}(\tau)|^2 \qquad 2.89$$

where γ is a constant which reflects the degree of spatial coherence of the incident light.

2.6.2 Scattering from polymer solutions.

As shown at the beginning of 2.6, the scattered intensity arises from fluctuations in the local dielectric constant. In polymer solutions, assuming the solvent dielectric constant to be small compared with that of macromolecules, then the macromolecules dominate the behaviour of the dielectric fluctuations. The nature of the scattering depends on the size of the scattering centres, L, compared with the magnitude of the inverse scattering vector, K^{-1} (see section 2.4.3).

Dilute polymer solutions at low momentum transfer, $KL \ll 1$.

In dilute solution the polymer chains are well separated and consequently act as independent entities. Sufficiently small polymers having characteristic length , L , act as

point scatterers. For such scatterers the factor exp ($i\underline{k}.\underline{r}$) in the scattering amplitude term (eqn 2.75) is the same for all $\underline{r}$ within one scatterer. Thus the electric field scattered by different dipole radiators within one scatterer are in phase at the detector. Being point scatterers, only motions of the centre of mass comtribute to the time dependence of the scattered light. For non-interacting, identical scatterers under simple Brownian diffusion the field function is given by

$$g^{(1)}(K,t) = \exp^{-\Gamma t} \qquad 2.90$$

where Γ is $D_t K^2$ and D_t the translational diffusion coefficient in the limit c=0. D_t can be related to molecular size by the Stokes-Einstein relation

$$D_t = \frac{kT}{6\pi\eta_s R_H} \qquad 2.91$$

where R_H is the hydrodynamic radius. These measurements can thus be used to give an indication of polymer size and have been employed to study the molecular weight dependence of both D_t and R_H ($\simeq R_G$) [102].

Dilute polymer solutions at high momentum transfer, KL >> 1

If the polymer molecules are sufficiently large or K is sufficiently large, such that $L >> K^{-1}$, the field scattered by dipoles within one scatterer will not be in phase at the detector. There will therefore be some degree of destructive interference and the scattered light will reflect the internal as well as centre of mass motion of the molecules (47) Much work has been done theoretically and experimentally on the internal motions of flexible coil polymers (6,46,47,48) . This work concerns the wavevector dependence of the characteristic relaxation times, τ_c, of the different Rouse-Zimm type modes. The field scattered by large flexible macromolecules fluctuates due to internal motions and thus will contribute to the time dependence of the scattered light. For this case the field autocorrelation function has the form (104)

$$g^{(1)}(K,t) = A_o(K)\exp^{-\Gamma_1 t} + A_1(K)\exp^{-(\Gamma_1+\Gamma_2)t} + . \qquad 2.92$$

where A_o, A_1, are K-dependent amplitudes, $\Gamma_1 = D_t K^2$ and $\Gamma_2 = 2\tau^{-1}$ i.e. the inverse of the relaxation time associated with the

dominant internal mode. A_o, A_1 etc are dependent on scattering angle in such a way that at low angles (low K) A_o dominates and eqn. 2.92 reduces to eqn. 2.90: as K increases, contributions from the internal modes increase and the function becomes non-exponential. The angular dependence of $g^{(1)}(K,t)$ over the angular range for which A_o and A_1 dominate the scattering has been used to obtain information about the relaxation time τ_1. At higher angles, other terms enter eqn. 2.92 corresponding to the higher internal modes. If the polymer molecules are rigid, the resultant scattered field for K>>1 will fluctuate in time as the particle undergoes rotational Brownian motion. The field correlation for this situation is the same as in eqn. 2.92 [103, 104] but with $\Gamma_2 = 6D_r$ where D_r is the rotational diffusion coefficient.

2.6.3 Light scattering from non-dilute polymer systems

At finite concentration, the polymer molecules will interact and the rates of motion of individual chains are consequently modified. However in cases where the mean chain separation a_c is smaller than K^{-1}, the scattering will be influenced by motions which are no longer characteristic of isolated chains, but represent co-operative diffusion of the whole system. Several authors have addressed this problem.

Brochard and de Gennes [50] have predicted the PCS behaviour of flexible polymer molecules dissolved in theta solvents. In this semi-dilute region their model predicts that the field correlation function (the dynamical structure factor) has two distinct components, each of the form

$$g^{(1)}(K,t) = \frac{S(K,t)}{S(K,0)} = \exp^{-\Gamma_i t} \qquad 2.93$$

The correlation function consists of a fast initial decay with a characteristic frequency given by

$$\Gamma_1 = 1/\tau_r + \rho D_c K^2 \qquad 2.94$$

followed by a subsequent slow decay with the frequency

$$\Gamma_2 = \frac{D_c K^2}{1 + \rho \tau_r D_c K^2} \qquad 2.95$$

where τ_r is the characteristic time for the relaxation of

entanglements and ρ is the ratio of the high frequency elastic modulus, E_{gel} to the isothermal osmotic rigidity E_o, and D_c is the co-operative diffusion of the entangled polymer chains.

Hence for $KL << 1$ the slow decay $\Gamma_2 = D_c K^2$ while the fast initial decay $\Gamma_1 = 1/\tau_r$. However the authors argue that because of the low amplitude of the fast mode, it would be difficult to observe τ_r experimentally. At high momentum transfer, $KL >> 1$, they predict that the slow mode relaxation frequency $\Gamma_2 \rightarrow {}^1/\rho\tau_r$ while for the fast mode $\Gamma_1 \rightarrow D_c K^2$. Again for the same reason the high amplitude of the slow mode makes the fast mode unobservable.

Reihanian and Jamieson (51) modified the theta solvent approach of Brochard and de Gennes, to include good solvents. Their model which considered the Rouse-Beuche-Zimm model chain of n-segments, also showed bimodal behaviour, with a fast initial decay

$$\Gamma_1 = {}^1/\tau_r + (D_c + D_t)K^2 \qquad 2.96$$

and a slow decay

$$\Gamma_2 = \frac{D_t K^2}{1 + (D_c + D_t)K^2\tau_r} \qquad 2.97$$

where D_t ($= {}^{D_c}/\rho$) is the chain centre of mass diffusion coefficient. Here, for small values of $\rho \simeq 1$, the relative amplitudes of the slow and fast modes are comparable and as a result both modes of decay should be observable.

Rigid rods

The light scattering equations applicable to interacting thin rigid rods have been modelled by Doi and Edwards(DE) (4) In the semi-dilute regime the rods are severely constrained by neighbouring rods (see Fig 2.9 b). Orthogonal motion of the rods is therefore inhibited, leaving motion to occur mainly along the thin chain axis with a diffusion coefficient D_t. Their analysis also leads to non-exponential characteristics of the dynamical structure factor. They predict that the initial slope should be

$$\left.\frac{\partial S(K,t)}{\partial t}\right|_{t=0} = \frac{1}{3}\Gamma_1 = \frac{1}{3}D_r K^2 \qquad 2.98$$

which is one half the dilute solution slope,

$$\frac{\partial S(K,t)}{\partial t}\Big|_{t=0,c=0} = \frac{2}{3}\Gamma_1$$

At long times the dynamical structure factor $S(K,t)$ depends on concentration and approximates to an exponential decay

$$S(K,T) = S(K,0)\exp^{-\Gamma_2 t} \qquad 2.100$$

with characteristic frequency,

$$\Gamma_2 = (K^2 D_{rc} D_t)^{\frac{1}{2}} \qquad 2.101$$

D_{rc} is the concentrated solution rotational diffusion coefficient related to the infinite dilution value (see section 2.3.2) by

$$D_{rc} = D_r\{c_n L^3\}^{-2}$$

since D_r is given by eqn 2.5, Γ_2 has the following concentration and molecular weight dependence

$$\Gamma_2 \propto \frac{|K|}{c_n L^5} \propto \frac{|K|}{c\,M^4} \qquad 2.102$$

At high concentration , the $S(K,t)$ concentration dependence is predicted to disappear. This is attributed to a transition from mixed rotational and translational diffusion to pure long axial translation, which Doi and Edwards argue will remain essentially independent of concentration.

Edwards and Evans [19] have extended the argument to higher concentration, c, near the upper limit of the DE regime , C^{**}. Their model predicts that the effective translational diffusion coefficient decreases with increasing concentration until a freezing of molecular motion occurs, at a certain concentration in a glass-like transition. Their treatment shows a concentration dependence of the form

$$D_{eff} = D_t\{1 - \gamma(c_n d L^2)^{\frac{3}{2}}\} \qquad 2.103$$

where c_n is the number concentration of the rods and γ is a numerical constant close to unity . Therefore in contrast to the Doi and Edwards theory which predicts that D_t should decrease with concentration initially and then become independent of concentration in the semi-dilute region (where diffusion is still relatively unrestricted), Edward and Evans predicted that at higher concentrations the translational diffusion coefficient should again be concentration dependent, decreasing as $D_{eff} \propto c^{1.5}$

Chapter Three

APPARATUS AND DATA ANALYSIS

This Chapter is divided into two sections, section A deals with a detailed description of the Kerr electro-optic effect apparatus, experimental procedure and finally the methods of analysis employed. Section B deals with the same aspects of the Photon correlation spectroscopy.

Section A : The Dynamic Kerr Effect.

3.1 The Kerr effect technique apparatus.

A schematic diagram of the Kerr electro-optic apparatus is shown in Fig. 3.1. A plane polarised monochromatic laser light (source(LL)) is incident on a rotatable Glan-Thompson quartz prism(P) which ensures complete polarisation of the incident light. The light then passes into the Kerr cell (KC)

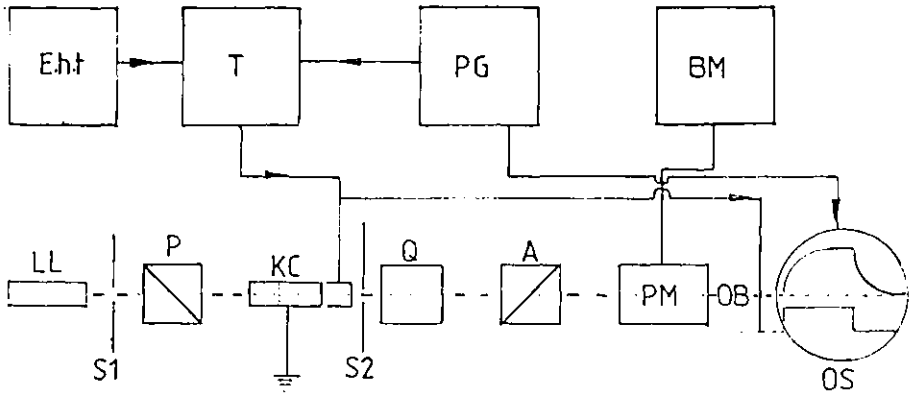

E.h.t	High tension power supply	KC	Kerr cell
T	Thyratron	Q	Quarter wave plate
PG	Pulse generator	A	Analyser
LL	Laser light source	PM	Photomultiplier
S1,S2	Slits to cut down stray light		
P	Polariser	OS	Oscilloscope

Fig 3·1 Block diagram of the Kerr electro-optic apparatus.

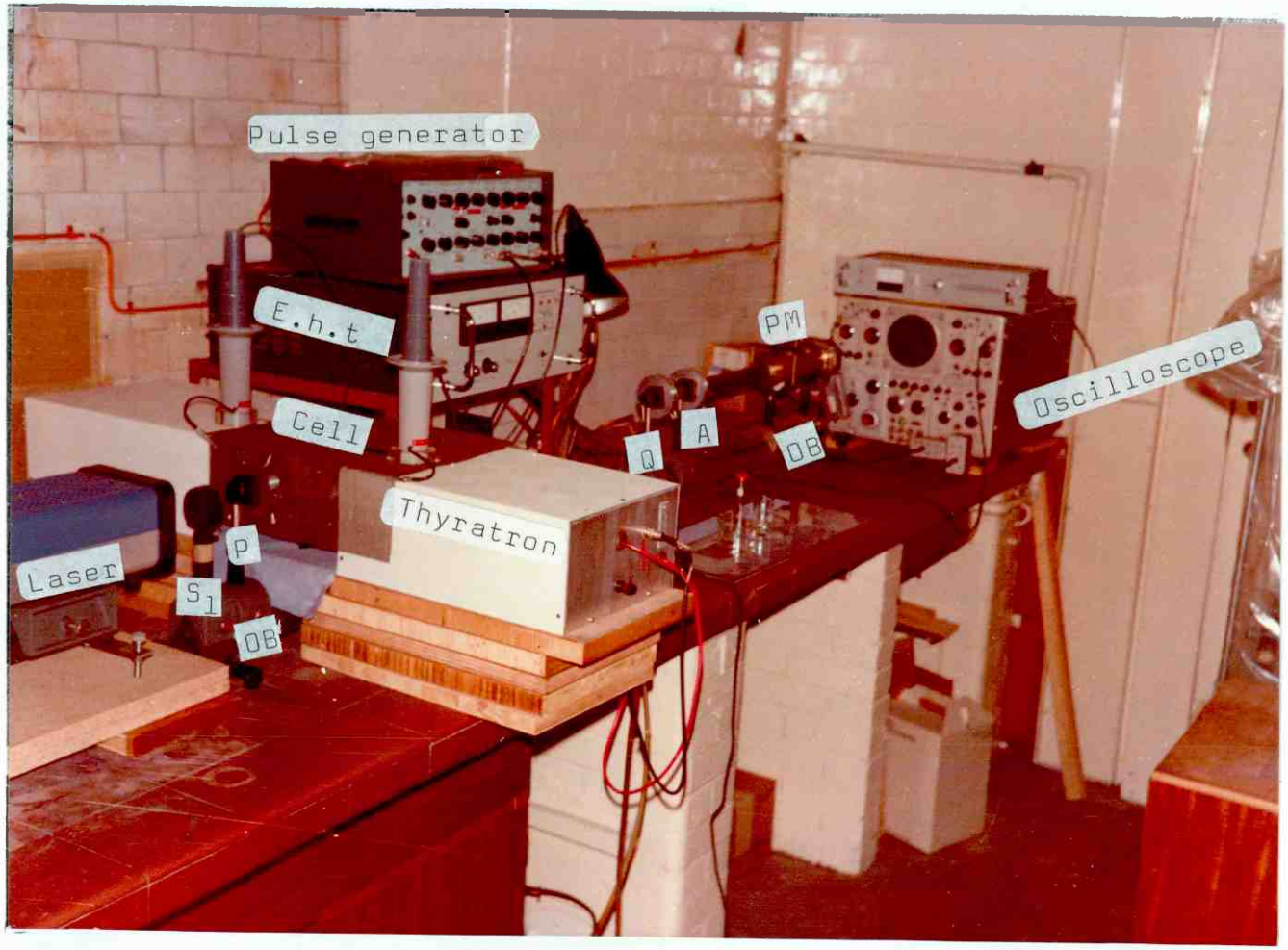

Photo No. I The Kerr electro-optic equipment.

which contains the polymer solution. The electrodes which are arranged so that the electric field direction is at 45^{o}to the direction of polarisation of the light are connected to a high voltage pulse generation system which consists of : a Brandenburg Model 728R high tension supply ,(E.h.t) capable of delivering up to 20kV, a twin hydrogen thyratron discharge unit,T and a Farnel type low voltage twin pulse generator,(PG). The cell is maintained at constant temperature by circulation of thermostatting fluid through its outer jacket from either a water thermostat or for low temperature work, a Lauda Ultra-Kryomat type K120W refrigerator unit. On emerging from the Kerr cell the light beam can pass through a quarter wave plate (Q), which restores the elliptically polarised beam into a planar polarisation. It then passes through another rotatable Glan-Thompson prism, the analyser, A whose crossed position with the polariser ensures complete extinction of the beam when no electric field is applied to the cell. Any light emerging from the analyser is detected by a photomultiplier (PM) powered by a Brandenburg model 476R power supply.The output from the detector is fed via a load resistor to a Tektronix type 556 Dual beam oscilloscope, where the signal is displayed before being photographed using a polaroid CR-9 land oscilloscope camera. The field applied to the cell is monitored using two Tektronix P6015 high tension probes and is displayed on the oscilloscope for simultaneous recording alongside the birefringence.

3.2 The Kerr cell

The Kerr cell, designed and constructed during this study and whose schematic diagram is shown in Fig 3.2, consists of two concentric stainless steel cylinders A and B of length 65mm and internal diameter 40mm and 25mm respectively. The inner cylinder houses the stainless steel electrodes, C, of dimensions 50 x 10 x 2mm which are embedded in a glass-filled Teflon (PTFE) block D giving a 2mm gap between the electrodes. The PTFE was chosen because of its good insulating properties and general inertness to chemical attack.The PTFE and the electrodes are held in position by stainless steel rods,E which also serve as electrical connections, through which the voltage is applied across the cell. The cell windows,G are made of glass

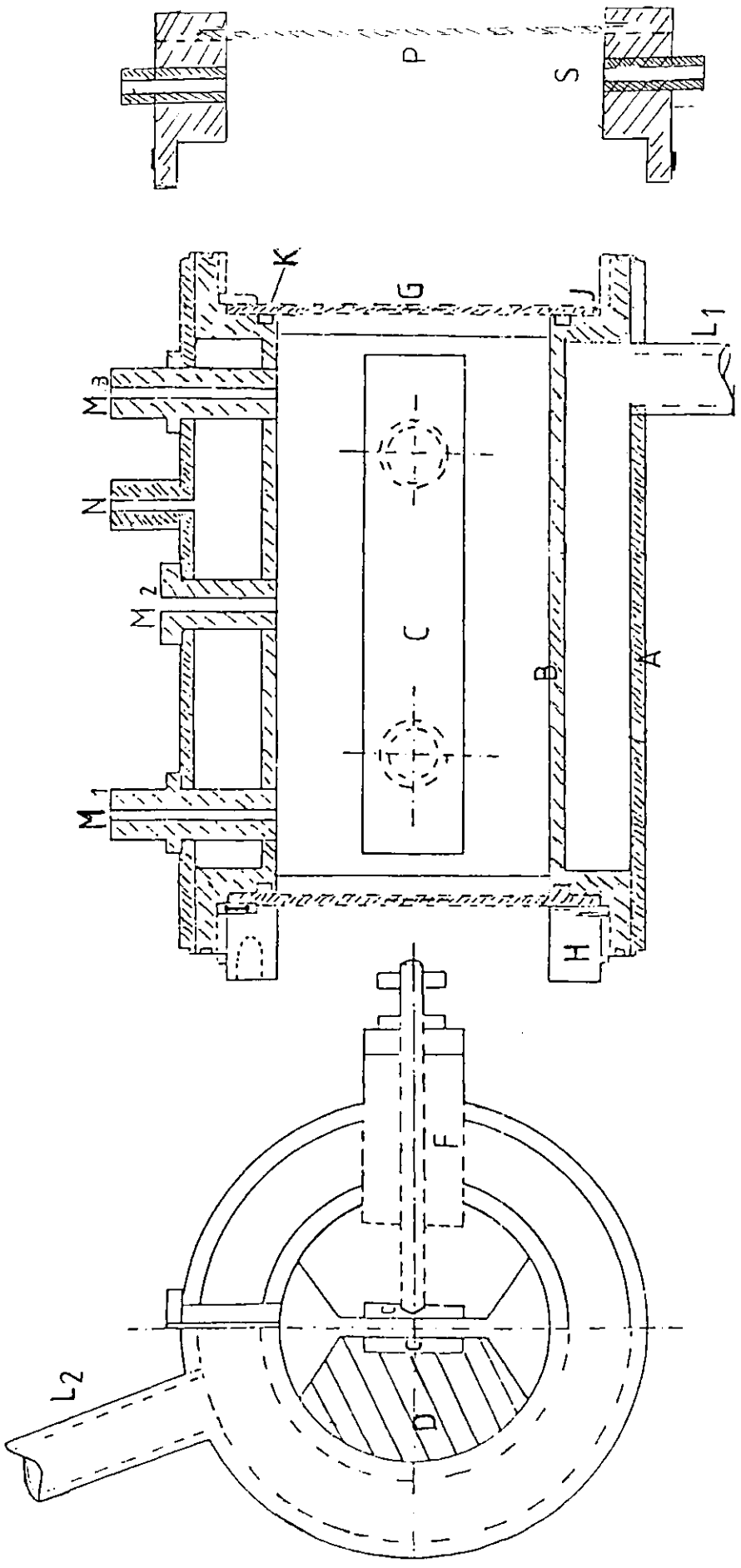

Fig 3. 2 The Kerr Cell.

with a 10mm hole at the centre. Microscope slide glasses are glued to close these windows in order to minimise strain birefringence. The glass windows are held in place by means of threaded stainless steel end rings,H which press onto a thin PTFE washer, I. thus pressing the windows onto a groove J. The groove is fitted with a PTFE o-ring K,to ensure a tight leak proof joint.

The outer jacket is provided with an inlet L_1, and an outlet L_2 for the circulation of the thermostatting fluid used to maintain the cell temperature as required. The third hole N,serve as an opening for inserting a thermocouple to monitor the temperature of the thermostatting fluid. The three other holes, M_1, M_2, M_3 on the top of the cell give access to the inner cylinder compartment. Through these holes, the polymer solution is introduced and withdrawn using microsyringes. These access tubes ensure that air bubbles do not become entrapped between the electrodes, and provide a means of monitoring the solution temperature using a thermocouple.

For low temperature measurements (below $0^{o}C$) the additional component S, is attached to the end of the Kerr cell to prevent water condensation and ice formation on the cell windows. It consists of a glass window screwed onto a groove in a PTFE tube, with a gap (20mm) left between the glass windows G and P. This gap is intermittently swept with dry air to keep the windows free of condensation. The entire attachment is fixed in position by means of jubillee clips.

The cell has a volumetric capacity of 11 ml and has been designed:
(i) to be easily dismantled for washing, cleaning and drying;
(ii) with a provision for adjusting the electrode gap.

3.3 The Pulse generator and the Thyratron system.

Two types of waveforms were used in this work: a) a single rectangular pulse and b) a reversing rectangular pulse.

3.3.1 The singular rectangular pulse unit.

The low voltage twin pulse generator, the Farnel type generating system, is a versatile pulsed waveform source. The system comprises of modules arranged to perform specific

functions and these are;
(i) the stabilised power supply unit;
(ii) the trigger unit, which controls the mode of operation of the pulse generating system either through an internal pulse repetitive frequency (PRF) generator directly or externally via a push button contact or contact sockets which provide the facility to use camera shutter contact closure;
(iii) the PRF generator, which determines the pulse repetition frequency (1 Hz to 10M Hz) available from the instrument;
(iv) two pulse width units which control the duration (0.1μs to 1.0 s) of the output pulses available from the pulse generator.
(v) two output units, which control the pulse amplitudes (30 mV to 20 V) and polarities;
(vi) two pulse delay units which determine the time delay between the input trigger and the pulse output. For twin pulse operation, the delay time for the first pulse is set at zero and that for the second pulse governs the time separation between the occurrence of the pulses. This is adjustable from 0.1μs to 1.0 s;

The pulses from the pulse generator are used to discharge hydrogen filled thyratrons thereby acting as a simple switching circuit for the electrode e.h.t supply. Fig 3.3 (a) shows the circuit diagram of the thyratron assembly which was designed and constructed in the Chemical Engineering Department Electronic Workshop. It consists of two parallel resistors R_1 and R_2, each 10 MΩ, connected to the Brandenburg model 728R high tension power supply. These loads ensure that small currents are delivered to the circuit for safe operation. The capacitors C_1 and C_2 connected in parallel with the thyratron Y_1 and Y_2 are charged when the e.h.t. is switched on and maintain a constant voltage at the cell electrodes. The thyratron Y_1 and Y_2 act as switches for discharging the electrode as desired.

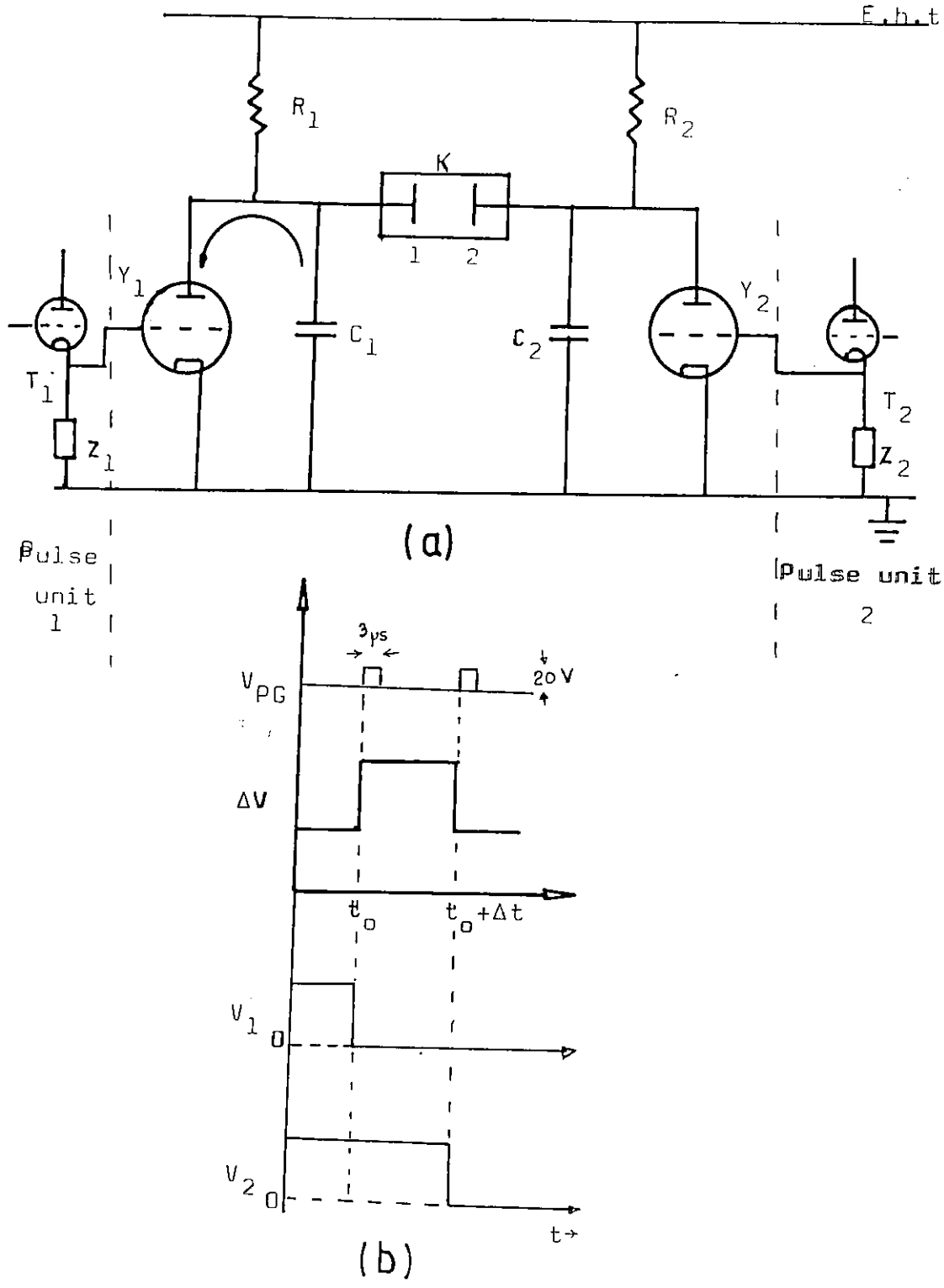

Fig 3.3 (a) The Thyratron circuitry
(b) Rectangular wave

Operation and generation of a rectangular pulse.

When the e.h.t is switched on the voltage is applied through the parallel resistors to the cell electrode. The two capacitors become simultaneously charged, so that both the capacitors and the electrodes are at the same voltage V. At time , t_o say, a 20 volt pulse of 3.0 μs duration from the pulse generator ,T , triggers thyratron Y_1, causing current to flow to earth through Y_1 as shown in Fig 3.3(a) consequently discharging capacitor C_1 and connecting electrode K_1 to earth. With electrode K_1 at zero potential and K_2 and C_2 at the e.h.t potential, V, a potential difference V volts becomes developed across the cell. At a later time t, $(=t_o + \Delta t)$, thyratron Y_2 is triggered by a similar small voltage, T_2 from the pulse generator, causing the rapid discharge of the electrodes K_2 and capacitor C_2 to zero potential. Both electrodes are now at zero potential and there is no potential difference across the cell electrodes. Within the time interval Δt a rectangular pulse of the form shown in Fig 3.3 (b) has therefore been generated. The capacitors will recharge again ready for the pulse sequence to be repeated.

During the course of this work three sets of capacitors of value 50 pF, 300 pF, and 0.1 μF were employed. These were altered according to the conductivities of the various polymer solutions studied. A conducting medium between the cell electrodes can cause the discharge of the capacitor C_2 across the cell during the time interval Δt. The time dependence of the volage of the condenser of capacitance C, discharging through a resistance R, is given by

$$V(t) = V_o \exp -t/\tau_c \qquad 3.1$$

where the time constant $\tau_c = RC$ and V_o is the initial capacitor voltage. If such a flow of current takes place through the sample the voltage across the cell decreases continuously throughout the period Δt , and the pulse form is no longer rectangular. By increasing the capacitance C, the time constant can be made sufficiently long that the electrode voltage remains essentially constant for the period of the pulse Δt. However, such a change also means that the rate of capacitor charging is also decreased and so the rate of the pulse repet-

ition that can be achieved is reduced. This was not a limitaion except for very short pulse times ($\Delta t < 5\ \mu s$) when single shot operation did not give a sufficiently intense CRO display.

3.3.2 The reversing pulse unit

The unit, designed and constructed in the Departmental Electronic Workshop , utilies transistorised technology. It was designed to ;

i) overcome the problems associated with the conductive media, an improvement on the single pulse unit discussed above;

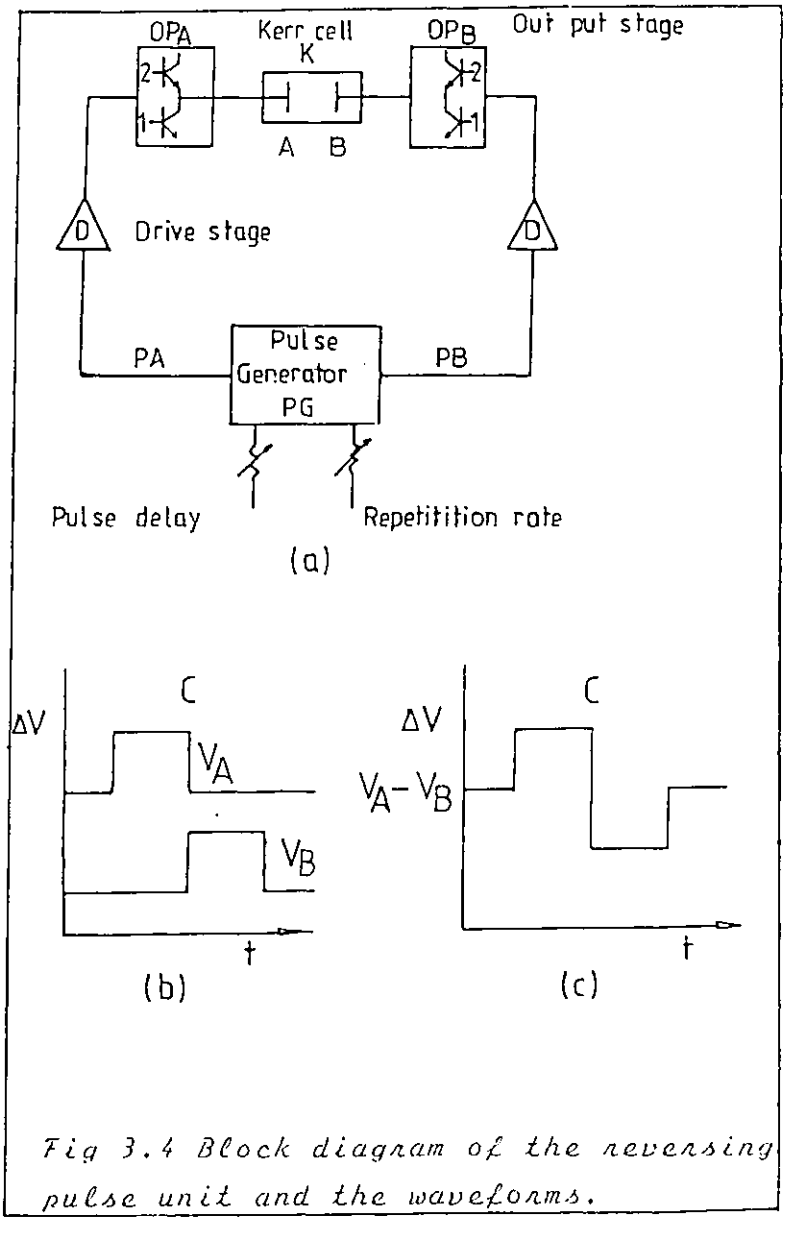

Fig 3.4 Block diagram of the reversing pulse unit and the waveforms.

ii) produce both rectangular and reversing pulse waveforms. The reversing pulse generator (block diagram in Fig 3.4 (a)) consists of a pulse generator PG, an integrated circuit with facility for setting the pulse duration ,PD, and the pulse repetition rate ,PR. The generated pulse is driven through the drive stage D, which amplifies the pulse generator output to the required power to drive the output stage OP. This output stage consists of two sets of transistors,1 and 2, connected to the electrodes A and B of the Kerr cell,K. The output transistor 1 facilitates the fast build up of the voltage on the electrodes, while the transistor 2 is responsible for fast discharge of the field to earth. The operation is similar to the thyratron arrangement.

Generating the reversing pulse

The pulse generator is a standard unit with in built pulse duration and repetition rate facilities. The reversing waveform is generated as follows: at time t_o the pulse generated along PA, keeps the electrode K_A at the potential of D, while K_B is at zero potential. This leads to a potential V being developed across the Kerr cell K. At a later time t ($= t_o+\Delta t$) corresponding to position C in Fig 3.4(b) the electrode K_B is activated by the pulse generated along PB. Simultaneously transistor 2 in OP_A discharges the voltage on electrode K_A. With K_A now at zero potential and K_B at the pulse potential V a voltage is again developed across the cell, but opposite in polarity to that previously applied. The net effect is the generation of a reversing pulse waveform of the type shown in Fig 3.4 (c).

The reversing pulse unit was designed to operate between 0 to 1.0 kV, however, technical problems restricted operation to voltages less than 0.6 kV.

3.4 The detection circuit

This consists of the photomultplier PM, oscilloscope CRO, the variable load resistors and the camera. When a blue light source (λ=441.6 nm) was employed, the detector was an EMI 9813 KB bialkali cathode photomultiplier which has its maximum sensitivity in the blue region of the visible spectrum. For the later experiments using a red laser (λ=632.8 nm), an

EMI 9658 R , S-20 trialkali cathodes, PM was used. The PM power supply was a stabilised Brandenburg unit model 476R, capable of delivering 0.4 to 2.0 kV. The output of the PM was taken through a load box, in which a variety of resistances in the range 50Ω to 20 kΩ could be selected, to a Tektronix 556 Dual beam oscilloscope. The oscilloscope displayed both the voltage pulse and the birefringence signal on the screen. Facilities existed for expansion of the time scale to amplify the detail of selected portions of the detected signal. A polaroid CR-9 land camera using polaroid 107C film was used to record the displayed oscillogram.

3.5 The optical system

The optical system is shown schematically in the lower section of Fig 3.1. The laser light source (LL) was initially an RCA-LD 2186 He-Cd laser, emitting monochromatic plane polarised light of wavelength 441.6 nm and power 15 mW. However, during the course of this work this was replaced, first by a Liconix model 4110, He-Cd laser operating at the same wavelength, and power 11.5 mW , and later by a Rofin NEC GLG 5350 .5 mW He-Ne laser operating at 632.8 nm. The slits S1 and S2 were used to reduce the effects of stray light. The rotatable Glan-Thompson prism P, is positioned with its plane of vibration parallel to the plane of polarisation of the beam in order to increase the degree of polarisation obtained. The quarter waveplate Q, (when inserted) converts the elliptical polarised beam emerging from the cell into a plane polarised beam before it passes through another rotatable Glan-Thompson prism, A, the analyser. The polariser and the analyser and the quarter wave plate are mounted on rotatable graduated holders which could be adjusted to within 0.05^{o}. These components have their axes of vibration set 45^{o} (P)/ 135^{o}(A ,Q) with crossed position, the analyser and the polariser reduce the light intensity impinging on the photomultiplier to a minimum.

3.5.1 Optical theory

The optical components described above, can be arranged in two modes for birefringence measurements

Mode A - Optical arrangement without λ/4-plate

In this mode, the analyser and the polariser are crossed and are at 45^{o} to the field direction. Rotating the analyser through an angle α away from the crossed position allows light of intensity I_{α}, to reach the photomultiplier. This intensity is related to the angle α and the optical retardation , δ due to the birefingence according to equation { 1 } .

$$I_{\delta} = \tfrac{1}{2}KI_{o}\{ 1 - \cos 2\alpha\cos\delta \} \qquad 3.2$$

where I_{o} is the incident light intensity on the cell and K is an efficiency factor accounting for any loss of intensity due to reflection and absorption by the optical components. Without an electric field ($\delta = 0$), the intensity reaching the PM becomes,

$$I_{\alpha} = \tfrac{1}{2}KI_{o}\{ 1 - \cos 2\alpha \} = KI_{o}\sin^{2}\alpha \qquad 3.3$$

The effect of any residual strain birefringence δ_{o} in the cell windows is to modify this transmitted intensity to:

$$I_{\alpha+\delta_{o}} = \tfrac{1}{2}KI_{o}\{ 1 - \cos2\alpha\cos\delta_{o}\} = KI_{o}\{ \sin^{2}\alpha\cos\delta_{o} + \sin^{2}\tfrac{1}{2}\delta_{o}\} \qquad 3.4$$

When an electric field pulse is applied, the solution birefringence increases the intensity reaching the detector to

$$I_{\alpha+\delta_{o}+\delta} = \tfrac{1}{2}KI_{o}\{ 1 - \cos 2\alpha \cos (\delta+ \delta_{o})\} \qquad 3.5$$

where δ is the retardation due to the solution. The change of light intensity on application of the pulse is here given by

$$\Delta I_{\delta} = I_{\alpha+\delta_{o}+\delta} - I_{\alpha+\delta_{o}} = \tfrac{1}{2}KI_{o}\{\cos 2\alpha\cos\delta - \cos 2\alpha\cos(\delta+\delta_{o})\} \qquad 3.6$$

When the analyser and the polariser are crossed (α=0) this equation reduces to

$$\Delta I_{\delta} = \tfrac{1}{2}KI_{o}\{ \cos\delta - \cos(\delta+\delta_{o})\} \qquad 3.7$$

$$= KI_{o}\{ \sin^{2}(\tfrac{1}{2}(\delta+\delta_{o})) - \sin^{2}\tfrac{1}{2}\delta_{o}\} \qquad 3.8$$

For very small angles for which $\delta = \sin\delta$ eqn 3.8 simplifies

$$\Delta I_{\delta} = KI_{o}\{ \tfrac{1}{4}\delta^{2} + \tfrac{1}{2}\delta\delta_{o} \} \qquad 3.9$$

and for a case for which $\delta_o << \delta$.

$$\Delta I_\delta = \tfrac{1}{4} K I_o \delta^2 \equiv K I_o \{(\pi \ell \Delta n)/\lambda\}^2 \quad 3.10$$

Such an optical system therefore gives a signal proportional to the square of the induced retardation or birefringence i.e. quadratic detection.

Noting that $\delta = 2\pi B \ell E^2$ eqn.2.40, when the Kerr law holds, substitution into eqn. 3.9 yields

$$\Delta I_{\delta}/E^2 K I_o = \pi^2 \ell^2 B^2 E^2 + \pi \ell B \delta_o \quad 3.11$$

an equation originally developed by Orttung and Meyers [71]

Mode B - Optical arrangement with λ/4-plate.

With a λ/4-plate, positioned with its slow axis at 135° to the electric field direction (parallel to the analyser) the light intensity transmitted by the analyser when it is rotated by an angle α from the crossed position in the absence of the field is given by

$$I_{\alpha+\delta_o} = \tfrac{1}{2} K I_o \{1 - \cos(2\alpha+\delta_o)\} \quad 3.12$$

When the electric pulse is applied to the sample introducing a retardation δ, the transmitted intensity becomes [1],

$$I_{\alpha+\delta_o+\delta} = \tfrac{1}{2} K I_o \{1 - \cos(2\alpha+\delta_o+\delta)\} \quad 3.13$$

Thus the intensity change due to the field pulse, ΔI_δ is given by

$$\Delta I_\delta = I_{\alpha+\delta_o+\delta} - I_{\alpha+\delta_o} = \tfrac{1}{2} K I_o \{\cos(2\alpha+\delta_o) - \cos(2\alpha+\delta_o+\delta)\} \quad 3.14$$

$$= K I_o \{\sin(\alpha + \tfrac{1}{2}\delta_o + \tfrac{1}{2}\delta) - \sin^2(\alpha + \tfrac{1}{2}\delta_o)\} \quad 3.15$$

For small angles we have

$$\Delta I_\delta / K I_o = (\alpha + \tfrac{1}{2}\delta_o + \tfrac{1}{2}\delta)^2 - (\alpha + \tfrac{1}{2}\delta_o)^2 \quad 3.16$$

$$\tfrac{1}{2}\delta(\alpha+\delta_o) - \tfrac{1}{4}\delta^2 \quad 3.17$$

$$\Delta I_\delta / K' I_o \simeq \tfrac{1}{2}\sigma\delta \quad 3.18$$

This optical arrangement therefore leads to linear detection characteristics.

Substitution of eqn 2.40 into eqn. 3.17 yields

$$\Delta I/KI_o E^2 = \pi^2 \ell^2 B^2 E^2 + \pi \ell B (\alpha+\delta_o) \qquad 3.19$$

The linear detection mode is often preferred because:
(i) it results in greater amplification of the birefringence signal
(ii) it could be used to determine the sign of the birefringence .

It is noted that eqns. 3.3 and 3.4 are useful for evaluating δ_o, KI_o and testing the linearity of the photomultiplier. Equations 3.11 and 3.19 could be used to evaluate not only the Kerr constant B , but also the strain birefingence δ_o.

3.6 Experimental procedure

3.6.1 Preparation of cell assembly

Before measurements on a new polymer system, the cell was completely dismantled and the components washed, rinsed with acetone and allowed to dry. The cell was then re-assembled and rinsed with the solvent to be studied. After drying the cell was finally filled with the polymer solution, ensuring that no air bubbles were trapped between the electrodes. When changing concentrations the cell was thoroughly rinsed with solvent,with the windows removed, between runs.

3.6.2 Alignment of optical system.

In the quadratic detection mode, the polariser and the analyser were crossed, to ensure complete extinction of the laser beam. The analyser was then rotated away from the cross position and the intensity impinging on the photomultiplier recorded. The reading was used to determine KI_o using eqn. 3.3 and to check that the photomultiplier was operating within its linear response range. After the solution was introduced into the cell, the thermostatting fluid was circulated around the cell jacket. When temperature equilibrium was reached, the cell was mounted at 45^o to the polarisation direction and the $I(\alpha)$ relationship again recorded in order to characterise KI_o and $\delta_o$using eqn. 3.4.

If the linear detection mode, was to be used the $\lambda/4$-plate was then introduced between the cell and the analyser with its marked fast axis set at 45^o to the field direction. Fine adjustment of the $\lambda/4$-plate position was achieved by

rotating it to restore extinction. As before the alignment of the apparatus was checked by recording the transmitted intensity as the analyser was rotated away from the crossed position, using eqn. 3.12

3.6.3 Measurement of electric birefringence

When examining a solution for the first time, the following procedure was used. A rectangular low voltage pulse of width ≈ 200 μs was applied to the cell, and the amplititude gradually increased monitoring the induced birefringence and field signals on the CRO screen. When an adequate signal was displayed, the pulse width was either increased or decreased to ensure that the pulse was sufficiently long to achieve steady state orientation.

Various methods could be used to amplify the birefringence signals. The major ones were:

(a) Pulse amplitude. Increasing of the e.h.t supply increases the degree of orientation of the polymer in solution and consequently increases the birefringence signal. However, an excessively high field can cause distortion of the birefringence signal, and care has to be exercised that the transient characteristic times are not affected by field changes. The maximum pulse amplification that can be used is also limited by the maximum current which can be drawn from the photocurrent diode chain - 0.2 mA for EMI 9813 KB and 1.0 mA for the EMI 9858 R. (photomultiplier).

(b) Photomultiplier load. The higher the load R, the greater the voltage generated across it and hence the higher the amplitude of the recorded signal. However, this has the effect of also increasing the time constant of the detection circuit (RC) and care must be taken that this does not approach any of the characteristic times of the polymer system under investigation.

(c) Analyser position. This is only applicable in the linear detection mode using the $\lambda/4$-plate. Increasing the analyser angle α away from the crossed position amplifies the signal, as shown by eqn. 3.18 and its more accurate form 3.15.

Once the signal had been optimised, the CRO display was photographed either for a single shot experiment or for improved intensity and semi-continuous observation, in a repetitive pulse experiment at a frequency of typically 10 to 50 Hz.

3.7 Data analysis

3.7.1 The linearity of detection circuit and strain birefringence

In analysing the observed birefringence signals, it was necessary to establish (a) that the photomultiplier detector was operating within the linear response and (b) the extent of the strain birefringence δ_o, introduced by the Kerr cell. To check the former, the optical system was set up without the Kerr cell or $\lambda/4$-plate and detected signal (V volts) measured as a function of the angle, α between the analyser direction and the laser polarisation plane . The intensity of light reaching the detector under these circumstances is given by the Malus law;

$$I = KI_o \sin^2\alpha \qquad 3.3$$

Fig 3.5 shows a typical plot of V versus $\sin^2\alpha$, where it can be seen that above a measured voltage of 2 volts, corresponding to an anode current of 0.7mA, the photomultiplier response was non-linear i.e. the voltage is no longer proportional to light intensity.($V \not\propto I$). In all experiments care was taken to ensure that the current drawn never exceeded this initial value of 0.7mA. Consequently in all subsequent discussion , the detector signal voltage, V and the light intensity, I, will be used synonymously. Such a plot was also used to determine KI_o.

The cell containing the solution was then mounted in the optical path and the intensity variation with angle α was again recorded (see Fig 3.5). In this case, where an additional optical retardation δ_o due to strain birefringence may be present, the detected intensity is given by

$$I = KI_o \sin^2\alpha\cos\delta_o + KI_o \sin^2\tfrac{1}{2}\delta_o \qquad 3.4$$

Hence,

$$\frac{\text{intercept, C}}{\text{slope,}} = \tfrac{1}{2}(\sec\delta_o - 1) \qquad 3.20$$

which for this example gave $\delta_o = 0.4$. This was in fact the maximum value of δ_o observed; values were typically 0.2^o and made a significant contribution to the birefringence only for the molecules with low Kerr constants (PPG,PPO,PMPS). In these cases δ_o was subtracted from the measured optical retardations before evaluation of Kerr constants etc.

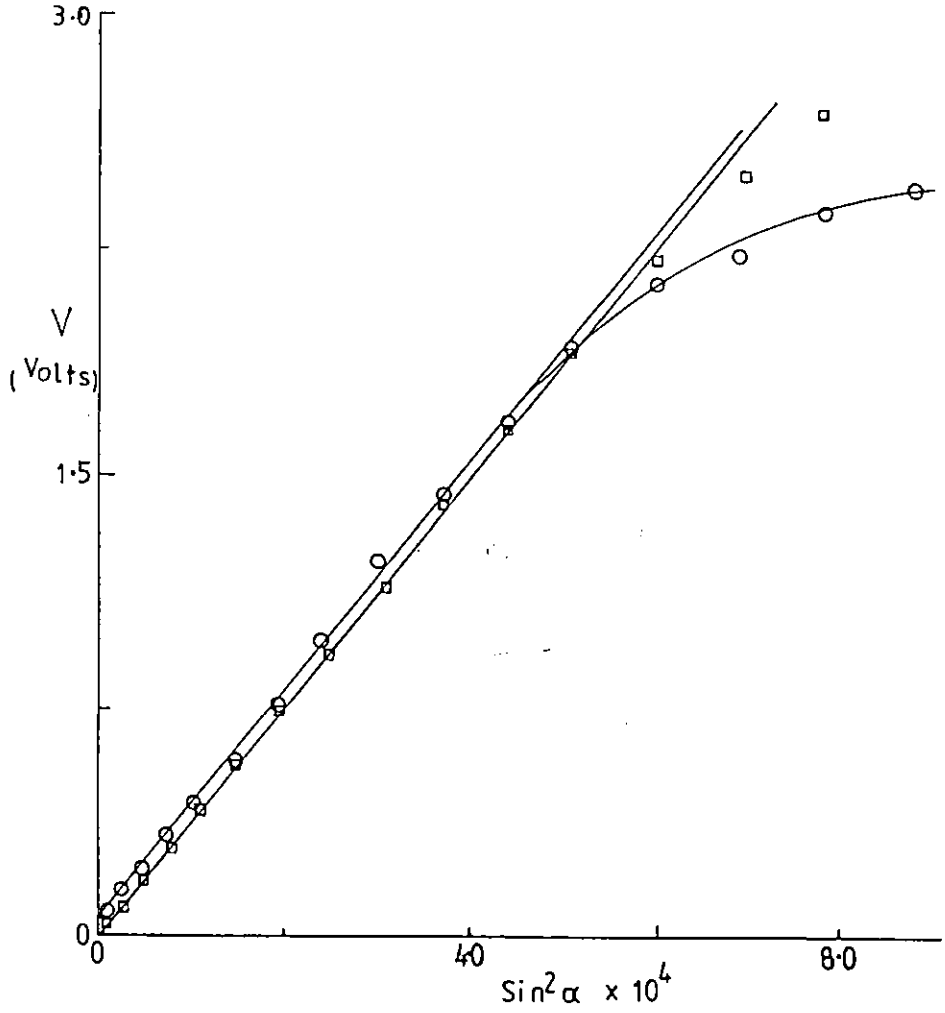

Fig 3·5 The voltage, V, variation with $\sin^2\alpha$, the analyser angle for a solution of 12·7 kg m^{-3} ethyl cellulose, (○), and no cell on the optical path, (□).

3.7.2 The optical retardation, δ and the birefringence Δn

For the case without a quarter wave plate, the retardation δ is related to the intensity according to eqn. 3.8

$$\Delta I_\delta = KI_o\,(\sin^2\tfrac{1}{2}(\delta_o+\delta) - \sin^2\tfrac{1}{2}\delta_o) \qquad 3.8$$

KI_o and δ_o were evaluated as in section 3.7.1 enabling δ_o to be calculated. The birefringence, Δn can then be calculated using eqn. 2.37

$$\Delta n = \frac{\lambda\delta}{2\pi\ell} \qquad 2.37$$

3.7.3 The Kerr constant, B

The Kerr constant calculation, will be illustrated with data obtained for polypropylene glycol PPG 0402 at 223 K. The steady state birefringence at various field strengths was recorded for the macromolecular liquid. The Kerr cell strain birefringence δ_o was calculated as in 3.7.1, and subtracted from the overall retardation δ', to obtain the polymer

retardation $\delta=\delta' - \delta_o$. This is plotted as a function of E in Fig 3.6 From the slope of this plot the Kerr constant was calculated using eqn. 2.40. In this case B = $3.13 \times 10^{-15} V^{-2} m$.

Alternatively, for cases where the obtained birefringence is $<10^o$ the Kerr constant can be calculated using eqn. 3.11

$$\frac{\Delta I_\delta}{E^2 K I_o} = \pi^2 \ell^2 B^2 E^2 + \pi \ell B \delta_o \qquad 3.11$$

As expected the Kerr constants from the two methods are in good agreement.

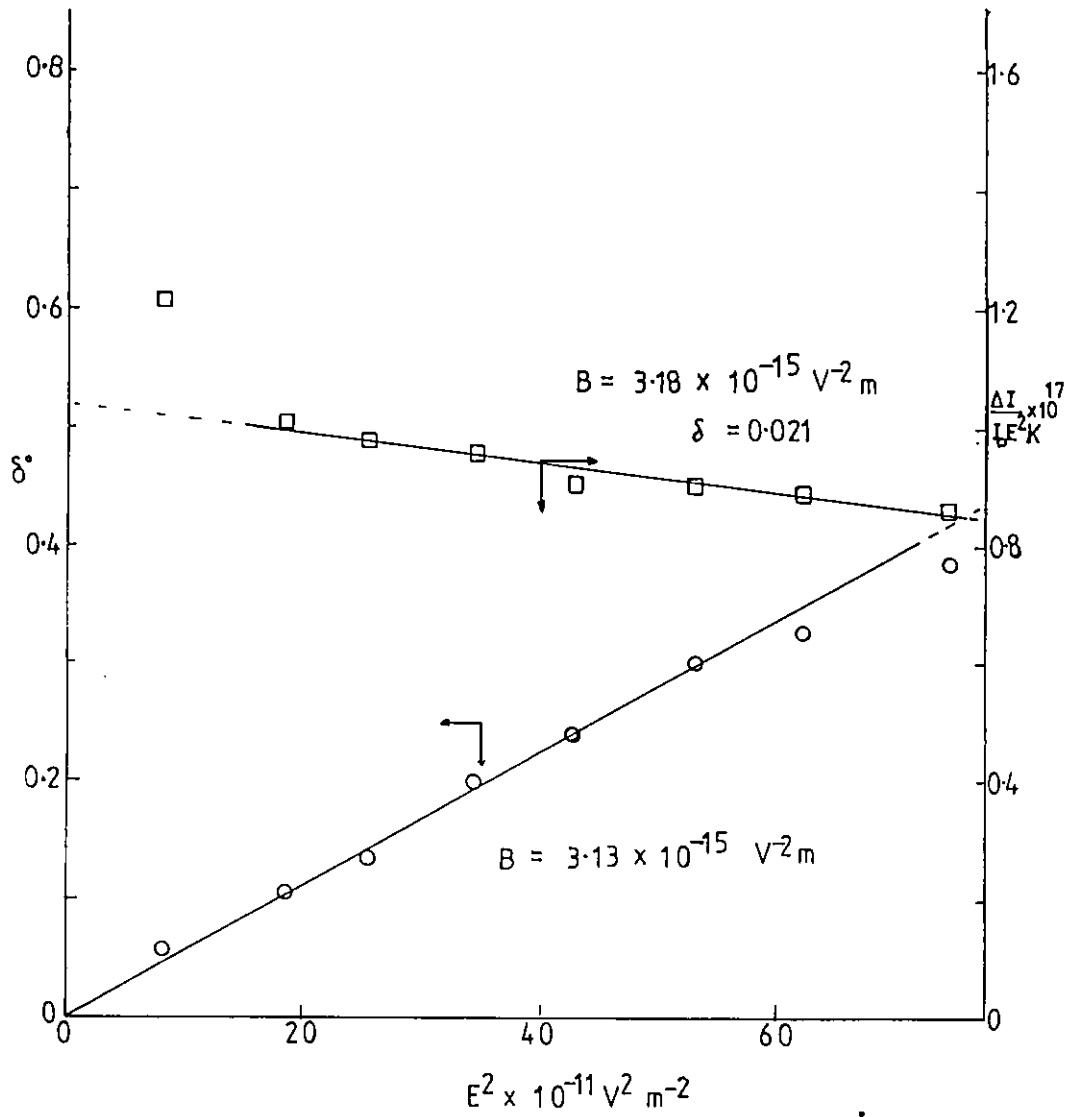

Fig 3·6 The field dependence of the birefringence, δ (○) and $\frac{\Delta I}{KI_o E^2}$ (□) for polypropylene glycol PPG 0402 at 223 K .

3.7.4 Relaxation time determination.

(a) The decay transient

The polymer solutions studied in this work in general gave decay birefringence transients that were non-exponential These curves were characterised in a number of ways:

(i) the initial relaxation time, τ_{in}.

The initial slope relaxation time, τ_{in}, is defined as the gradient of a $\ln(\delta(t)/\delta_{max})$ versus t plot as $t \to 0$

$$\Delta n\Big|_{t \to 0} = \Delta n_o \exp^{-t/\tau_{in}} \qquad 3.21$$

(ii) the e^{-1} relaxation time, τ_e

The time at which the decay birefringence reaches e^{-1} of the value at field removal, Δn_o is termed the τ_e relaxation time (see Figs 3.7 and 3.8)

$$\frac{\Delta n(\tau_e)}{\Delta n_o} = e^{-1}$$

(iii) the average decay relaxation time, $\langle\tau\rangle_d$

The average relaxation time $\langle\tau\rangle$ can be evaluated as the area S_2 under the normalised decay birefringence curve as discussed in section 2.5.5 and illustrated in Fig 3.8

(iv) the peeling method.

The decay birefringence could also be characterised in terms of a superposition of several exponetial functions

$$\frac{\Delta n(t)}{\Delta n_o} = \sum_{i=1}^{N} A_i \exp^{-t/\tau_i} \qquad 2.62$$

Such an interpretation is not particularly useful when large number of terms must be taken to fit the curve. However when $N < 2$ (or at most 3) and the time scales of the contributing terms are significantly different (i.e. $\tau_1 < \tau_2$ etc) then it is possible to extract the parameters, A_i and τ_i from the experimental data with little ambiguity. Furthermore in such a situation it is more likely that the individual relaxation times will have a real physical interpretation.

When the contributing terms were well separated in time the long relaxation time was obtained, by fitting a straight line at long times to the linear portion of a $\ln \delta$ versus time

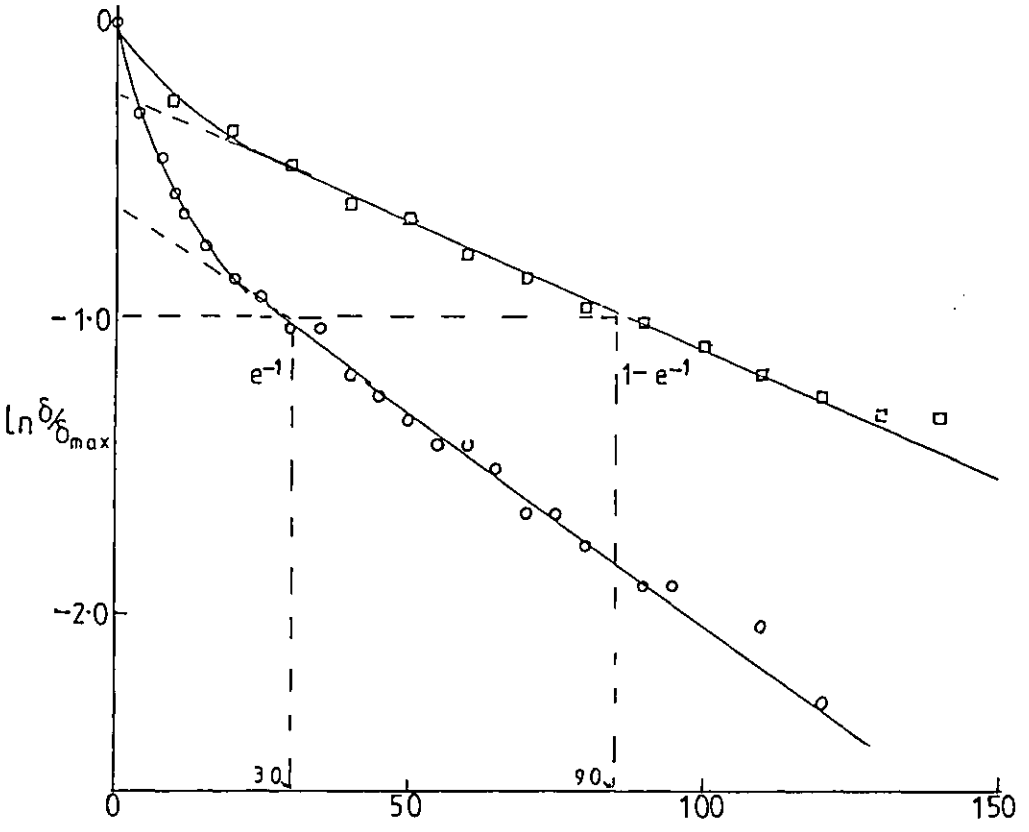

Fig 3.7 Typical $\log_e$ versus time plot of the rise, □, and decay, o, birefringence transients for PBIC #21 of concentration 1.3 kg m^{-3}.

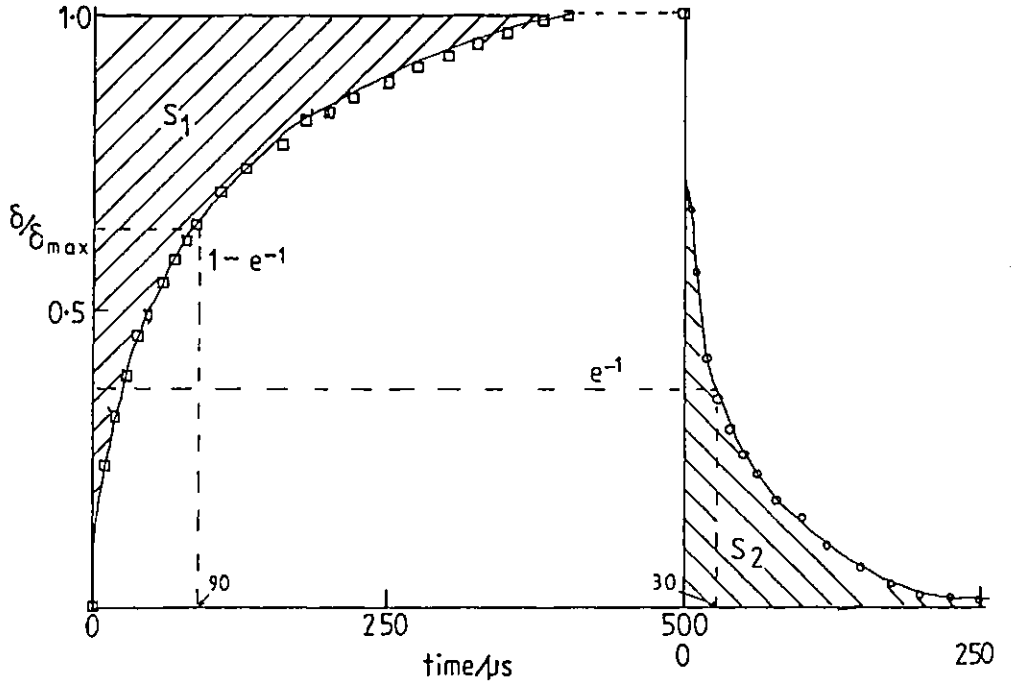

Fig 3.8 A typical birefringence transient for PBIC #21 of concentration 1.3 kg m^{-3} showing the areas above, S_1, and below, S_2, of the rise and decay transients respectively; and the times when $(\delta(\tau_e)_n/\delta_{max})_{rise} = 1 - e^{-1}$ and $(\delta(\tau_e)_d/\delta_{max})_{decay} = e^{-1}$.

plot. The slope of this time yielded the long relaxation time τ_ℓ, and amplitude of this term, A_ℓ. Subtracting the contribution of this term at anytime from the full decay curve gave the contribution due to other terms operating at shorter times. The linear long time portion of this residual curve then gave the next relaxation time τ_{p1}. By repeated subtraction in this manner (the so called 'peeling method'), the curve can be characterised in terms of a series of peeled relaxation times of decreasing magnitude ($\tau_\ell, \tau_{p1}, \tau_{p2}$ etc). This procedure was performed by computer using a linear least squares procedure , and the criterion that the correlation coefficient for each linear portion should be greater than 0.97. A typical example of such an analysis is shown in Fig 3.9 for PBLG II at C=20 kg m^{-3} for which just two relaxation times (τ_ℓ and τ_{p1}) were obtained. In this work, usually one or two relaxation times were sufficient to characterise the curves, in no case did the number of terms needed exceed three.

(v) Williams - Watts relationship

Another method of characterising the non-exponential form of the birefringence is to use the empirical relaxation function of Williams - Watts (70)

$$\phi(t) = \frac{\Delta n(t)}{\Delta n_o} = \exp^{-(t/\tau)^\beta} \qquad 0 < \beta < 1 \qquad 2.63$$

The relaxation spread factor, β is a measure of the deviation from single exponential behaviour.

For square law detection the above relationship can be written:

$$\phi_d(t) = \frac{\Delta I(t)}{\Delta I_o(0)} = \exp^{-(2t/\tau)^\beta} \qquad 3.22$$

Thus the slope of s plot of $\ln(-\ln\phi_d)$ versus ln t yields the spread factor β, while the intercept yields the relaxation time τ . In practice, it was found that a better way to obtain τ was from the time at which

$$\ln(-\ln \phi_d(t)) = 0$$

where $\tau = 2t_o$

The average relaxation time $\langle\tau\rangle$ of section (iii) can also be evaluated since

$$\langle\tau\rangle = \int \phi(t)\, dt \qquad 3.24$$

which for equation 2.86 yields

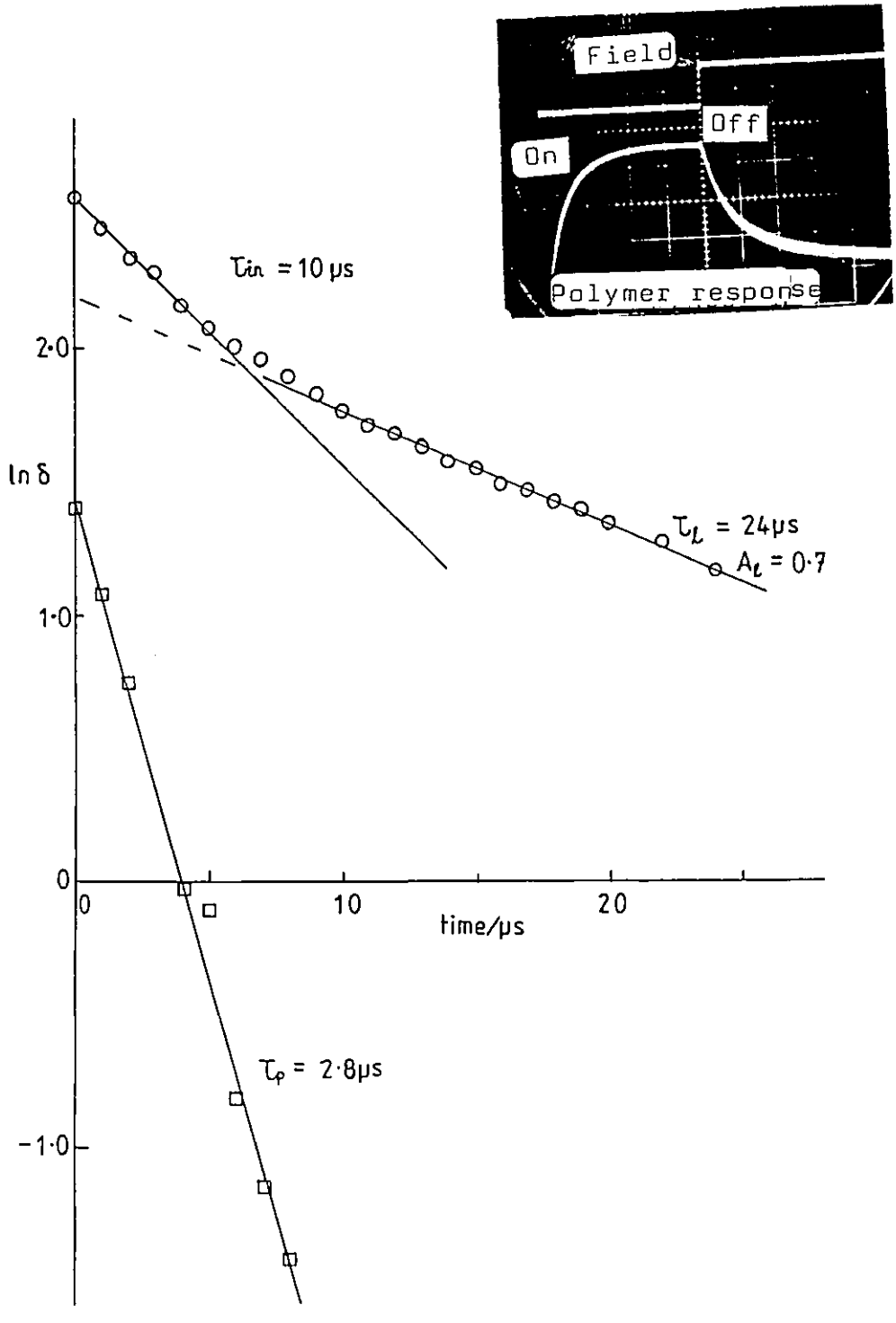

Fig 3.9 Ln δ versus time of 20 kg m^{-3} PBLG II in C-F at 293 K, showing τ_{in}(o), τ_{ℓ}(o), τ_{p} (□).

Insert: The oscillogram showing the field and the polymer response to a rectangular pulse field.

$$\langle\tau\rangle = (\tau/\beta)\,\Gamma(1/\beta) \qquad 3.25$$

A typical Williams-Watts analysis is illustrated in Fig 3.10 for the case of a liquid propylene glycol at 228 K.

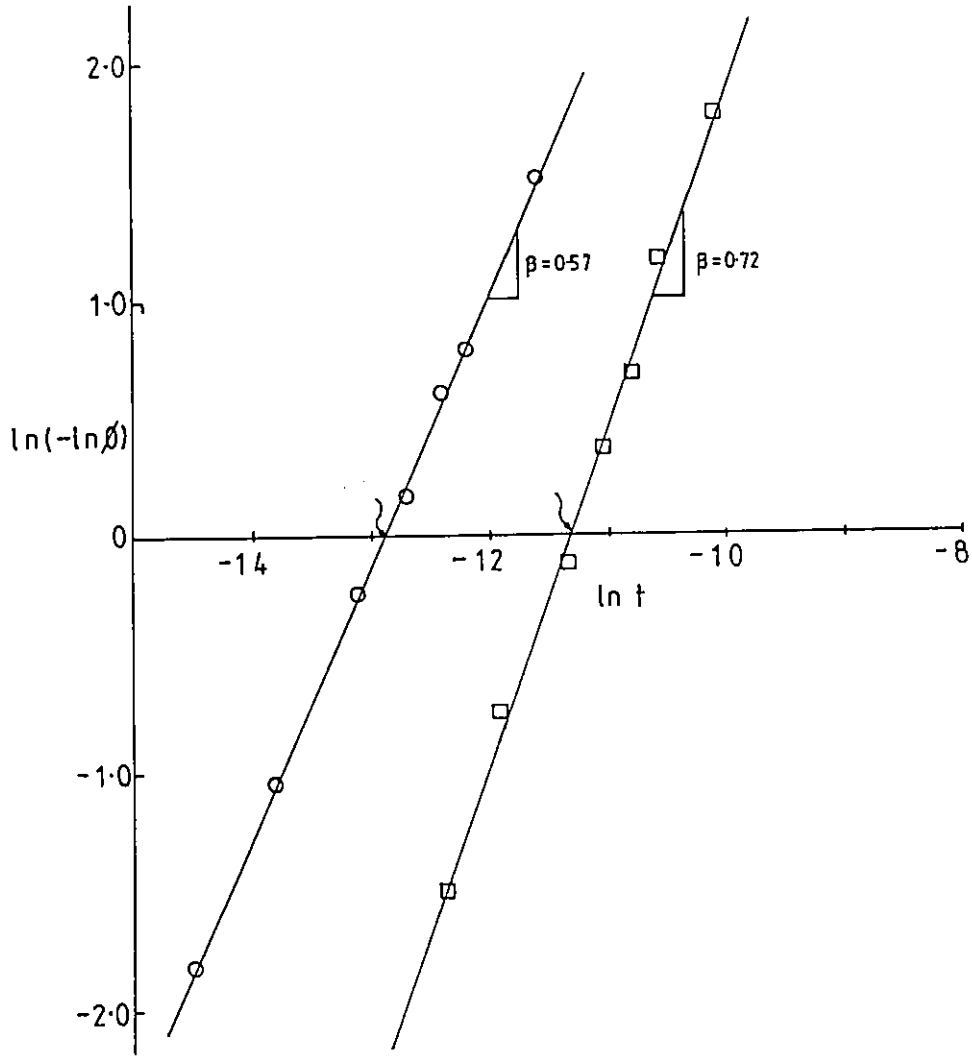

Fig3·10 Ln(-lnØ) versus ln t of the primary rise,(○), and decay,(□), processes of polypropylene glycol (PPG 0402) at 228 K

(b) The rise transient

The rise birefringence curve has been characterised in terms of the following;

(i) the $1 - e^{-1}$ relaxation time, τ_r

By analogy with τ_e this is defined by

$$\psi_r(t) = 1 - \frac{\Delta n(t)}{\Delta n_\infty} = e^{-1} \text{ at } t = \tau_r \qquad 3.26$$

where Δn_∞ is the steady state value of the birefringence (see Figs 3.7 and 3.8). In terms of the measured intensities

$$\phi_r(t) = \frac{\Delta I(t)}{\Delta I_\infty} \qquad 3.27$$

and for square law detection

$$\psi_r(t) = 1 - \phi_r^{\frac{1}{2}}(t) \qquad 3.27(a)$$

where as for linear detection

$$\psi_r(t) = 1 - \phi_r(t) \qquad 3.27(b)$$

(ii) the average rise relaxation time, $\langle\tau\rangle_r$

The average rise relaxation time $\langle\tau\rangle_r$ is evaluated from the area over the normalised rise transient as illustrated in Fig 3.8 i.e.

$$\langle\tau\rangle_r = \int\psi_r(t)\,dt \qquad 3.28$$

(iii) William - Watts relationship.

For the rise birefringence the Williams - Watt representation becomes

$$\psi(t) = \exp - (t/\tau)^{\beta_r} \qquad 3.29$$

For square law detection a plot of $\ln(-\ln(1-\phi_r^{\frac{1}{2}}(t))$ against $\ln t$ yields the slope, β_r. τ was obtained again as the time at which $\ln(-\ln(1-\phi_r^{\frac{1}{2}}(t)) = 0$. The average relaxation time, $\langle\tau\rangle_r$ for this case becomes

$$\langle\tau\rangle_r = (\tau/\beta_r)\Gamma(1/\beta_r) \qquad 3.30$$

(c) Transients containing birefringence components of opposite sign

For some systems, complex birefringence transients containing contributions of opposite sign were obtained, Fig 3.11 insert, illustrates a typical case obtained using a $\lambda/4$-plate for a polypropylene glycol (PPG 2002) sample at 238 K. The rise transient obtained using a $\lambda/4$-plate consists of rapid negative birefringence transient superimposed on a much slower positive transient. In cases such as this the slow secondary, process was analysed by plotting $\ln(I(t)-I_\infty)$ versus time ($t>t_s$), in all cases linear plots were obtained corresponding to a single relaxation time (see Fig 3.11)

$$\phi_s = I(t) - I_\infty\Big|_{t>t_s} = \text{constant} \times \exp^{-t/\tau_s} \qquad 3.31$$

The fast, process them corresponds to the function

$$\phi_p = I(t) + \phi_s \qquad 3.31(a)$$

which was in general non-exponential and usually characterised in terms of the Williams - Watts function.

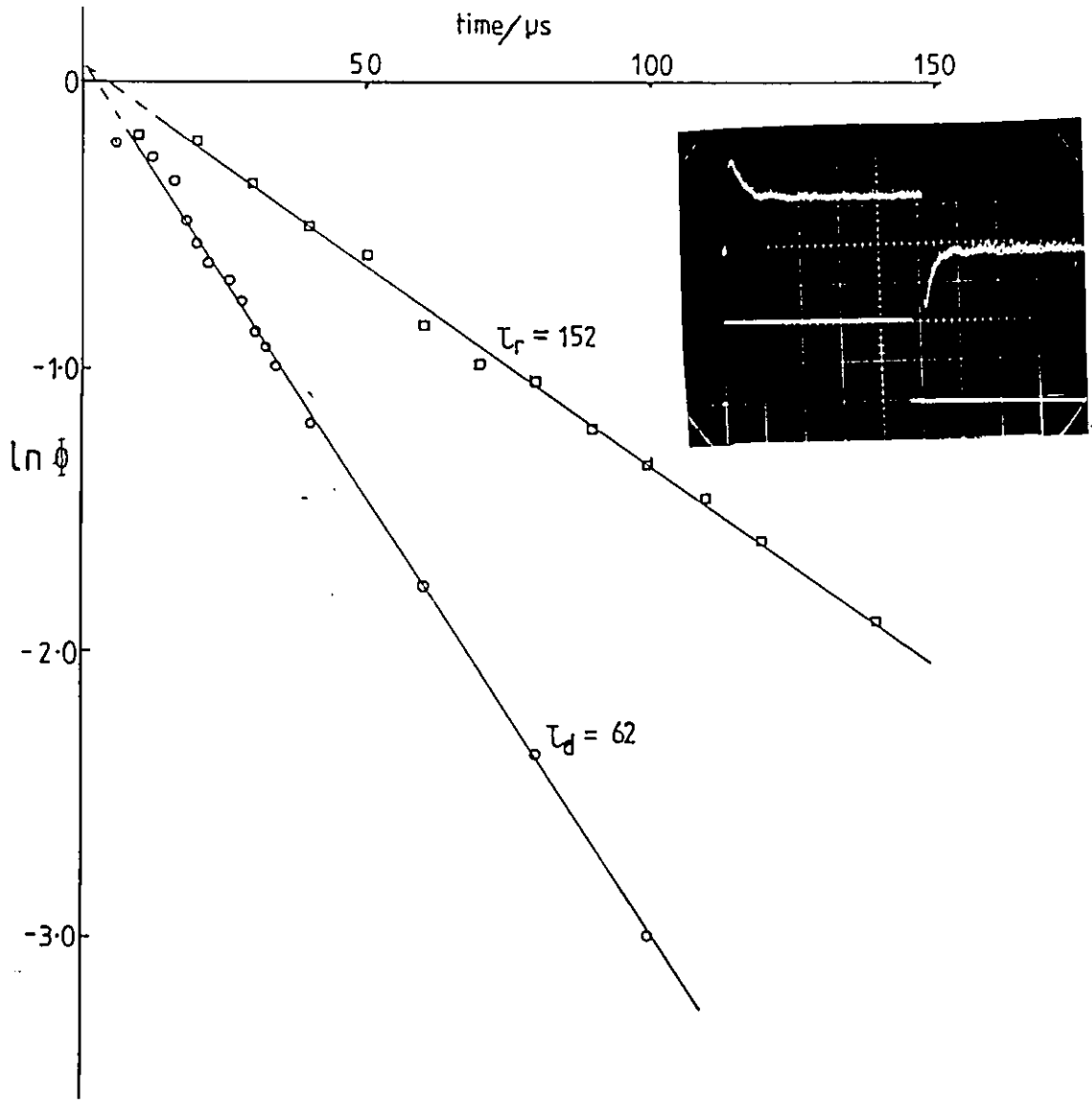

Fig 3·11 Typical plot of $\ln \phi_s$ ($\phi_s = I(t) - I_\infty$) versus time for the rise secondary, □ and decay secondary, o processes of polypropylene glycol PPG 2002 at, 238°K

3.7.5 The dipole moment.

Eqn 2.47 relating the field dependence of the birefringence to molecular properties such as polarisability and dipole moment may be rearranged to give

$$\frac{\Delta n}{E^2} = \frac{2\pi C_\nu}{15n}(g_1 - g_2)\, Q\left[1 + P/Q + \frac{E^2Q^2}{21}\{1 + 2P/Q - 2(P/Q)^2\}\right] \qquad 3.33$$

Thus a plot of $\Delta n/E^2$ versus E^2 should be linear with intercept

$$C = \frac{2\pi C_\nu}{15n}(g_1 - g_2)Q(1 + P/Q) \qquad 3.33(a)$$

and slope

$$m = \frac{2\pi C}{15n}\nu\,(g_1-g_2)Q^2(1 + 2P/Q - 2(P/Q)^2) \qquad 3.34$$

so that

$$\frac{|m|}{C} = \frac{Q}{21}\left(\frac{1 + 2r - 2r^2}{1 + r}\right) \qquad 3.35$$

Here r=P/Q which can be determined independently using the reversing pulse technique. Hence the polarisability anisotropy and dipole moment can both be obtained as shown in the following example.

Fig 3.12 shows a typical plot obtained from 0.8 kg m^{-3} poly-γ-benzyl-L-glutamate(PBLG) I in chloroform-formamide . From the slope of m=1.51 x $10^{-24}V^{-4}m^4$ and intercept,C=2.1 x $10^{-11}V^{-2}m^2$ obtained from this graph together with the value of r=0.47 obtained from reversing pulse unit the polarisability $(\alpha_1 - \alpha_2)$ and the dipole moment $(\mu_{\alpha\beta})$ are found to be 6.0 x 10^{-33}F m^2 and 3.38 x 10^{-27}C m respectively.

For the permanent dipole moment and induced polarisability are simultaneously evaluated without prior knowledge of the partial volume C_ν or the optical anisotropy factor (g_1-g_2).

If values of r are not available, it is necessary to make simplifying assumptions in eqn.3.33 regarding the relative magnitudes of P and Q. If P >> Q the eqn 3.33 reduces to

$$\frac{\Delta n}{E^2} = \frac{2\pi C_\nu}{15n}(g_1-g_2)\,P\{1 - \frac{2}{21}PE^2\} \qquad 3,36$$

and in this case

$$\frac{|m|}{C} = \frac{2}{21}\,\frac{\mu^2}{k^2T^2} \qquad 3.37$$

giving the dipole moment μ_β . If Q >> P, then

$$\frac{|m|}{C} = Q/21 = \frac{\alpha_1 - \alpha_2}{21\ k\ T} \qquad 3.38$$

and the polarisability anisotropy, $\Delta\alpha$, is obtained . Applying these procedures separately to the data already analysed in Fig 3.12 gave μ_β = 3.5 x 10^{-27} C m, $(\alpha_1-\alpha_2)$ = 6.1 x 10^{-33} F m^2 in surprising good agreement with the full analysis. This is discussed further in section 5.7

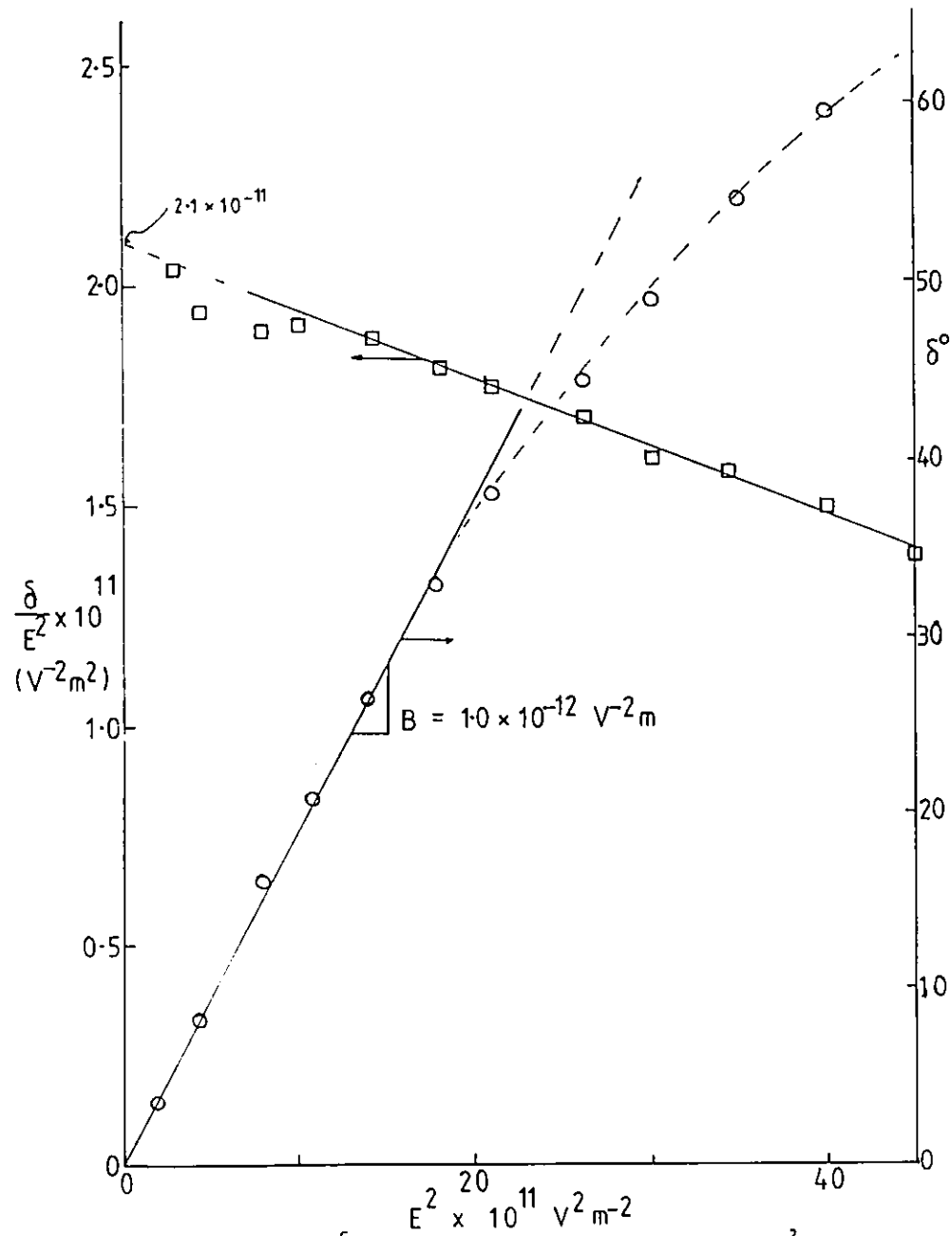

Fig 3.12 Plots of δ/E^2 and δ against field strength, E^2, for 0·8 kg m^{-3} PBLG I in chloroform-formamide at 293 K.

3.7.6 Apparent activation energy

It was found that both the relaxation times and the birefringence signal decreased with increasing temperature. By assuming that the relaxation time may be related to an activation energy, E_a for the orientation process, by the expression

$$\tau = \tau_o \exp^{-E_a/RT} \qquad 3.39$$

then the activation energy may be obtained from a plot of ln τ versus 1/T (see Fig 3.13). In this instance the apparent activation energy is found to be 62 kJ mol^{-1} and is considered to give, a measure of the energy required for this particular (segmental) motion to occur in the viscous polymer solution. All the relaxation times measured in this work were found to be well represented by an Arrhenius expression of the form of eqn. 3.39.

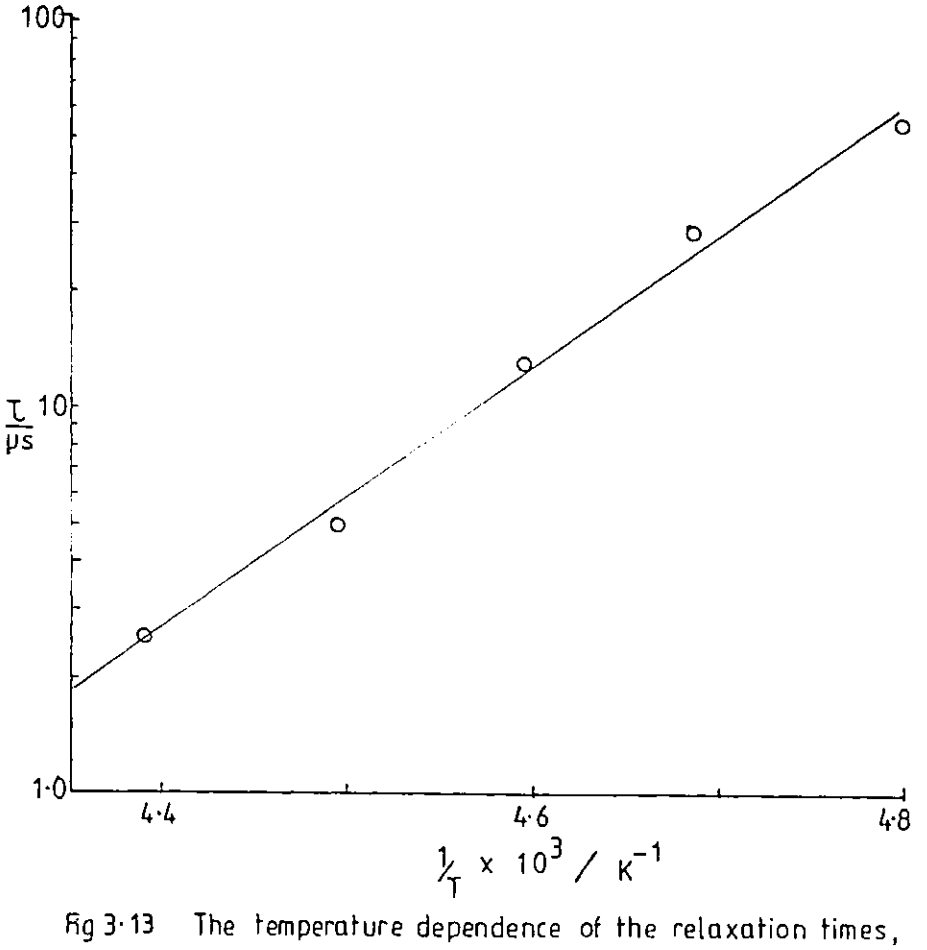

Fig 3·13 The temperature dependence of the relaxation times, typified by the primary process of polypropylene glycol (PPG 0402)

3.8 Error analysis.

The analysis of errors associated with the measurements will be illustrated with a typical measurement using a 0.53 kg m^{-3} solution of PBIC ($M_w=6.4 \times 10^5$) at 294 K using a field gradient 500 kV m^{-1}. There are two main sources of error in a relaxation time evaluation. The first is associated with the reading of individual points from the oscillogram and the second associated with the method of analysis of the data.

Error in oscillogram reading.

The amplitude of the birefringence was measured with a millimeter grating which was placed on top of the oscillogram. This amplitude could be read to within 0.2mm. With the various techniques employed to amplify the signal, this led to an average error of about 1% in the determination of the static birefringence. However in the case of dynamic measurements, the range of errors could vary from 1 to 50% as t increased from zero to high values i.e. steady state was approached. (the rise steady state birefringence or the decay equilibrium birefringence). This error at high times was minimised by curtailing measurements when the signal had fallen to about 5% of its initial amplitude.

Error in curve analysis.

In most cases $\ln \delta/\delta_{max}$ versus time plots for the various systems were non-linear (see Fig 3.14 for the example chosen) and were well represented by a double exponential function:,

$$\frac{\Delta n(t)}{\Delta n_o} = \psi_d(t) = A_p \exp^{-t/\tau_p} + A_\ell \exp^{-t/\tau_\ell} \qquad 3.40$$

The relaxation time τ, was evaluated using a least squares analysis on the long time data. The least squares computer programme starts by fitting a straight line to the last two points, and then progressively adding other points, calculating at each stage (a) the correlation coefficient (b) the intercept C, (c) the slope m , and hence the relaxation time , τ , and (d) the standard deviation of the slope. When the correlation coefficient becomes less than 0.97 the fitting is suspended and the above parameters listed.

The peeled relaxation time, τ_p is obtained by subtracting the birefringence contribution of the long time relaxation

process from the total birefringence and applying least square regression analysis, as above, to the new data. (see Fig 3.14).

The initial relaxation time, τ_{in}, is obtained by performing a least squares analysis, this time beginning with the first two data points and including further points until the correlation coefficient falls below 0.97, as above.

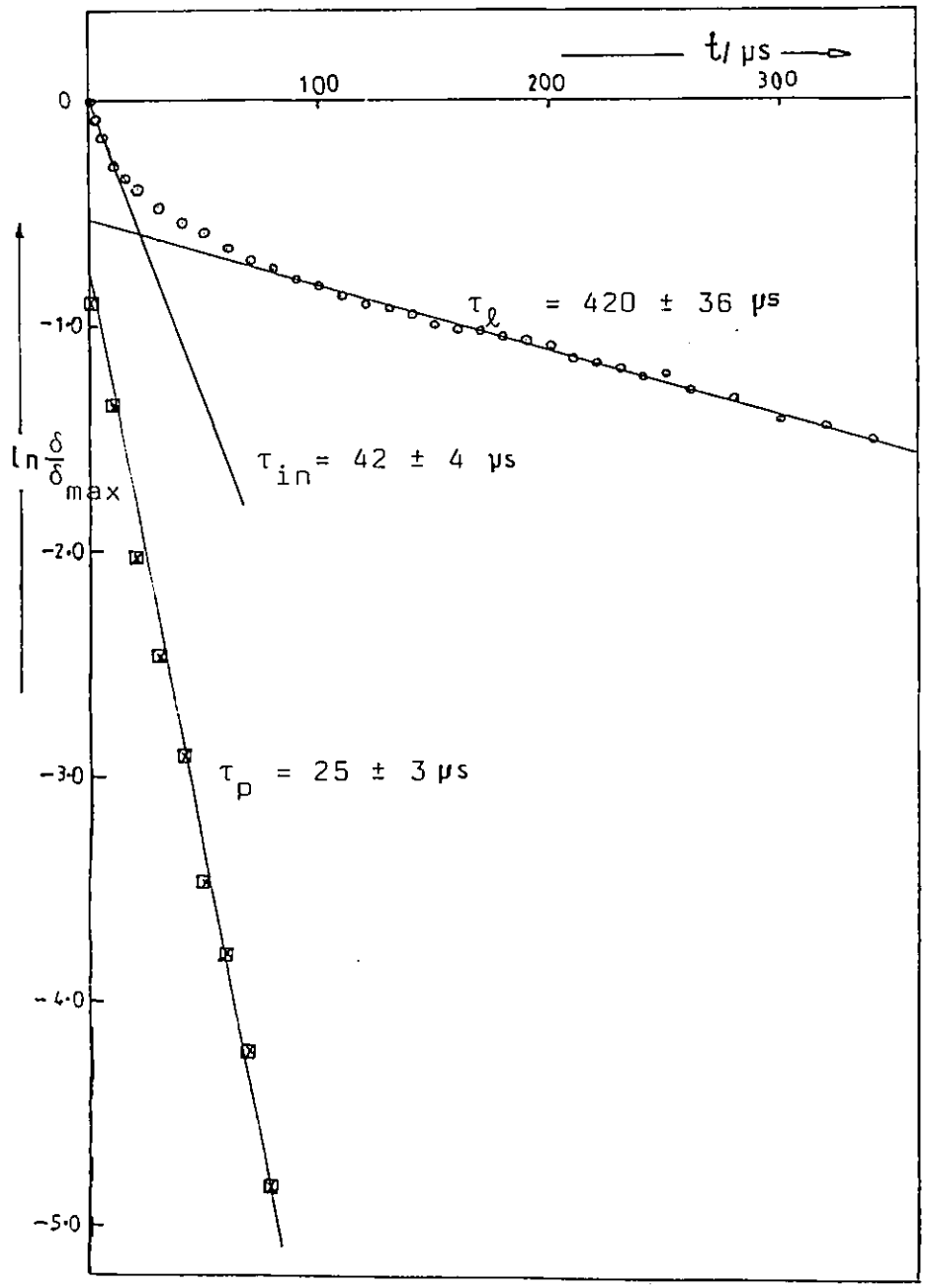

Fig 3.14 Ln δ/δ_{max} versus time for 0.53 kg m^{-3} PBIC #29 , E = 500 kV m^{-1} , temperature 294 K.

Table 3.1 shows the results from a typical single run experiment as compared with seven repeat experiments using the same sample under the same comditions. The uncertainty in the relaxation time τ as measured by the standard deviation in a single experiment lies between 8 and 12%. This is larger than the mean square deviation of the mean values obtained from the repeat experiments indicating a high degree of reproducibility in the results.

Table 3.1 Relaxation times of a 0.53 kg m^{-3} solution of PBIC #29 at 294 K

	Single experiment	Mean and standard deviation of seven experiments.
τ_p/μs	25 ± 3	29 ± 2
τ_{in}/ μs	42 ± 4	47 ± 4.6
τ_ℓ /μs	420 ± 36	439 ± 40

3.9 Equipment performance.

After assembling the Kerr effect equipment, a series of test experiments was carried out to determine the characteristics of some of the components, especially the optical components and the detection circuit , and to ensure that the equipment was functioning correctly.

3.9.1 The detection circuit.

The performance of the detection circuit was tested by conducting Kerr effect measurements on nitrobenzene, an accepted standard for such work because of its high birefringence

stability and fast relaxation time.

By measuring the detected intensity at varying field strength, the optical retardation δ, was calculated as outlined in section 3.7.2. From a plot of δ versus E^2 the Kerr constant B was determined to be $6.4 \times 10^{-12} V^{-2} m$ at $18 \pm 0.5\ ^{o}C$ and 441.6 nm wavelength. This value compares reasonably with the literature value (73) of $4.5 \times 10^{-12}\ V^{-2}\ m$ determined at 21.3 ^{o}C and 578 nm wavelength.

The relaxation time of nitrobenzene is of order $10^{-12} s$ (118) This is many orders of magnitude faster than the nominal response time of the photomultiplier and therefore measurements of the apparent relaxation time of nitrobenzene were used to determine the time constant of the detection circuit, τ_{RC}. τ_{RC} may be varied by changing either the load resistance R or the capacitance C, of the detection circuit. However the oscilloscope has a fixed capacitance quoted by the manufacturer as 20 pF. Thus apparent relaxation times were determined as a function of load resistance, as shown in Fig 3.15. The slope of this plot gives the capacitance of the oscilloscope ,leads, etc as 2.02×10^{-10} Farad. Thus a load of 50Ω (the lowest value used in this work) limits measurements to solutions having relaxation times greater than $10^{-2} \mu s$.

3.9.2 The optical components:

Having obtained a satisfactory result for the Kerr constant of nitrobenzene and noted the limitations of the detection circuit, the optical arrangement was tested using a solution of ($10\ kg\ m^{-3}$) PBLG III in dimethylformamide (DMF). The solution was subjected to a rectangular pulse of strength $2.5\ kV\ m^{-1}$ and duration 6.0 μs and the resulting birefringence analysed in both the linear and quadratic detection modes. In the case of linear detection, tests were carried out for both clockwise and anticlockwise rotation of the analyser with respect to the crossed position. The relaxation times obtained are shown in table 3.2.

These results show that:

(a) The decay birefringence, obtained from anticlockwise rotation of the analyser was characterised by a single relaxation time which was independent of the magnitude of angle of rotation α.

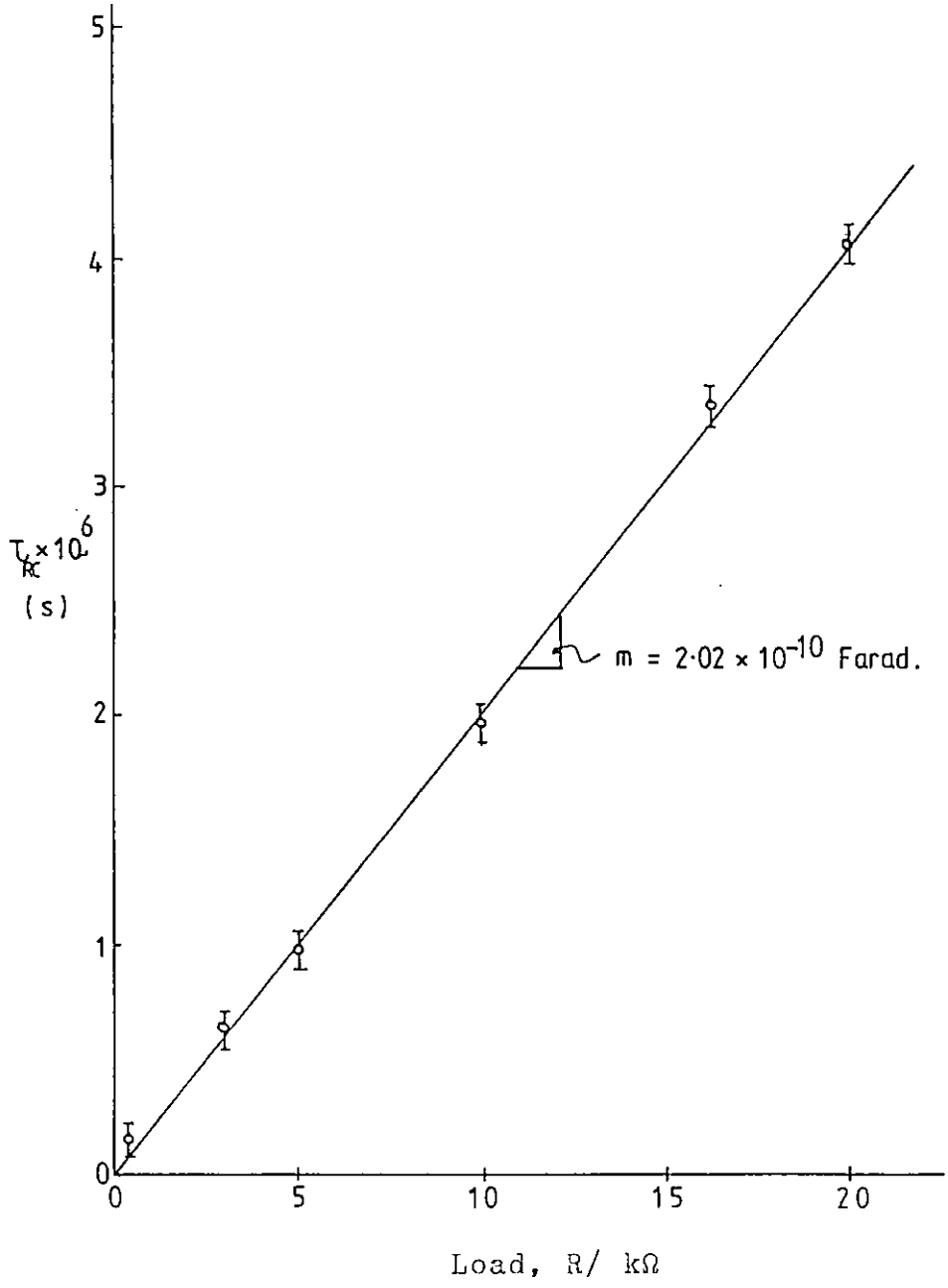

Fig 3.15 The experimental time constant, τ_{RC}, variation with load, R, using nitrobenzene.

Table 3.2 Relaxation time variation with optical arrangement and analyser angle rotation.

With λ/4-plate; clockwise rotation of analyser.				
Analyser angle from the crossed position, α°	0.6	1.6	2.6	3.6
Measured relaxation times τ/μs From initial slope	3.6	3.6	3.6	3.3
From final slope	5.2	5.1	5.2	5.1
With λ/4-plate; anticlockwise rotation of the analyser				
Analyser angle from the crossed position, α°	2.4	3.4	4.5	6.4
Measured τ/μs From initial slope	4.1	4.1	4.0	4.0
From final slope				
Without the λ/4-plate				
Measured τ/μs From initial slope	1st run 4.1		2nd run 4.1	
from final slope	9.7		6.5	

(b) For clockwise rotation of the analyser at least two relaxation times were evident. Again these times were independent of the extent of rotation.
(c) In the quadratic detection mode, two relaxation times were observed with the initial time in good agreement with that obtained from anticlockwise rotation of the analyser in the linear mode. The strain birefringence in the cell was very small (0.03)

Exhaustive examination of the polariser and the analyser alignment and that of the cell relative to the plane of polarisation of the laser beam established that the source of these discrepancies was the quarter wave plate.

The quarter wave (λ/4-) plate was therefore tested to determine the retardation introduced at a wavelength of 441.6 nm

In the absence of the cell, and with the analyser in crossed position with the polariser, the intensity transmitted by the analyser is related to the retardation introduced by the λ/4-plate, δ, and the angle θ between the analyser axis and the quarter wave plate axis according to the expression;

$$I_n(\theta) = \frac{2I(\theta)}{KI_o} = (1 - \cos 2\theta \cos\delta) \qquad 3.41$$

With the λ/4-plate positioned so that its slow axis is at 45^o to the plane of polarisation, δ introduced should be $\pi/2$. Hence the beam emerging from the plate should be circularly polarised, giving an intensity at the detector $I_n(\theta)$ which is independent of the analyser rotation, see Fig 3.16 (a).

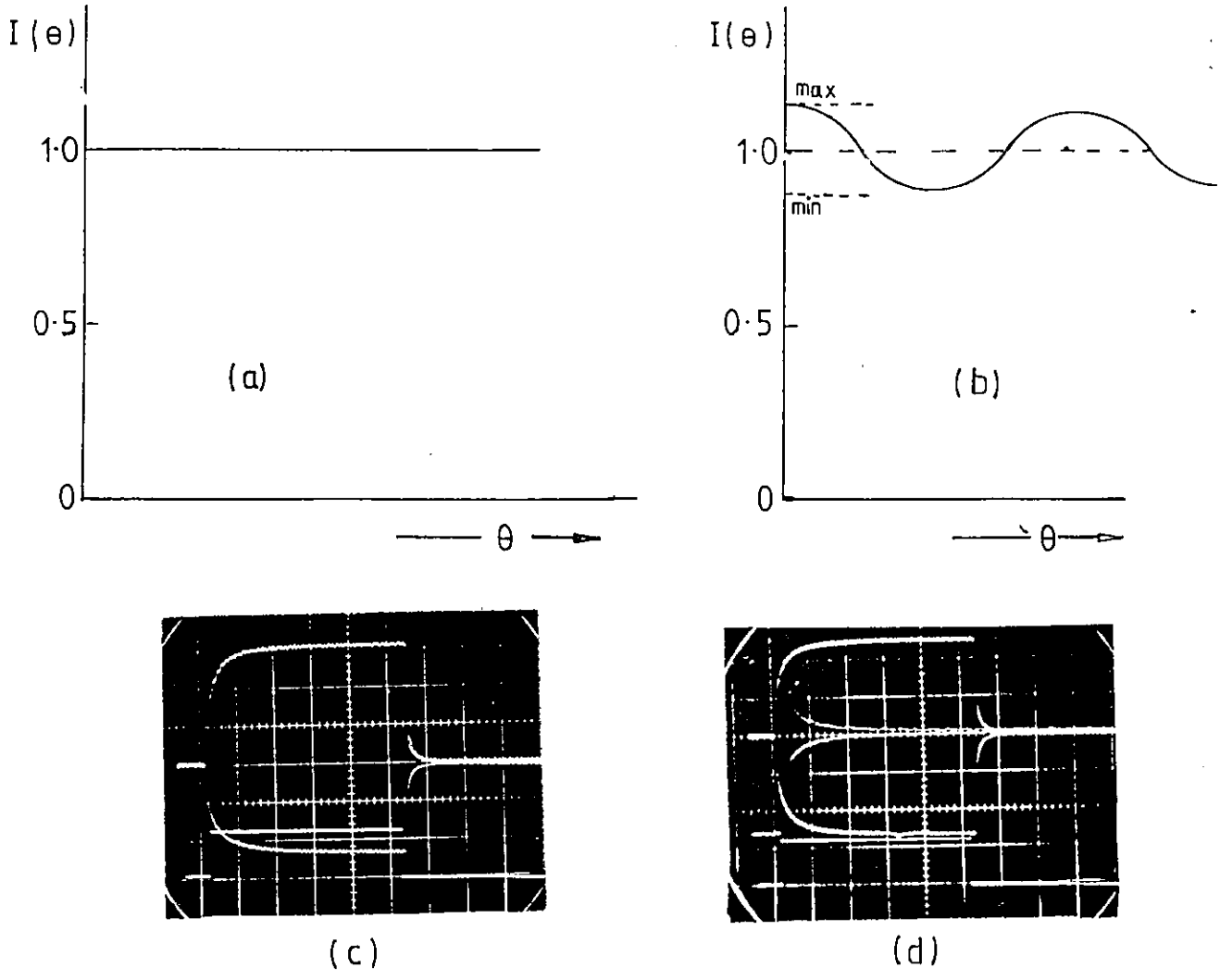

Fig 16 The intensity, I(θ) - angular variation for proper (a) and improper (b) behaviour of the quarter wave plate. (c) birefringence transients for same angle α, for the clockwise (+) and anticlockwise(-) rotation of analyser using improper λ/4-plate. (d) birefringence transients for same, α, using proper λ/4 plate; the transients are identical.

However if the quarter wave plate is defective and instead of a phase shift of exactly $\pi/2$, gives a shift $(\pi/2+\Delta)$ then

$$I_n(\theta) = 1 - \cos 2\theta\cos(\pi/2+\Delta) = 1 + \cos 2\theta\sin\Delta \qquad 3.42$$

The implication of equation 3.42 is that as θ is varied a periodic maxima and minima will be observed in the intensity transmitted by the analyser (see Fig 3.16(b)). The maximum and minimum intensities, I_{max} and I_{min}, are related by

$$\frac{I_{max} - I_{min}}{I_{max} + I_{min}} = \sin\Delta \qquad 3.43$$

For the experiments listed in Table 3.2 the plate was found to have a phase shift of $\Delta=14^{o}$. This is the source of the discrepancy between the birefringence transients and the relaxation times observed for clockwise and anticlockwise rotation of the analyser (see Fig 3.16(c)). Adjustment of the plate mounting could not improve the phase shift to better than 85^{o}, indicating that the crystal was not exactly a $\lambda/4$-retarder at the blue laser wavelength of 441.6 nm. All subsequent measurements using the He - Cd laser were performed using quadratic detection. For the He - Ne laser, a $\lambda/4$-plate tuned to 632.8 nm was obtained which introduced a phase difference of exactly $\pi/2$. Fig 3.16(d) shows typical birefringence transients using this system where clockwise and anticlockwise rotations by the same angle α produced mirror image transients and identical relaxation times.

3.9.3 Overall equipment performance

In order to check the overall reliability of the equipment, a series of experiments were conducted on dilute solutions of a well characterised flexible rod-like macromolecule poly(n-butyl isocyanate),PBIC. The particular sample chosen was PBIC #21 having $\bar{M}_w = 1.33 \times 10^5$ and polydispersity, Z=1.1 kindly supplied by Dr. A.J. Bur of U.S.A. Bureau of Standards. This sample has been extensively studied in the past in Kerr effect and dielectric experiments by Jennings et al (36) Bur and Roberts (24) and Beevers et al (27) and so should prove a good test of the performance of the present equipment. An almost identical sample, $\bar{M} = 1.125 \times 10^5$ has been studied by Tsvetkov et al (26).

A solution of concentration 1.0 kg m^{-3} in carbon tetrachloride was prepared for this comparative study. A typical plot of ln δ/δ_{max} versus time (see Fig 3.17) is seen to be strongly curved, indicating a broad distribution of relaxation times. The relaxation curve was analysed in terms of τ_{in}, τ_{ℓ}, τ_e and $\langle\tau\rangle_{K,d}$ and the results are shown in Table 3.3. The relaxation times obtained agree reasonably well with those of Jennings et al [36] and also with the dielectric relaxation studies of Bur and Roberts [24] and Tsvetkov et al [26], assuming the mechanism of PBIC orientation, to be small angle.

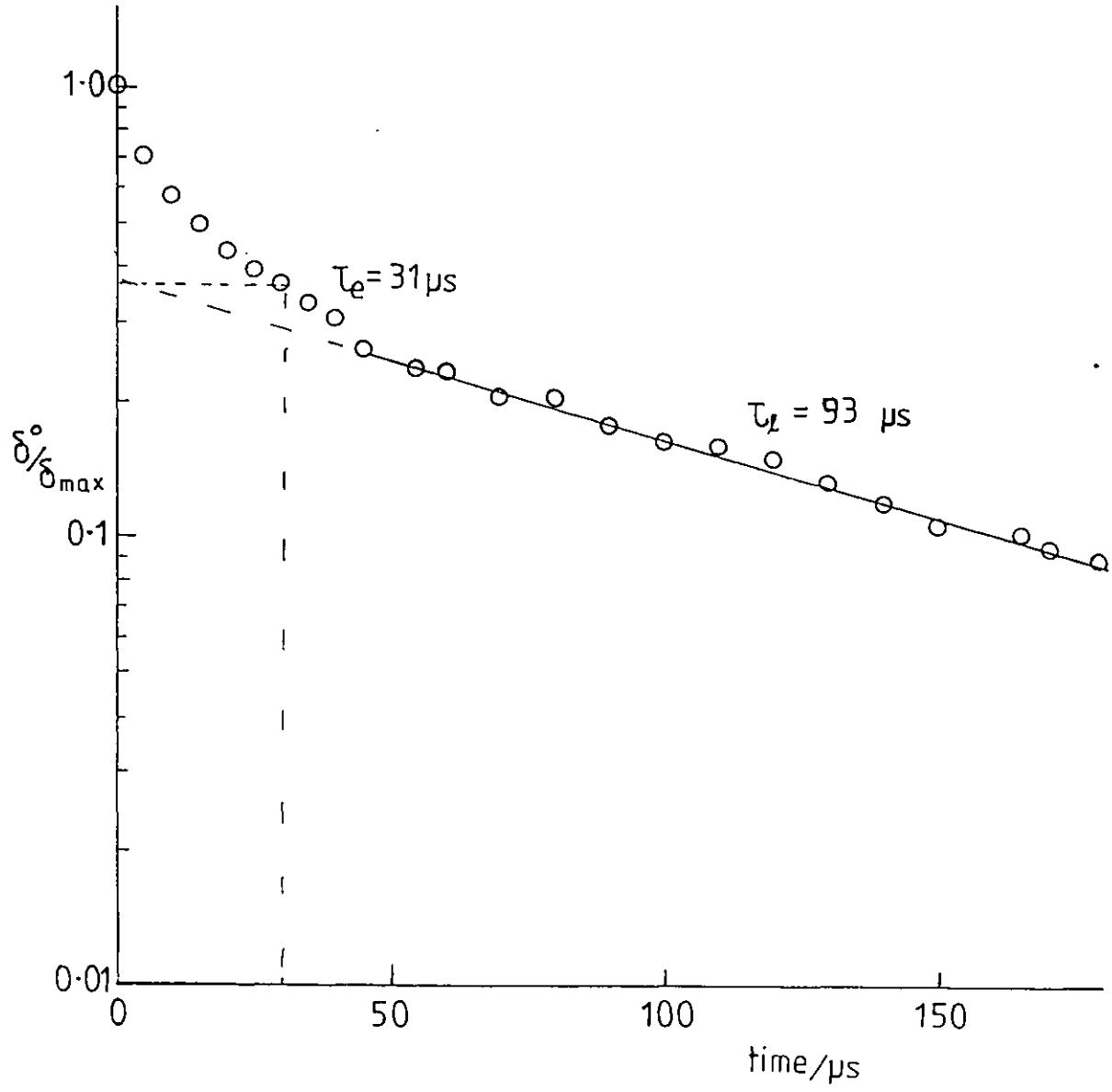

Fig 3·17 Plot of the retardation, δ against time for a 1·0 kg m^{-3} PBIC #21 at pulse duration 1·0 ms, E = 150 kV m^{-1} and temp. 293 K.

Table 3.3 Relaxation times from Rise and decay transients of 1.0 kg m^{-3}.

Temperature/ K	Rise transient τ/μs			Decay transients τ/μs							
	τ_r ref 27	τ_r	$\langle\tau\rangle_{K,r}$	τ_e ref27	τ_K ref36	τ_K ref24	τ_K ref26	τ_e	τ_{in}	τ_ℓ	$\langle\tau\rangle_{K,d}$
293	340	96	114	124	35±3(a)	42(b)	37(b)	31	20	53	43
303	320	78	87	103				23	15	40	34
313	280	65	69	84				19	11	31	26
323	220	56	70	68				14	10	26	26

(a) Kerr relaxation time in benzene 30±3.3 μs corrected to CCl_4 viscosity at 293 K

(b) dielectric relaxation time converted to τ_K assuming $\tau_K = \frac{1}{3}\tau_D$

rotational diffusion for which $\tau_D = 3\tau_K$ This gives confidence in the performance of the present apparatus. However, all these results, including the present ones differ significantly from the recent Kerr effect measurements of Beevers et al. In all cases, their rise and decay times were a factor of about four higher than the present values. The cause of this disagreement is unclear, however their investigation was performed at much higher field strengths in the region of 1300 kV m^{-1} as compared with 250 kV m^{-1} in this work. Repeating the present measurements at such higher fields produced a distorted transient birefringence signal, with two extrema before the steady state was reached. However with this distortion the decay relaxation time (τ_e) at 293 K was found to be only 44μs .The cause of this disagreement between Beevers et al and ourselves still remains unresolved.

In contrast with the large disagreement between the absolute values of relaxation times obtained by Beevers et al and those of this work, the temperature dependence is found to be similar. The rise and decay relaxation times decrease with increasing temperature in the manner well represented by an Arrhenius expression (eqn. 3.39);the apparent activation energies obtained (see Table3.4) are in reasonable agreement with those found by Beevers et al. There is also reasonable agreement on the ratios of the rise to the decay relaxation times for the two sets of measurements. For the present results it is worth pointing out that the ratio of the mean relaxation times $\langle\tau\rangle_{K,r}/\langle\tau\rangle_{K,d}$ was reasonably constant at 2.6±0.1 over the temperature range studied, implying that the contribution of the induced dipole term is significant; and that the orientation mechanism is not of the 'fluctuation jump type' (see section 2.5.5).

Table 3.4 Apparent activation energy E_a/ kJ mol^{-1}

	This work	Beevers et al
Rise	9.4	12.4
Decay	16.3	14.8

Section B: Photon Correlation Spectroscopy

3.10 The light scattering apparatus.

A detailed description of the apparatus used in this section of the work, has been given by Letherby [49] and is shown diagrammatically in Fig 3.18. It consists of a Rofin He - Ne laser (light source)(2), of 5 mW power output and wave length 632.8 nm. This is powered by stablised power supply unit(1). The laser beam is collimated and focussed to the centre of the specimen contained in a 10x10x40 mm optical cell (3), immersed in a trough (4) filled with the refractive index matching fluid m-xylene. Filtered m-xylene having the same refractive index as the cell windows is used in order to minimise flare and internal reflections. The cell, and the

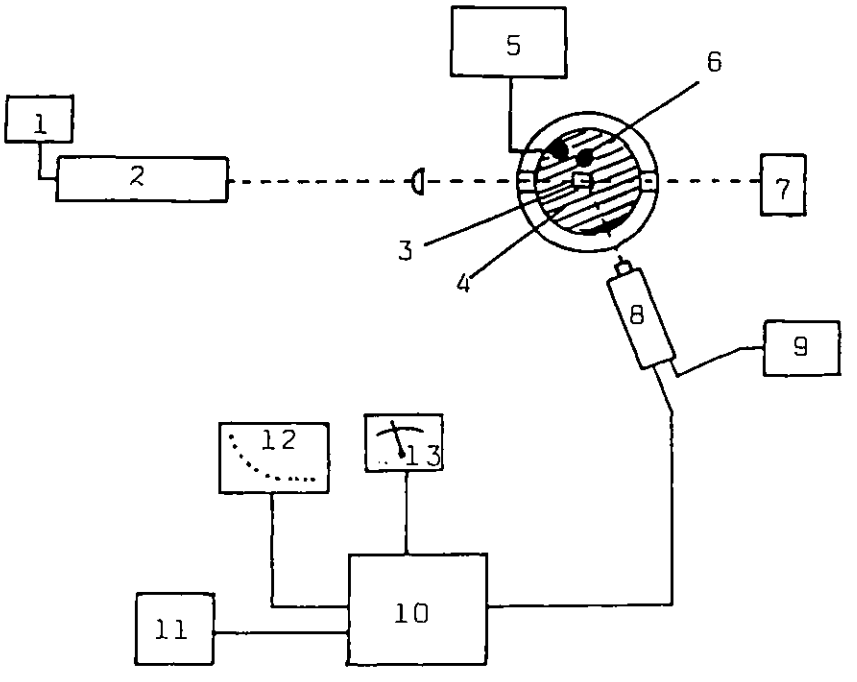

1. Laser power supply
2. Laser
3. Sample cell
4. Index matching bath
5. Heater controller
6. Thermometer
7. Light trap
8. Photomultiplier
9. H.T. supply for photomultiplier
10. Malvern K 7023 digital correlator
11. Microcomputer
12. Oscilloscope
13. Ratemeter

Fig 3.18 Photon correlation spectroscopy apparatus.

fluid are maintained at the same temperature by a set of electrical heaters controlled by thermistors (5). A mercury in glass thermometer inserted in the trough (6) is used to monitor the temperature to within ±0.2 ^{o}C. The scattered laser light was monitored using a photomultiplier, PM (8) fixed on a movable mount, capable of being rotated through scattering angles from 5^{o} to 135^{o}. The entire spectrometer assembly was mounted on a concrete slab to minimise the influence of vibrations.

The autocorrelation functions are obtained using a Malvern K7023, 96 channel correlator (10). With this arrangement the dynamic autocorrelation function can be displayed on the the oscilloscope (12), while the output of the PM is monitored via the ratemeter (13) , which indicates the noise in the signal and hence gives an indication of the cleanness of the sample. The output from the correlator is fed directly to a micro-computer (11) which enables the correlation function to be stored and analysed.

3.11 Experimental procedure.

3.11.1 The cell: The cell was normally soaked overnight in a concentrated nitric/chromic acid mixture, then washed with water, rinsed with acetone and dried.

3.11.2 Sample: A weighed quantity of the polymer sample was dissolved in a known volume of filtered solvent. The solution was then filtered using a 0.45 µm Millipore filter. Subsequent comcentrations were made by dilution of this master solution using known volumes of filtered solvent. The solutions were allowed to stand overnight before decanting about 2 cm^{3} of solution into the cell, which was then immersed in the thermstatted m-xylene bath. Sufficient time was allowed to attain temperature equilibrium before measurements were started. The sample was left overnight in the bath to permit complete dust settlement; before a repeat run was made on the following day.

3.11.3 Operation of the correlator.

The correlator uses 92 of its 96 channels to store the autocorrelation function $g^{(2)}$ in a digital form. The function is accumulated over N (typically 10^{5} - 10^{6}) interval of time each of duration t_{c} (termed the 'channel time'). The number

of photons arriving at the detector during a particular time interval at a time t, n(t), is recorded in an accumulator . This count is simultaneously separately multiplied with the contents of 92 'shift registers' which contain the photon counts, $n(t+ xt_c)n(t)$, are the incremental contributions to the photon count correlation function over the time interval $t=t_c$ to $t=92t_c$. By accumulating these values in the 92 counters or 'channels', over the large number (N) of sample times, a digital representation of the intensity autocorrelation function is obtained.

In order that the multiplication and transfer operation described above can be achieved in the hardwired correlator in times much less than t_c, 'clipping' of the observed signal is introduced. The observed photon count, n, is compared with a set clipping level n_c(a number in the range 0 - 9) ; if $n<n_c$ then the number of clipped counts, n_k, is set equal to zero, if $n>n_c$ then $n_k=1$. By having only two digits 0 or 1 the necessary speed of manipulation can be achieved. The function that is actually measured is therefore the single clipped photon count correlation function $\langle n(t)\ n_k\ (t + xt_c)\rangle$, which for large N is a good approximation to $G^{(2)}(\tau)$. Normalisation to give $g^{(2)}(\tau)$ can be done either by using a machine normalisation - a mean intensity obtained using the remaining four channels of the correlator - or as preferred in this work, by using the value of $\langle n(t)\ n(t + xt_c)\rangle$ for sufficiently large values of xt_c that $n(t_c)$ and $n(t + xt_c)$ are essentially uncorrelated.

It was necessary to select three parameters for each correlation measurement:

(a) the channel time, t_c, was chosen so that complete decay of the correlation function occured in the total run time ($=92t_c$). The aim was to ensure that at least the last ten channels had approximately the same value. The visual display of the correlation function on the oscilloscope aided this decision. The accurate determination of the normalisation value from the long time channels was crucially dependent on a correct choice of t_c.

(b) the clipping level, n_c, was adjusted using the probability analysis mode.This mode plots on the oscilloscope a trace of the distribution of the number of photons received per sample

time. It has been shown that the most efficient choice of clipping level is to set n_c equal to the mean of the number of counts per channel time.

(c) the photomultiplier aperture, if the mean number of photons per channel time was either less than 1 or greater than 9, then the photomultiplier aperature was adjusted to bring the intensity of scattered light incident on the PM within the appropriate range.

With the settings completed, the accumulation of the autocorrelation function was commenced and continued until statistics of the displayed function were judged to be adequate for the accurate definition of the correlation function. The stored function was then fed to the microcomputer for analysis and displayed graphically on the printer. The accumulation could be continued to obtain a more accurate function or cleared and the run repeated. Typical run times in this work ranged from 5 to 30 minutes.

3.12 P.C.S Data analysis.

The function recorded by the correlator is the single clipped photon count autocorrelation function $\langle n(0)n_k(t)\rangle$. For sufficiently long accumulation times this is a close approximation to the intensity autocorrelation function $G^{(2)}(K,t)$. This must be normalised with respect to the mean scattering intensity $\langle I\rangle$, which in this work has been obtained from the time limit of $G^{(2)}(K,t)$.

$$g^{(2)}(K,t) = \frac{\langle I(K,0)I(K,t)\rangle}{\langle I\rangle^2} = \frac{\langle n(0)n_k(t)\rangle}{\langle n\rangle\langle n_k\rangle} = \frac{G^{(2)}(K,t)}{G^{(2)}(K,t\to\infty)} \qquad 3.44$$

The normalised field autocorrelation function $g^{(1)}(K,t)$ (or dynamic structure factor $S(K,t)$ is obtained from the experimental function $g^{(2)}$ using the Siegart relation of equation 2.86.

$$g^{(1)}(K,t) = \left[\frac{G^{(2)}(K,t)}{G^{(2)}(K,t\to\infty)} - 1\right]^{\frac{1}{2}} \qquad 3.45$$

Fig 3.19 illustrates a typical photon count autocorrelation function for a solution of ethyl cellulose (EC) in toluene of concentration 47.2 kg m^{-3} using an iris aperture of $\frac{1}{2}$ and a channel time t_c of 1.8ms. This function was accumulated in 14 minutes.

As shown in section 2.6.2, for dilute non-interacting spherical particles, undergoing Brownian motion the field autocorrelation function decays exponentially with a single relaxation time, related to the translational diffusion coefficient D_t and the scattering vector, K (see eqn 2.90):

$$g^{(1)}(t) = A \exp^{-} D_t K^2 t \qquad 3.46$$

Hence equation 3. 45 becomes

$$g^{(2)}(t) - 1 = [A \exp -D_t K^2 t]^2 \qquad 3.46(a)$$

and a plot of $\ln[g^{(2)}(t) - 1]$ versus time is linear with a slope Γ, where

$$\Gamma = \tau^{-1} = 2D_t K^2 \qquad 2.47$$

and is the characteristic relaxation (or correlation) time. In contrast to this simple behaviour photon count autocorrelation function for concentrated ethyl cellulose solutions studied in this work were in general non-exponential. However, the $\ln[g^{(2)}(t) - 1]$ versus time plots usually showed two distinct linear regions, well separated in time, and have been characterised by a two exponential expression of form:

$$\left[g^{(2)}(t) - 1\right]_{t\to 0} = A_1 \exp -\Gamma_1 t \qquad 3.48$$

$$\left[g^{(2)}(t) - 1\right]_{t\to \infty} = A_2 \exp -\Gamma_2 t \qquad 3.49$$

The logarithmic correlation functions i.e. plot of $\ln[g^{(2)}(t) - 1]$ versus time yielded two slopes, that at long times being designated Γ_2, while that at short times being designated Γ_1. A least squares fitting procedure was used in evaluating the slopes. Fig 3.19 (b) shows the logarithmic correlation function corresponding to the data of Fig 3.19 (a).

The behaviour of $g^{(2)}(K,t)$ at shorter times was examined in more detail by repeating experiments using smaller values of channel time t_c. For these cases, the total run time ($=92t_c$) was insufficient to observe the long time asymptotic limit of $G^{(2)}$ for normalisation purposes. The procedure adopted was to ensure that for any channel time t_c, at least the last 20 channels overlapped in absolute time with the long time linear portion of, slope Γ_2, the logarithmic correlation function from a previous run obtained using a larger value of t_c.

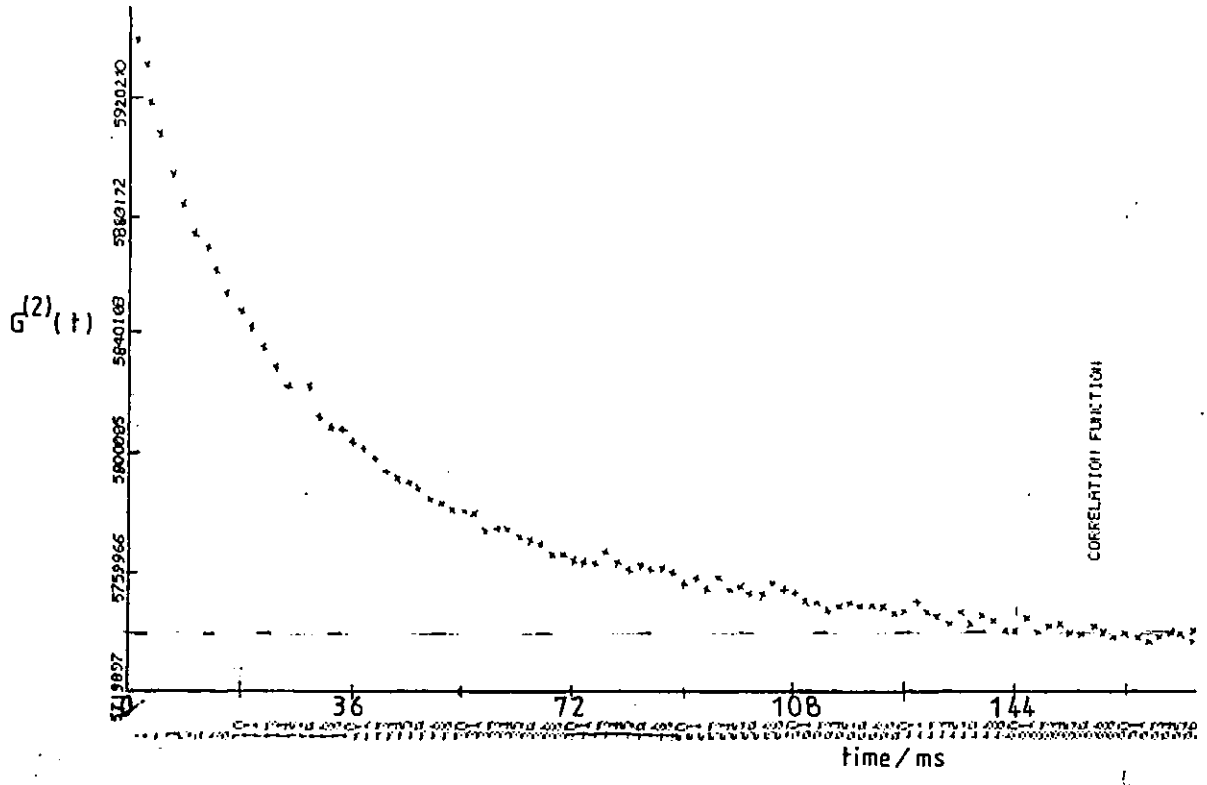

Fig 3.19(a) A typical experimental autocorrelation function , EC in toluene at 47.2 kg m^{-3}, 298 K and channel time 1.8 ms .

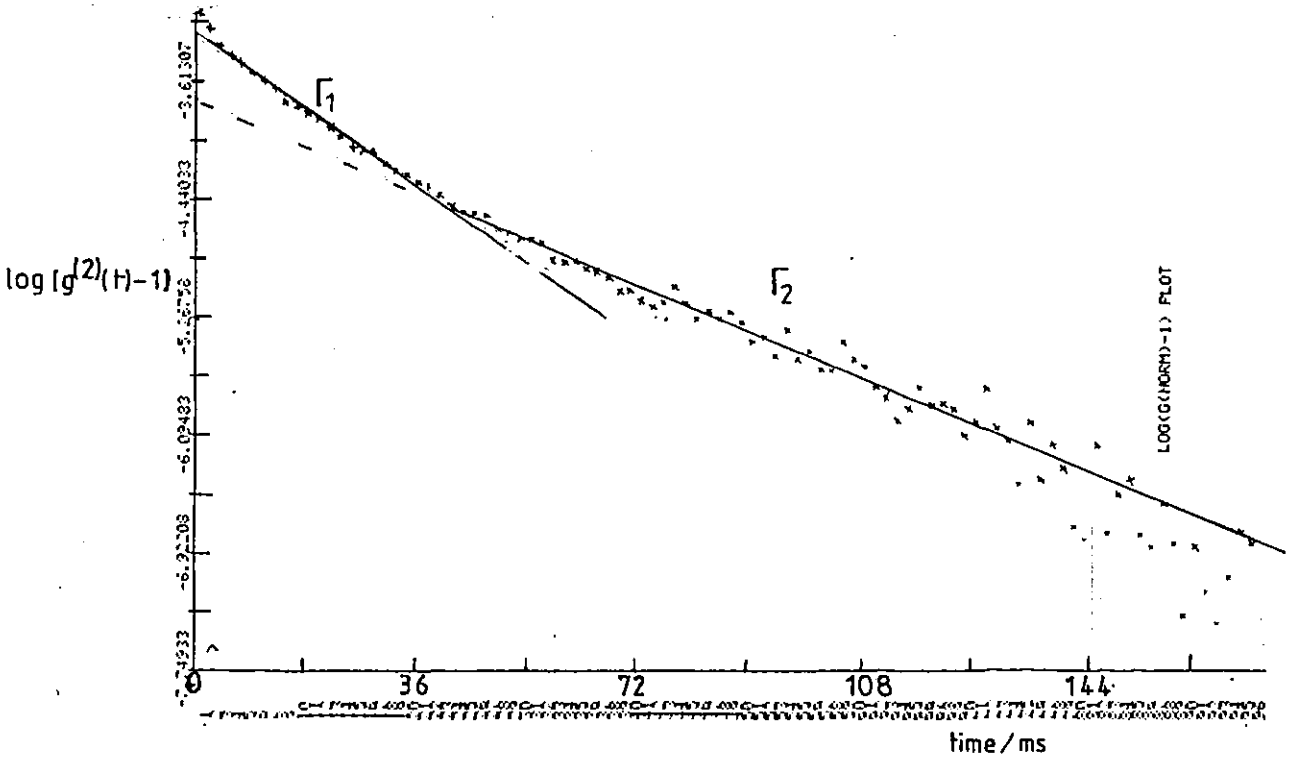

Fig 3.19 (b) A typical logarithmic correlation function of a 47.2 kg m^{-3} EC in toluene at 298 K and 1.8 ms channel time.

The normalisation factor $G^{(2)}(\infty)$ was then obtained by fitting these last 20 points to the functional form;

$$G^{(2)}(t) = G^{(2)}(\infty)\left[1 + \exp -\Gamma_2 t\right] \quad 3.50$$

Thus, in expanding the time scale of the example shown in Fig 3.19(b) a suitable choice of t_c, would be 900 μs. Further reductions in t_c would necessitate fitting the long time slope to Γ_1. By progressively reducing t_c, in this way, ensuring that the functions from successive experiments overlap sufficiently, the whole correlation function was investgated down to very small times. For some of the samples studied, the region of the slope Γ_1 was itself revealed to consist of at least two linear regions which nevertheless persisted over several decades of the time scale. A detailed description of this behaviour is given in Chapter 5.

Chapter Four

MATERIALS

4.1 Polymer studied

4.1.1 Poly-γ-benzyl-L-glutamate, PBLG

This polymer has the structure

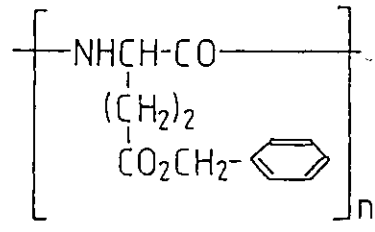

Strong hydrogen bonding between the C=O and N=H groups causes the chain to adopt a helical structure in polar solvents such as dimethylformamide (DMF), dichloroethane, and chloroform-formamide (C-F). Three samples of this synthetic polypeptide were obtained from Phase Separation Limited. The samples were designated PBLG I, PBLG II, PBLG III in order of their decreasing molecular weight. The solvents used were DMF and chloroform-Formamide mixture, mixed in the volume ratio 99.5% chloroform to 0.5% formamide, in both of which PBLG has been shown to be essentially unaggregated (72) In the mixed solvent formamide acts as a deaggregant; this C-F mixture was usually used in preference to dimethylformamide because it was less conductive and has been shown to preserve the rod-like configuration of PBLG (72). The molecular weights of the samples were determined by measuring their intrinsic viscosities at 25°C in DMF using a modified Ubbelohde dilution viscometer. The weight average molecular weights were determined using the Mark-Houwink equation, (see Fig 4.1).

$$[\eta] = K\bar{M}_w^{\alpha} \qquad 4.1$$

where $\alpha = 1.7$ and $K = 2.9 \times 10^{-10}$ m^3 kg^{-1}. The results are shown in Table 4.1

4.1.2 Poly(n-butyl isocyanate), PBIC

The structure of this polymer is

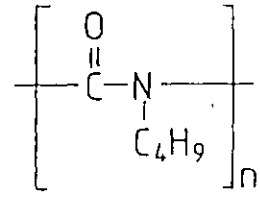

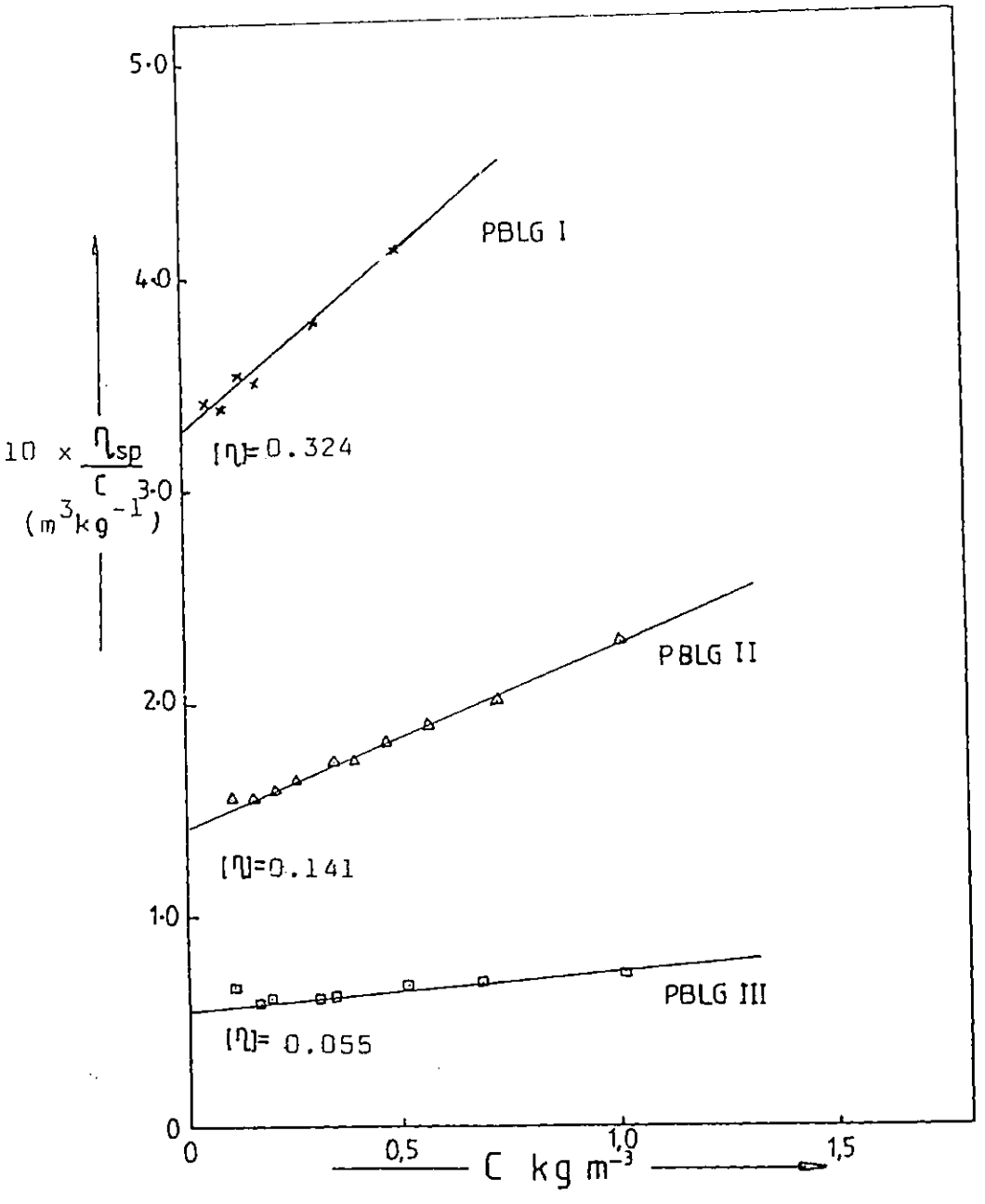

Fig 4.1 The intrinsic viscosity determination for PBLG.

Table 4.1 Molecular weights of PBLG ($\bar{M}_w$)

Sample	[η] x 10 m^3 kg^{-1}	Molecular weight
PBLG III	0.55	74000
PBLG II	1.41	129000
PBLG I	3.24	210000

Again, specific interactions between the carbonyl group and the nitrogen atom cause the chains to adopt a helical structure in certain solvents such as carbon tetrachloride (CCl_4). The PBIC sample used were kindly supplied by Dr. A.J.Bur, National Bureau of Standards, U.S.A. They comprise of two fractionated samples, designated PBIC #21 (M_w=1.33 x 10^5 and polydispersity $Z_p=M_w/M_n$=1.1) and PBIC CN-1 (M_w=1.3 x 10^6 and Z_p=1.0), and unfractionated sample, PBIC # 29 (M_w=6.4 x 10^5 and Z_p=4.6). The solvent used was analytical grade carbon tetrachloride supplied by BDH Chemicals Ltd.

4.1.3 Polypropylene glycols,PPG

The structure is

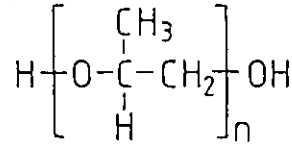

The four samples used were low molecular weight liquids (kindly donated by Lankro Chemicals Ltd) and coded according to their molecular weights. They were Propylan D400 of nominal molecular weight 400 referred to in this work as PPG 0402; Propylan D1002 of nominal molecular weight 1000 designated PPG 1002; Propylan D2002 of molecular weight 2000, designated PPG 2002; and finally Propylan DP2257 of molecular weight 2200, designated PPG 2257. The solvent used was 'Analar' grade toluene from BDH Chemicals Ltd.

4.1.4 Polypropylene oxide, PPO

The structure is

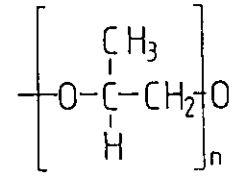

The two samples used in this work were kindly supplied by Dr. C. Booth of Department of Chemistry, University of Manchester and were identified according to their batch numbers. The batch sample S3.3, of viscosity average molecular weight M_v=1.44 x 10^6, was designated PPO 3.3 while the batch S4.4, of viscosity average molecular weight M_v=2.93 x 10^6, was designated PPO 4.4. The solvent used was 'Analar' grade toluene (BDH).

4.1.5 Polysulphone

(i) Poly(2-methyl pentene-1 sulphone),PMPS

The structure is

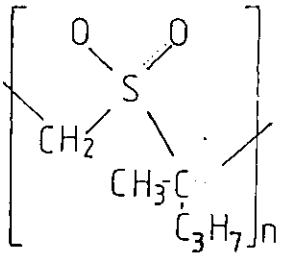

The sample used was kindly supplied by Dr. A. Fawcett, Department of Chemistry, Queen's University Belfast. It has a molecular weight $M_w=3.2 \times 10^5$ and is referred to as PMPS in this work. The solvent used was 'Analar' grade benzene.

(ii) Polyethersulphone,PES

The structure is

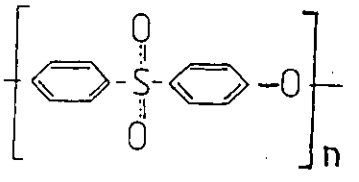

Three samples of this polymer were kindly supplied by Dr. J. Rose of Imperial Chemical Industries Ltd (Petrochemicals and Plastics Division). They were designated PES I, PES II, and PES III according to their molecular weights as determined by gel permeation chromatography GPC. PES I has $M_w=7.4 \times 10^4$ and $Z_p=2.1$; PES II has $M_w=1.23 \times 10^5$ and $Z_p=2.4$ and PES III has $M_w=1.1 \times 10^5$ with $Z_p=2.1$. The solvent used for this polymer is reagent grade N-pyrrolidone.

4.1.4 Ethyl cellulose,EC

The structure is

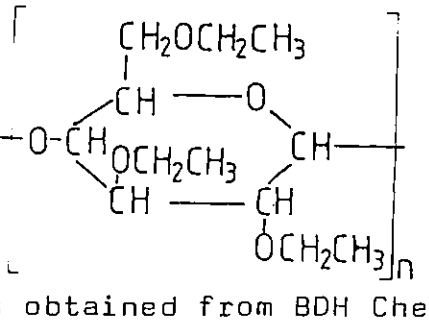

The ethyl cellulose sample used was obtained from BDH Chemicals Ltd and has ethoxy content of 48.3% and a mean degree of hydroxyl substitution 2.48 per monomer unit. The molecular weight (M_n) determined viscometrically in benzene was found to be 2.63×10^4 Solutions for the dynamic studies were made in 'Analar' grade toluene.

4.2 Sample preparation

4.1.1 Solvent filtration.

Two sets of 0.45 µm Millipore filters - Metricel GN and Metricel alpha 6 - were used in solvent filtration, depending

on their compatibility. The alpha 6 filters were used for formamide, chloroform, dimethylformamide, and N-pyrrolidone, while toluene, benzene, nitrobenzene and carbon tetrachloride were filtered using the GN membranes. The solvents were filtered before the dissolution of the polymer and no subsequent filtration of the solution was carried out. This was because attempts to filter polymer solutions can lead to preferential adsorption on the membrane material - and/or blocking of the filter pores, with subsequent loss of polymer.

4.2.2 Concentration

Master solutions were made up by dissolving a weighed quantity of the polymer in the solvent contained in a volumetric flask, which had previously been cleaned and rinsed with the solvent. The solution was virgorously shaken for a few minutes, then left overnight under gentle stirring until complete dissolution was achieved. Lower concentrations were prepared by progressive dilution of this master solution.

Three factors limited the maximum concentration which could be studied i.e. the concentration of the master solution:
(i) the availability of the polymer sample - this was the limiting factor in the cases of PBIC, PMPS and PPO;
(ii) the viscosity of the polymer solution, preventing satisfactory transfer of the sample to the cell and the production of bubble free samples - thus was the limitation in the cases of PBLG and PES;
(iii) solubility limitations, producing turbid solutions - this was the limiting factor in the case of ethyl cellulose in toluene.

Chapter Five

RESULTS AND DISCUSSION

The experimental results are presented in two sections. The first section contains information concerning the dynamic relaxation phenomena of various polymers, with emphasis placed on the effects of concentration, molecular weight, temperature and field strength. The second section contains the measured (static) equilibrium properties of the macromolecules which characterise their interaction with an electric field. Within each of these sections the results are presented for each of the polymers studied. A comparison is made with available theoretical models for each system in turn. Comparison of the various systems with each other and a rationalization of the differences in their behaviour is given in Chapter six.

Section One

Molecular Dynamics

5.1 Poly-γ-benzyl-L-glutamate,(PBLG).

5.1.1 Dilute solution behaviour

Most previous studies on PBLG have been concerned with dilute solutions. Measurements of intrinsic viscosities and light scattering on this system have shown it to be a rod shaped polypeptide with α-helical coil structure in some non-polar solvents [72]. Their studies showed them to be rod-like up to 300,000 molecular weight and to exhibit small amount of flexibility at $M_w = 8.0 \times 10^5$. The α-helical structure in some solvents was confirmed by Luzzati et al[105] by X-ray diffraction technique; although the discrepancy between their inferred value of the monomer length and that from static measurements led to conclusions that PBLG,[92] though rod-like, exhibits some flexibility. The first dynamic Kerr effect study on PBLG was undertaken by Tinoco [86], who showed that the technique was an effective tool for probing the dynamics of PBLG molecules and ascertaining their size and shape.

Dielectric studies by Marchal and Marchal [22] ,carried out on PBLG of molecular weight ranging from 3200 to 217000 showed it to be rigid throughout this range. This was supported by the studies of Wada [23], who covered molecular weights from 70000 to 180000. However the studies by Block et al [21] on the range 25000 to 275000 showed that considerable flexibility was exhibited by high molecular weight samples. The molecular weight dependence of the relaxation times, τ ($\propto M^{\zeta_m}$) gave exponents, ζ_m which changed from the expected value of three for rods at low values of M to two as M was increased. Other workers such as Tsuji and Watanabe [32], Powers [98] Powers et al [35] and Watanabe [89] carried out extensive electro-optic measurements on PBLG, concentrating on the effect of solvents, aggregation and flexibility on measured characteristics such as size,Kerr constants and dipole moments.

As the above studies showed PBLG to be a rod-like macromolecule with a small degree of flexibilty, it was chosen as a starting material in our studies, being a molecule whose dilute solution dynamics has been well characterised and representing the rigid extreme of the polymers to be studied. The molecular weights of the samples used in this work were PBLG III, M_w=74000, PBLG II, M_w=129000, and PBLG I, M_w= 210000. All the PBLG samples in the dilute regime showed significant deviation from single exponential Kerr relaxation. Consequently the decay birefringence curve was characterised by the relaxation times τ_{in}, τ_p, τ_ℓ, and τ_e as described in section 3.7.4 .

PBLG has been shown to have monomer length and solvated diameter of 0.15 nm and 1.5 nm respectively [72] . In analysing our dilute solution data, we have used Broersma's equation (eqn 2.6) for the rotational diffusion coefficient, D_r, because it accounts explicitly for the end effects of a rigid rod. The relaxation times ($\tau=(6D)^{-1}$) of PBLG III, PBLG II and PBLG I based on this equation are 1.2μs, 5.2μs and 37μs respectively. The present experimental values of $\tau_{in}(\tau_\ell)$ 1.5 (2.8)μs, 5.2 (14.8)μs, and 17 (58) μs are in reasonable agreement considering the uncertainties in the molecular weight distribution of the samples used. This indicates that the PBLG samples studied can be adequately represented by a rigid rod-type model in dilute solution, in keeping with the finding of Marchal and Marchal [22],

Block et al [21] and Wada [23] . The present results are compared with previous Kerr effect and dielectric ($\tau_K=\tau_D/3$) results at 298 K in Fig 5.0. There is reasonable agreement between the different sets of data.

5.1.2 Concentrated solutions

For concentrated, non-rigid or polydisperse systems decay birefringence transients are in general non-exponetial, hence they have been characterised in terms of the relaxation times, τ_{in}, τ_e, τ_p, and τ_ℓ as described in section 3.7.4.

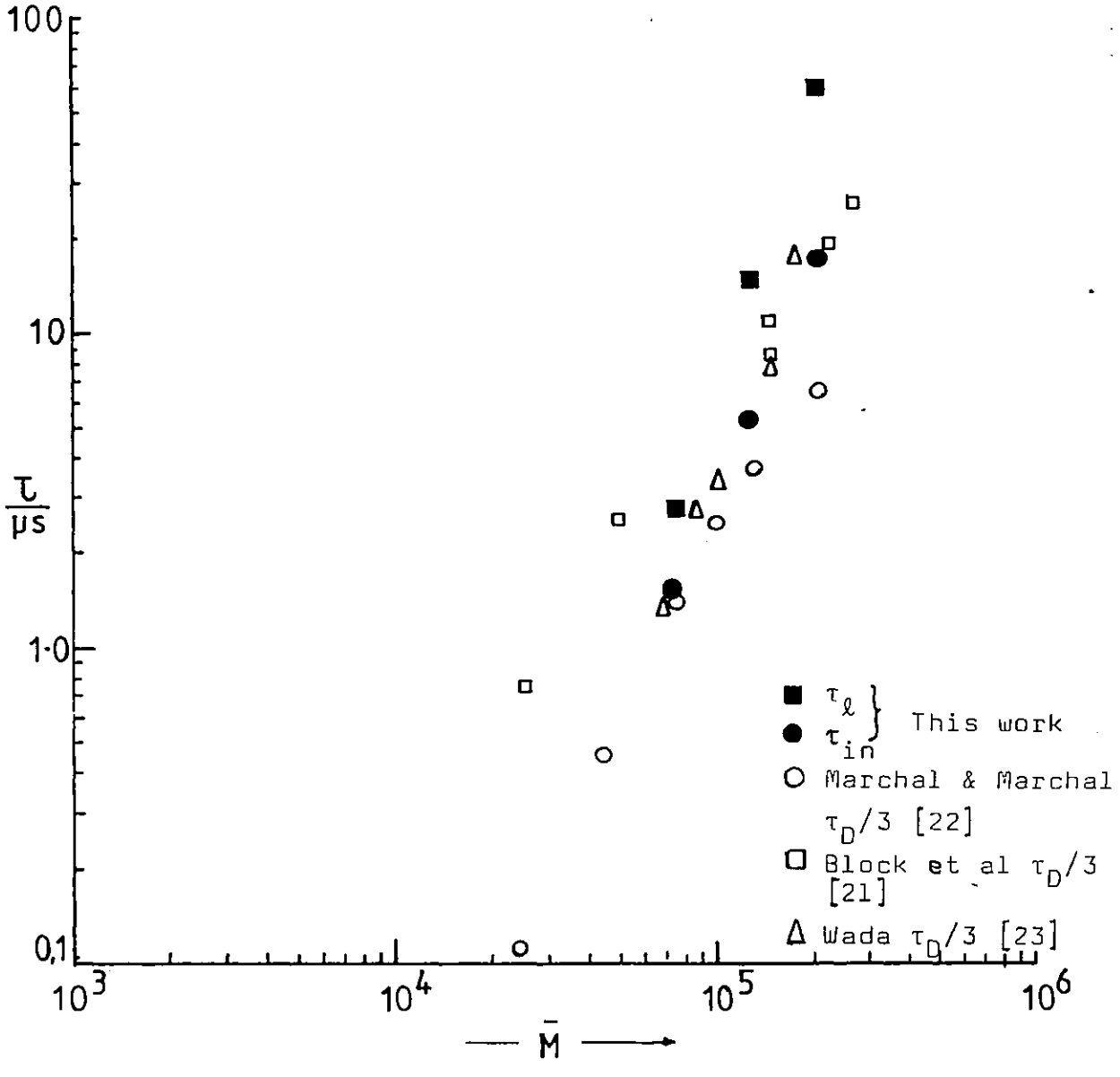

Fig 5.0 The molecular weight dependence of the infinte dilution relaxation times of PBLG results here, compared with previous results of other workers.

A typical analysis in terms of these quantities for the case of 21.2 kg m^{-3} solution of PBLG I in C-F is shown in Fig 5.1. The sharp break in the slope and the good representation of the curve by the sum of two exponentials (characterised by τ_p and τ_ℓ) is typical of all the PBLG transients in this work.

The spread factor, β (eqn 2,63) calculated for PBLG I over the concentration range 0.12 to 21.2 kg m^{-3} decreases with increasing concentration from 0.84 to 0.66, indicating that at least some of the deviation from non-exponential behaviour is due to concentration effects. Where measurements were made under comparable conditions in the two solutions DMF and C-F (see, for example, Table 5.1(a)) there was good agreement between the relaxation times after correction had been made for viscosity differences. This suggests the absence of specific solvent or aggregation effects in agreement with ealier work which has shown PBLG to be aggregate free in these solvents [72].

The effect of field strength and pulse duration

The effects of field strength and pulse duration on the observed relaxation times were studied in order to identify suitable conditions for studying the effects of concentration on the polymer dynamics. Table 5.1(b) shows results obtained on a 10kg m^{-1} solution of PBLG III in DMF at various field strengths and three pulse widths. The results reveal that the relaxation times are independent of field strength at the low field strengths employed. At high field gradients (E>350 kV m^{-1}) however, the birefringence transients became distorted (see

Table 5.1(a) Solvent dependence of relaxation time τ_{in} for a 10 kg m^{-3} solution of PBLG III

Solvents	Relaxation time τ/μs	$\tau_{in}\eta_{DMF}/\eta_{C-F}$
DMF	4.0 ± 0.1	
C-F †	3.5 ± 0.5	4.4 ± 0.6

† 0.5% Formamide in Chloroform.

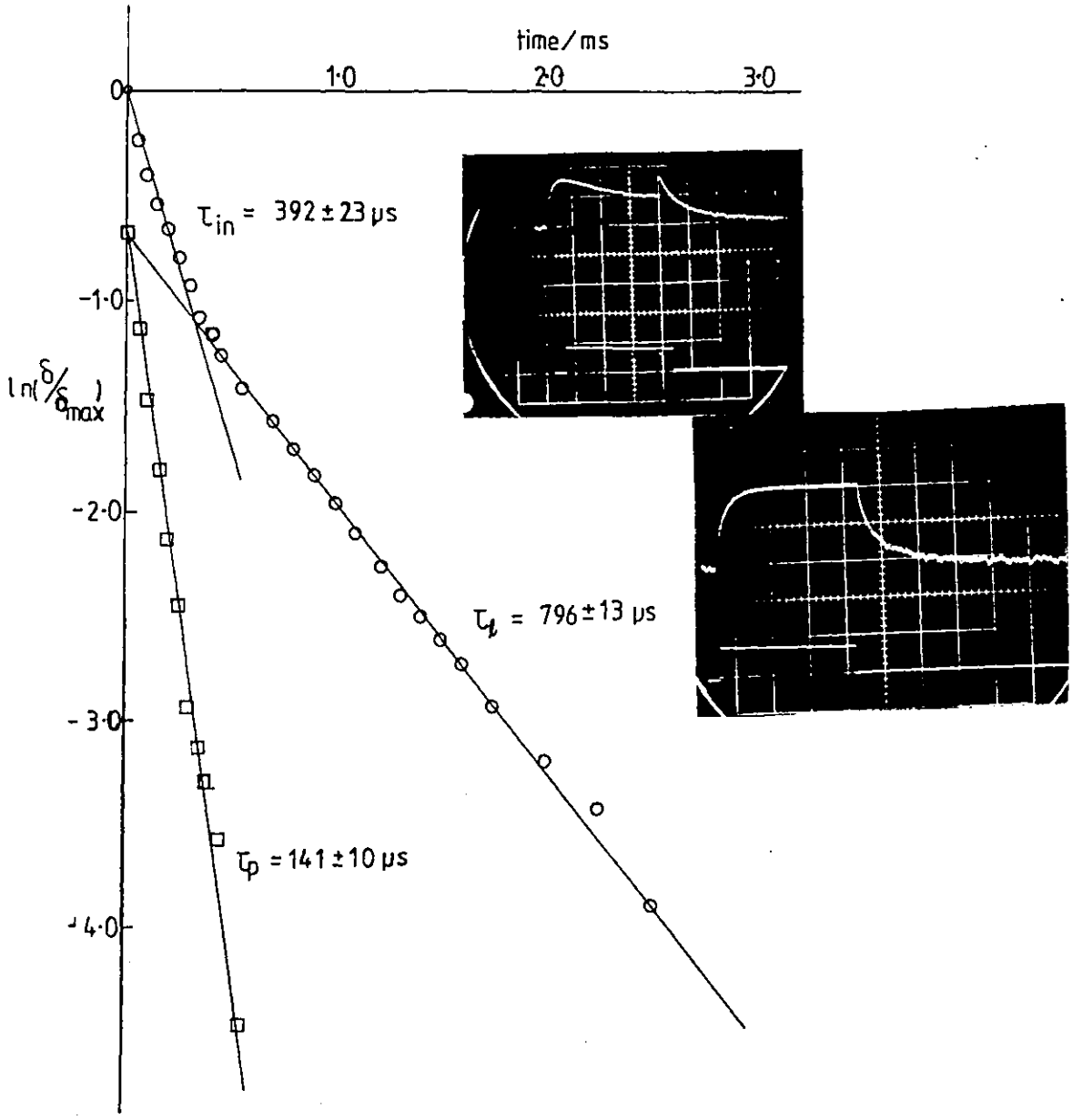

Fig 5·1 Ln δ/δ_{max} versus time/ms for PBLG I sample in chloroform-formamide, of concentration, 21·2 kg m^{-3}, pulse amplitude of 250 kV m^{-1} and duration 2·5 ms.

The inserts are the oscillograms of 10 kg m^{-3} PBLG III in DMF at field strengths 300 and 400 kV/m showing distorted signal.

Table 5.1(b) Effect of field strength and pulse width on relaxation time, τ_{in}/μs and τ_{ℓ}/μs

Pulse width (μs) \ Field, E/ kV m^{-1}		25	50	100	150
6	τ_{in}	3.1	3.0	3.1	3.2
	τ_{ℓ}	11.0	9.7	10.2	9.9
20	τ_{in}	3.0	2.9	3.3	2.9
	τ_{ℓ}	9.6	12.0	10.1	10.5
50	τ_{in}	3.0	3.3	2.9	3.1
	τ_{ℓ}	9.7	10.1	11.2	10.0

insert Fig 5.1). The birefringence reached a maximum and gradually decreased towards a steady value, and when the field was cut off it rapidly returned to the maximum steady state value before decaying to zero. However, the evaluated relaxation time, τ_{in} associated with the decay process was 3.1 μs for both the distorted and the undistorted signals, a result in good agreement with those in Table 5.1 (b) obtained at lower fields.

Normal transients were observed at relatively low field gradients. The shape of the distorted birefringence transients suggests that at high fields an additional negative birefringence component appears having a characteristic time significantly longer than the initial orientation time. This is presumably a field induced effect, possibly chain distortion or aggregation, which relaxes almost instantly as soon as the high field is removed. In all cases where this effect occurred the slope of the decay transients was identical to that obtained for undistorted transients. Consequently for the purposes of this work it did not prove necessary to investigate this phenomenon further. However, a more detailed study of the transients of this type should yield significant information on the field induced effects in helical macromolecules.

At the three pulse widths presented, the observed relaxation times were independent of the pulse duration. This implies that for this particular example steady state orientation of

the macromolecules had occurred within 6 μs, and that prolonged application of the field did not affect the subsequent relaxation process. All experiments were carried out using a pulse duration in excess of that required for equilibrium orientation of the macromolecules.

5.1.3 Dependence of relaxation times on concentration.

All measurements on concentrated solutions were conducted in the chloroform-formamide (C-F) solvent, The values of the relaxation times and the relative amplitudes for the concentrations studied are given in Tables 5.2 and 5.4. Fig 5.2 is a plot of ln τ versus ln C for the highest molecular weight sample, PBLG I. This shows that all the relaxation times have similar concentration dependence. The log-log plots each have two distinct linear regions with a sharp change in the slope at about the same concentration, which we refer to as the critical concentration, C_r. This implies a relationship of the form,

$$\tau \quad \propto \quad C^{\zeta_C} \qquad 5.1$$

Table 5.2 Relaxation times of PBLG I at 294 K

Concentration/kg m^{-3}	Relaxation times τ/μs				† A_ℓ	β
	τ_{in}	τ_e	τ_p	τ_ℓ		
0.125	18.4 ± 1	19	6.3 ± 1	34 ± 1	0.55	0.70
C* ∿0·22						
0.34	20.1 ± 1	20	7.6 ± 1	57 ± 3	0.6	0.66
0.80	33 ± 1	34	14.3 ± 1	62 ± 2	0.56	0.84
1.70	37 ± 2	37	12.1 ± 2	81 ± 3	0.52	0.76
$C_r \simeq 3.0$						
4.23	48 ± 4	50	30 ± 1	147 ± 9	0.41	0.66
10.6	163 ± 10	165	95 ± 4	515 ± 31	0.45	0.66
$C^{**} \sim 14.3$						
15	324 ± 30	340	78 ± 15	606 ± 29	0.5	0.64
21.2	456 ± 43	450	146 ± 20	815 ± 61	0.5	0.72

† $\frac{\Delta n(t)}{\Delta n_o} = A_1 \exp^{-t/\tau_p} + A_2 \exp^{-t/\tau_\ell}; \quad A_1 + A_2 = 1.0$

C_r = experimental critical concentration, C* and C** are concentrations at onset of overlapping and onset of isotropic nematic transitions respectively (see section 2.3.2)

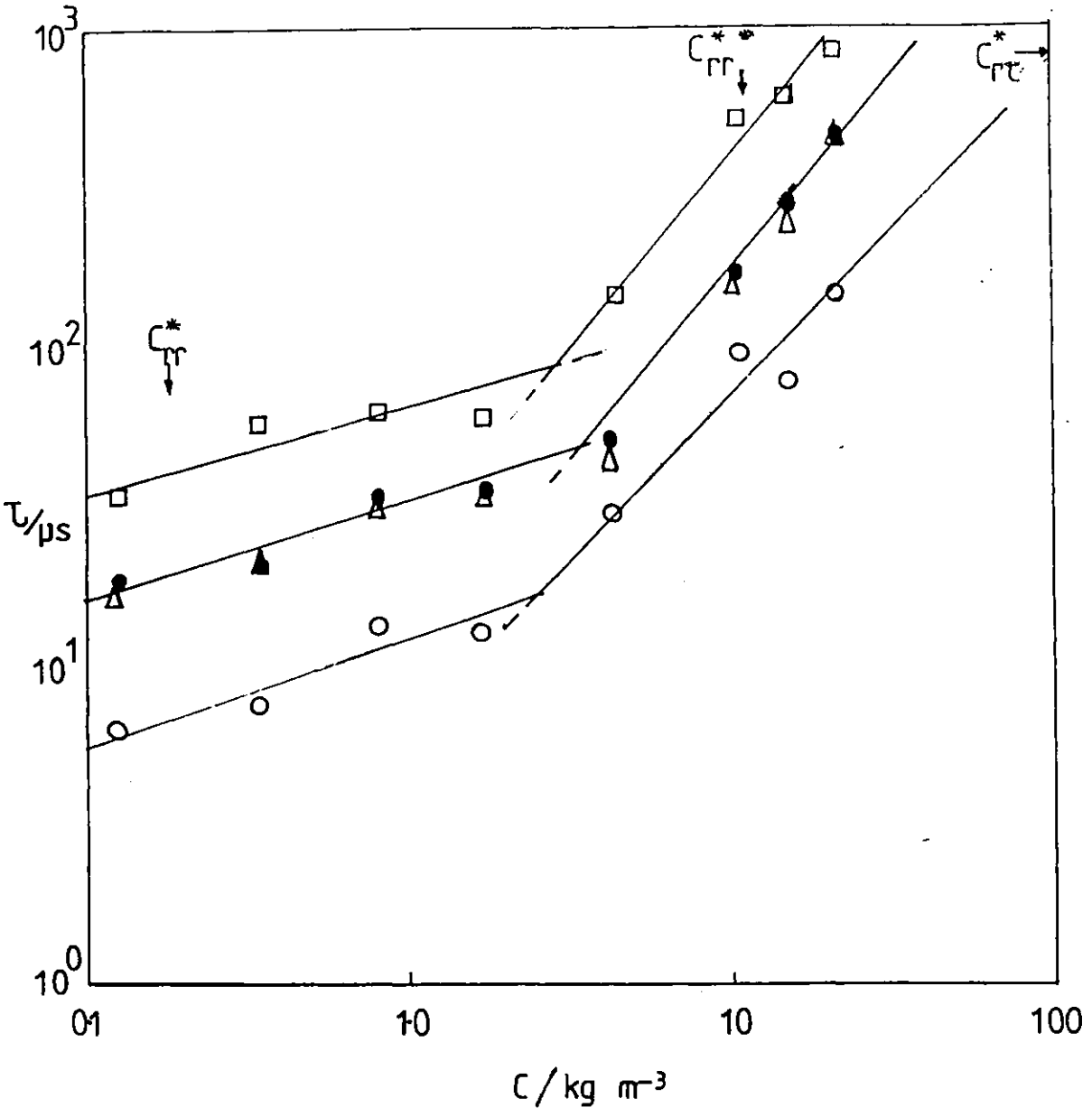

Fig 5·2 Concentration dependence of the relaxation times of PBLG I in chloroform-formamide, (C-F), τ_{in} (Δ), τ_e (●), τ_l (□), and τ_p (○).

Irrespective of the relaxation time chosen to characterise the decay transient, a sharp change was observed in the concentration dependence from a value of ζ_c=0.35 below C_r (≃3 kg m^{-3}) to a value of ≃1.2 above C_r. The values of the exponent ζ_c and the critical concentration, C_r, for the various relaxation times of all three samples are given in Table 5.3.

A comparison of the concentration dependence of the relaxation times τ_{in} and τ_{ℓ} for all PBLG samples studied is given in Figs 5.3 and 5.4 respectively. The concentration dependences of the relaxation times of all the three samples are similar. All show sharp changes over a narrow range of concentration, the plots merely being shifted along the τ and C axes. Within the limits of experimental error the concentration exponents are independent of molecular weight, but the critical concentration decreases with increasing molecular weight.

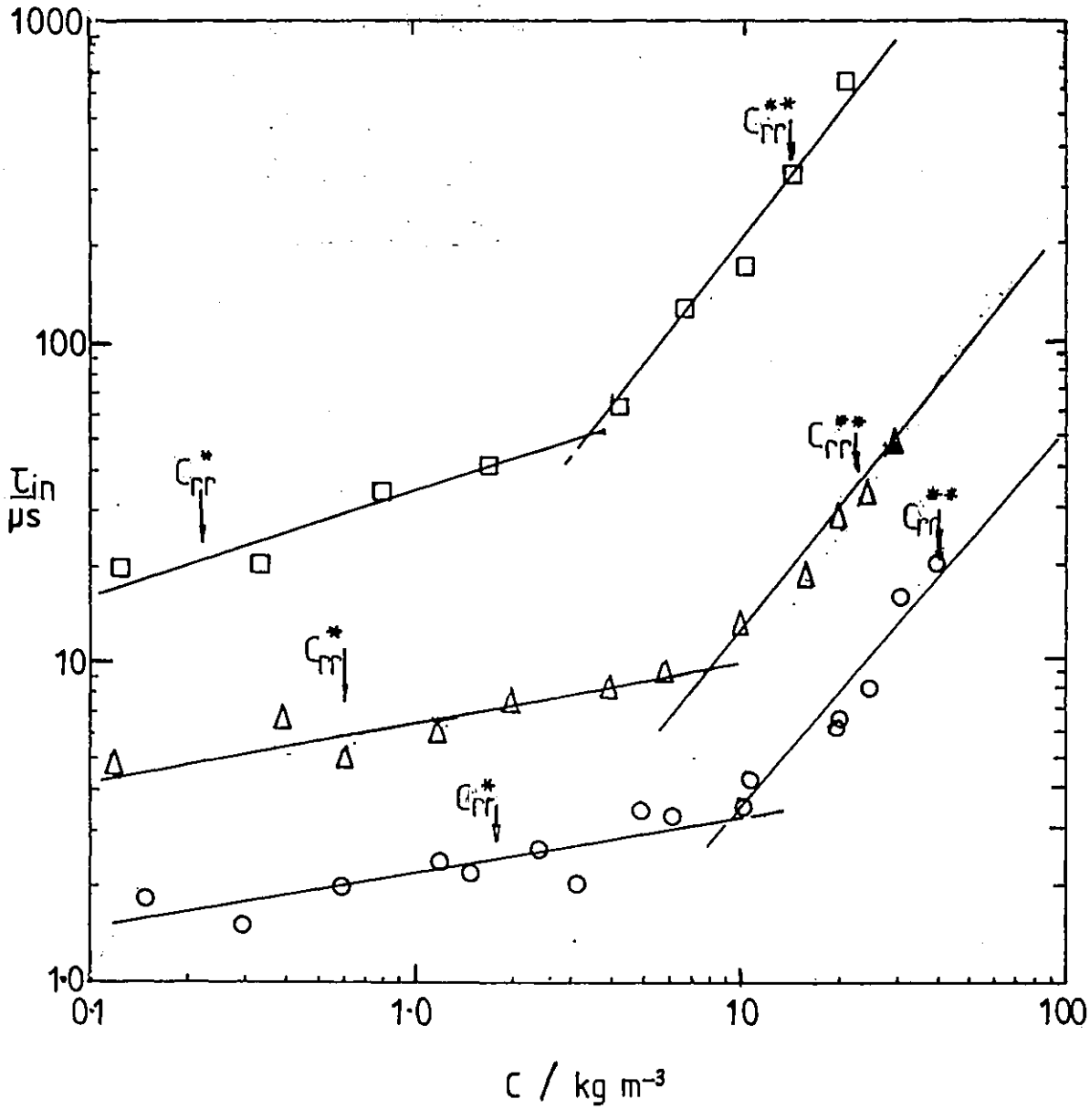

Fig 5·3 Concentration dependence of the initial relaxation times, τ_{in}, of PBLG I (□), PBLG II (Δ), PBLG III (○) in chloroform-formamide.

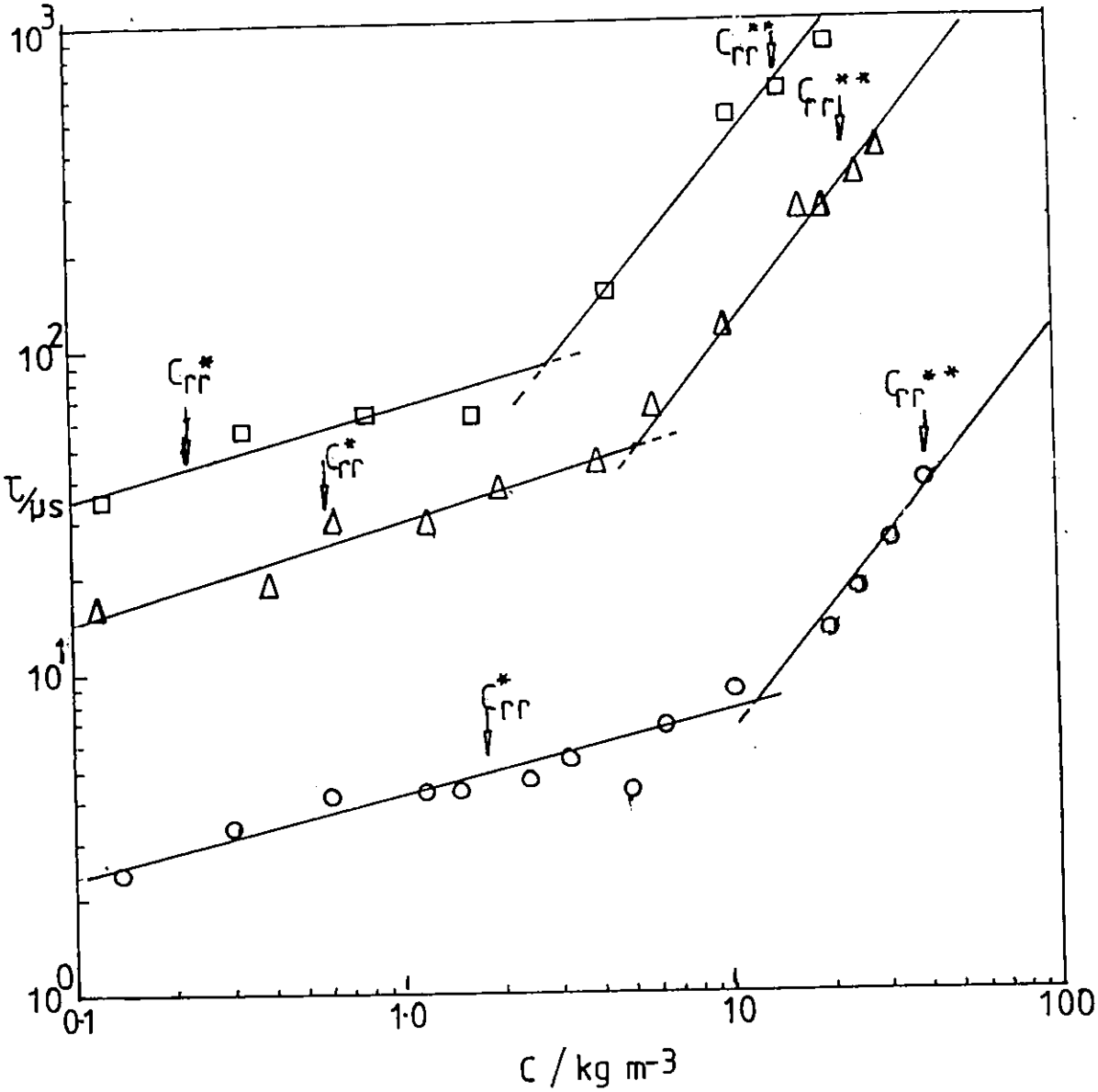

Fig 5·4 Concentration dependence of the long relaxation times, τ_L, of PBLG I (□), PBLG II (Δ), and PBLG III (○) in C - F.

Table 5.3 The exponents and the critical concentration observed in the PBLG measurements.

Sample	Relaxation type	Experimental C_r	Exponent, ξ_c	
			$C < C_r$	$C > C_r$
PBLG I	τ_{in} & τ_e	∿ 3.0	0.25 ± 0.05	1.26 ± 0.100
	τ_p		0.30 ± 0.10	1.19 ± 0.10
	τ_ℓ		0.24 ± 0.10	1.22 ± 0.10
PBLG II	τ	∿ 6.5	0.2 ± 0.03	1.20 ± 0.10
	τ_ℓ		0.29 ± 0.04	1.28 ± 0.12
PBLG III	τ	∿ 11.0	0.21 ± 0.03	1.25 ± 0.16
	τ_ℓ		0.26 ± 0.04	1.31 ± 0.15

5.1.4 Molecular weight effects

The molecular weight dependence of the relaxation times is illustrated here by choosing two concentrations one well below C_r and the other well above C_r. The concentrations were chosen such that the reduced concentration C/C_r was constant 0.12 for $C<C_r$ and 1.7 for $C>C_r$. Fig 5.5 is a plot of $\ln \tau_{in}$ against $\ln M$ for these two cases. The low concentration results are in reasonable agreement with the values obtained from the dielectric relaxation data of Block et al [21] carried out in the concentrations range 5 to 10 kg m^{-3} in trans-1,2 dichloro-ethylene saturated with DMF. The linearity of the plots for both reduced concentration again implies a relation of the form

$$\tau \quad \propto \quad M^{\zeta_m} \qquad 5.2$$

There is a small increase in the exponent, ζ_m with increasing concentration from a value of 2.2 ± 0.2 below C_r to 3.5 ± 0.8 for $C>C_r$.

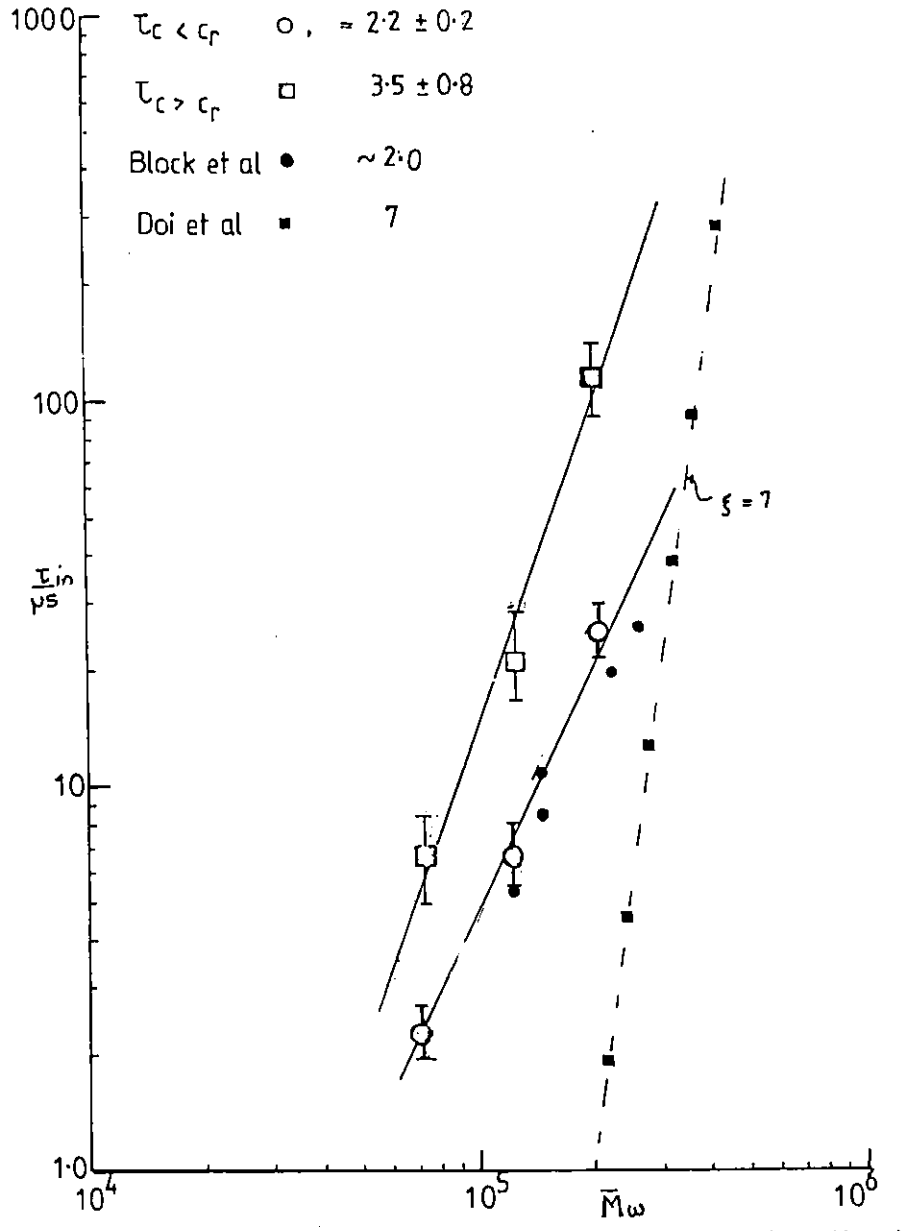

Fig 5·5 The molecular weight dependence of the relaxation times of the PBLG samples.

Table 5.4 Relaxation times of PBLG II and PBLG III

PBLG IT			PBLG III		
Concentration C, kg m^{-3}	Decay		Concentration C, kg m^{-3}	Decay	
	τ_{in}/ µs	τ_{ℓ} / µs		τ_{in}/ µs	τ_{ℓ}/ µs
0.12	4.8	16	0.15	1.8	2.3
0.40	5.3	18	0.3	1.5	3.2
C_{rr}^{*} = 0.6			0.6	2.0	4.0
0.62	6.0	30	1.2	2.4	4.2
1.2	6.2	29	1.5	2.2	4.1
2.0	7.2	36	C_{rr}^{*}= 1.8		
4.0	8.0	44	2.4	2.6	4.5
6.0	9.2	65	3.2	2.0	5.2
C_r = 6			5.0	3.3	4.1
10.0	12.5	111	6.4	3.2	6.6
17.0	18.1	260	10.5	3.9	8.8
20.0	28.2	263	C_r =		
C_{rr}^{**}			20.3	6.5	13.2
25.0	31.5	336	25.4	8.2	17.0
30	48	397	31.0	16.0	24.0
			40.0	20.0	38.0
			C_{rr}^{**} =41		

5.1.5 Discussion

As concentration increased, a sharp change in ζ_c was observed at some critical concentration C_r. This is in qualitative agreement with the predictions of Doi and Edwards (DE) [4] (see section 2.3.2) that at some concentration near molecular overlap, a significant change from dilute solution type behaviour to moderately dilute should occur. The extent to which the experimental results agree quantitatively with the DE theory can be examined as follows.

The volume swept out in space by a chain by virture of its rotational motion is given by

$$V_m = \frac{4}{3}\pi r_m^3 \qquad 5.3$$

where r_m is an appropriate chain dimension defining its spatial extent. For a rigid rod of length L, r_m=L/2 while for a random coil chain it is appropriate to take r_m equal to the radius of gyration R_G. The mean number of chains, n_U, occupying this volume V_m is

$$n_U = \frac{1000\ C\ N_A V_m}{M} \qquad 5.4$$

where C is the concentration in kg m^{-3}, N_A is the Avogadro's number, and M the molecular weight(in grams). As long as ,n_U, in such a volume, V_m is less than one the system is considered to be dilute but chain interactions begin to increase markedly for n_U>1. The critical concentration for this onset of inter-chain 'entanglements' occurs when n_U=1 and is given as

$$C^*_{kg\ m^{-3}} = \frac{M}{1000 N_A V_m} \qquad 5.5$$

For rigid rod type molecules, another critical concentration C** at which the isotropic-nematic transition should occur can be estimated by defining a characteristic volume V_m' = $\pi r_m^2 d$ where r_m=L/2 and d is the rod diameter. C** is the concentration at which n_U reaches 1 for this volume i.e.

$$C^{**}_{kg\ m^{-3}} = \frac{M}{1000 N_A V_m'} \qquad 5.6$$

Table 5.5 gives the values of C* for PBLG I, II and III calculated assuming the molecules to be (a) rigid rods (C^*_{rr}) and (b) random coils, C^*_{rc} (assuming $R_G = n^{\frac{1}{2}}\ell/\sqrt{6}$ where ℓ = monomer length and n is the degree of polymerisation) and of C**

Table 5.5 The critical concentration parameters for PBLG. All concentrations, C, in kg m^{-3}.

Sample	Experimental C_r	Calculated			Ratio $\frac{C_r}{C^*_{rr}}$
		C^*_{rr}	C^{**}_{rr}	C^*_{rc}	
PBLG III	11.0	1.8	40.6	20500	6.1
PBLG II	6.5	0.6	23.3	15600	10.6
PBLG I	3.0	0.22	14.3	12200	13.6

assuming rigid rod behaviour . The rigid rod values are also marked on Figs 5.2, 3 and 4 . The DE theory is designed to cover the concentration range $C^*_{rr} \leqslant C \leqslant C^{**}_{rr}$. The relaxation data obtained experimentally cover the whole DE concentration range up to C^{**}_{rr} and provide a good test of the applicability of the theory to synthetic polypeptides.

In terms of those two models, the PBLG samples are much closer to rigid rods than random coil macromolecules. The experimentally observed critical concentrations, C_r certainly confirm this although they are significantly greater than the calculated C^*_{rr} values ($C_r/C^*_{rr} > 6$, see Table 5.5).

The concentration exponent, $\zeta_{C>C_r} = 1.2$ is rather low compared with the DE predicted value of $\zeta_{C>C_r} = 2$. At low concentrations, $C<C_r$, the molecular weight exponent ζ_m of 2.2±0.2 is less than the value of 3 expected for perfectly rigid rod macromolecules (eqn 2.6). This is consistent with the dielectric observation of Block et al [21] and can be attributed to some degree of chain flexibility. At high concentration $C>C_r$, the ζ_m value of 3.5±0.8 is significantly lower than the the DE prediction of $\zeta_m=7$. In view of the deviation of ζ_m from the rigid rod value at low concentrations, it is not unexpected that $\zeta_{m,(C>C_r)} < \zeta_{m,DE}$ although the extent of the discrepancy with the DE value is surprising.

The present results contrast with Maguire's recent publication on Kerr relaxation studies of rigid rod viruses which showed $\zeta_c \simeq 2$ and $\zeta_m \simeq 5.7$. This suggests that DE behaviour is

only approached by extremely rigid systems and that any flexibility in rod-like leads to a marked reduction in both τ_c and τ_m. These findings are consistent with other work on PBLG and similar α-helical molecules. Fig 5.6 shows plots of the relaxation times obtained in this work for PBLG I (M_w=210000) ploted alongside those of Tsuji and Watanabe [32] and of Tinoco [86] on PBLG of M_w=310000 and 350000 respectively both in dichloroethane. The concentration (10 to 90 kg m^{-3}) covered by Tsuji et al is far in excess of both C* (0.10 kg m^{-3}) and C** (7.5 kg m^{-3}) for their molecular weight. Even in this regime the concentration exponent, ζ_c, = 1.5 is still below the DE prediction of 2 . These data are consistent with the present results in the region of overlap. Tinoco's results at lower concentrations appear consistent with Tsuji's work. These two sets of data taken together show behaviour analogous to that observed in this work, with $\zeta_{C<C_r} \sim 0.2$ and $\zeta_{C>C_r} \sim 1.5$.

It is interesting to note that an electro-optic study of the chain dynamics of another α-helical molecule, paramyosin by Delaney and Krause, [75] (see Fig 5.6) shows similar behaviour to that observed here for PBLG. These workers obtained Kerr relaxation times for this molecule ($\bar{M}$ = 210000 and C_{rc}= 0.32 kg m^{-3}) in 1mM citrate buffer at 293 K, over a range of concentrations. Their data has been reanalysed and shows abrupt change in the concentration exponent from ζ_c=0.1 to ζ_c =0.56 at a concentration of $C_r \simeq$ 0.8 kg m^{-3}. As for PBLG, C_r is significantly greater than C*. However, the concentration exponent ζ_c for $C>C_r$ is only about half that observed for PBLG.

For PBLG, therefore, although the dependence of relaxation times, τ, on concentration and molecular weight in concentrated solution is in qualitative agreement with the DE model, the values of the exponents are significantly lower than those predicted by the theory. One reason for this discrepancy is probably that the PBLG, α-helix is not perfectly rigid and that the rods become increasingly flexible as molecular weight increases. In addition, there are likely to be significant long range interactions between these polar molecules which were neglected in the DE treatment, where the rods were only considered to interact on contact. The critical concentrations at which there was a marked change in the observable effect of chain interactions on the rotational relaxation times were

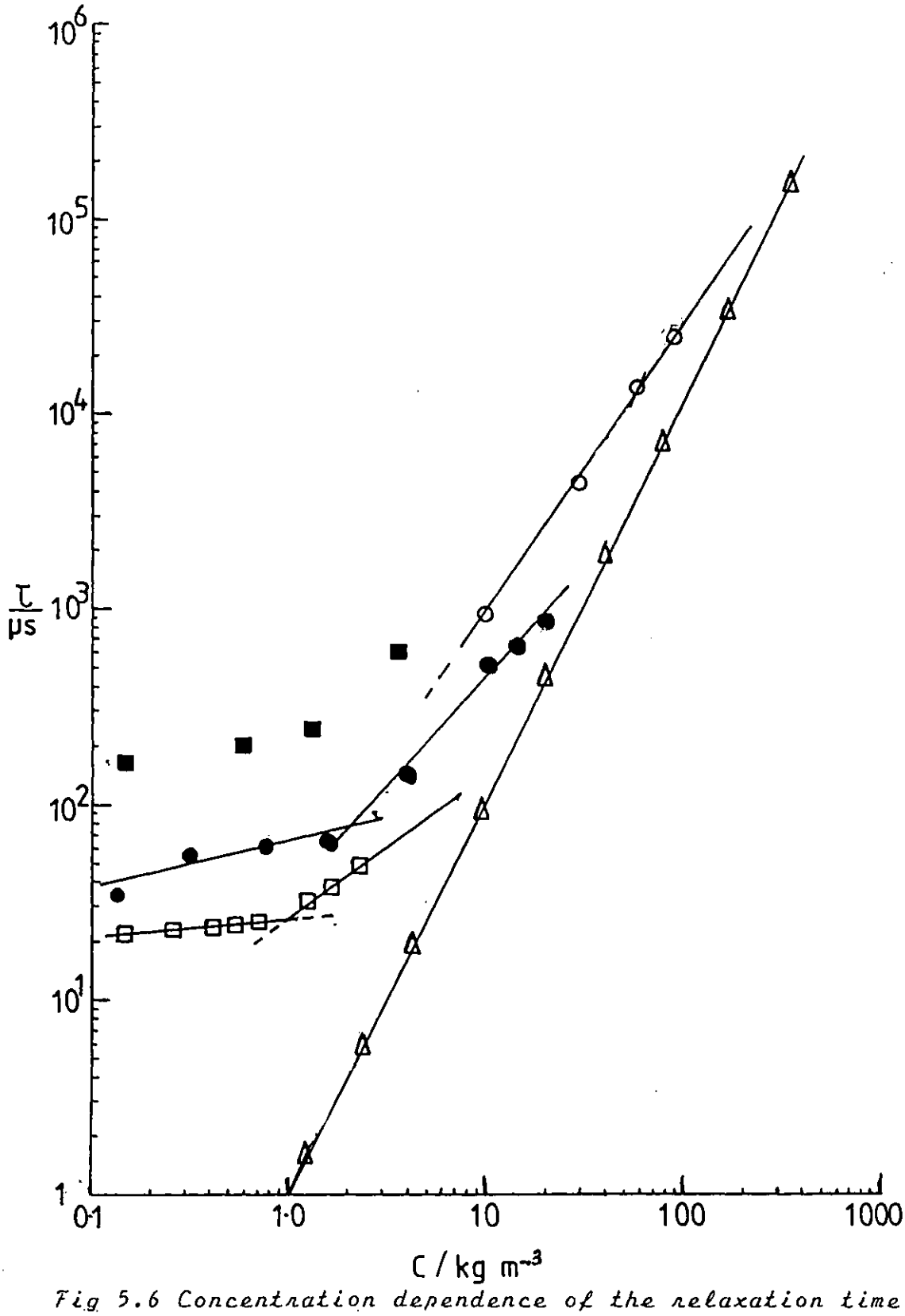

Fig 5.6 Concentration dependence of the relaxation time results for various α-helical molecules: PBLG Tsuji and Watanabe(○), PBLG this work(●), Paramyosin, Delaney and Krause (□), Tinoco (■) and theoretical prediction of Doi and Edwards(——△——)

in all cases greater than those expected on the basis of rigid rod overlap. This is again an indication that chain flexibility causes qualitative changes in the rotational dynamics to occur at higher concentrations than would be expected for rigid sytems. The ratio C_r/C^* may be taken as an indication of chain flexibility for these rod-like molecule.

The observed values of the ratio $C_r/C^*_{rr} > 6$ suggest an alternative explanation for the change in concentration dependence of τ. In a system of rotating rods, although interactions will begin to increase once the mean separation between centres a_c, is less than the rod length L (i.e. at C*), the restrictions on relative rotational motion might be expected to increase significantly once a_c becomes less than L/2. To see this, consider two molecules as in Fig 5.7. For the case $L > a_c > L/2$, rotation of the molecule A will cause molecule B to rotate in a sense which does not increase its interaction with A. However, once $a_c < L/2$, rotation of A causes B to rotate in such a way that A-B interactions are maintained or even increased. Although such an argument is obviously crude, it does suggest that a qualitative change in the effect of concentration on rotational motion might be expected when $a_c = L/2$ i.e. by evaluating V_m in eqn 5.3 using $r_m = L/4$ rather than L/2. This would increase C* by a factor 8 and bring the observed C_r values more into line with expectation. The extent to which this effect may contribute obviously needs more quantitative investigation.

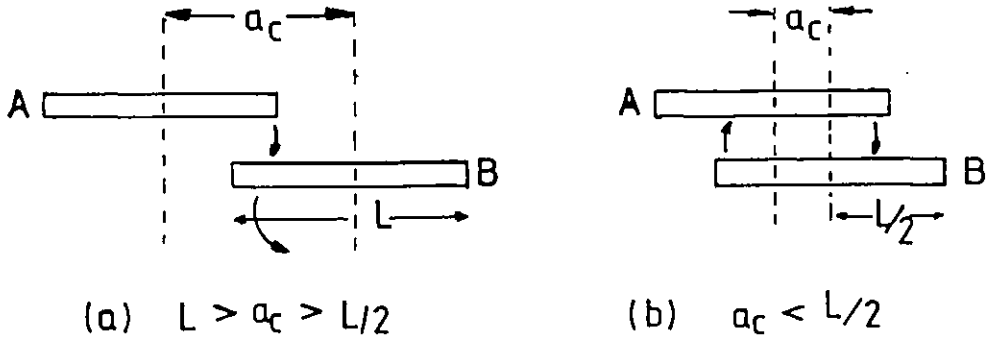

Fig 5.7 Probable rotational model of a rigid rod under varying degree of mean separation, a_c in an 'entangled' polymer solution.

5.2 Poly (n-butyl isocyanate), PBIC.

PBIC has been shown to possess a helical coil chain conformation and to behave as an essentially rigid rod for low molecular weights [24,25, 36]. The precise limiting molecular weight for such behaviour is a matter of some contention, but appears to lie in the range 10^4 - 10^5 [36]. Significant chain flexibility is encountered for molecular weights in excess of 5×10^5 [24,36].

The present experiments were designed to study the effects of concentration on the rotational dynamics of weakly flexible chains of this type. The three samples of PBIC studied had molecular weights of (a) PBIC #21 $M_w = 1.33 \times 10^5$ and $Z_p = 1.1$ (b) PBIC #29 $M_w = 6.4 \times 10^5$ and $Z_p = 4.6$ and (c) PBIC CN-1, $M_w = 1.3 \times 10^6$ and $Z_p = 1.0$. All the experiments were conducted in carbon tetrachloride solutions.

A representative normalised birefringence ($\Delta n(t)/\Delta n_{max}$) transient typical of those obtained for all the PBIC solutions studied is shown in Fig 5.8. The decay transients are faster than the rise transients. As was observed in the dilute solution

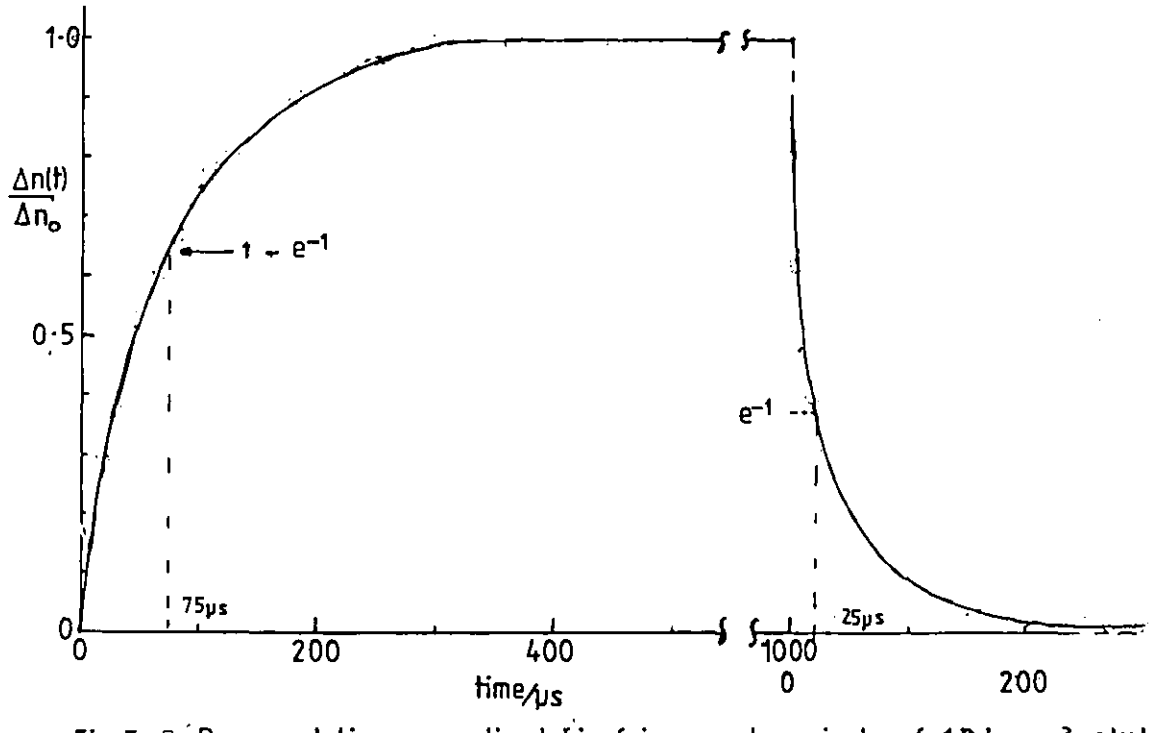

Fig 5·8 Representative normalised birefringence transient of 1·0 kg m^{-3} solution of PBIC #21 under a field of 400 kV/m and pulse width, 1·0 ms at 294 K.

(see section 3.7) the ratio of the characteristic relaxation times of the rise, τ_r, and the decay, τ_e transient for this case is 3.0 ± 0.4. This indicates a rotational diffusion mechanism for the dynamics, and that orientation is dominated by the permanent chain dipole. The ratio τ_r/τ_e was found to be 3.0 ± 0.5 for all the PBIC solutions studied in this work, suggesting that this same mechanism persisted up to the highest concentration examined.

The plots of $\ln \delta(t)/\delta_{max}$ versus time were found to be curved as in Fig 5.9 . Again the transient was characterised in terms of the four relaxation times τ_{in}, τ_ℓ, τ_p, and τ_e . In general the decay birefringence curves could be well represented by a two term exponential fit, characterised by the relaxation times τ_ℓ and τ_p.

5.2.1 Concentration dependence of the relaxation times

The relaxation times obtained for the lowest molecular weight sample PBIC #21 at various concentrations are given in Table 5.6 and plotted in the form $\ln \tau$ versus $\ln C$ in Fig 5.10. All four relaxation times show significant concentration dependence with no change in the concentration exponent over the concentration range studied, which extends into the region for which significant rod overlap should be occurring. The most marked dependence on concentration is exhibited by the long relaxation times, τ_ℓ and by τ_e for which the exponents ζ_c are found to be 0.47±0.07 and 0.65±0.11 respectively. The fastest relaxation time τ_p also shows significant concentration dependence with an exponent ζ_c of 0.37±0.14, whilst the time characterising the initial slope, τ_{in} is somewhat less concentration dependent, with ζ_c=0.22±0.2.

The relaxation measurements conducted on the intermediate molecular weight (unfractionated) sample PBIC #29 are given in Table 5.7 and plotted in Fig 5.11. At low concentrations all four relaxation times are only weakly dependent on concentration (ζ_c 0.1 - 0.2). However above C_r, 0.9 kg m^{-3} there is an abrupt change in the concentration dependence of τ_ℓ, τ_e, and τ_{in} and ζ_c rises to 0.5. For the fastest relaxation time τ_p, however, no such sharp change is observed and the exponent, τ_c remains ~0.1 up to the highest concentrations

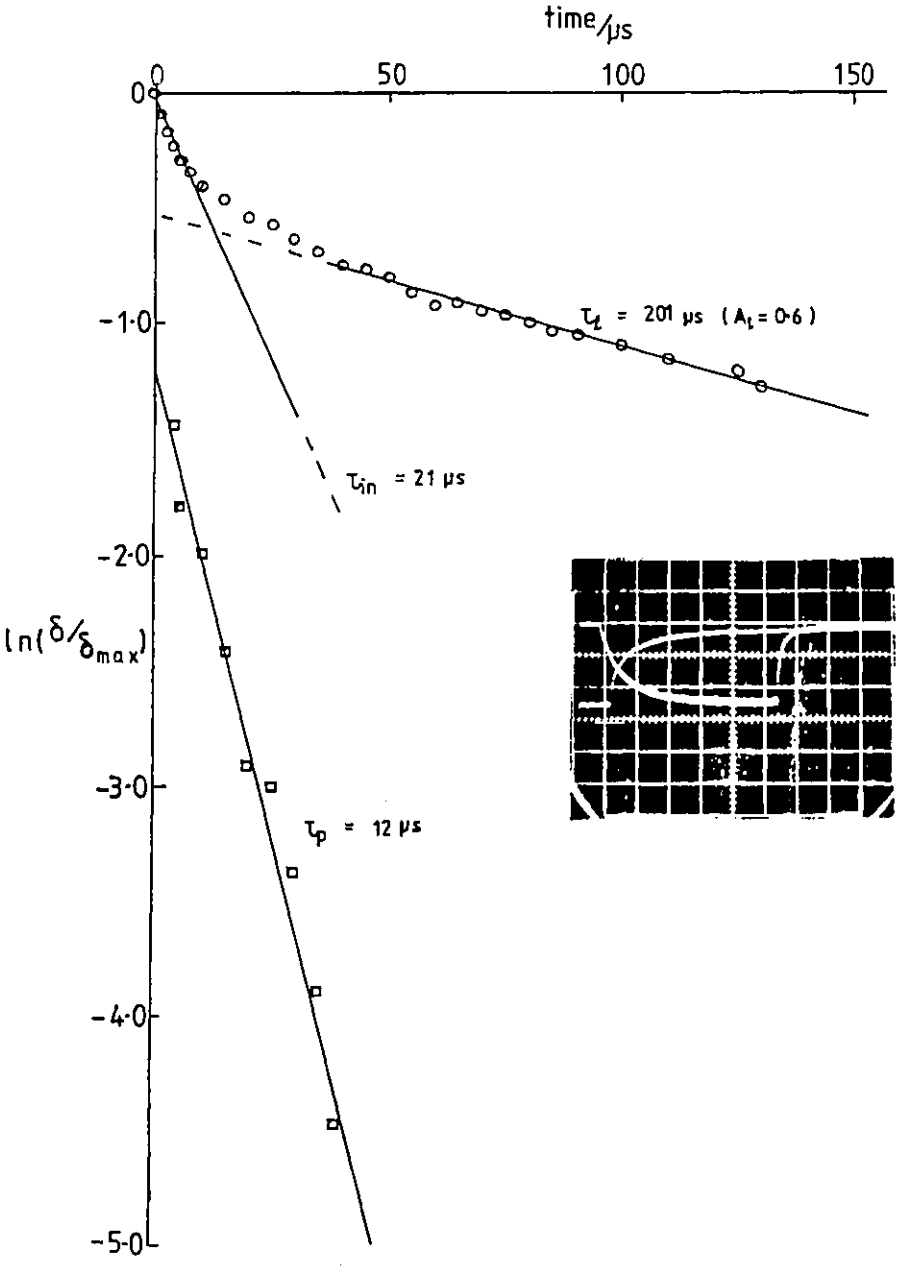

Fig 5·9 A representative plot of $\ln(\delta/\delta_{max})$ versus time/μs for 1·3 kg m^{-3} PBIC #21 decay transient. Field, E = 400 kV/m, and pulse width 1·0ms.

The insert is the oscillogram showing the full birefringence on 200μs/cm and the expanded decay transient on ~50μs/cm.

Table 5.6 Concentration dependence of rotational relaxation times for the PBIC #21 sample in CCl_4 at 294 K

Concentration C/kg m^{-3}	Relaxation times τ / μs			
	τ_{in}	τ_e	τ_p	τ_ℓ
$C^* = 0.1$				
0.5	20.0 ± 2.0	27.8 ± 3.4	6.1 ± 0.6	72.3 ± 14
0.73	24.3 ± 2.4	33.0 ± 13.0	7.7 ± 1.9	90.0 ± 24
0.88	19.8 ± 3.7	33.0 ± 6.0	7.8 ± 1.2	82.2 ± 32
1.0	21.1 ± 7.7	30.0 ± 8.0	8.2 ± 1.5	97.5 ± 20
1.34	39.4 ± 7.2	46.0 ± 13.0	11.3 ± 3.8	118.0 ± 13
1.73	23.3 ± 5.3	60.0 ± 4.2	7.8 ± 1.3	129.0 ± 24
3.46	30.8 ± 3.3	78.0 ± 12.0	14.4 ± 5.3	168.0 ± 47
$C^{**} = 9.8$				

Standard deviation based on over five measurements.

Table 5.7 Concentration dependence of rotational relaxation times for the PBIC #29 sample in CCl_4 at 294 K

Concentration C kg m^{-3}	Relaxation times τ / μs			
	τ_{in}	τ_e	τ_p	τ_ℓ
$C^* = 0.0043$				
0.024	29. ± 3	64.0 + 2	17	205 ± 37
0.053	49.0 ± 4	88.0 ± 3	13	308 ± 45
0.107	42.0 ± 4	130· ± 14	20	360 ± 66
0.53	46.0 ± 5	178· ± 17	18.5	486 ± 21
0.75	53.0 ± 5	143· ± 4	17	378 ± 56
C_r 1.0				
1.07	62.0 ± 6	207 ± 40	21	420 ± 12
2.67	64.0 ± 22	310 ± 46	27	662 ± 134
3.67	115.0 ± 21	311 ± 62	26	915 ± 25
5.34	143.0 ± 3	390 ± 42	23	1350 ± 56

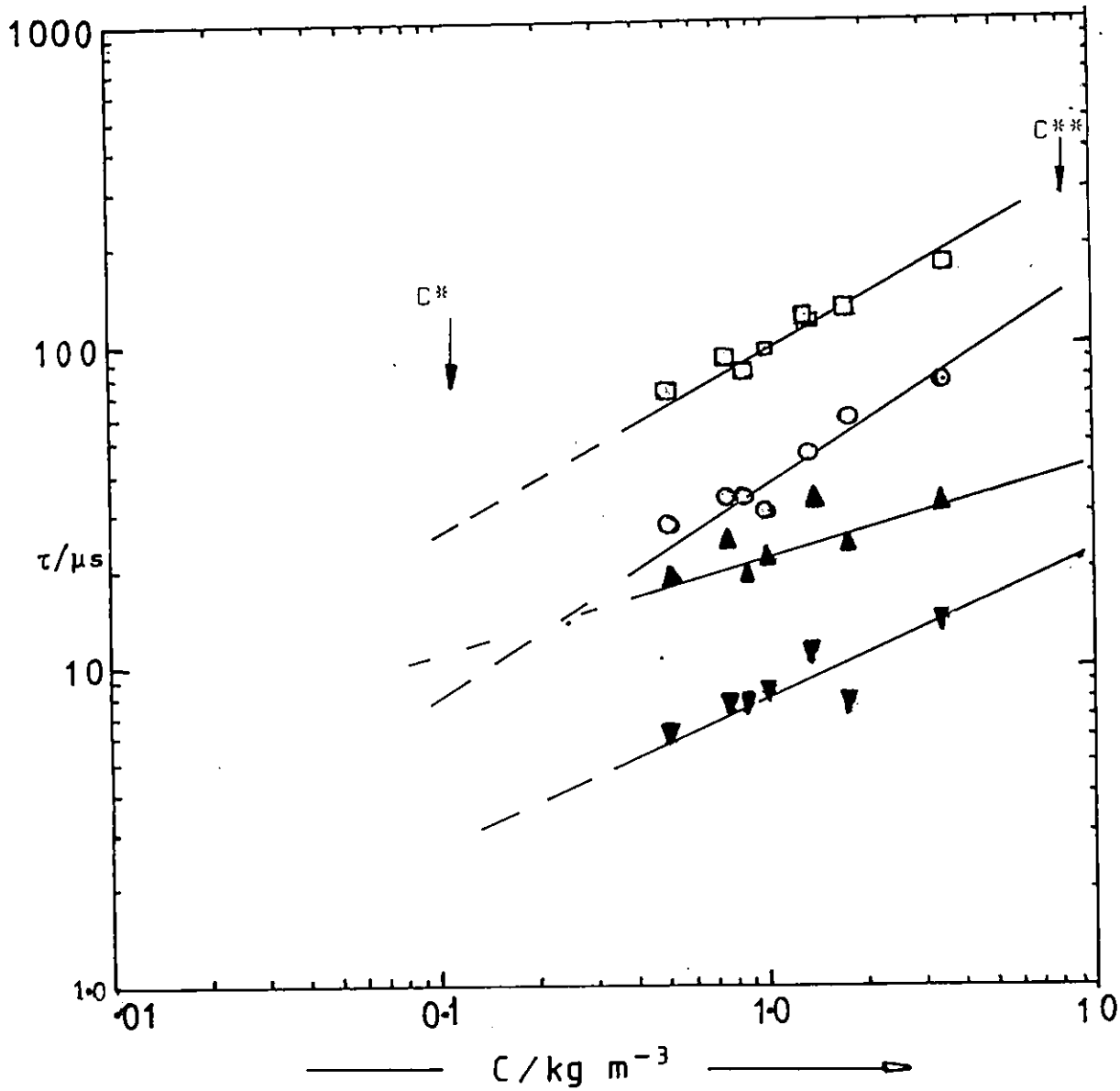

Fig 5.10 The concentration dependence of the relaxation times, τ_ℓ(□), τ_e(⊙), τ_{in}(▲) and τ_p(▼) for PBIC #21.

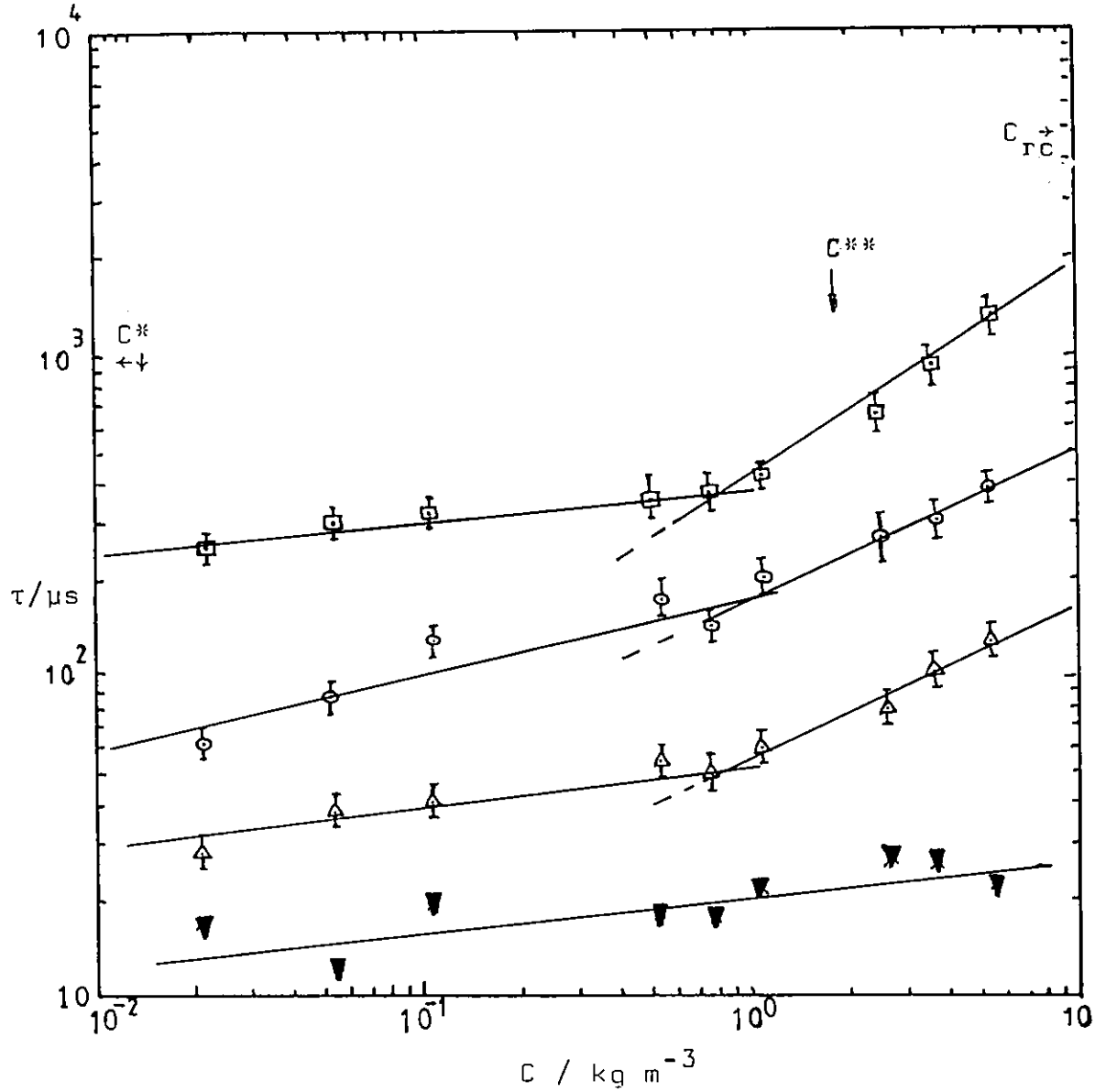

Fig 5.II The concentration dependence of the relaxation times of PBIC #29, τ_ℓ(□), τ_e(○), τ_{in}(△), τ_p (▼).

studied. The values of C_r and ζ_c for the various relaxation times are summarised in Table 5.8.

Results for the highest molecular weight sample PBIC CN-1 studied are tabulated in Table 5.9 and are plotted in Fig 5.12. Again τ_ℓ, τ_e and τ_{in} show an abrupt change in concentration dependence from ζ_c= 0.21 below C_r (=0.22 kg m^{-3}) to ζ_c= 0.5 above C_r, with τ_p exhibiting no change in ζ_c(=0.3) at C_r.

A direct comparison of the concentration behaviour of τ_ℓ for the three samples is shown in Fig 5.13. The data for both the PBIC CN-1 and PBIC #29 samples lie on two distinct straight lines of different slopes, whereas no break in slope is observed for PBIC #21. The intersection of the two linear regions occurs at a critical concentration, C_r, which shifts to higher values with decreasing molecular weight.

5.2.2 Molecular weight effects.

The molecular weight dependence of the relaxation times above and below the critical concentration C_r, is illustrated by choosing two reduced concentrations : C/C_r = 0.14 and C/C_r = 1.8((Fig 5.14). Since there was no critical concentration observed in the case of the lowest molecular weight sample, PBIC #21, (see Fig 5.10) the comparison has also been made at two values of C/C^* (=13 and 30), using C^* values from eqn. 5.3 assuming PBIC to be rigid rod. However this method of comparison based on equal values of C/C^* (y say) covered only the low concentration regimes of the three samples i.e. in all cases $C = yC^* < C_r$.

It is difficult to draw firm conclusions regarding the molecular weight dependence of the relaxation times from the $\ln \tau$ - $\ln M_w$ plots of Fig 5.14 since only three samples were studied and the intermediate sample PBIC # 29 had a considerably broader MWD (Z_p=4.6) than the other two samples. However in general ζ_m for τ_ℓ is somewhat lower than τ_e and for the two highest molecular weight samples there appears to be no significant change in ζ_m as C is increased through the critical concentration C_r. Even allowing for the large uncertainties in ζ_m due to the restricted range of M over which the studies were made it is clear that the molecular weight dependence in the concentrated region is significantly lower than that

Table 5.8 The exponents and the critical concentration observed in the PBIC measurements.

	Relaxation type	Exp. C_r/kg m^{-3}	Exponent		Calculated C/ kg m^{-3}	
			$C < C_r$	$C > C_r$	C^*	C^{**}
PBIC 21	τ_{in}	-	0.22 ± 0.20	-	0.10	9.8
	τ_e		0.65 ± 0.11			
	τ_ℓ		0.47 ± 0.07			
	τ_p		0.37 ± 0.14			
PBIC 29	τ_{in}	0.9	0.13 ± 0.01	0.45 ± 0.05	0.004	2.05
	τ_e		0.15 ± 0.06	0.46 ± 0.05		
	τ_ℓ		0.10 ± 0.06	0.63 ± 0.07		
	τ_p		0.20 ± 0.11			
PBLG CN-1	τ_{in}	0.22	0.20 ± 0.11	0.68 ± 0.06	0.001	1.0
	τ_e		0.17 ± 0.10	0.52 ± 0.12		
	τ_ℓ		0.23 ± 0.12	0.51 ± 0.08		
	τ		~ 0	-		

standard deviation based on computer fit.

Table 5.9 Concentration dependence of the rotational relaxation times for P8IC CN-1 sample in CCl_4 at 294 K

Concentration C/ kg m^{-3}	Relaxation times $\tau/\mu s$			
	τ_{in}	τ_e	τ_p	τ_ℓ
C^*				
0.015	130 ± 18	430	70	600
0.021	163 ± 6	343 ± 166	41	436 ± 50
0.025	250 ± 10	550 ± 75	48	642 ± 30
0.038	169 ± 17	298 ± 35	35	685 ± 123
0.05	268 ± 30	618 ± 60	91	710 ± 110
0.10	345 ± 5	573 ± 60	117	811 ± 75
0.25	367 ± 47	793 ± 44	130	938 ± 61
0.28	410 ± 21	741 ± 31	123	1538 ± 59
0.50	669 ± 29	992 ± 63	170	1705 ±± 77
1.00	1122 ± 88	1100 ± 270	125	3116 ± 151
2.01	1434 ± 298	2530 ± 680	168	3362 ± 160

the quoted errors are the standard deviation based on at least three measurements on each concentration.

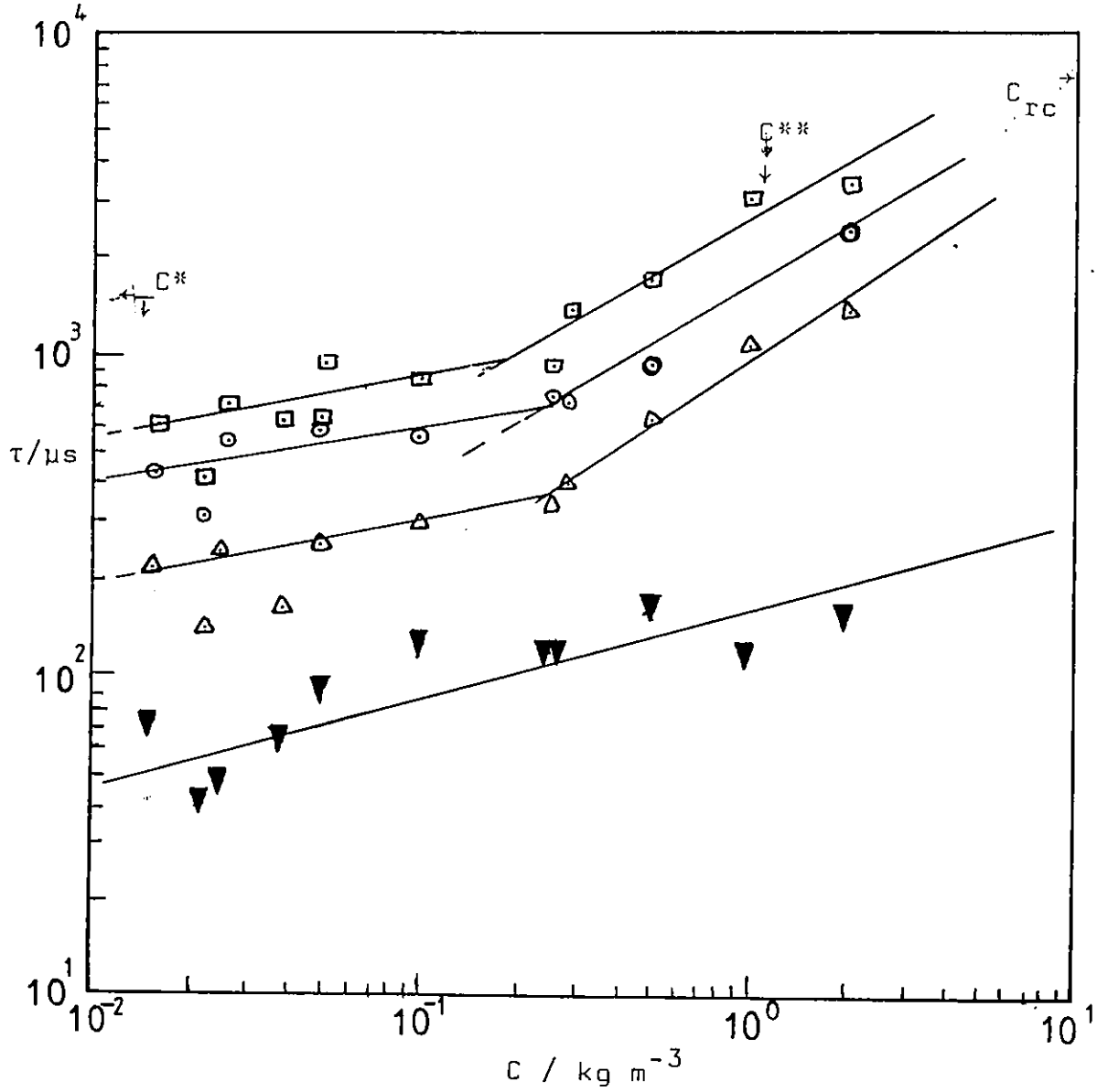

Fig 5.12 Concentration dependence of relaxation time of PBIC CN-I; τ_ℓ (□), τ_e(○), τ_{in} (△), τ_p(▼).

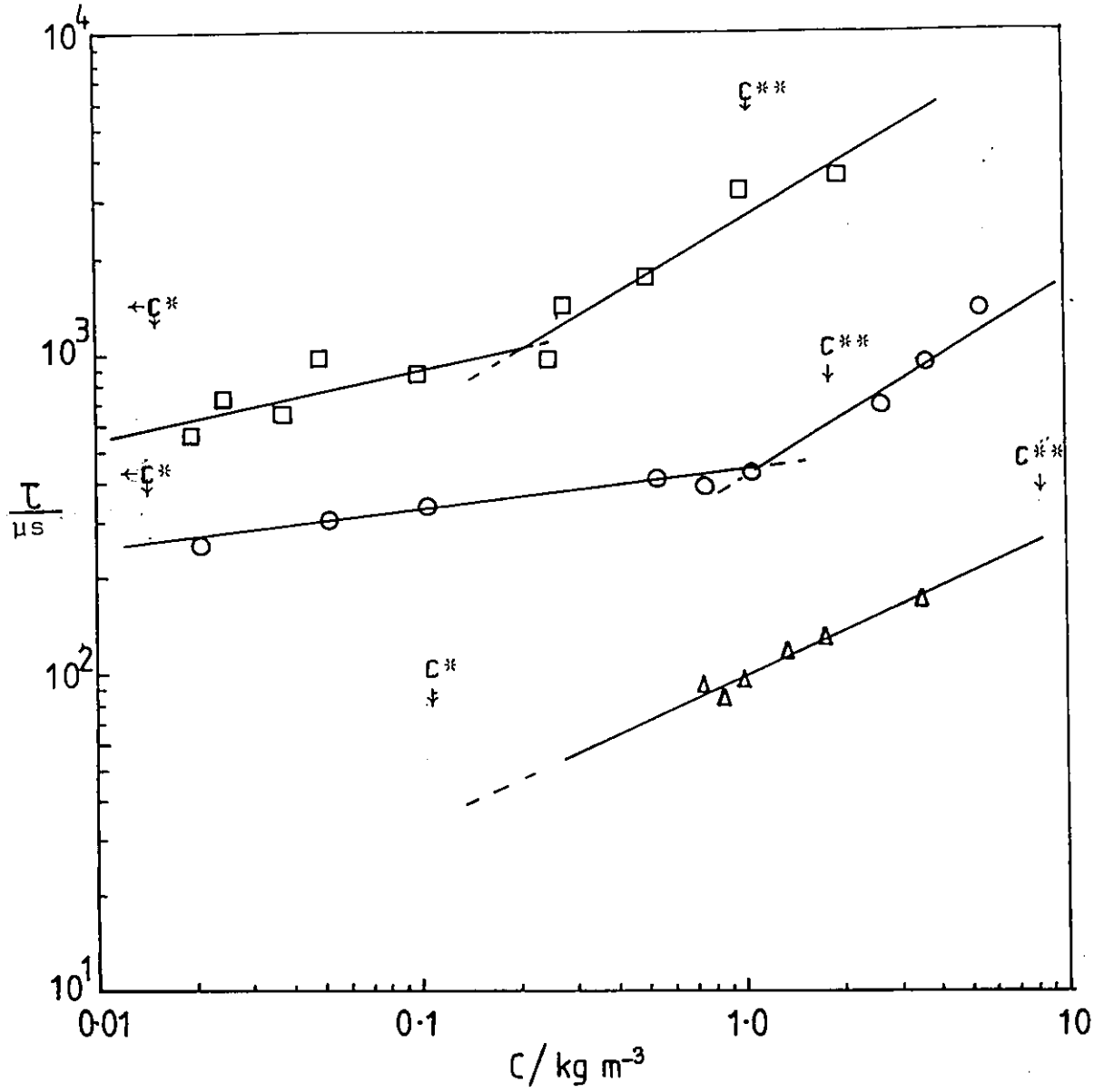

Fig 5·13 Concentration dependence of the long relaxation times, τ_l for poly(butyl isocyanate) PBIC #21 (▲), PBIC #29 (○), and PBIC CN-1 (□).

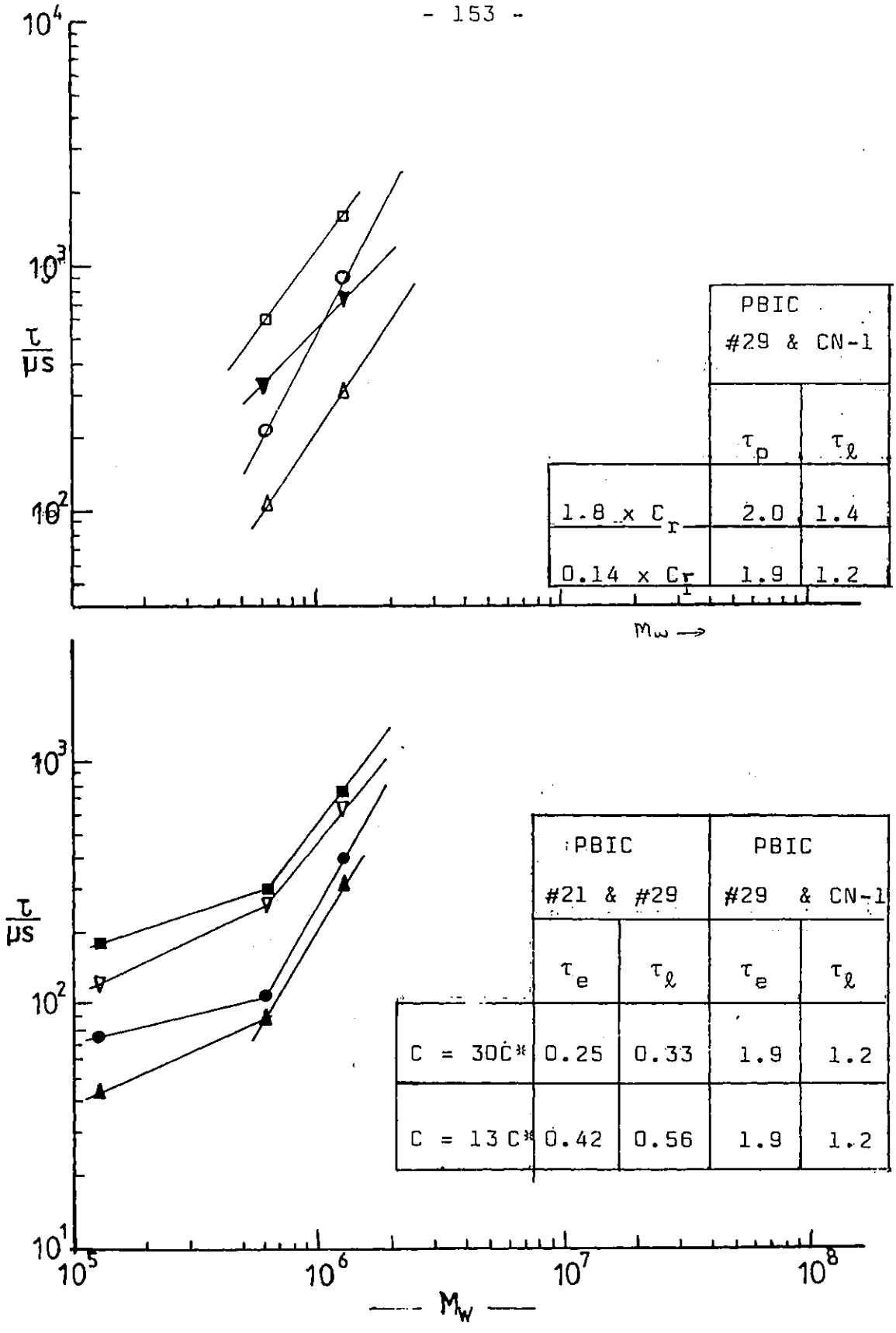

Fig 5.14 The molecular weight dependence of the PBIC relaxation times based on C_r and C at two concentrations.*

predicted by Doi and Edwards and is not very much higher than in dilute solution.

5.2.3 Temperature dependence of relaxation times

Another parameter of interest in this work is temperature. The variation of relaxation times with temperature can be represented by an Arrhenius expression of form,

$$\tau = A \exp - E_a/T \qquad 5.7$$

where E_a is the apparent activation energy, evaluated from a plot of $\ln \tau_e$ versus $1/T$. Fig 5.15 shows the temperature dependence of the relaxation times, τ_e of nominally 1.0 kg m^{-3} solutions of the three samples, together with that for the rise relaxation times τ_r, for PBIC #21. The resulting apparent activation energies are tabulated in Table 5.10. That for the decay process is found to increase with increasing molecular weight, and to be significantly greater than that for the decay transient. This is to be expected since the rate of

Table 5.10 Apparent activation energy of PBIC

Sample	Transient	Concentration C/ kg m^{-3}	Apparent energy E_a/ kJ $mole^{-1}$
PBIC 21	decay	1.3	13.8 ± 0.5
PBIC 21	rise	1,3	18.0 ± 1.0
PBIC 29	decay	1.1	20.1 ± 0.7
PBIC CN-1	decay	1.1	28.0 ± 0.8

alignment of the molecules is determined by the response to the electrical field in opposition to random thermal motions, whereas the decay process is determined by the temperature dependent Brownian forces. The linearity of the various plots shows that Arrhenius behaviour is maintained for both

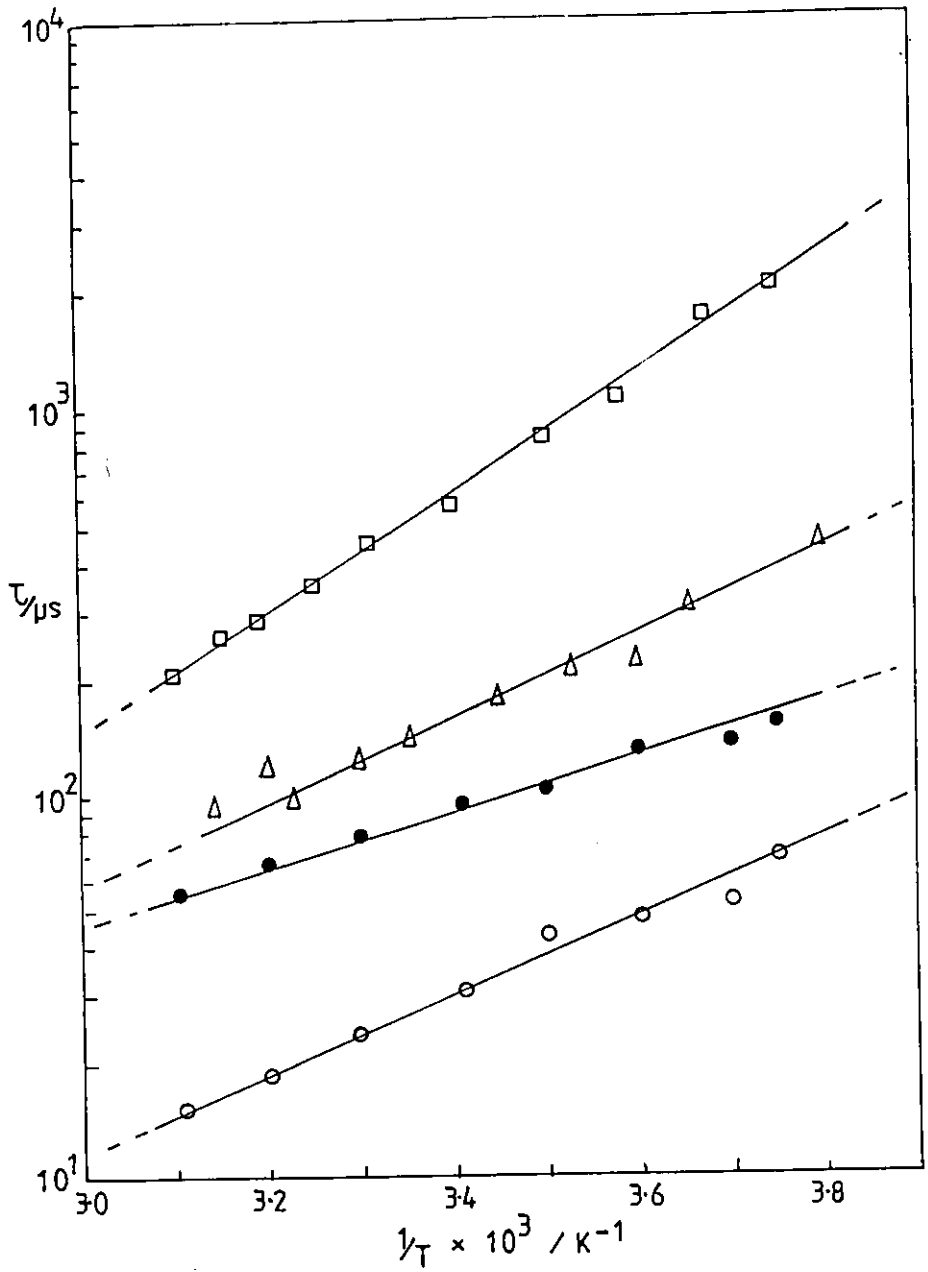

Fig 5·15 Temperature dependence of relaxation times, for PBIC#21 decay (○), rise (●); PBIC #29 decay (Δ); PBIC CN-1, decay (□).

increased molecular weights and concentrations. The results for PBIC #21 (Tables 3.4 and 5.10) suggest that the apparent activation energy increases with polymer concentration.

5.2.4 Field dependence of the relaxation times

Since it was observed that increased concentrations required lower field strengths to align the molecules, it was decided to check the effect of field strength on the observed relaxation times. The effect of field strengths covering the entire range used for PBIC was investigated using a 1.3 kg m^{-3} solution of PBIC #21; the results are shown in Table 5.11. It is evident that within their mutual uncertainties the relaxation times are independent of applied field strength. The ratio of the average relaxation times $\langle\tau\rangle_r/\langle\tau\rangle_d$, lies in the range 2.5 to 2.8 over the whole range of fields used.

Table 5.11 Field dependence of relaxation time for 1.3 kg m^{-3} PBIC #21 in carbon tetrachloride at 294 K.

Field, E/kVm^{-1}	Decay, $\tau/\mu s$			Rise, $\tau/\mu s$			$\frac{\langle\tau\rangle_r}{\langle\tau\rangle_d}$
	τ_e	τ_ℓ	$\langle\tau\rangle_d$ †	τ_r	τ_ℓ	$\langle\tau\rangle_r$ †	
.150	41.5	75	37	97	136	100	2.8
250	53.6	90	50	100	148	124	2.5
400	43.5	83	38	93	128	97	2.6
650	41.5	81	28	97	131	75	2.7

† The average error in the τ values is ±10% except for the values $\langle\tau\rangle_d$ and $\langle\tau\rangle_r$ where errors in estimation of the areas under/over the transient may amount to ±16%.

5.2.5 Discussion.

The molecular weight dependence of τ_ℓ and τ_e extrapolated to infinite dilution is shown in Fig 5.16 along with previous Kerr effect and dielectric measurements ($\tau_K \doteq \tau_D/3$) on PBIC. Although there is a broad spread of results at any given value of M_w, presumably due to variations in MWD between the sample , there is general agreement between the data in a change over from M^3 to $M^{1.5}$ dependence as M is increased. This indicates a change from rigid-rod towards flexible rod-type (even coil-like) behaviour as the chain length increases. The present data are in reasonable agreement with the previous measurements and indicate that the three samples studied straddle this change over region from stiff to flexible behaviour. The larger difference between τ_e and τ_ℓ for PBIC # 29 ($M_w = 6.4 \times 10^5$) may well reflect the large polydispersity of this sample.

The dilute solution relaxation times for the three samples have been analysed using Broersma's equation. Studies of PBIC in dilute solution have suggested a monomer length, ℓ_o and diameter , d_o of 0.12 nm and 1.2 nm respectively [36]. Using these parameters in the Broersma's equation (eqn. 2.6) the three poly(n-butyl isocyanate) samples PBIC #21, PBIC #29, PBIC CN-1 studied here should yield relaxation times of 42 μs, 3.4 ms and 26 ms respectively, if they are behaving as isolated rigid rods. The experimental values (τ_e, τ_ℓ) for these samples are (28,63), (64,205) and (410,600) μs respectively. This suggests that the two higher molecular weight samples at least are far from rigid rod molecules. The experimental relaxation times for these two samples interpreted using the Broersma's equation give equivalent monomer lengths of 0.044 nm and 0.032 nm respectively. This reduction in the effective monomer length with increasing molecular weight suggests a considerable increase in the chain flexibility as M increases. This is in accord with the findings of Bur and Roberts [24], and of Jennings and Brown [36], that PBIC deviates increasingly from rigid rod behaviour above a molecular weight of $\sim 10^4$

Turning to the behaviour in the concentrated solutions, the relaxation times exhibited the same sharp changes at some

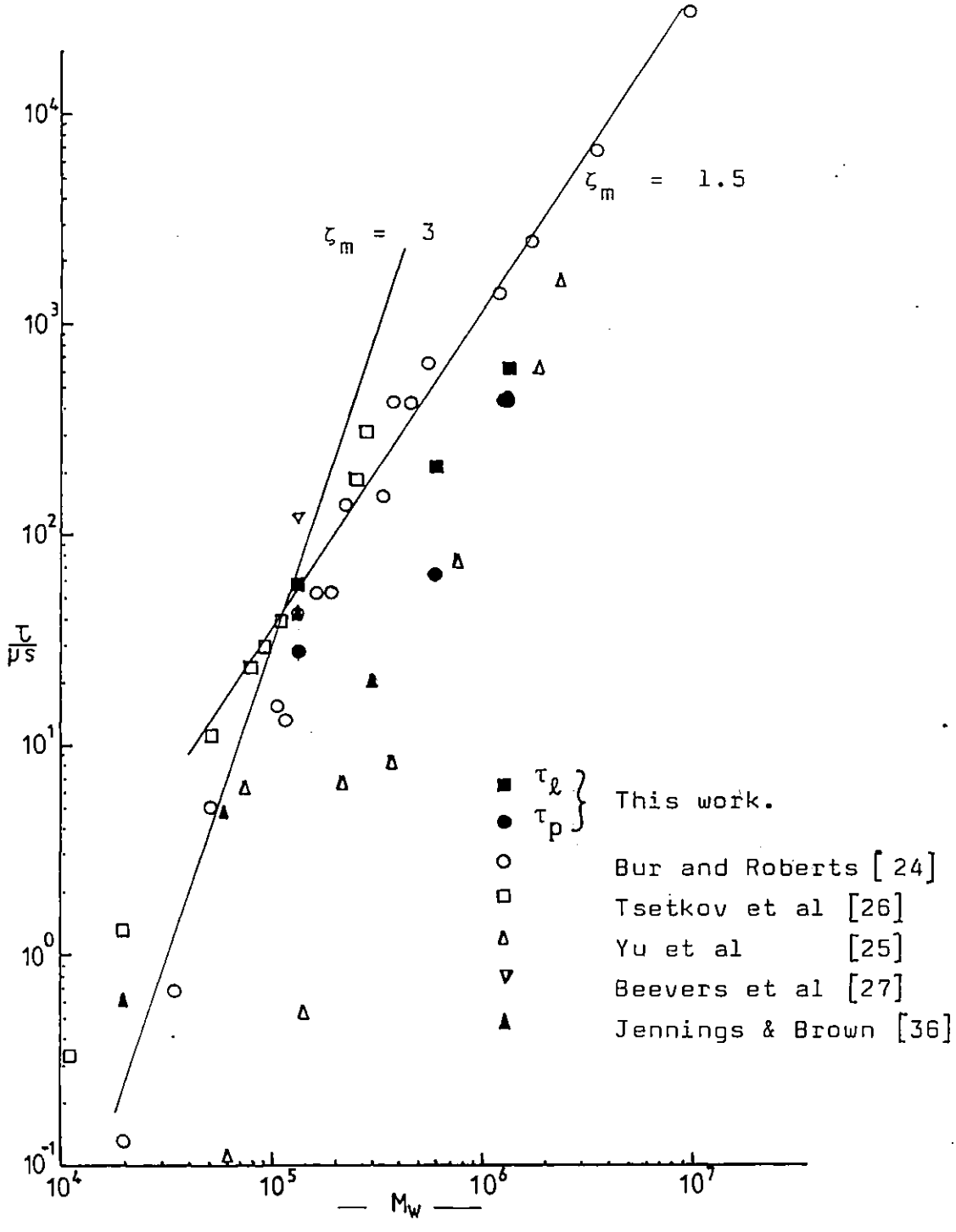

Fig 5.16 The molecular weight dependence of the infinite dilution relaxation times τ_ℓ(■) and τ_e(●), compared with previous Kerr and dielectric results of other workers.

critical concentration as were observed in the case of PBLG. This behaviour is in qualitative agreement with the predictions of Doi and Edwards (DE). However the concentration exponent $(\zeta_c)_{C<C_r} \sim 0.2$ and $(\zeta_c)_{C>C_r} \sim 0.6$ are about half the values obtained for PBLG, and are in even worse quantitative agreement with the DE prediction of 2 .

Table 5.12 shows a summary of the concentration C_r, C^*, and C_r/C^* for the cases of all the PBIC for comparison purposes. As observed for PBLG, the PBIC C_r values decrease with increasing molecular weight. However C_r/C^*, which may be taken as a measure of rod flexibility, indicates that flexibility increases with molecular weight. Also $(C_r/C^*)_{PBLG} << (C_r/C^*)_{PBIC}$ indicating that PBIC is significantly more flexibility than PBLG.

Within the PBIC samples, the lowest molecular weight PBIC #21, is expected to be the 'most rigid'. Unfortunately we were unable to reach its critical concentration experimentally due to shortage of material. The concentration exponent $(\zeta_c)_{C<C_r}$ for the sample, is greater than the $(\zeta_c)_{C<C_r}$ values of the other PBIC samples and is comparable with $(\zeta_c)_{C<C_r}$ for PBLG. For the two molecular weights, the exponent for the peeled relaxation time shows no break at the critical concentration. The reason for this τ_p behaviour could be:
(a) τ_p corresponds to relaxation of the dipole component perpendicular to the chain backbone which relaxes by local motion;

Table 5.12 The critical concentration parameters for PBIC. All concentrations, C, in kg m^{-3}.

Sample	Experimental	Calculated			Ratio $\frac{C_r}{C^*_{rr}}$
	C_r	C^*_{rr}	C^{**}_{rr}	C^*_{rc}	
PBIC = 21	> 3.5	0.1	9.8		>35
PBIC = 29	0.9	0.004	2.1		209
PBIC CN-1	0.22	0.001	1.0		220

(b) or τ_p corresponds to relaxation by end-over-end rotation of small species for which C_r is much greater than that for the larger species, characterised by τ_ℓ.

Using equations analogous to 5.3 and 5.4, we can relate the observed values of the critical concentration C_r to a characteristic length ℓ_q, corresponding to the value of the mean interchain distance below which an abrupt change in the chain dynamics occurs, i.e.

$$C_r = \frac{M}{1000 N_A V_c} \quad \text{where } V_c = \frac{4\pi}{3}(\ell_q/2)^3 \qquad 5.8$$

This gives ℓ_q = 0.14 μm for PBIC #29 and ℓ_q = 0.27 μm for PBIC CN-1. The ratio of these values to the 'rigid rod' length L for the two samples is 0.17 in both cases. One possible interpretation of ℓ_q is that it is the persistence length. Although those values are slightly greater than those obtained by various workers in the dilute solution studies (0.04 to 0.13 μm) [36].

There was no break in slope of the τ versus C plot observed at $C^{**}_{\text{rigid rod}}=(C^{**}_{rr})$ nor was there evidence of anisotropy (liquid crystal behaviour) above C^{**}. This again indicates that estimation of critical concentrations based on rigid rod behaviour for PBIC leads to an underestimation when compared with experiment.

It is interesting to note that the behaviour of paramyosin observed by Krause et al (see section 5.1.5) in which $(\zeta_c)_{C<C_r}$ = 0.1, $(\zeta_c)_{C>C_r}$ = 0.56 is very similar to that observed here for PBIC.

The molecular weight dependence of the relaxation times for both $C<C_r$ and $C>C_r$ is again far lower than the DE prediction of ζ_m = 7. The values of ζ_m for PBIC are also significantly lower than for PBLG, a further indication of the increased flexibility of these helical molecules.

5.3 Poly (2-methyl pentene-1 sulphone), PMPS

Studies of the dynamics of the 'rod-like' macromolecules PBLG and PBIC have shown that chain flexibility exhibits a considerable effect on molecular dynamics in the concentrated solution. Poly(2-methyl pentene-1 sulphone) has been shown to behave as a non-helical stiff coil in dilute solution [77,78]. The alternative type of stiff chain was therefore chosen to investigate further the effects of flexibility on chain dynamics. The individual segment dipoles lie predominantly parallel to the chain backbone and combine to give an overall component which will cause orientation of the whole chain in the direction of the applied field, and which upon removal of the field can relax by whole molecule rotation. The smaller perpendicular dipole compoment may relax independently via more local segmental motion. All measurements reported here were for a sample of $M_w = 3.2 \times 10^5$ in solution in bemzene.

5.3.1 Concentration dependence of the relaxation times

Because of the strong curvature of the ln δ versus time plots, the decay transients were characterised by at least two relaxation times τ_p and τ_ℓ. Fig 5.17 shows the concentration dependence of these relaxation times together with τ_{in} and τ_e. Because of the large difference in the values of τ_ℓ and τ_p, τ_e and τ_ℓ are essentially identical. These plots reveal that the 'peeled' relaxation time, τ_p has a value of about 10 μs and is essentially independent of concentration over the range studied. The values of τ_ℓ and τ_e are weakly concentration dependent at low concentrations $(\zeta_c)_{\tau_\ell} \simeq 0.12$, $(\zeta_c)_{\tau_e} \simeq 0.05$ but change abruptly over a narrow range of concentrations near the critical concentration $C_r = 6$ kg m^{-3} to become strongly concentration dependent with an exponent, $(\zeta_c)_{\tau_\ell} = (\zeta)_{\tau_e}$, of 0.60±0.07. The initial relaxation time (which merely reflects the combined effect of τ_ℓ and τ_p at short times) has a lower concentration exponent of 0.41±0.07.

5.3.2 Effect of temperature on relaxation times.

Fig 5.18 shows a plot of ln τ_e versus 1/T for two concentrations, chosen such that one (3.2 kg m^{-3}) is below C_r and the other (20 kg m^{-3}) significantly above C_r and close to the concentration C** at which PMPS should exhibit liquid crystal

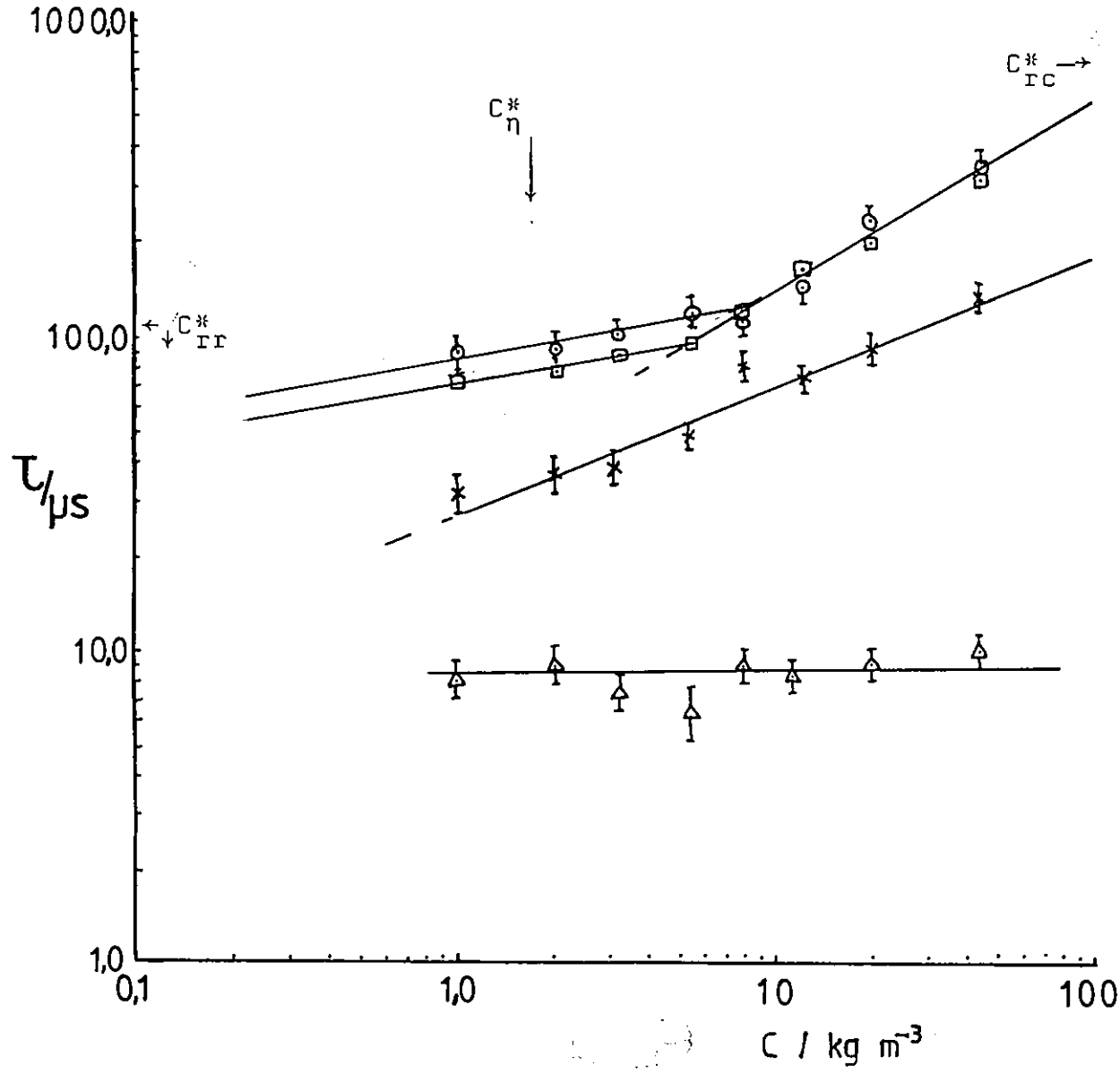

Fig 5.17 The concentration dependence of the relaxation times of PMPS in benzene at 294 ; τ_ℓ(○), τ_e(□), τ_{in}(x), τ_p(Δ).

Table 5.13 (a) Concentration variation of relaxation times of PMPS ($\bar{M}$ = 3.2 x 10^5) in benzene at 293 K

Concentration C / kg m^{-3}	Decay relaxation times, τ/μs			
	τ_ℓ^D	τ_p	τ_{in}	τ_e
1.0	76 ± 4	8.0	32 ± 4	67
2.1	80 ± 5	9.0	35 ± 5	79
3.2	89 ± 3	7.2	39 ± 3	87
5.5	97 ± 6	6.4	50 ± 2	84
8.0	107± 10	9.0	80 ± 7	119
12.7	208 ± 8	8.5	74 ± 5	197
20.0	221 ±11	9.0	79± 10	200
40.0	280 ±24	10.0	131 ± 5	300

Table 5.13 (b) Temperature dependence of the τ_e relaxation times for 20 kg m^{-3} and 3.2 kg m^{-3} solutions of PMPS in benzene.

Temperature / K	Relaxation times, τ/μs	
	20 kg m^{-3}	3.2 kg m^{-3}
300	225 ± 25	98
294	320 ± 20	100
291	360 ± 10	111
286	960 ± 50	127
281.5	1113 ± 130	132
273	2350 ± 250	150
270	4120 ± 293	173

behaviour were it to act as an elongated rod. The apparent activation energies for the two concentrations are 12.5±0.5 kJ mol^{-1} and 61.5±2.5 kJ mol^{-1} respectively.

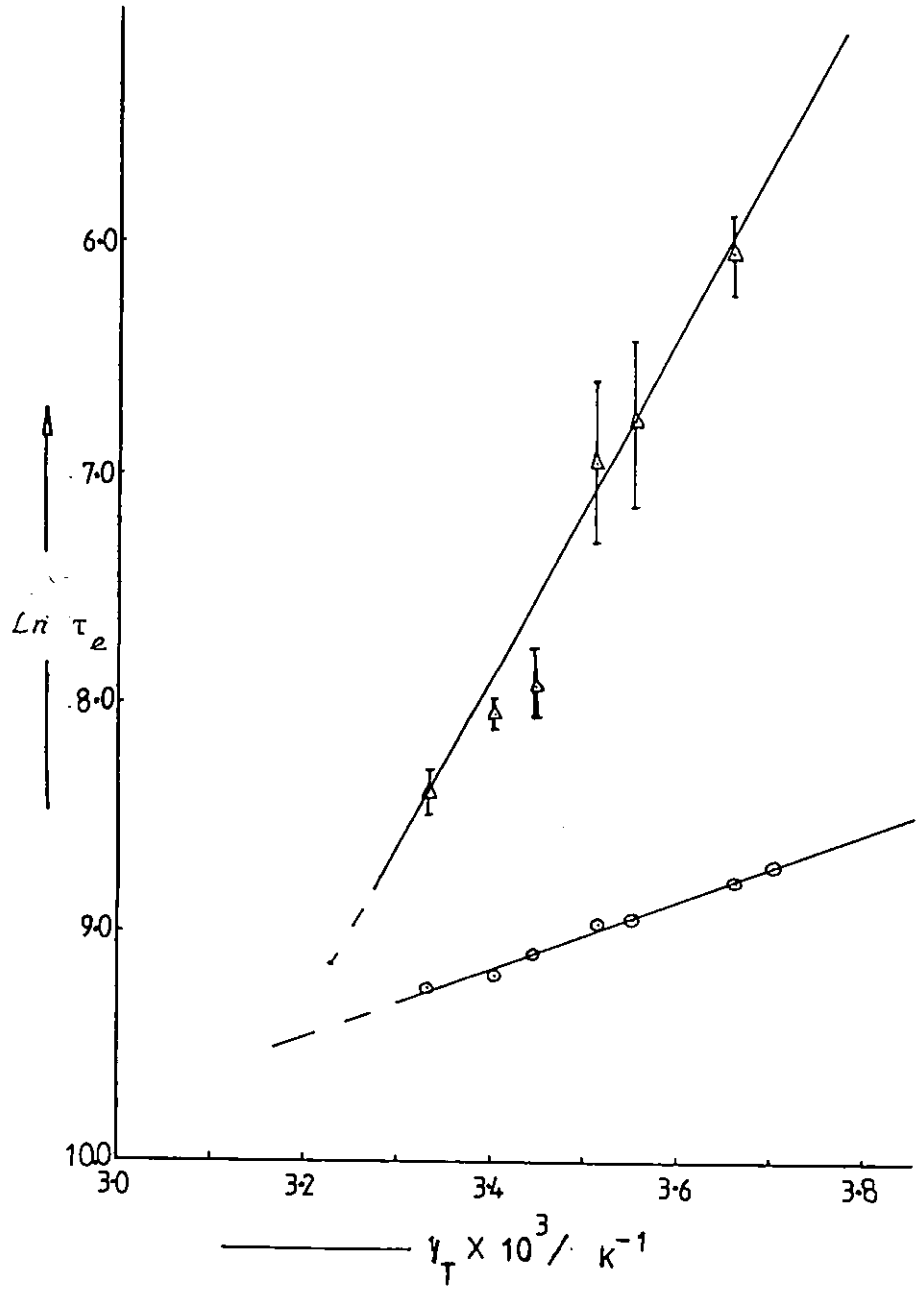

Fig 5.18 Ln τ versus 1/T (K^{-1}) of 20 kg m^{-3},(Δ) and 3.2 kg m^{-3}(○) for PMPS (M_v = 3.2 x 10^5) in benzene.

5.3.3 Discussion

It is not surprising that for this stiff coil type polymer the concentration exponents of τ_ℓ, τ_e and τ_{in} are significantly less than that predicted by the Doi and Edwards theory for rigid rods. However, it is probably surprising that the behaviour of PMPS is very similiar in this respect to that found for the helical rod-type macromolecule PBIC. This seems to suggest that once molecules have sufficient flexibility to depart from perfectly rigid rod-type behaviour the changes in concentration exponent with chain flexibility are relatively small. However the 'peeled' relaxation times, τ_p, for PMPS do differ from those for PBIC in that they are essentially independent of concentration. This contrasts with τ_p for the helical macreomolecules which did depend on concentration, albeit weakly for the higher molecular weight PBIC samples. The values of τ_p for PMPS may be attributed to relaxation of the the perpendicular component of the chain dipole due to local segmental rotation, arising, because of the flexible coil nature of PMPS molecules and the unsymmetrical olefin unit. In the concentrated solution studied here, such segmental motions would be expected to be still dominated by the local intermolecular interactions and be relatively insensitive to the effects of chain interactions and hence concentration.

On the basis of the model of section 5.1.5 the volume V_m swept out by the PMPS chain assuming it to be a rigid rod with monomer length ℓ_o = 0.49 nm using equation 5.3 is 6.3 x $10^{-19} m^3$ and this gives an overlap concentration C* = 8.4 x 10^{-4} kg m^{-3}. On the other hand if PMPS is assumed to be random coil, using the radius of gyration, R_G $(=(n/6)^{\frac{1}{2}}\ell_o)$ in eqns 5.3 and 5.4 yields an overlap concentration of 156 kg m^{-3}. However, using the Simha and Cornet interaction parameter expression [82,83]

$$C^*[\eta] = 1 \qquad 5.9$$

and the experimentally obtained intrinsic viscosity (0.565 m^3 kg^{-1}) gives an overlap concentration C* of 1.8 kg m^{-3}. Experimentally the observed critical concentration C_r was 6 kg m^{-3}. The rigid rod assumption underestimates C_r, the ideal random coil assumption overestimates it. The Simha value, based on an experimental measure of the dilute solution coil size through

$[\eta]$, comes closest to predicting the observed value of C_r, although again gives an underestimate. The characteristic length, ℓ_q, obtained from C_r (using equation 5.8) is 50.2 nm compared with a monomer length of 0.49 nm and the contour length L of 1.06 μm. This indicates that the abrupt change in dynamical behaviour occurs when the mean distance between chain interactions is ≈100 monomer units. There are L/ℓ_q = 20 such segments per chain; again the interpretation of ℓ_q as a measure of the persistence length of PMPS is at least plausible.

Assuming this molecule to be a fully extended rigid chain and applying Broersma's equation (with $\ell_o = d_o$) gives a relaxation time of 4.1 ms. This result is greatly in excess of the observed result (76 μs) for the most dilute solution of this work. Applying the bead and spring models (see section 2.3.1) to this polymer gives a calculated Rouse relaxation time of 50 μs and a Zimm relaxation time of 35 μs. These results suggest therefore that PMPS behaves as a partially draining coil-like molecule in dilute solution.

The contribution to the apparent activation energy due to solvent viscosity changes alone [78] is 11 kJ mol^{-1} for the system studied here. This is close to the 12.5 kJ mol^{-1} obtained for the 3.2 kg m^{-3} solution of PMPS in benzene, suggesting that the effect of temperature on the relaxation of this concentration is mainly due to solvent viscosity effects. It also provides indirect evidence that chain interaction effects here remain small. At high concentrations $C>C_r$ the solvent viscosity effect becomes far less significant and the large activation energy observed at 20 kg m^{-3} reflects the high degree of molecular interaction present, resulting in marked reductions in the rotational mobility of the macromolecules.

5.3.4 Polyether sulphone, PES

Although it was chosen as a 'stiff coil' the poly(olefine sulphone) PMPS used in the above section in the event showed a great degree of flexibility. A more rigid poly(ether sulphone) PES, having a dipole moment component along the chain backbone and having a benzene ring in the chain backbone to reduce segmental rotation was selected in an attempt to investigate

a stiffer system. Three samples of PES as described in Chapter 4 were studied in N-methyl pyrrolidone solution. The relaxation results obtained with these samples are presented in Table 5.14 . The Kerr constant for this system was found to be very low, so that loads of 5 kΩ or 10 kΩ had to be applied across the photomultiplier in order to obtain signals of sufficient amplitude. These loads raised the time constant of the detection circuit to values (determined using the solvent) of 1.2μs and 1.7μs respectively.

The transients obtained were highly non-exponential and decayed very rapidly. Even the relaxation time, τ_ℓ was barely significantly greater than the time constant of the detection circuit. These values of τ_ℓ were all in the range 2-3 μs, being essentially independent of concentration and molecular weight. Evidently the parallel dipole component was insufficient to produce appreciable molecular alignment and the signals observed were probably due to some (surprisingly rapid) local motion. Consequently these systems were not pursued further.

Table 5.14 (a) Kerr effect relaxation times of Poly ethersulphone (PES)

Concentration C kg m^{-3}	Decay		Concentration C kg m^{-3}	Decay	
	τ_ℓ/μs	τ_p / μs		τ_ℓ / μs	τ_p / μs
PES I load 10 kΩ			PES II load 5 kΩ		
6.4	3.4 ± 0.6	1.42± 0.6	0.91	1.8 ± 0.03	
15.9	3.4 ± 0.5	0.6 ± 0.1	2.3	2.3± 0.07	
39.7	2.7 ± 0.4	0.85± 0.1	5.7	2.02± 0.8	0.55± 0.1
146.0	2.96± 0.1		11.4	1.9 ± 0.3	0.35 ± 0.1
PPES II load 5 kΩ			35.6	2.12± 0.4	0.38 ± 0.1
22	1.9		71.2	2.1 ± 0.2	0.42 ± 0.15
43	1.7				

Table 5.14 (b) Time constant variation with load.

Load / kΩ	5	10	15	20
Time constant /μs	1.2	1.7	2.1	2.9

5.4 Polymers of propylene oxide and propylene glycol.

The studies on relatively stiff rod-like and coil-like polymers have revealed a marked dependence of the rotational chain dynamics on concentration. The effects are somewhat less than those expected theoretically for completely rigid molecules and one probable cause of this discrepancy is significant chain flexibility. Moreover, it appears that the effects of concentration become less marked the more flexible the molecules become . In order to examine further the effects of increased molecular flexibility, it was decided to study concentration effects in poly(propylene oxide/glycol) which has relatively low energy barriers to internal rotation and has been shown in dilute solution to behave as a very flexible coil [28]. Two types of system were studied - low molecular weight poly(propylene glycols)and high molecular weight poly(propylene oxides).

5.4.1 Propylene glycols

Fig 5.19 (a) is a representative birefringence transient obtained for the low molecular weight liquid glycols PPG 1002 ($\bar{M} \sim 1000$), PPG 2002 ($\bar{M} \sim 2000$) and PPG 2257 ($\bar{M} \sim 2200$). The characteristic birefringence response obtained on application of the pulsed field using the quarter wave plate † shows that the birefringence is initially negative, decreasing rapidly to a minimum, then rising gradually to a steady state value at long pulse widths. When the field is cut off, the transient rises rapidly to positive values before decaying to zero. This unusual birefringence behaviour has also been observed by Beevers et al [29] on liquid glycols. The phenomenon can be explained in terms of a superposition effects due to two processes, one rapid with negative birefringence and the other slow with positive birefringence.

Fig 5.19 (b) shows a schematic representation of the data in which the birefringence is resolved into two such components - a negatively birefringent primary process characterised by rapid rise/decay and a positively birefringent secondary process which exhibits far slower rise/decay characteristics. The dipole moment of poly(propylene glycols) can be resolved into

† *Similar transients, of reduced amplitude, were observed without using the quarter wave plate. These transients were recorded at low temperatures using double cell windows which*

were screwed tight to allow air circulation and prevent water condensation on the windows. It is probable that the tightening of the screw fitting produced significant strain in the cell windows, having the effect of introducing a constant phase retardation δ_o, and may thus act in a similar fashon to a $\lambda/4$-plate. Such problems have been reported previously in low temperature measurements [80]

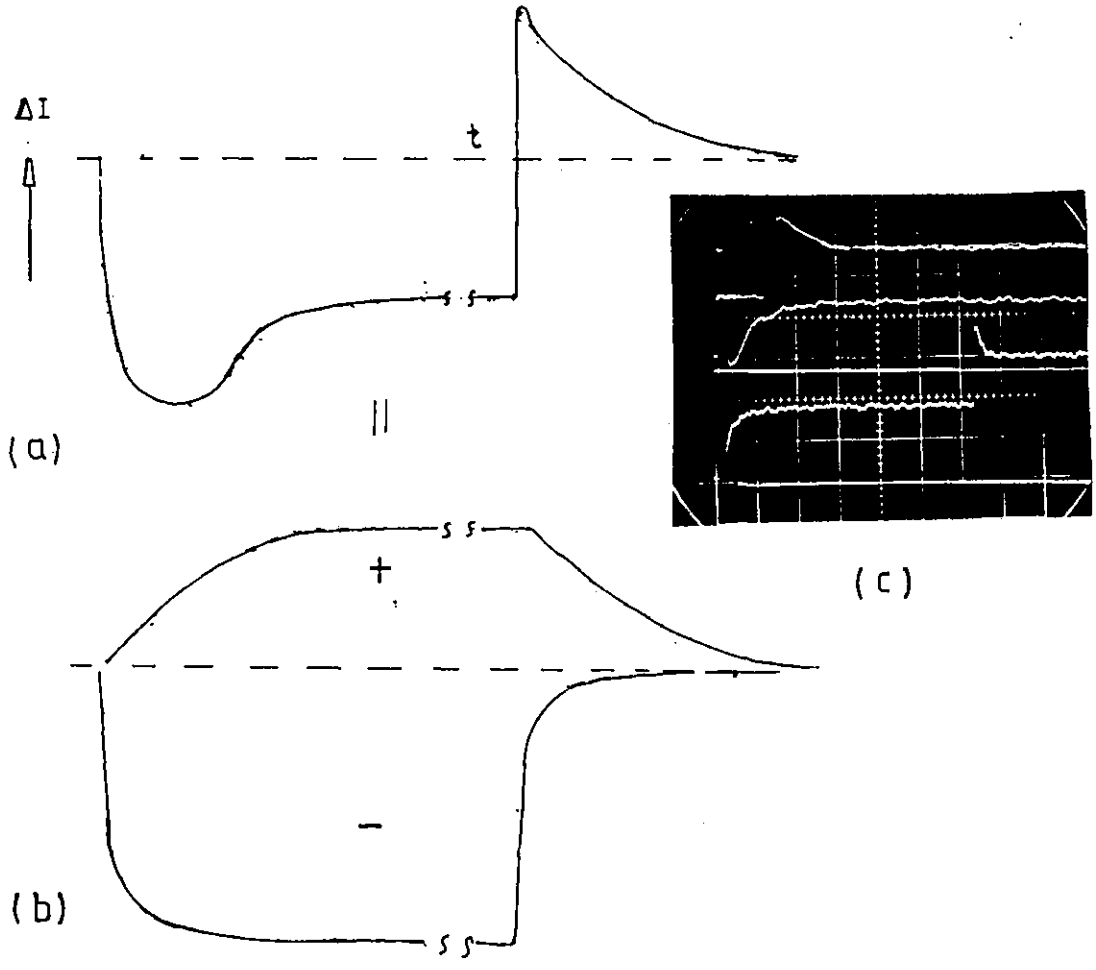

Fig 5.19 (a) Representative plot of ΔI versus time and the oscillogram (photo) transients of liquid glycols.

(b) Schematic representation of resolved components of fast negative and slow positive processes.(c) Diluted PPG transients.

two components, one directed along the chain contour and the other perpendicular to it . Application of an electric field to the polymer causes some degree of orientation and alignment of the macromolecules in the field. The dipole component parallel to the chain contour will lead to orientation of the whole chain and its subsequent relaxation may only occur by whole molecule rotation. Thus the slow secondary process is associated with rotation of the whole molecule. On the other hand the perpendicular dipole component can align and relax

by means of local segmental rotation and it is this faster motion which is associated with the primary process.

The observed signals were either of the form illustrated in Fig 5.19 (a) or its mirror image, depending on the direction of rotation of the analyser. The relaxation times determined from the transients were independent of the extent and direction of the analyser rotation (see Table 5.15)

Table 5.15 Relaxation times obtained rotating the analyser in clockwise(+) and anticlockwise(-) directions using a 3000 kV m^{-1} pulse of 3 ms duration.

Sample	Temperature/ K	Analyser rotation + x			Analyser rotation -x		
		Decay		Rise	Decay		Rise
		2^o $\frac{\tau}{\mu s}$	1^o $\frac{\tau}{\mu s}$	2^o $\frac{\tau}{\mu s}$	2^o $\frac{\tau}{\mu s}$	1^o $\frac{\tau}{\mu s}$	2^o $\frac{\tau}{\mu s}$
PPG 2002	228	614	22	1592	630	18	1650
PPG 2257	223	620	25	2830	797	23	2910

A rather different transient behaviour was observed for the lowest molecular weight sample PPG 0402 ($\bar{M} \simeq 400$) Fig 5.20 (a). The birefringence response shows that when the pulsed field was applied, the birefringence was initially negative, decreased rapidly to a minimum, then rose steeply to positive values before gradually rising to a steady state value. When the field was removed, the transient exhibited a further low amplitude rise before falling rapidly to below 60% of its steady state value and gradually decaying to zero. These observations can also be explained in terms of a superposition of the effects of three processes, a rapid negative birefringence process, followed by a rapid positive birefringence and finally by a slow positive birefringence. Fig 5.20 (b) shows the schematic representation of the data in which the birefringence is resolved into three parts; a negatively birefringent primary process, A, a higher positively birefringent primary process, C, and another positively birefringent secondary process B, exhibiting the slowest rise/decay characteristics.

The slight positive jump at field removal seems to reflect the fast recovery of the initial negative primary process. Both the amplitude and the time scale of this process are small, consequently the birefringence transients were analysed only in terms of the positive primary rise and decay processes and the positive secondary rise and decay processes.

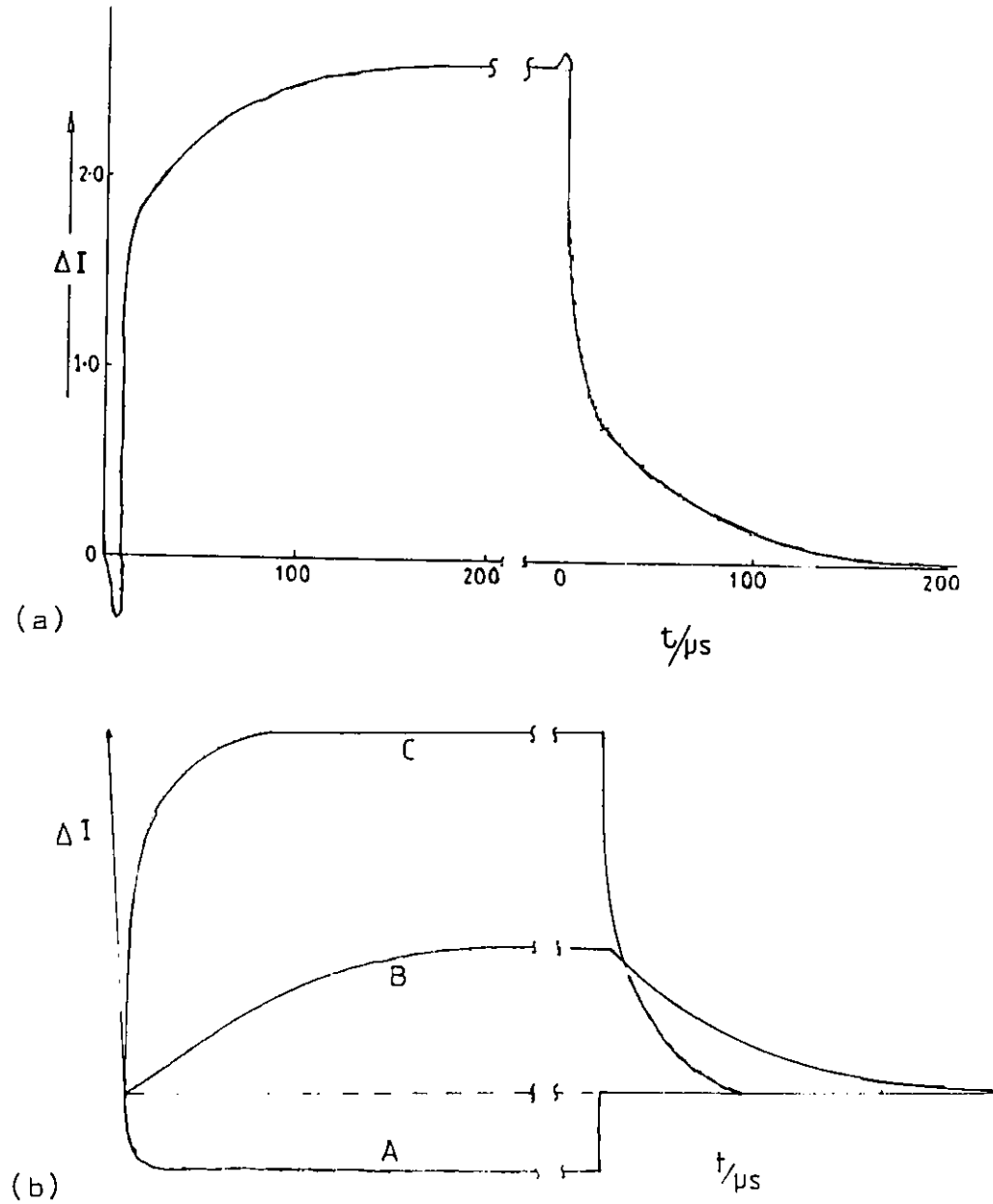

Fig 5.20(a) Typical birefringence transients of PPG 0402.
(b) Schematic representation of resolved components (A,B,C).

5.4.2 Glycol relaxation times

At room temperatures these low molecular weight polymers are liquids but have very low Kerr constants. In order to obtain sufficient birefringence for accurate measurement even for the undiluted polymers, experiments were conducted at temperatures in the range 238 K to 213 K.

The rise and decay transients of the secondary process were exponential and the single characteristic relaxation time obtained as illustrated in section 3.7.4 are given in Table 5. 16 . The primary process showed deviations from a single exponential, therefore the transient was analysed in terms of the Williams and Watts function (see section 3.7.4). The relaxation times corresponding to this fit, together with the spread factor β, are given in the same Table 5.16 .

As expected, the secondary relaxation times increase with both sample molecular weight and the decreasing temperature. The ratio of the secondary rise time $\tau_{K,r}$ to the decay time $\tau_{K,d}$ varies over a wide range lies in general in the range 2.0 to 4.0. There is some evidence that this ratio increases as the temperature is lowered, especially for the highest molecular weight sample where the ratio increases from 1.7 to 7.2. The dielectric relaxation times obtained by Beevers et al [27] for a sample of $\bar{M}$ = 2025 is compared with our sample PPG 2002 ($\bar{M}$ ~2000) in Fig 5.22 (c). These dielectric relaxation times compare well with the Kerr effect secondary rise times obtained in this work or, equivalently , with about three times the secondary decay values. The dielectric and the Kerr results are therefore consistent with each other within the framework of a rotational diffusion mechanism.

(a) Molecular weight dependence of the relaxation times.

Figures 5.21 (a), (b) show plots of the relaxation times versus molecular weight at two selected temperatures 228 K and 218 K. The relationship of relaxation times to molecular weight is of the form,

$$\tau = K M^{\zeta_m} \qquad 5.10$$

with values of ζ_m essentially the same for the rise and decay times of each process. The secondary process is found to have

Table 5.16 The variation of Polypropylene glycol relaxation times with molecular weight and temperature. †

Sample	Temp K	Rise relaxation times τ/μs			Decay relaxation times τ/μs		
		2^o	1^o	β_r	2^o	1^o	β_d
PPG 0402	228	112	12.4	0.72	55	2.5	0.57
	223	230	16.7	0.68	84	4.6	0.56
	218	607	38.0	0.6	237	13.0	0.62
	213	1627	91.0	0.62	478	28	0.56
	208	4100	112.0	0.56	1130	49	0.56
PPG 1002	238	57			18		
	233	202			58		
	228	525	19.0	0.68	194	7.1	0.6
	223	1360	51.0	0.70	255	15.0	0.74
	218	7900	150.0	0.56	2501	32.0	0.52
PPG 2002	243	62			24		
	238	145			67		
	233	743	18.0	0.56	195	6.1	0.62
	228	1592	63.1	0.62	632	17.0	0.58
	223	6336	234.0	0.64	2004	32.0	0.54
PPG 2257	243	117	3.1	0.82	70		
	238	253	25.0	0.76	105	2.5	0.60
	233	800	57.0	0.58	217	14.0	0.54
	228	2843	80.0	0.64	620	25.0	0.62
	223	11180	182.0	0.52	1557	62.0	0.52
	218	31021	560.0	0.62	5800	240.0	0.56

† Results are the mean values from at least two, experiments with an estimationed error of about 10%

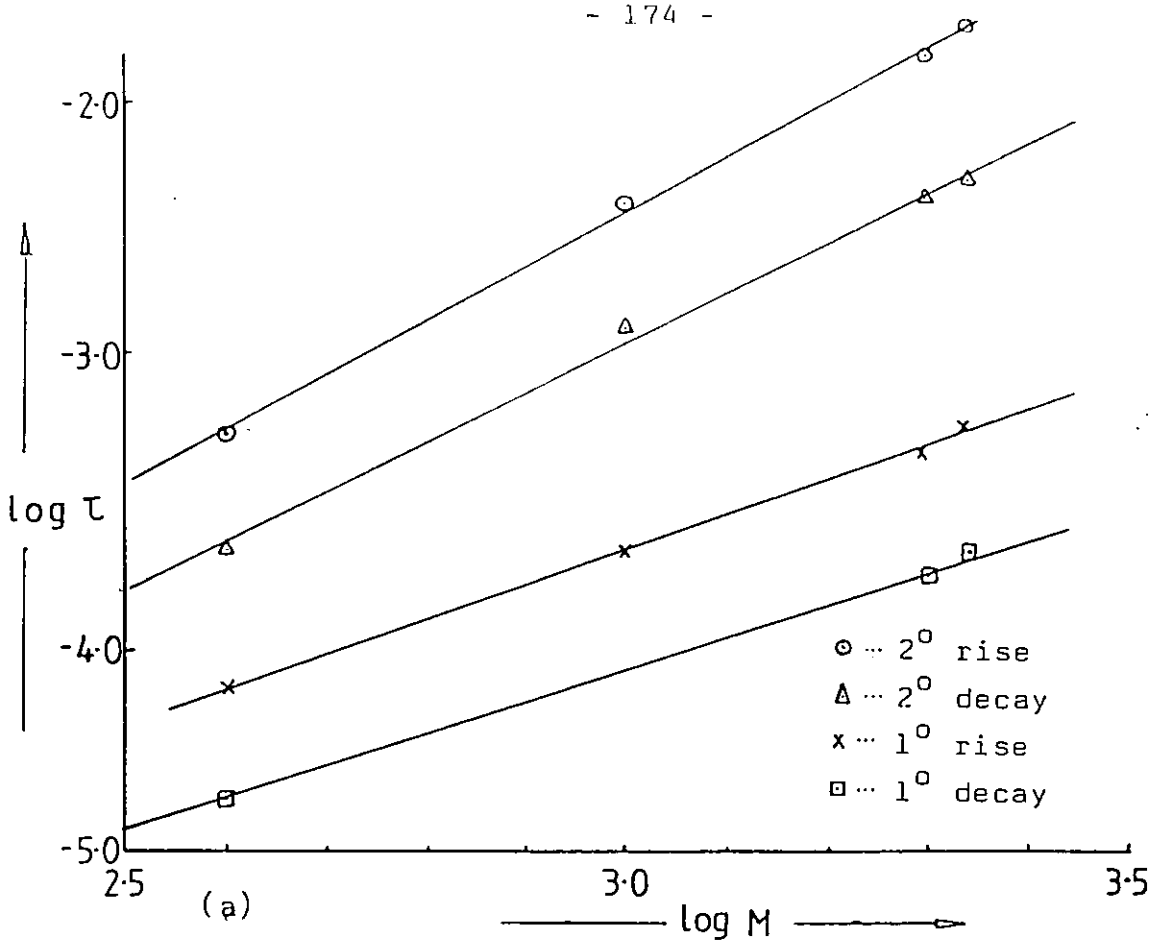

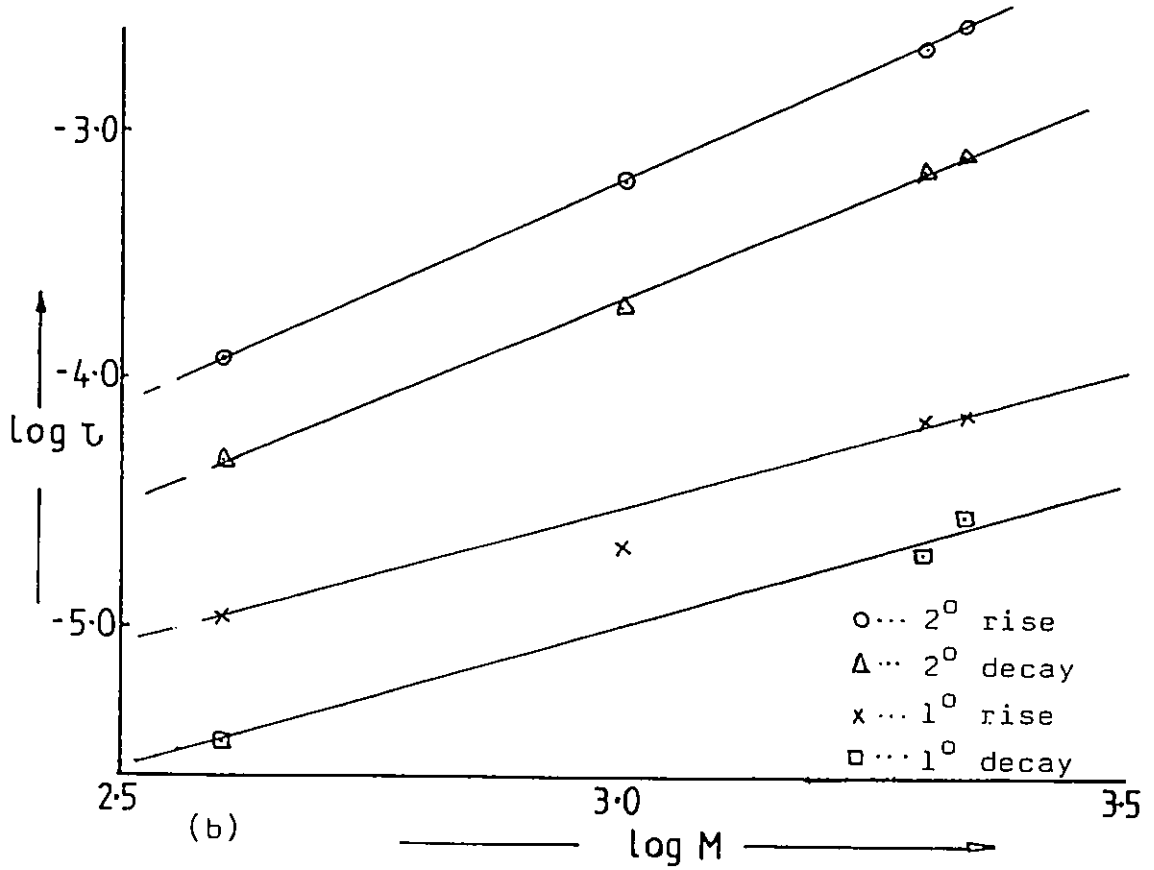

Fig 5.21 Molecular weight dependence of the Polypropylene glycol relaxation times at temperatures (a) 228 K and (b) 218 K.

an exponent , ζ_m = 1.95±0.2 while the primary process exponent is 1.25±0.2. The linear dependence of the primary relaxation time on molecular weight suggests that for these short chains (incorporating 7 - 40 monomer units) this process is not entirely due to independent rotation of small localised segments of the chain.

(b) The temperature dependence of the relaxation times

Figures 5.22 (a) - (d) are log linear plots of relaxation time versus 1/T for PPG 0402, PPG 1002, PPG 2002 and PPG 2257 respectively. The rise and decay relaxation times associated with both the primary and secondary processes are well represented by an Arrhenius expression. The apparent activation energy obtained for the various relaxation processes are shown in Table 5.17 .

Table 5.17 Apparent activation energies associated with Glycol relaxation processes, E_a/kJ mol^{-1} †

Sample	M	2^o Rise	2^o Decay	1^o Rise	1^o Decay
PPG 0402	400	73	63.4	55.4	55.7
PPG 1002	1000	102	100.3	92.0	89
PPG 2002	2000	109	106.4	102.0	97
PPG 2257	2200	129	124.6	115.7	116.7

† Field gradient > 3000 kV m

The apparent activation energy associated with the relaxation processes in these bulk polymers are large, in contrast to those observed for the relatively dilute PBIC systems. The energy requirement increases with increasing molecular weight. As expected the secondary process, corresponding to whole molecular orientation has a higher activation energy than the primary fast process associated with more local chain motions. The energies associated with the rise and decay processes are comparable in both cases.

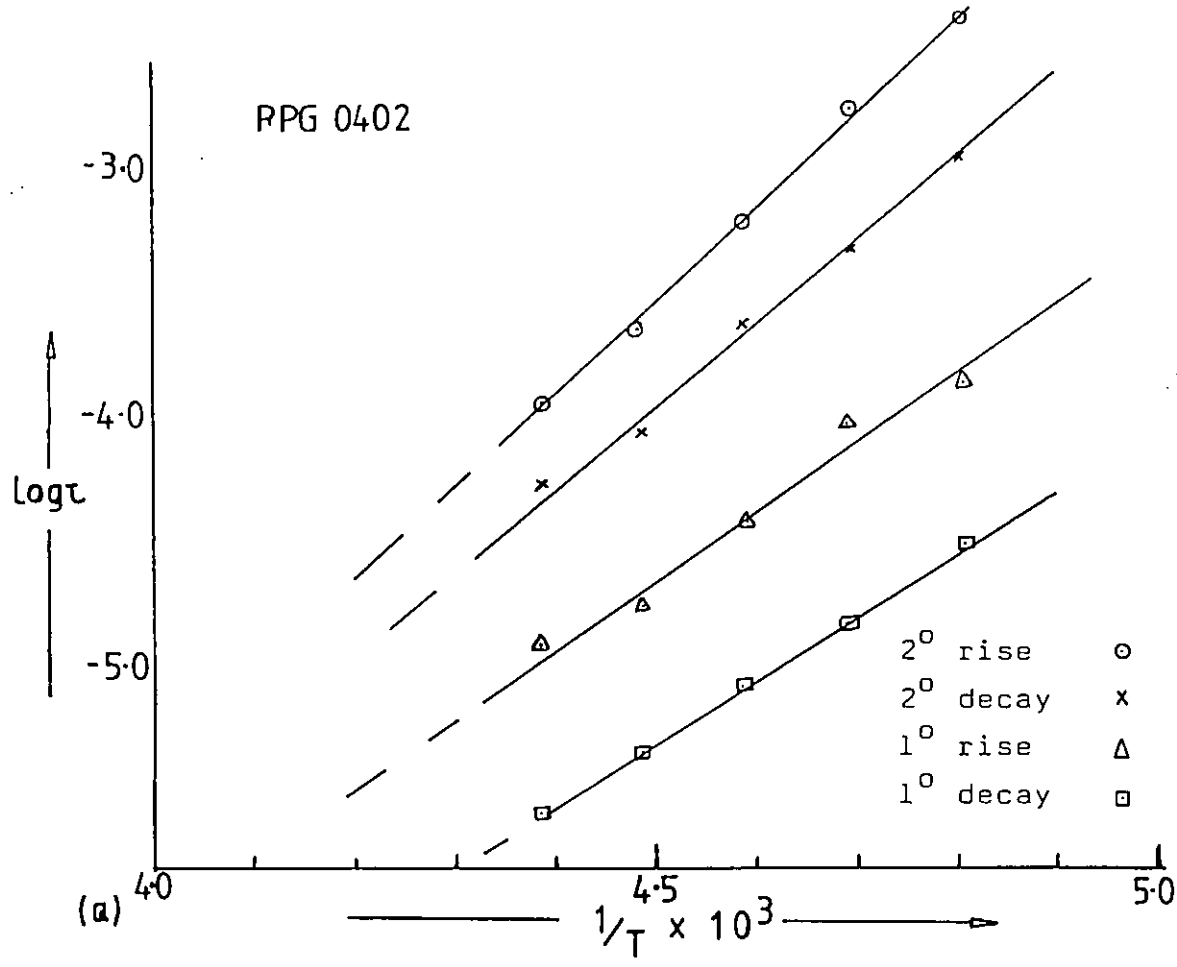

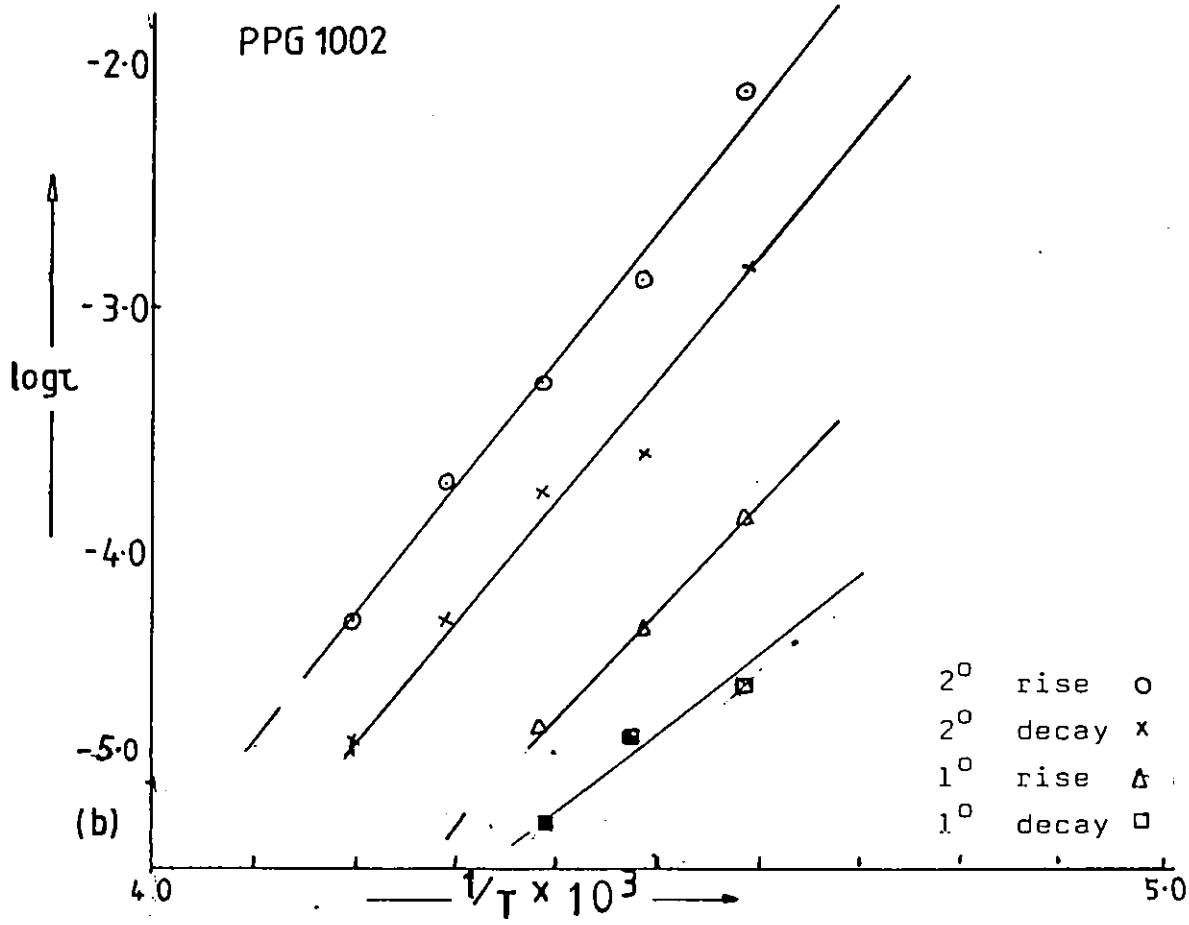

Fig 5.22 The temperature dependence of the relaxation times of (a) PPG 0402 and (b) PPG 1002

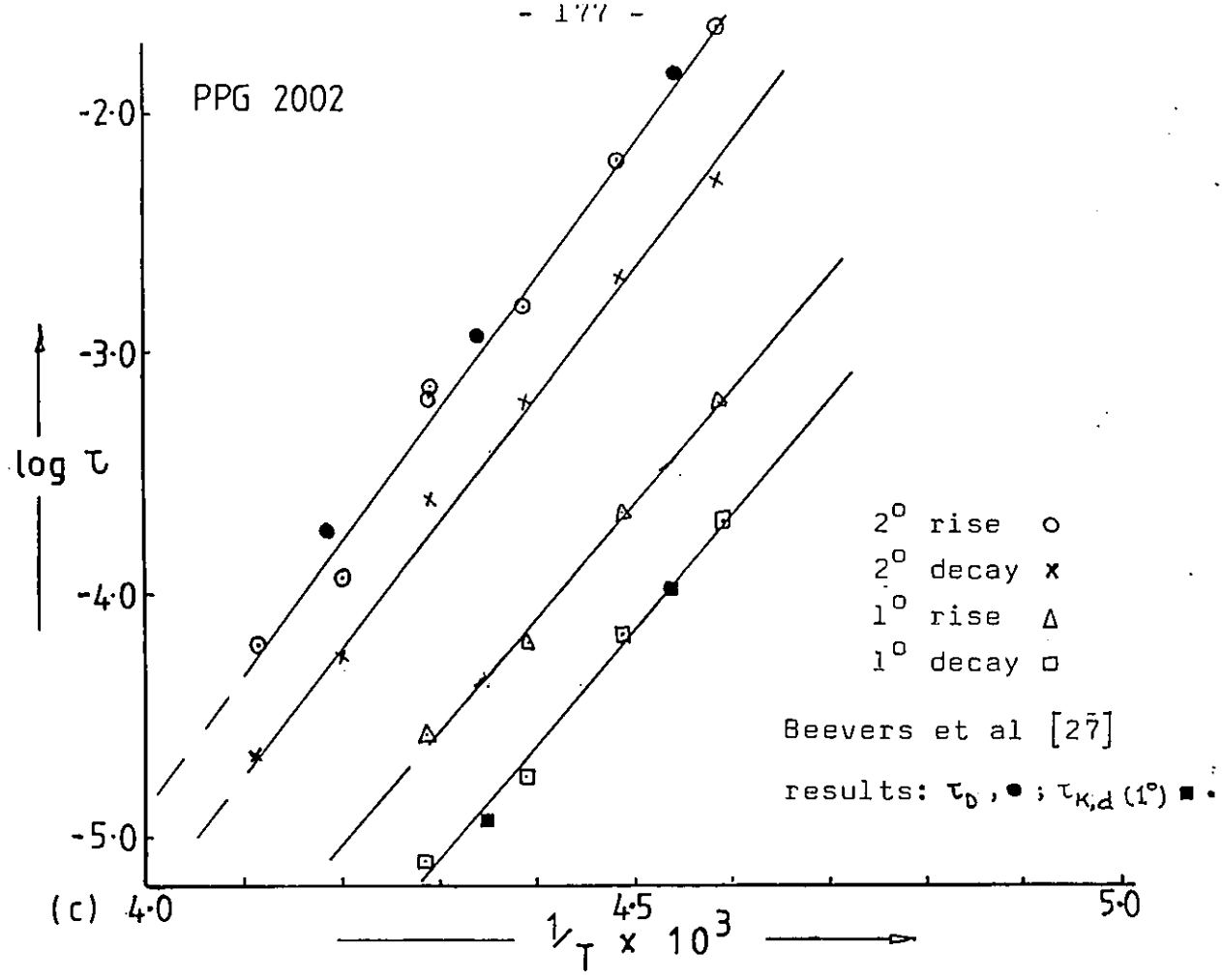

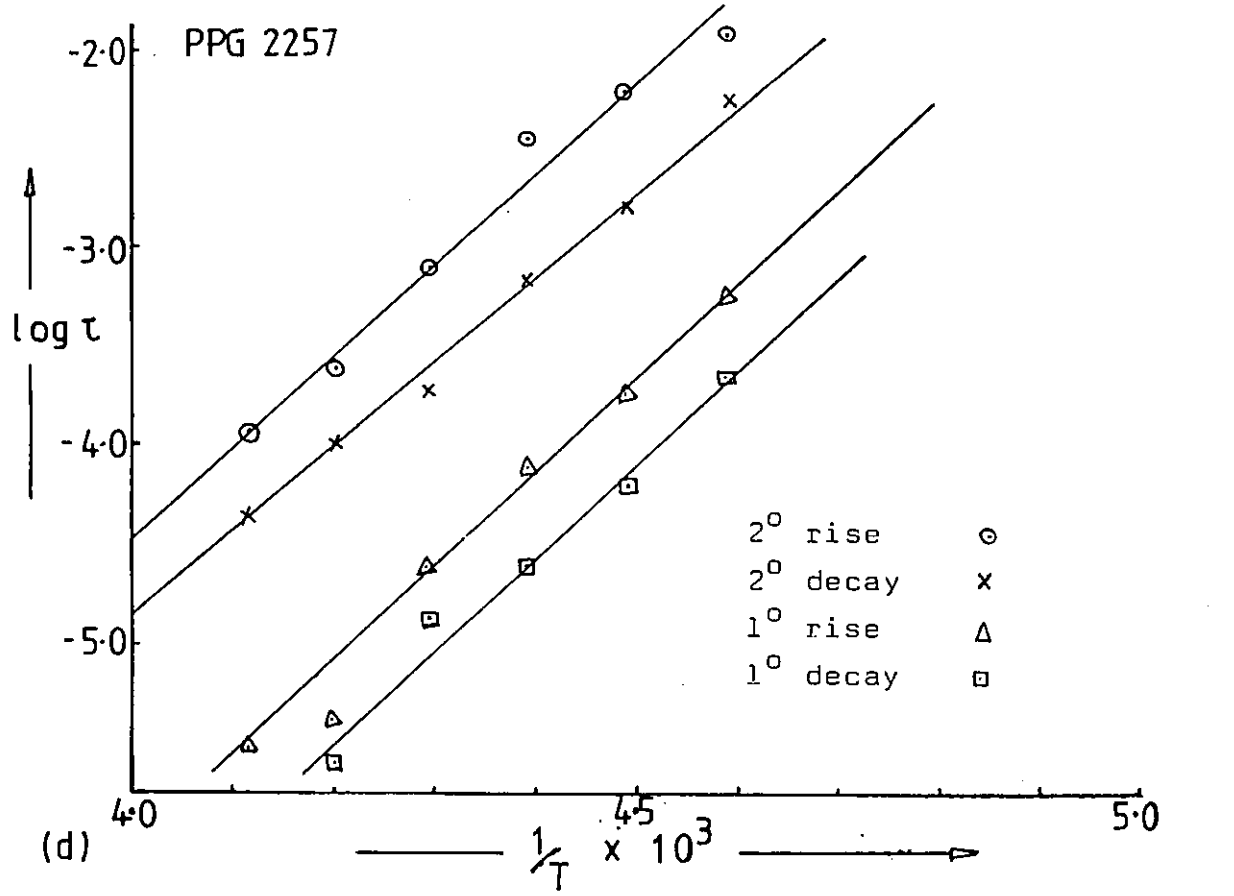

Fig 22 (c) The temperature dependence of the relaxation times of PPG 2002 and (d) PPG 2257.

(c) Concentration dependence of the relaxation times

The liquid glycols, being miscible with toluene, offered an opportunity of studying the relaxation behaviour over a wide range of concentrations from very dilute through to pure polymer (liquid or 'melt'). However limitations due to low birefringence restricted studies to the two highest molecular weight samples PPG 2002 and PPG 2257 at concentrations above 20 v/v %.

A typical birefringence transient for the diluted systems is shown in Fig 5.19c. The main difference from the bulk systems was that the negative primary process was considerably quicker, resulting in a time dependence dominated by the secondary process. In all cases, these decays were well represented by a single exponential function. The results for the secondary relaxation times obtained at various temperatures are shown in Table 5. 18 .

Significant birefringence was observed in solution at higher temperatures than for the bulk liquids, but as temperature decreased the amplitude of the birefringence for the bulk liquid increased relative to that obtained for the solution and eventually being much greater. Also at higher temperatures, e.g. 238 K for PPG 2257 and 243 and 238 K for PPG 2002, both the rise (τ_r) and decay (τ_d) relaxation times in the bulk were less than the corresponding times in solution. The data show that the concentration dependence of τ_r and τ_d was different and that this dependence varied with temperature.

At lower temperature ($T < 233$ K) the bulk values of both $(\tau_r)_{bulk}/(\tau_r)_{sol}$ and $(\tau_d)_{bulk}/(\tau_d)_{sol}$ eventually become much greater than one. As temperature was lowered, the solution values of τ_r and τ_d at first increase and then, at about 238 K, level out to values which are essentially constant within the experimental errors. At all temperatures the ratio τ_r/τ_d for the bulk polymer was greater than two while that for solutions varied between 1 and 1.3.

The temperature dependence of the liquid glycol viscosity is expected to be greater than that of the solution, and as the relaxation times should be roughly proportional to the viscosity we expect the relaxation time to increase with increasing viscosity and hence decreasing temperature.

Contrary to this expectation, the solution relaxation times levelled out and, moreover, the absolute values of the relaxation times of the solutions were greater than the bulk relaxation times at high temperatures. This suggests therefore that the relaxation processes in the solution are different from those occurring in the bulk liquid.

The ratios τ_r / τ_d for solution and bulk are also different, in the two cases. Although evidence is meagre, the values

Table 5.18 Secondary relaxation times variation, with Polypropylene glycol concentration in toluene.

Sample Sample	Concentration C/(v/v)%	Temp. K	Relaxation times, τ/μs		$\frac{\tau_r}{\tau_d}$
			Rise τ_r	Decay τ_d	
PPG 2257	20	238	343±33	314 ± 36	1.1
		233	383±33	342 ± 34	1.1
		223	353±47	378 ± 42	1.0
	50	253	213 ± 5	221 ± 6	1.0
		243	347±15	335 ±17	1.0
		238	425±27	329 ± 17	1.3
		233	437 ±32	338 ± 45	1.3
	100	238	253±14	105 ± 5	2.4
		233	797±45	210 ± 17	3.8
		228	2843±89	618 ± 43	4.6
		223	11180±140	1557± 70	4.0
PPG 2002	50	253	318	248	1.3
		243	366	266	1.4
		233	380	317	1.2
	100	243	62	22	2.8
		238	118	59	2.0
		233	635	265	2.4
		228	1600	638	2.5
		223	6336	2004	3.1

of this ratio for solutions are more in line with that expected for a 'fluctuation jump' mechanism than for rotational diffusion. However, the fact that the relaxation curves for the solutions were always close to a single exponential function is not in line with such mechanism, for which highly non-exponential relaxation curves have been observed in previous Kerr effect studies [90,91], on supercooled liquids and solutions. These differences between the τ_r/τ_d ratios for the bulk glycols and the solutions may be due to some extent to changes in local field effects in the different systems causing changes in the relative contributions of permanent and the induced dipole effects.

The concentration dependence of τ_r and τ_d observed here over a wide range of concentrations is very different from that observed on the other systems, where studies were restricted to semi-dilute solutions. The dynamical behaviour of these diluted bulk systems obviously requires a more detailed investigation than has been possible in this work. It was not possible to study the glycol systems at lower concentrations. In order to study the semi-dilute region for this polymer it was necessary to use the much higher molecular weight poly(propylene oxides).

5.4.3 Polypropylene oxide

In order to examine the concentration dependence of the dynamics of flexible chains in more detail, the studies were therefore extended to a range of polypropylene oxides (PPO) of higher molecular weight ($>10^6$), which have not previously been studied using the Kerr effect. Except for the -OH end group in the glycols, the oxide is structurally the same and has dipole components parallel and perpendicular to the chain backbone. The parallel component is again responsible for a slow relaxation via whole molecule rotation while the perpendicular component is responsible for fast relaxation via backbone segmental rotation [29].

Fig 5. 23 shows a typical birefringence transient obtained using a quarter wave plate. The rise transient is characterised by two regimes, a very fast initial portion followed by a gradual approach to the steady state. Upon

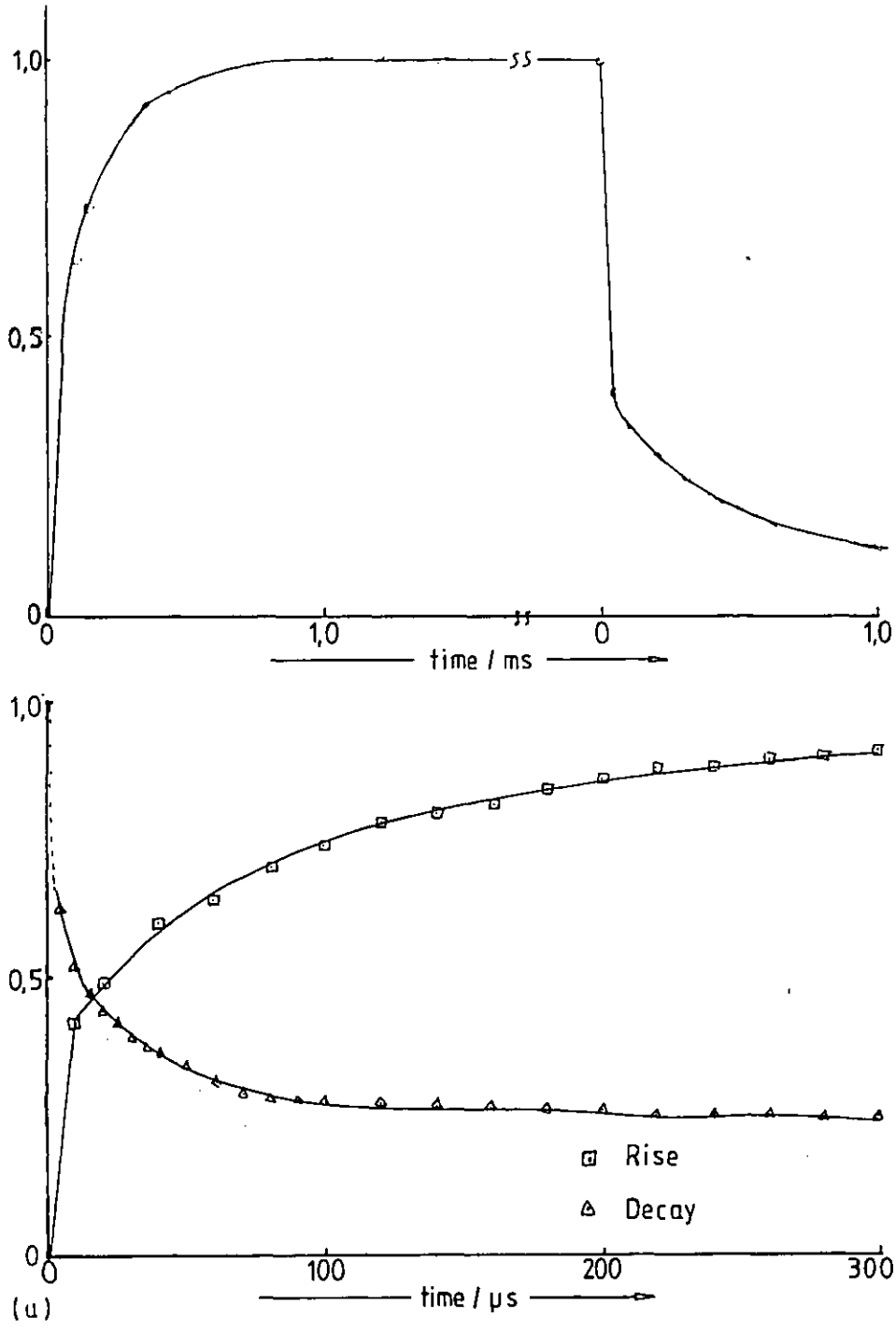

Fig 5·23 Representive birefringence transient for Polypropylene Oxide, $Mv = 1,44 \times 10^6$ in toluene.
(a) Expanded scale

field removal the decay transient follows same pattern, an initial rapidly decaying section followed by a much slower decay. This is clearly shown in the expanded scale of Fig 5.23 (a). In contrast to the low molecular weight glycols, both components give positive birefringence. The transients are in fact more similar to those for the lowest molecular weight glycol, PPG 0402, than to those of the other glycols.

5.4.4 Relaxation times for poly(propylene oxide)

The PPO transients were highly non-exponential. They have been characterised by three relaxation times, τ_ℓ , τ_{p1} and τ_{p2} obtained by 'peeling' method. The rise and decay transients have also been characterised in terms of their e^{-1} values, τ_r and τ_e respectively. All these times, together with their relative amplitudes and the ratio τ_r to τ_e, are shown in Table 5.19 , for the two samples studied, (M_v = 1.44 x 10^6 [S3.3] and 2.93 x 10^6 [S4.4])in toluene at 295 K. For both samples, the fastest relaxation time τ_{p2} contributes 50% of the decay transient whereas τ_ℓ and τ_{p1} contribute essentially equal amounts. These relative contributions do not vary significantly with concentration. The ratio τ_r/τ_e remains constant at a value ≈ 2, lower than that for the bulk glycols but significantly greater than for the glycol solutions.

The concentration dependence of the relaxation times is illustrated in Figs 5.24 (a), (b) for the two samples studied. In both cases, the relaxation times τ_ℓ, τ_{p1}, and τ_e have essentially the same concentration dependence with an exponent of 1.0±0.1 . In contrast the fastest relaxation time τ_{p2} is independent of concentration over the range studied. At the lowest concentrations studied the two fastest relaxations merge into one and the decay is then characterised by just one fast and one slow process.

No critical concentration, C_r was observed experimentally For S3.3 the calculated concentration, C_{rr}, giving the onset of entanglement, based on a rigid rod model, is 3.5 x 10^{-6} kg m^{-3} and that based on the random coil model C_{rc} is 10.5 kg m^{-3}. The fact that 10.5 kg m^{-3} was exceeded experimentally seems to suggest that C_r, occurs at a concentration less than the lowest concentration studied, and thus suggests that PPO is not a completely flexible random coil but has some degree of rigidity.

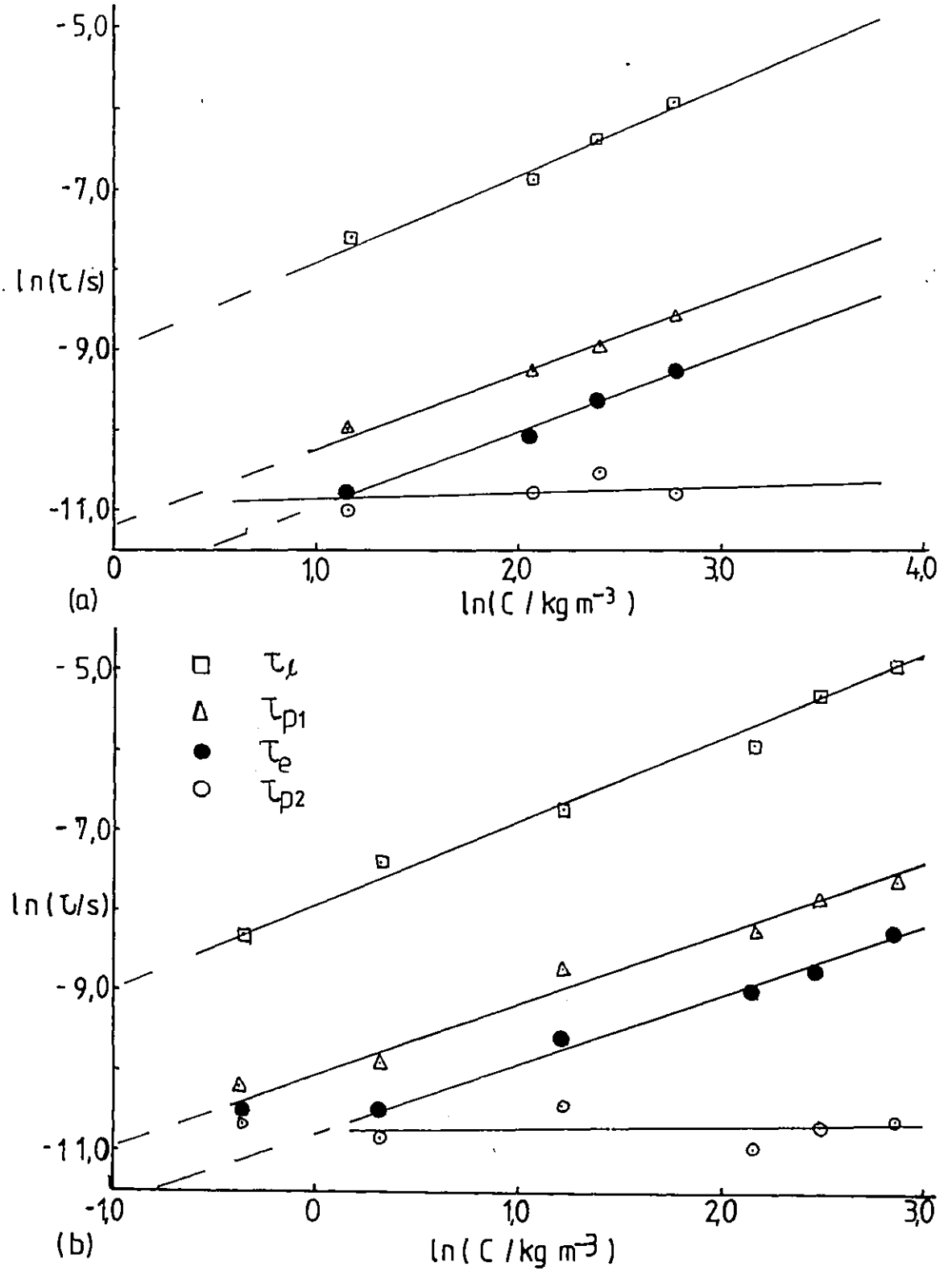

Fig 5·24 Concentration dependence of Polypropylene Oxide relaxation times.

(a) PPO S3·3 $M_v = 1.44 \times 10^6$

(b) PPO S4·4 $M_v = 2.93 \times 10^6$

Table 5.19 The relaxation times, τ, and the amplitudes, A_i, for the Kerr effect relaxation of Polypropylene oxide in toluene solution as a function of concentration. ($\tau/\mu s$)

Sample	Concentration kg m^{-3}	Long time		Relaxation data				τ_e	$\frac{\tau_r}{\tau_e}$
				First 'peeled'		Second 'peeled'			
		τ_ℓ	A_ℓ	τ_{p1}	A_{p1}	τ_{p2}	A_{p2}		
PPO S3.3	3.2	506 ± 28	0.29	61 ± 1.5	0.22	16	0.48	25	2.3
(M_v = 1.44	7.9	1010 ± 138	0.29	95 ± 6.0	0.24	22	0.48	42 ± 3	2.2
x 10^6)	11.1	1692 ± 76	0.26	127 ± 11.0	0.26	38	0.47	65 ± 5	1.9
	15.8	2587 ± 278	0.24	184 ± 23.0	0.27	22	0.48	98 ± 18	2.1
PPO S4.4	0.68	249 ± 9	0.22	36 ± 5	0.29	24	0.49	30 ± 10	1.7
(M_v = 2.93	1.4	618 ± 12	0.24	49 ± 3	0.27	20	0.50	26 ± 3	2.1
x 10^6)	3.4	1173 ± 221	0.22	164 ± 7	0.27	31	0.52	70 ± 10	2.2
	8.6	2577 ± 120	0.26	255 ± 13	0.27	17.2	0.47	120 ± 11	2.2
	12.0	5018 ± 250	0.26	375 ± 25	0.23	23.2	0.51	158 ± 20	2.0
	17.3	6840 ± 134	0.31	470 ± 32	0.14	25	0.56	270 ± 10	1.8

On the basis of the Rouse model, the relaxation times at 298 K calculated using the literature values of K = 12.9 x 10^{-6} m^3/kg and α = 0.75 [74] to give intrinsic viscosity in equation 2.2 are 1.6 μs and 5.3 μs for samples S3.3 and S4.4 respectively. However assuming some hydrodynamic interaction and using Zimm's model, the relaxation times associated with whole molecule rotations are 4.4 μs and 15.0 μs for S3.3 and S4.4 respectively. Experimentally the long relaxation times, τ_ℓ, observed for both samples are significantly higher than the values predicted by these models. However experiments were never made in the region where τ becomes independent of concentration. Extrapolation to zero concentration gives values of 295 μs and 270 μs. These are still significantly higher than the infinite dilution model values, presumably due to extrapolation from such high concentrations.

Although only two samples have been studied and so a precise study of the molecular weight dependence can not be made, it appears that τ_ℓ, τ_p, and τ_e all depend on molecular weight in a similar fashion, with an average exponent of 1.3 ± 0.1. This exponent does not vary significantly with concentration over the region studied (see Fig 5.25). However the fastest relaxation time τ_{p2} (≈22 μs) is independent of molecular weight (see Fig 5.25).

5.4.5 Discussion

In the PPO studies two relaxation times τ_ℓ, τ_{p1} both showed concentration and molecular weight dependence while τ_{p2} was independent of both. This contrasts with the observation for the bulk glycols, where there were only two relaxation times, τ_ℓ and τ_p and both were dependent on molecular weight. The contrasting behaviour of the shortest relaxation time indicates that the stiffness is such that the length of chain involved in backbone segmental motion is equal to that of the whole macromolecule for these shorter glycol chains ($M/M_o < 40$), but is small compared with the overall length of the high molecular weight PPO ($M/M_o > 24000$). This behaviour is akin to an observation made in the work of North on poly(N-vinylcarbazole) [87,77] in which the polymer behaved as a stiff coil for $M_w < 10^4$ giving a molecular weight dependent relaxation time but changed to flexible coil at higher molecular

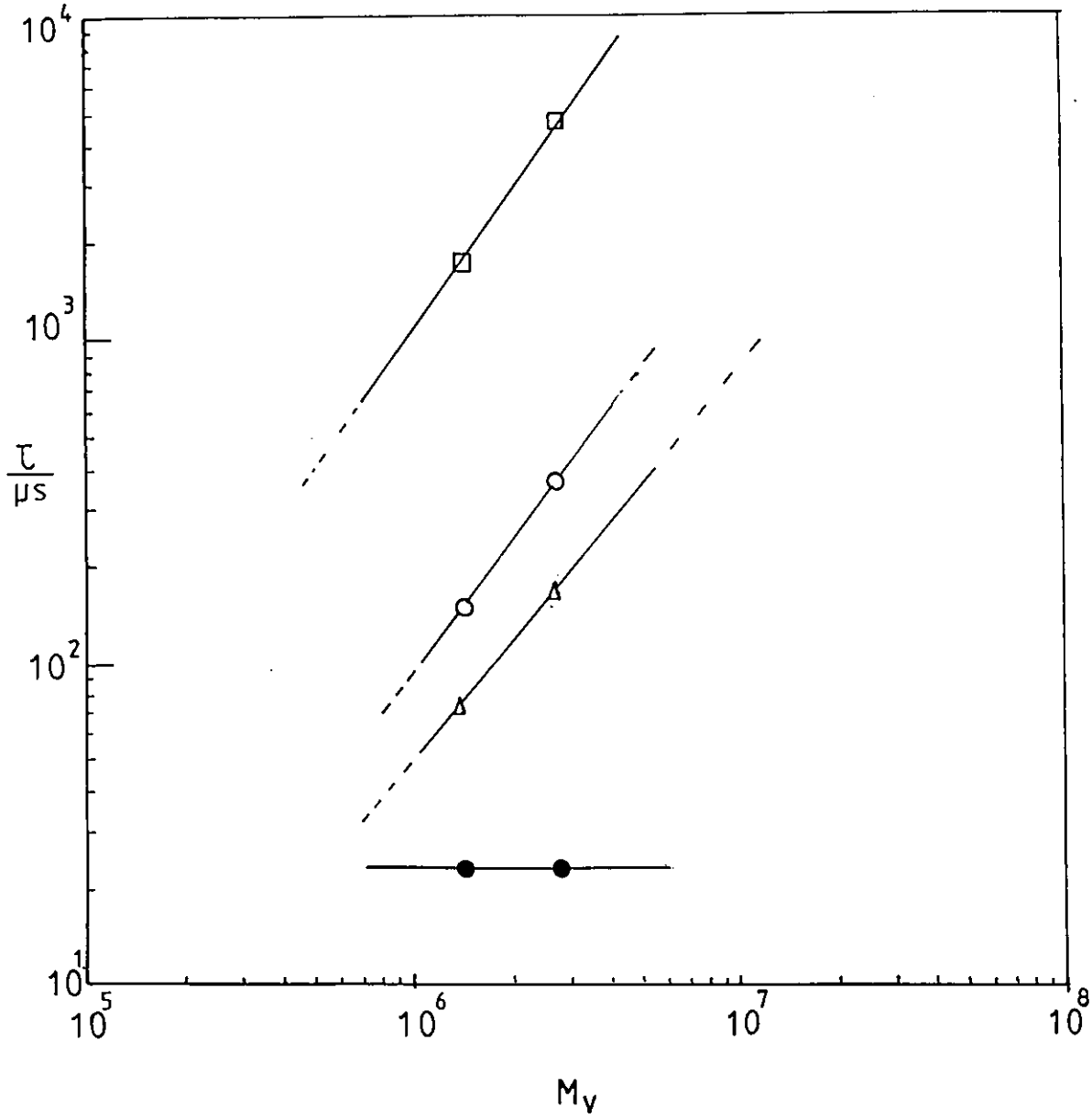

Fig 5·25 Molecular weight (M_V) dependence of the relaxation times of Polypropylene oxide, at concentration 12·2 kg m^{-3} : τ_t (□) , τ_{p_1} (○) , τ_e (Δ) , τ_{p_2} (●) .

weight ($M_w > 5 \times 10^4$), for which the relaxation time was independent of M.- The observed behaviour of τ_{p2} in PPO therefore suggests a truly local motion; τ_{p1} may be characteristic of longer segments and therefore molecular weight dependent.

The M dependence of τ_p for the glycols ($\zeta_m = 1.25 \pm 0.2$) is similar to that for τ_{p1} in PPO ($\zeta_m \simeq 1.3 \pm 0.1$), which suggests that they may both be associated with relaxation of the perpendicular dipole component via backbone rotation of long chain segments. By contrast, the value of ζ_m for τ_ℓ for the glycols (1.95 ± 0.2) is significantly greater than for the oxides ($\simeq 1.3$). Both these relaxation times are believed to be associated with motions of the whole chain. The Rouse-Zimm 'bead and spring' model (see 2.3.1) predicts that the relaxation time associated with whole molecule rotation for flexible coils in dilute solution should vary with the molecular weight as

$$\tau_1 \propto M[\eta] \propto M^{1+\alpha} \qquad 5.11$$

where the Mark-Houwink coefficient α varies from 0.5 to 0.8 and is 0.75 for PPO in toluene. For concentrated systems, on the other hand, de Gennes [16] in his reptation model (see section 2.3.2) predicted that the time associated with the reptation of molecules should scale as the square of M. The exponent $\zeta_m = 1.95$ observed for the secondary process in glycols agrees with such reptation model. The PPO solutions, in which the chain density is much lower , do not appear to behave in this way and are more consistent with the predicted exponent based on isolated molecule rotation.

The concentration exponent ζ_c, for the PPO τ_ℓ and τ_{p1} values is fairly constant, 1.0 ± 0.1. The exponent is not surprisingly less than the DE predicted value of 2 in view of the flexibility of the PPO chains. However it is about the same as that obtained in the PBLG studies for $C > C_r$ and for ethyl cellulose at $C < C_r$ (see section 5.5), both of which are relatively stiff chains. The fact that the concentration and molecular weight dependences of τ_ℓ and τ_{p1} are the same suggests that they may simply reflect polydispersity of the sample, in which τ_ℓ reflects the whole molecule behaviour of the long chains and τ_{p1} that of the shorter ones.

5.5 Ethyl cellulose, EC

5.5.1 The Kerr effect

Cellulose derivatives have been shown to behave as stiff random coil polymers in solution [77], in which the individual monomer dipole moments have components both parallel and perpendicular to the chain contour. The presence of a large parallel dipole component along the chain backbone results in the orientation of the macromolecule as a whole when an electric field is applied. When the field is removed, the way in which this component reverts to a random orientation will reflect the whole molecule rotational motion of the polymer chain.

Fig 5. 26(a) shows a typical normalised time dependent phase shift ($\delta(t)/\delta_{max}$) for ethyl cellulose in toluene. In contrast to the transient behaviour observed in the other polymer systems studied the rise and the decay transients here have approximately the same shape. The plot of log δ/δ_{max} versus time for the decay transient shows that the function is not a single exponential (see Fig 5.26 (b)). There is a rapid initial response followed by a slow approach to equilibrium . One method of characterising the non-exponential form of the birefringence is to use the empirical relaxation function of Williams and Watts [79] (see section 3.7 4). Fig 5.27 shows the plot of this function for the rise and decay data for the example shown in Fig 5.26. This reveals that the rise and decay transients are essentially identical and are both described well by the Williams-Watts function with

$$\beta_{K,r} \simeq \beta_{K,d} \simeq 0.51 \pm 0.04$$

Values of τ, β and $\langle\tau\rangle$ obtained for the rise (r) and decay (d) transients for various concentrations of ethyl cellulose (M_n=26300) in toluene are shown in Table 5.20.

For the ethyl cellulose data, it was found that a good representation of the decay transient could also be obtained using a two exponential fit evaluating τ_i and A_i by the 'peeling' procedure described in section 3.7.4(iv). For each concentration a slow relaxation time τ_ℓ and a much faster relaxation time τ_p were determined in this way and are also given in Table 5.20 alongside with their relative amplitudes

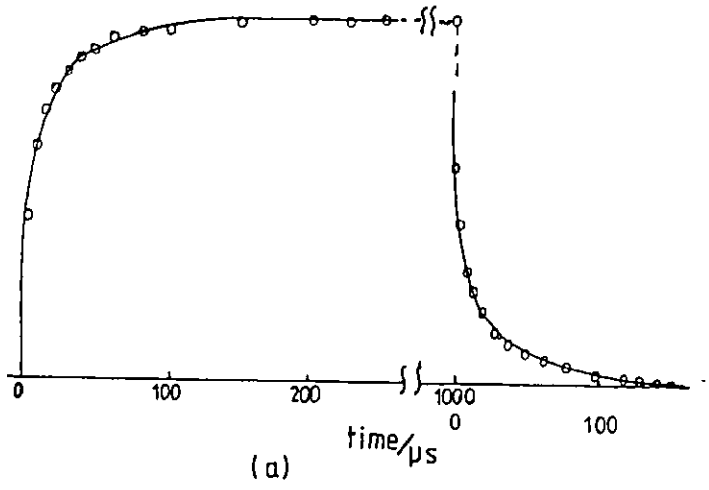

(a)

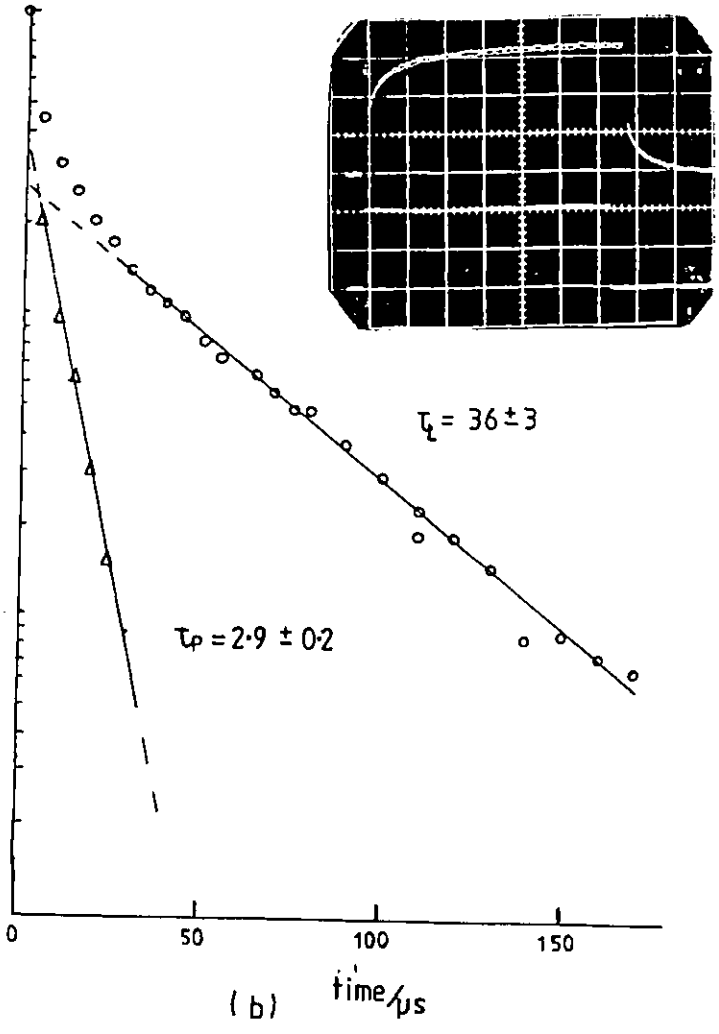

(b)

Fig 5.26 (a) Representative normalised transients δ/δ_{max} for ethyl cellulose .

(b) Log δ/δ_{max} against time for decay transient of 47.2 kg m^{-3} solution of ethyl cellulose in toluene .

and the e^{-1} relaxation times, τ_r and τ_e. The table shows that:

(a) $\beta_{K,d} \simeq \beta_{K,r}$

(b) $\langle\tau\rangle_{K,d} \simeq \langle\tau\rangle_{K,r}$

(c) the contribution of the slow relaxation to the decay process is about 40%, and varies little with concentration.

(d) the values of β decrease slightly with increasing concentration, implying a greater deviation from single exponential behaviour as concentration increases.

Fig 5.28 shows the concentration dependence of the relaxation times $\langle\tau\rangle$ and τ_ℓ the parameter $\beta_{K,d}$ ($\simeq\beta_{K,r}$) and the solution viscosity, η. The log-log plots for the relaxation times are essentially linear at low concentrations with a sharp transition to a steeper linear region over a narrow concentration range centred on $C_r \simeq 23$ kg m^{-3}. Representing the dependence of the relaxation time on concentration by the expression

$$\tau = KC^{\zeta_c} \qquad 5.1$$

the data indicate that for $\langle\tau\rangle$,

$$\zeta_c = 0.75 \pm 0.32 \quad C < C_r$$
$$\zeta_c = 1.75 \pm 0.2 \quad C > C_r$$

The concentration dependence of τ_e is essentially the same as for $\langle\tau\rangle$ in the two regions.

Interestingly the curve of log η versus log C (Fig 5.28) shows a similar pronounced change in slope over the same region of concentration. The transition is not as sharp in this case since the concentration exponent ζ_η for the viscosity increases gradually from zero as concentration increases from low values, changing very rapidly in the range $C \simeq 1 - 2$ kg m^{-3} and then becoming essentially constant (ζ_c 2.2±0.3) above C=2 kg m^{-3}. These two independent methods of observing the effect of concentration on the motion of polymer chains, show a sharp change in behaviour over the same narrow concentration range.

The $\beta_{K,d}$ - concentration plot (Fig 5.28) shows that $\beta_{K,d}$ increases with decreasing concentration, tending to a constant value above the critical concentration. For $C<C_r$, $\beta_{K,r}$ increases with decreasing concentration, with the implication that the Kerr decay transient for ethyl cellulose tends towards a single

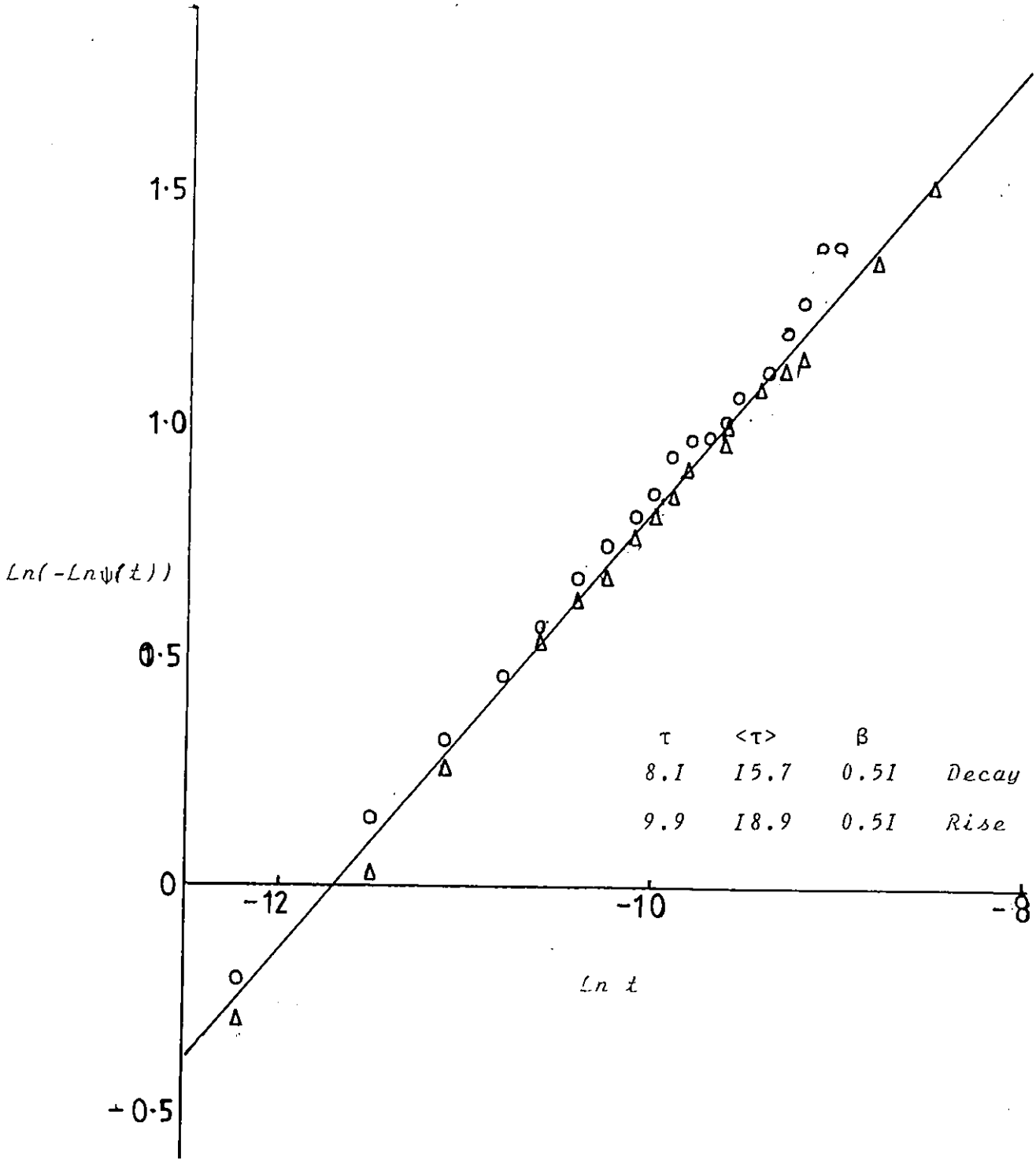

Fig 5.27 Ln(-Lnψ(t)) against Ln t for 47.2 kg m^{-3} ethyl cellulose in toluene at 293 K with ψ(t) = ϕ_d for the decay(○) and = 1 - ϕ_r for the rise(Δ). ϕ_r and ϕ_r are the normalised δ/δ_{max} rise and decay birefringence respectively.

Table 5.20 The relaxation times, τ, the spread factor β and amplitude A_ℓ, for the for the Kerr effect relaxation of ethyl cellulose in toluene as function of concentration.

Concentration, C ($kg\ m^{-3}$)	Decay							Rise		
	$\tau/\mu s$	$\langle\tau\rangle_{K,d}/\mu s$	$\beta_{K,d}$	$\tau_\ell/\mu s$	A_ℓ	$\tau_p/\mu s$	$\tau_e/\mu s$	$\langle\tau\rangle_{K,r}$	$\beta_{K,r}$	τ_r
5.1	0.86	0.96	0.82	2.6	0.55		0.7	1.1	0.78	1.0
6.6	1.3±0.2	1.74	0.71	2.9±0.4	0.45	0.8±0.1	1.0	1.8	0.62	1.3
9.5	1.6± 0.2	2.2±0.3	0.67	3.5±1.2	0.33	1.0±0.3	1.8	3.0	0.57	2.5
9.6	1.6± 0.2	3.4±1.3	0.48	3.9±1.2	0.47	1.2±0.4	1.8	4.4	0.53	2.1
12.7	1.7± 0.3	3.2±1.0	0.55	6.0±0.8	0.33	1.2±0.6	2.4	4.3	0.55	2.5
16.6	2.72±0.3	4.8±0.2	0.50	5.7±0.3	0.42	1.5±0.3		6.0	0.49	
$C_n = 20$										
25.4	3.9 ± 0.8	5.7±0.9	0.53	8.6±0.5	0.41	4.2±3.7	3.0	6.8	0.57	3.3
33.1	3.6 ± 0.1	6.3±0.8	0.55	13.7±3.2	0.4	1.9±0.7	4.2	8.2	0.55	5.3
40.0	4.4 ± 1.2	10.6±2.1	0.39	22.2±2.0	0.37	2.0±1.1		1332		
47.2	7.74±0.8	15.7±3.0	0.53	33. ± 2.7	0.4	1.9±1.0	6.9	18.9	0.51	6.6
57	9.9 ± 0.6	24.5±3.1	0.44	54.5±4.8	0.42	2.2±0.7		30.1	0.5	
70.2	20.1± 1.6	37 ± 4.4	0.56	68.5±12	0.38	2.1±1.3	8.5	42.3	0.48	9.2

The values of $\langle\tau\rangle$ β τ_ℓ A_ℓ given are the average values from 4 experiments for each concentration and the uncertainties quoted indicate the spread of results obtained.

exponential at infinite dilution behaviour which is reminiscent of perfectly rigid, monodisperse rods.

The concentration dependence of the fast process τ_p (Fig 5.28) is lower than for τ_ℓ but still significant, with an exponent of 0.42±0.1. However, this process does not show any break in slope as concentration is increased.

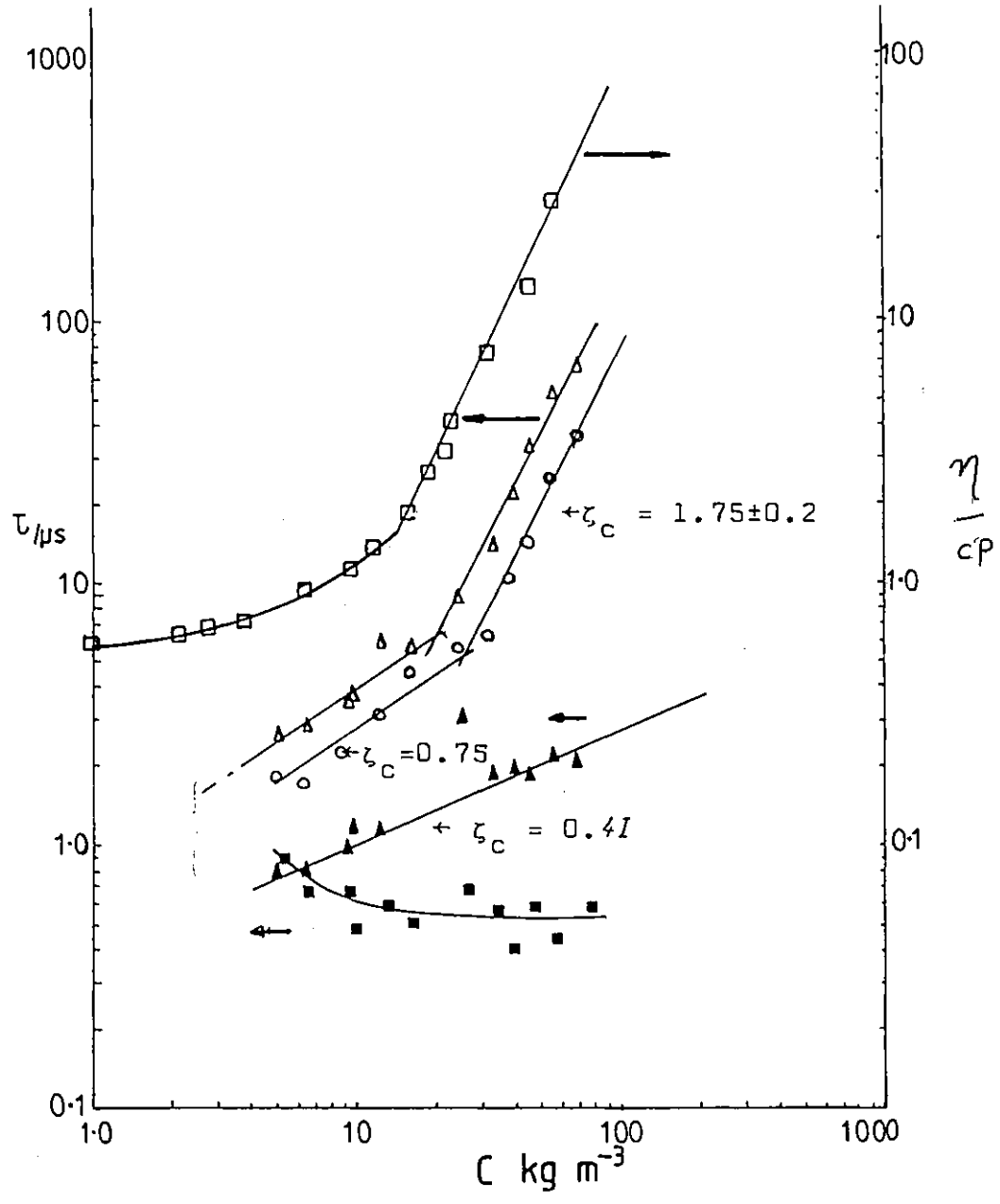

Fig 5.28 Log - Log plots of relaxation times $\langle\tau\rangle_{K,d}$(○); τ_ℓ (△); τ_p(▲); solution viscosity(□) and relaxation spread factor (■) against concentration, C for ethyl cellulose in toluene.

5.5.2 Photon Correlation Spectroscopy. PCS

The Kerr electro-optic measurements on the ethyl cellulose have given information on the rotational motion of these stiff chain macromolecules, and showed that there is a pronounced concentration dependence of the characteristic times for such processes. In order to study the translational motion of the molecules under similar conditions, photon correlation spectroscopy was used.

The autocorrelation functions were characterised by the method described in section 3.12. Fig 5.29 shows a plot of the logarithmic of the normalised autocorrelation function $[g^{(2)} - 1]$ (the 'logarithmic correlation function') versus time for a typical example (44 kg m^{-3} solution, 298 K using channel time of 10^{-3}s). The curve forms two distinct linear regions, well separated in time, and has been characterised by a two exponential expression of the form of eqn 3.48, 3.49:

$$\left[g^{(2)} - 1\right]_{t\to 0} = A_1 \exp^{-\Gamma_1 t} \qquad 5.12$$

$$\left[g^{(2)} - 1\right]_{t\to \infty} = A_2 \exp^{-\Gamma_2 t} \qquad 5.13$$

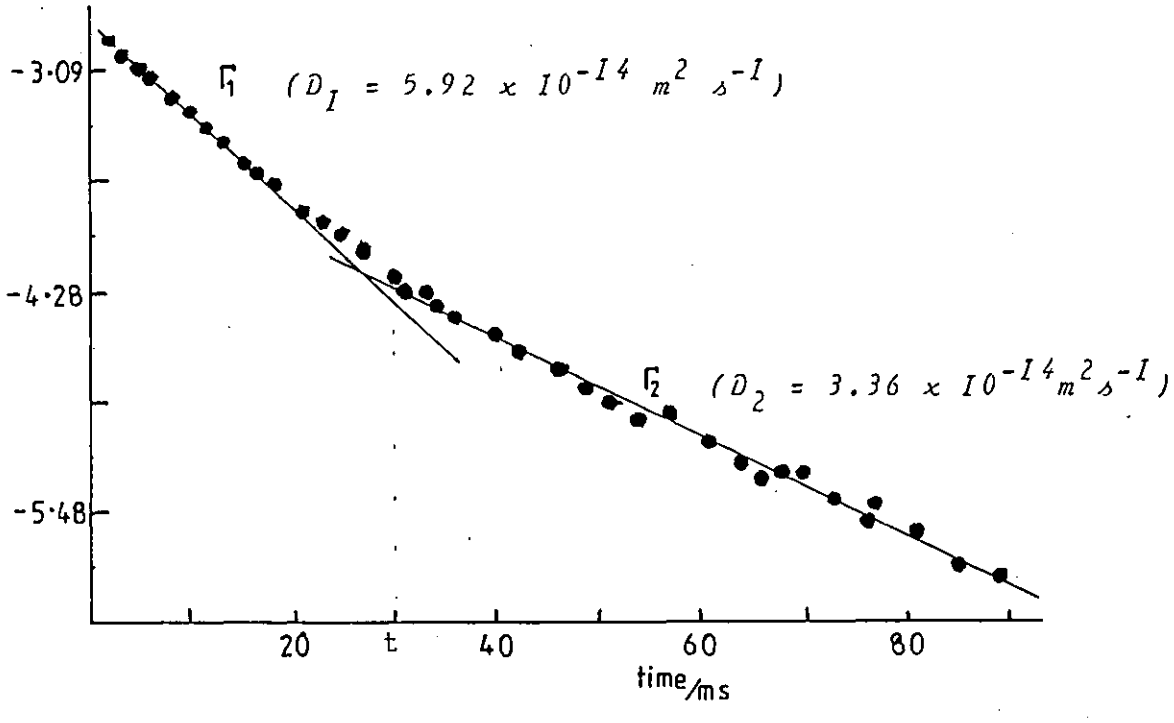

Fig 5.29 Semi-log plot of the logarithmic correlation function against channel time for 44 kg m^{-3} solution of ethyl cellulose in toluene at 298 K using a channel time of 1.0 ms.

The reciprocal time constants Γ_1 and Γ_2 were determined for many values of the scattering angle θ and hence of the wave-vector K.and are plotted against , K, $K^2$and K^3 in Fig 5.30. Despite the scatter in the data, these plots clearly indicate a K^2 dependence for Γ_1 and Γ_2. Consequently, these have been interpreted in terms of characteristic diffusion coefficients D_1 and D_2 according to the equations (see section 3.12).

$$\Gamma_1 = 2D_1K^2 \qquad 5\cdot14$$

$$\Gamma_2 = 2D_2K^2 \qquad 5\cdot15$$

A similar K^2 dependence was observed for all the Γ_i obtained in this work, and consequently the results are described in terms of characteristic diffusion coefficients associated with linear portions of the logarithmic correlation function. The short time behaviour of the functions was examined by reducing the channel time t_c and analysing the data as described in section 3.12. In Fig 5.31 (a) the channel time has been reduced to a quarter of that of Fig 5.29. This plot reveals that the portion of the curve for t<30 ms, which in Fig 5.29 was essentially linear, infact under higher resolution itself consists of two linear portions with a distinct change in slope at t = 6.3 ms. The long time slope in this case gives $D_2 = 5.7 \times 10^{-14}\ m^2s^{-1}$, in good agreement with D_1 value of Fig 5.29. At short times the slope increases and $D_1 = 7.3 \times 10^{-14}m^2\ s^{-1}$. Reducing the channel time still further to 62.5μs (Fig 5.31 (b) shows that this linear portion below 6.3 ms persists down to t= 0.6 ms. For very short times, a further sharp increase in slope is observed , characterised by $D_1 = 17.3 \times 10^{-14}\ m^2s^{-1}$.

These results suggest that the full logarithmic correlation function consists of three distinct regions, characterised by the diffusion coefficients D_ℓ, D_m and D_i ($D_\ell < D_m < D_i$). This is illustrated schematically in Fig 32. The coefficient $D_1$and D_2 obtained in different experiments change systematically from D_ℓ,D_m, to D_i as the channel time is reduced. This is illustrated for the example chosen in Table 5. 21

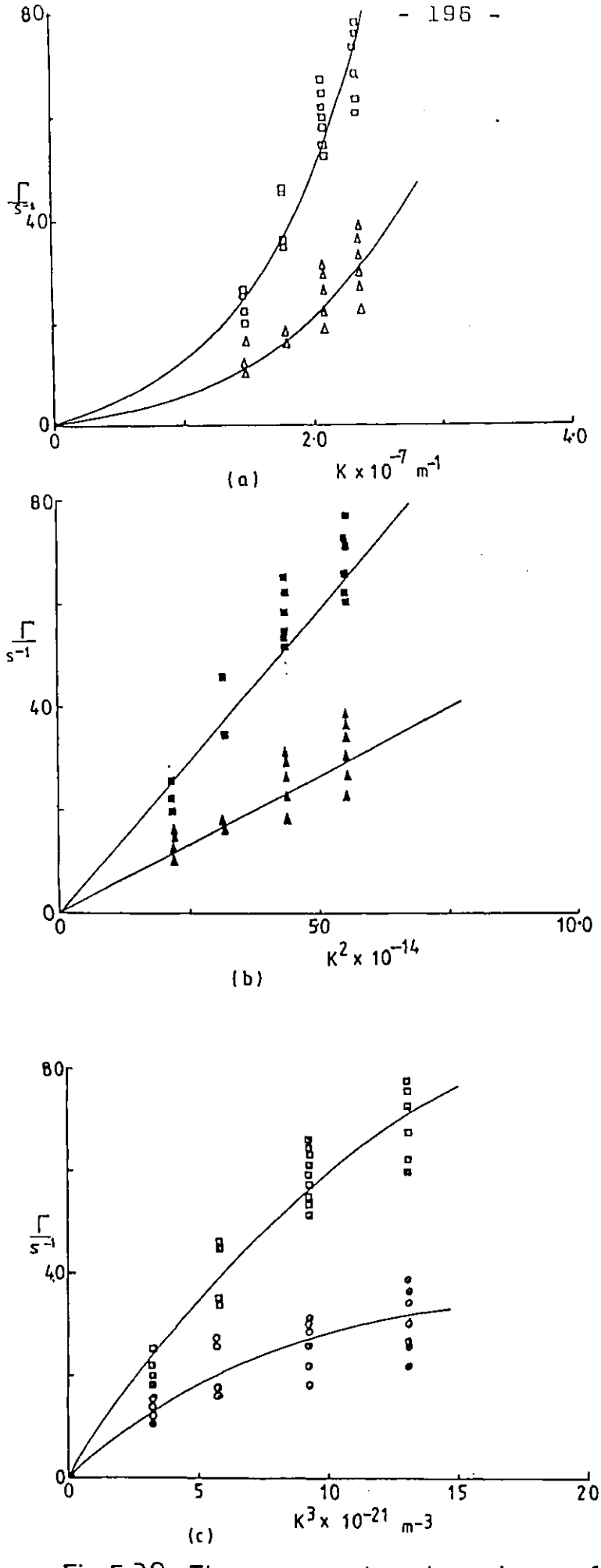

Fig 5.30 The wave vector dependence of the reciprocal time constants Γ_L,(□); Γ_m ,(○) of the autocorrelation function. (a) K (b) K^2 (c) K^3

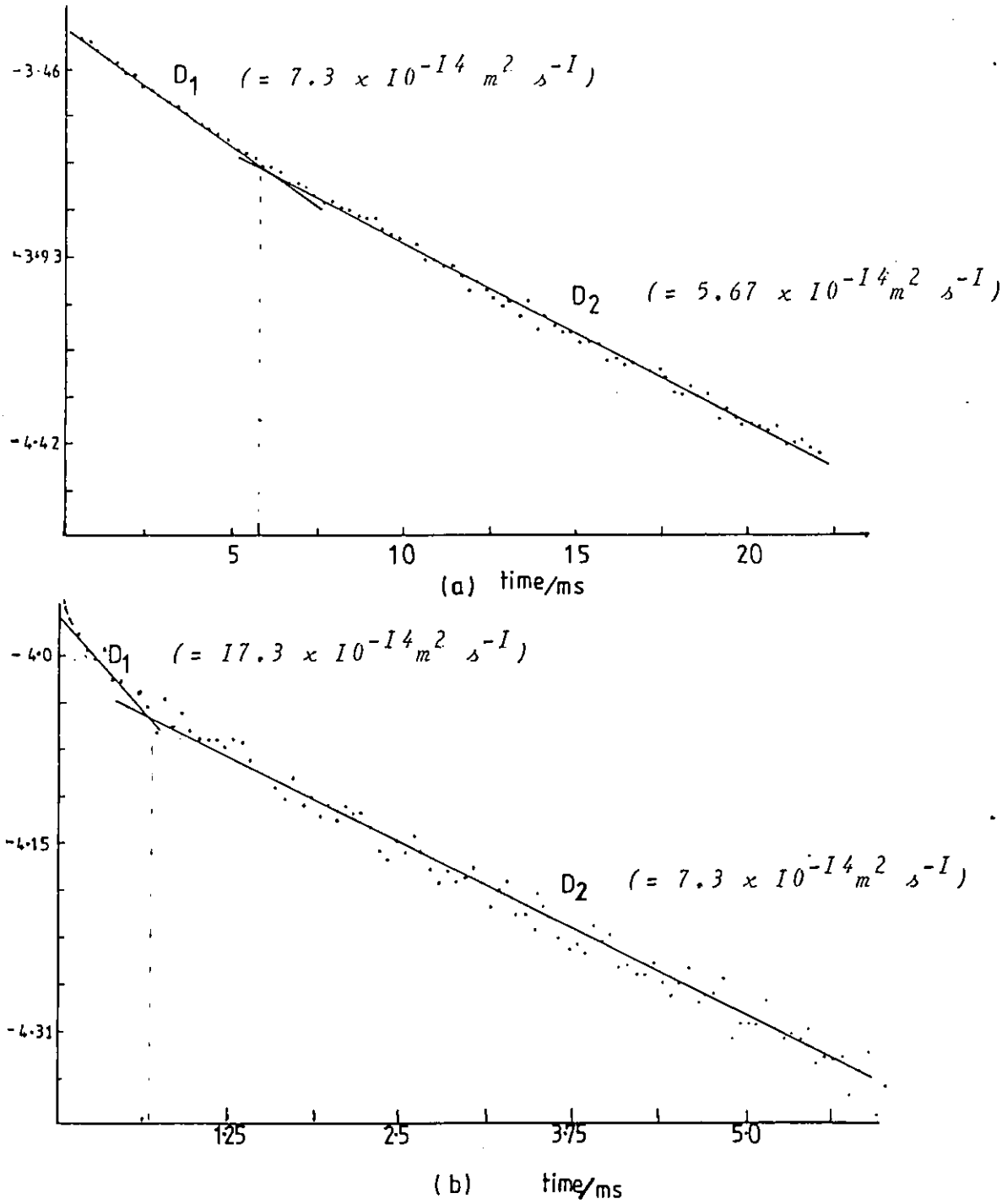

Fig 5.31 The plots of the logarithmic correlation function at (a) channel time t_c = 250 μs and (b) channel time t_c = 62.5 μs for 44 kg m^{-3} ethyl cellulose in toluene and 298 K

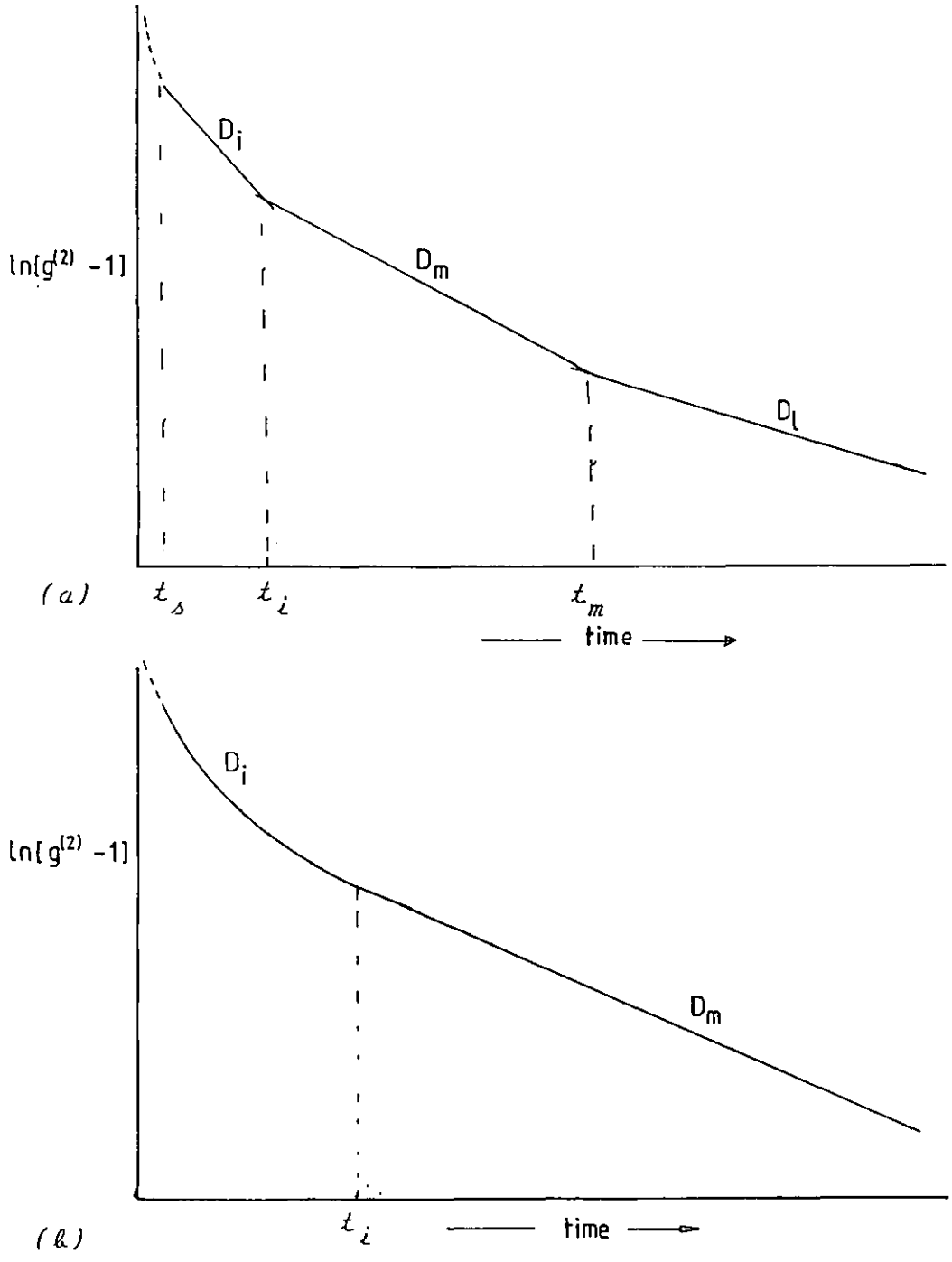

Fig 5.32 Schematic diagram showing the logarithmic correlation function.
(a) Full function showing D_l, D_m and D_i for 44 kg m^{-3} for $C>C_n$.
(b) Function for lower concentrations showing D_i and D_m for $C<C_n$.

Table 5.21 Variation of D_m and D_ℓ with channel time for a 44 kg m^{-3} solution of EC in toluene, 298K

Channel time/ms	$D_1 \times 10^{14}$ $m^2 s^{-1}$	$D_2 \times 10^{14}$ $m^2 s^{-1}$
1.8	5.96 ≡ D_m	3.4 ≡ D_ℓ
1.2	5.23 ≡ D_m	3.28 ≡ D_ℓ
1.0	5.92 ≡ D_m	3.36 ≡ D_ℓ
0.25	7.3 ≡ D_i	5.7 ≡ D_m
0.063	17.0 $t<t_c$	6.7 ≡ D_i

This behaviour is illustrated in an alternative way in Fig 5.33 in which values of D_1 and D_2 obtained in experiments in which only the D_i/D_m portions of the correlation function was observed (i.e. $t < t_m$ in Fig 5.32 (a)) are plotted as a function of K^2t_c. For the 44kg m^{-3} solution D_1 and D_2 remain comstant over wide ranges of K^2t_c, indicating the existence of distinct linear portion of the function of the form illustrated in Fig 5.32(a). Fig 5.33 also shows clearly the distinct increase in slope at short times $t< t_s$. The results for this 44 kg m^{-3} sample were typical of those observed for concentrations greater than C_r (23 kg m^{-3}).

Also shown in this figure are the corresponding data for a 23 kg m^{-3} solution at 298 K, which typifies the behaviour of solutions of lower concentration. It can be seen that the diffusion coefficients are of order of magnitude greater than those for the more concentrated system. In contrast to the latter, the values of D_1 and D_2 do not remain constant over a significant range of K^2t_c. This reflects the fact that, although in a single experiment distinct linear regions can still be identified, the slope of the logarithmic correlation function is changing much more rapidly with time in this case. In fact the shape of the overall correlation function for concentrations below C_r is of the form shown in Fig 5.32(b) where there is no long time (D_ℓ) region. Consequently, although D_m may still be readly characterised, the identification of a distinct D_i value for this system is not possible. Although this appears to contrast sharply with the behaviour of the more concentrated solutions, it is worth noting that

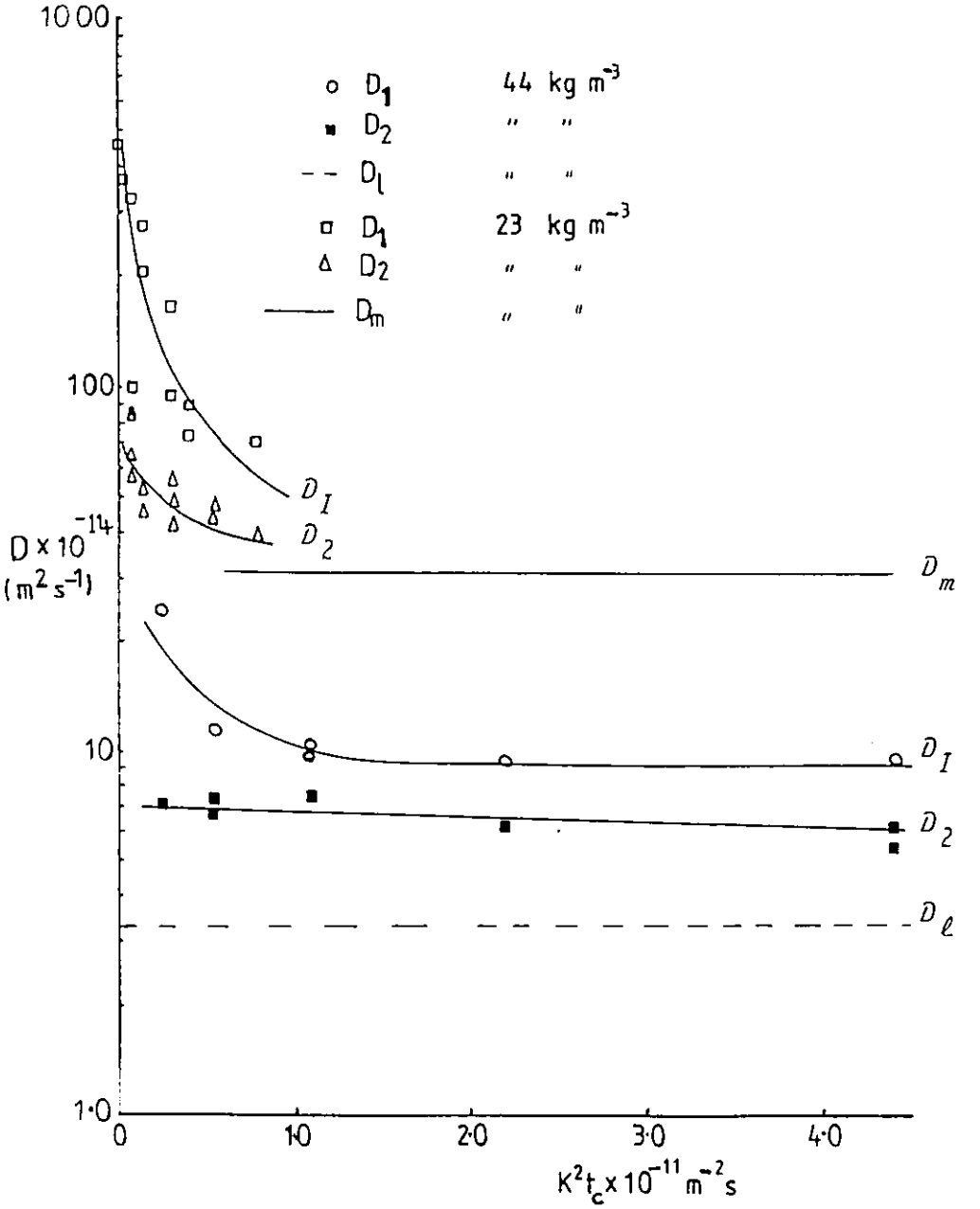

Fig 5.33 The diffusional coefficients D, variation with $K^2 t_c$ for 44 kg m^{-3} and 23 kg m^{-3} ethyl cellulose in toluene at 298 K.

the value of K^2t_c below which deviation from the longer time (D_m) slope is observed for $C < 23$ kg m^{-3} is essentially the same as K^2t_i for $C > 23$ kg m^{-3}. Hence the continuous increase in the slope of the logarithmic correlation function for the low concentration solutions only occurs in the same K^2t region in which the higher concentration systems exhibit the same behaviour. This is clearly seen in Fig 5.33, where D_1 and D_2 approach each other, and D_m, rapidly for $K^2t_c > 1.0 \times 10^{11}$ m^{-2} s.

Concentration dependence of the diffusion coefficients.

Dramatic changes were observed in the values of D_ℓ and and D_m as the concentration of ethyl cellulose in toluene was varied as illustrated in Fig 5.34. The long time slope characterised by D_ℓ was not observed until a critical concentration , $C_r \simeq 23 \pm 2$ kg m^{-3} was reached. Above this critical concentration within the rather large spread of the observations due to the low scattering intensities from these solutions, D_ℓ remained constant at $3.5 \pm 0.5 \times 10^{-14}$ m^2 s^{-1}. Such a dramatic change in the dynamics of the system at a concentration $\simeq 20$ kg m^{-3} is reminiscent of that observed for both the Kerr effect relaxation and the solution viscosity. In contrast to D_ℓ, at concentrations above 23 kg m^{-3} D_m changes gradually with concentration; Fig 5.34 shows an appropriate power law dependence of the form,

$$D_m = K C^{\zeta_c} \qquad 5.16$$

where $\zeta_c = -2.0 \pm 0.3$. At the highest concentrations studied D_m approached D_ℓ as the correlation functions obtained approached single exponential behaviour. Below the critical concentration, the variation of D_m with concentration was much less marked. Within the experimental scatter, D_m levelled out to a value of about $35 \pm 10 \times 10^{-14}$ m^2 s^{-1}. This change over from C^{-2} to C^0 behaviour at $C \simeq 25$ kg m^{-3} is emphasised in Fig.5.35.

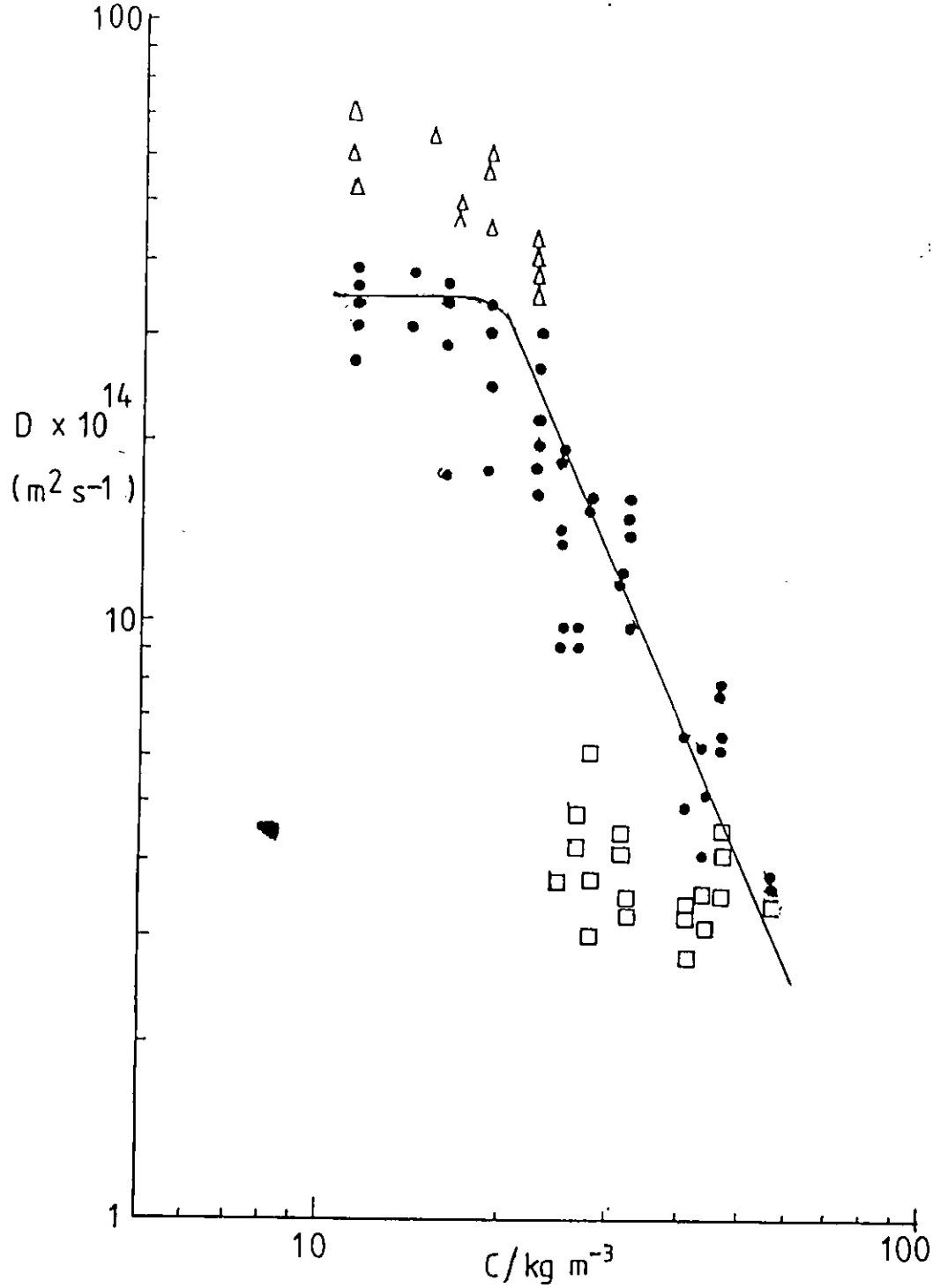

Fig 5·34 The concentration dependence of the translational diffusion coefficient, D_L (□) ; D_m (●) . and D_i (Δ)

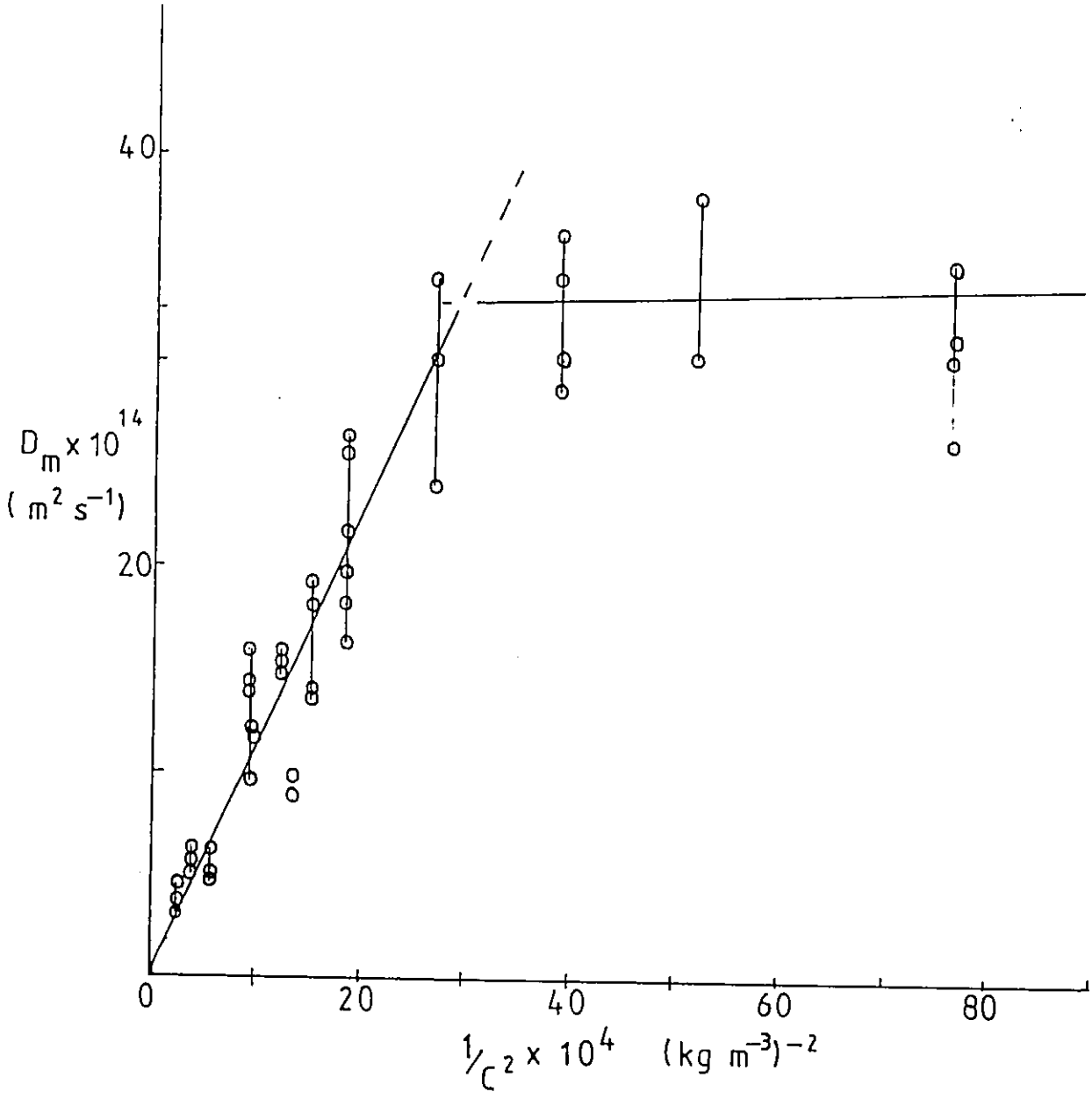

Fig 5.35 The concentration dependence of the translational diffusion coefficient, D_m, of ethyl cellulose in toluene.

5.5.3 Discussion.

The information obtained from the Kerr effect, viscosity and photon correlation spectroscopy (PCS) studies of ethyl cellulose in toluene is summarised in Table 5.22 . A possible explanation of these observations in terms of a simple physical model will be given first. Subsequently the extent to which the data can be interpreted in more quantitative terms using recent theories for the dynamics of semi-flexible chains in concentrated solution will be examined.

Interpretation of the results in terms of the physical model

(a) The model

The basis of the physical model for semi-flexible coil molecules like ethyl cellulose is shown in Fig 5.36 .In the dilute region Fig 5.36 (a), $C < C_1$, ethyl cellulose will undergo motions characteristic of an isolated stiff chain, characterised by a persistence length q, within which local monomer unit rotation is restricted. However local segmental chain motion can occur by rotation of lengths of the chain of order q.

As concentration is increased beyond some (low) value C_1, chain interactions become significant and the dynamics of the molecules will be modified. In this semi-dilute region, Fig 5.36(b), the mean separation between chain contact points, a_c is much larger than the persistence length q. Hence whilst the translational motion of the chains becomes increasingly hindered by the intermolecular forces, the more local segmental motions are relatively unaffected by these long range interactions. Furthermore, the chains can still move past one another relatively easily by undergoing changes in the shape by means of these local segmental motions to minimise the constraints on the translational motion.

Eventually, the concentration is increased to such a point, C_2, that the mean chain separation is now comparable with or smaller than q (see Fig 5.36(c)). In this concentrated region, chain translational motion is highly hindered and the system has a pseudo network structure in which the density of local chain interactions is high, although continually changing in time and space. Here, local segmental motion, though restricted, can still occur within the multi-chain

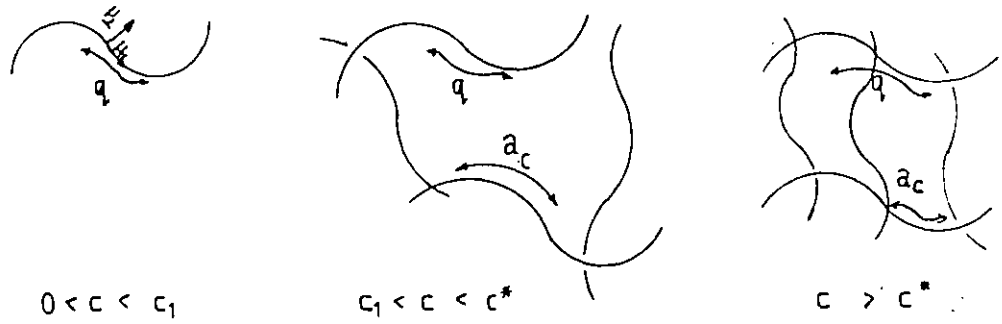

Fig 5·36 A simple physical model for the various regimes encountered in solution of stiff coil molecules as concentration is increased.

system but motions on a length scale q, do little to aid the relative translational motion of chains separated by a mean distance $a_c \lesssim q$.

(b) The Kerr effect

The dynamic Kerr effect probes the rotational motion of macromolecules. For ethyl cellulose, although the chain has a certain amount of rigidity, it is expected that the component of the dipole moment perpendicular to the chain backbone will relax by local motion of segments, whose length is of order q, at a somewhat faster rate than chain rotation. The results do indicate two distinct relaxation times, τ_p and τ_ℓ, rather than a broad distribution, and these are respectively identified with the relaxation of the perpendicular and parallel components of the chain dipole. In the concentration range $C<C_r$, both times increase with increasing concentration i.e. increasing chain interaction, but as expected on the basis of the physical model, τ_p is less sensitive to concentration than τ_ℓ, that is $(\zeta_c)_{\tau_p} < (\zeta_c)_{\tau_\ell}$. Above the critical concentration C_r, the concentration dependence of τ_ℓ increases dramatically $(\zeta_c)_{\tau_\ell} = 1.75$. Identifying C_r and C_2 in the model, this corresponds to the sharp reduction in overall chain mobility then $a_c \lesssim q$. By contrast no such sharp change is expected for local segmental motion and τ_p continues to increase with the same concentration exponent $(\zeta_c)_{\tau_p} = 0.4$ as for $C<C_r$.

Table 5.2.2 Summary of results from Kerr-effect, viscosity and PCS measurements for ethyl cellulose.

Technique	Parameter	C_r / † $kg\ m^{-3}$	Information		Comment
Kerr effect	τ_r / τ_e	20	∿1.3±0.1	$C<C_r$	Change in mechanism ?
			∿1.1±0.1	$C>C_r$	
	β		0.8-0.55	$C<C_r$	Tending to single exponential for low concentration
			∿ 0.55	$C>C_r$	Strong devation from single exponential
	$(\zeta_c)_{\tau_\ell}$		0.75	$C<C_r$	
			1.75	$C>C_r$	
	$(\zeta_c)_{\tau_p}$		0.4 for all C		No break in slope
Viscosity	ζ_η	17	<1.0	$C<C^*$	Change in slope not as sharp as for τ_ℓ.
			2.2	$C>C^*$	
PCS		23	D_i, D_m	$C<C^*$	D_i continuously increases as $t,c \to 0$ $D_i(t\to0, c\to0)$ isolated ≡Isolated chain?
			D_i, D_m, D_ℓ	$C>C^*$	
	$(\zeta)_{D_\ell}$		undefined	$C<C_r$	
			0	$C>C_r$	
	$(\zeta)_{D_m}$		∿-1	$C<C_r$	
			-2	$C>C_r$	

† C_r is the critical concentration at which there is sharp change in slope of the ln τ (or D)/ln C plots.

As concentration decreases, the contribution of the faster component to the Kerr effect decay transient decreases and the curve approaches single exponential behaviour. This is reflected in the increase of the spread parameter β from a constant value of 0.55 above C= C_r towards a value of unity at lower concentrations (Fig 5.28). Such a behaviour probably reflects the fact that as concentration decreases, the two relaxation times become closer in value. Eventually the rate of whole molecule rotation becomes comparable with or even faster than that for the rather restricted segmental motion of the stiff chain. In such circumstances both components of the dipole moment will relax via the faster whole molecule mechanism and in dilute solution it is possible that only one relaxation time would be observed.

This is in agreement with the work of Rjumtsev et al [54] on dilute solutions of cellulosis in dioxane .

It should be mentioned that the polydispersity of the sample is a potential source of non-exponential behaviour in the Kerr transients. However, although this will affect the interpretation of the relaxation times in terms of individual chain characteristics, and influence the precise values of τ and ζ_c observed , it is unlikely to be the source of the distinct relaxation times or the marked changes in their concentration dependence observed here.

Another interesting feature which changes with concentration is the relative shape of the rise and decay transients. At high concentration, $C > C_r$, they are essentially identical and $\tau_r/\tau_d \approx 1$. Such a situation can arise for at least two reasons:
(i) the relative contribution of the induced dipole moment term,Q, is very large (Q >> P) (see section 2.5.5(d))
(ii) the highly entangled ethyl cellulose molecules are relaxing by fluctuation (jump) mechanism (see section 2.5.6).

By contrast, as the concentration was decreased below C_r the shapes of the rise and decay transients become increasingly different. τ_r/τ_d increased with decreasing concentration, reaching a value of 1.4 for the lowest concentrations studied.

The reversing pulse unit could not be applied to establish the relative contributions of the induced and permanent

dipole moments because the field required to orientate ethyl cellulose is higher than the design capacity of the unit. However previous studies of ethyl cellulose derivatives suggest that the permanent dipole effect is dominant for these systems [54] and it is extremely unlikely that the relative contributions of P and Q would change significantly as the polymer concentration was increased. This suggests that the change in the shapes of the rise and decay transients as C increases through C_r may be due to a change in the orientation mechanism. The simple model suggested ealier indicates a physical mechanism whereby the molecules in the highly interacting state at $C > C_r$ can only rotate by a series of discrete jumps as persistence length segments become in turn free to rotate small distances as the molecules move past one another. For $C < C_r$, τ_r/τ_d does increase although not to the ideal rotational diffusion value of 4 for $P >> Q$. The source of this change in the shape of the transients with concentration obviously requires more detailed investigation.

(c) Viscosity

The increase of viscosity with concentration showed a continually varying concentration exponent, ζ_η for $C < C_r$ which levelled out to an essentially constant value of about 2 above C_r. This again indicates a significant change in the nature of the chain interactions in the region of $C \simeq 10 - 20$ kg m^{-3}. Moreover the exponent ζ_η of 2 indicates that the present experiments have been conducted in a moderately concentrated regime rather than a highly entangled system, for which much higher values of ζ_η ($\simeq 5$) would be expected [81]. An indication of the extent of coil overlap can be obtained by using the interaction parameter $C[\eta]$ of Simha [82]. A value of unity for this parameter corresponds to the concentration C^*_η for the onset of coil overlap. Cornet [83] has interpreted C^*_η as the concentration at which a uniform segment density is attained in the solution. The observed intrinsic viscosity of the ethyl cellulose sample used in this work in toluene is 5×10^{-2} m^3 kg^{-1}; using this value gives $C^*_\eta = 20$ kg m^{-3}, in good agreement with the critical concentration observed in the Kerr experiments.

(d) Photon Correlation Spectroscopy.

The correlation functions obtained with this technique have been characterised in terms of the diffusion coefficients D_i and D_m for $C < C_r$. At $C > C_r$ a long time tail emerged, leading to characterisation of the autcorrelation function at high concentrations in terms of D_i, D_m and D_ℓ. The concentration dependence of these coefficients has been illustrated in Figs 5.34 and 5.35. The fact that the long time tail does not persist into the regime $C < C_r$ suggests that D_ℓ is in someway associated with the transient network structure characteristic of the high concentration region. Here D_ℓ is ascribed to co-operative motions characteristic either of the network as a whole or of portions of the chains contained within it. Once significant chain overlap has occurred such motion would be expected to be relatively insensitive to the chain concentration (i.e. $\zeta_\ell \simeq 0$).

On the other hand, D_m in this region is ascribed to the translational diffusion of individual chains through the highly interacting chain system. Such a process becomes increasingly slower as concentration rises, and at the higher concentration studied (57 kg m^{-3}) the motion becomes so constrained that D_m tends towards D_ℓ, the experimental correlation function being essentially single exponential in form. Over the concentration range 57 kg $m^{-3} > C > C_r$, D_m varies as C^{-2} (see Fig 5.34). This behaviour is characteristic of reptative motion of chains in a semi-concentrated system [16,96] and will be discussed in further detail presently.

Below $C = C_r$, the cooperative motion characterised by D_ℓ disappears and the concentration dependence of the entangled chain diffusion coefficient D_m decreases markedly. The accuracy of the data from these weakly scattering solutions is not sufficiently high to define the concentration exponent in this region within narrow limits; it appears to be of order unity.

The physical significance of the coefficient D_i is not entirely clear since in general the value of the initial slope from which it has been derived increased as the channel time in the experiment was decreased. Consequently the values of D_i are only an approximation to the values obtained in the

$t \to 0$ limit. These quantities, on extrapolation to C=0, should correspond to the translational diffusion coefficient D_o of the isolated ethyl cellulose chains in toluene. A linear extrapolation of the present data suggests a value of $D_o \sim 7.5 \times 10^{-11} m^2 s^{-1}$. (estimated R_H = 5.2 nm)

Quantitative interpretation of data in terms of theoretical models:

Regarding ethyl cellulose as a fully extended rigid chain (containing M_n/M_o = 107 monomer units) and using Broersma's equation (with ℓ_o=0.515 nm, and d_o= 0.8 nm [54]) the calculated dilute solution relaxation times associated with the sample is 0.58 μs. On the other hand, regarding it as a random coil and using the experimental value of the intrinsic viscosity, of 5×10^{-2} m^3 kg^{-1}, the first normal mode relaxation time is 0.36 μs applying the Rouse model (eqn 2.1) or 0.25 μs using the Zimm non-free draining model (eqn 2.2).

The extrapolated, zero concentration value for τ_ℓ is 1.2 ±0.4μs, which is in disagreement with random coil model especially the Zimm value. Certainly the EC behaviour is far from being a fully extended rigid rod. Dilute solution dielectric studies [95] on ethyl cellulose in dioxane gave a relaxation time of 4.0μs for a narrow fraction of molecular weight 2.85×10^4 close to M_n of the present sample. Using $\tau_K = \tau_D/3$ this value corrected for the viscosity differences, corresponds to 0.7 μs, in reasonable agreement with the values obtained here. These workers examined a wide range of molecular weights and concluded that EC behaves as a rigid coil molecule which orientates as an entire unit in an electric field, in agreement with the interpretation of τ_ℓ put forward here.

A semi-quantitative measure of the extent of the interaction of polymer chains in solution at a concentration C, can be obtained by considerations based on the volume of the sphere of influence of a single molecule, V_m as presented in section 5.1.5. Equations 5.3 - 5.6 may be used to evaluate V_m, the mean number of chains occupying this volume n_v, and the critical concentration for the onset of strong chain interactions, C*. At C = C* any one chain interacts on average with two other chains at the periphery of the swept volume V_m,

(see Fig 5.37). Above C*, it will also interact closely with those chains which on average occupy part of the volume V_m. Conseqently at C > C*, the number of close chain-chain interactions ('entanglement junctions') per chain, ν, is simply $n_\upsilon+1$. The approximate mean distance between these entanglement points at a concentration C, a_c, is given by

$$a_c = \frac{2r_m}{\nu - 1} = \frac{\ell_q}{n_\nu} \qquad 5.17$$

For the present case, where we have ethyl cellulose of $M_n = 2.6 \times 10^4$ corresponding to n = 107 monomer units, each of length ℓ_o = 0.515 nm [54] we can estimate the above quantities for two extreme chain conformations:
(a) if the polymer behaves as a completely fully extended chain,

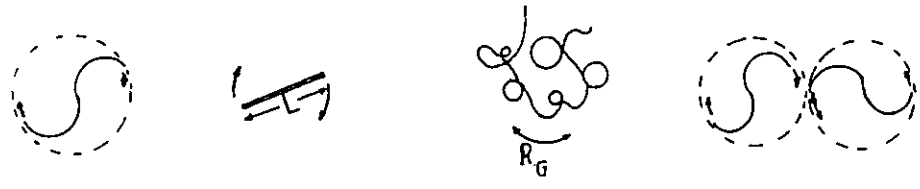

Fig 5·37 Chain configuration and probable interation model – (a) Sphere of influence of a chain (b) completely rigid rod molecule (c) coiled random coil molecule (d) simplified representation of the situation for $c = c^*$

the contour length L = 55 nm and the volume it sweeps out, V_m, is $8.7 \times 10^{-23} m^3$. This corresponds, by equation 5.3, to a critical concentration C* of 0.50 kg m^{-3}.
(b) if the polymer behaves as a random coil, the radius of gyration, R_G would be 2.2 nm and $V_m = 44.6 \times 10^{-27} m^3$. This gives a critical concentration C* = 980 kg m^{-3}.

The experimentally observed critical concentration C_r = 20 kg m^{-3} indicates that the behaviour of ethyl cellulose in toluene lies between that of a rigid rod and a random coil, i.e. it is a relatively stiff coil. The radius of the sphere of influence $r_m = \ell_q/2$ (see eqn 5.8) ,corresponding to the

observed critical concentration is 1.6×10^{-8}m. This value is similar to the persistence length of $1.8 \pm 0.3 \times 10^{-8}$m determined by Ryumtsev et al [54] using hydrodynamic properties and lends support to the interpretation of C_r in this way (see also section 5.1.5). Using q =10 nm shows that the present chains correspond to only about 5 (=L/q) persistence segments, again confirming the relative stiffness of the coil.

Table 5.23 gives the values of n_U, ν and a_c calculated using this ℓ_q value 1.6×10^{-8}m, for r_m in the equation of the simple model given here. This shows that over the range of concentration studied in this work 5 - 57 kg m^{-3}, the mean number of close intermolecular interactions per chain increases from zero to $\sim$ 5. Above $C = C_r$ the mean separation between such points decreases markedly until by C=60 kg m^{-3} $a_c \simeq 50 \times 10^{-10}$m, a value which is small compared with both the chain contour length and the spatial extent of the chain.

Table 5.23 The concentration variation of the number of chains n_U, per volume V_m, the number of interaction points, ν, and the mean distance between chains. a_c.

Concentration C/ kg m^{-3}	Number of chains in volume $V_m = n_U = \frac{1000CN}{M} A V_m$	Number of interaction points per chain $\nu = n_U + 1$	Mean distance between chains, $a_c = \ell_q / n_U$ $a_c \times 10^9$
1	0.05	-	-
5	0.25	-	-
10	0.5	-	-
20	1.0	2.0	16.1
30	1.5	2.5	10.7
40	2.0	3.0	8,1
50	2.5	3.5	6.5
60	3.0	4.0	5.4
75	3.75	4.75	4.3
100	5.0	6.0	3.2

Although it appears that the ethylcellulose used in this work behaves as a stiff coil rather than a fully extended rigid rod, it is interesting to compare the results with the prediction of Doi-Edwards (DE) model (sections 2,3.2 and 2.6.3). For the Kerr effect the rotational diffusion for C>C* should scale as

$$\tau \quad = \quad (6D_r)^{-1} \quad \propto \quad C^2 \qquad 2.25$$

The experimental relaxation time τ_ℓ, corresponding to this whole molecule rotation, varies as $C^{1.75}$ for $C>C_r$. Although this does not, and would not be expected to, agree exactly with the DE prediction, it is significant that this is the only one of the five systems studied in this work for which a value of $\zeta_c \simeq 2$ has been observed. The value of $(\zeta_c)_{\tau_\ell}$ observed below C_r, 0.75, is comparable with that obtained for the more rigid polymers over a wider concentration range.

For PCS studies of the translational motion of rigid macromolecules in the semi-dilute regime the DE model predicts that the autocorrelation function should have a concentration independent slope

$$\Gamma_1 \quad = \quad \tfrac{1}{3} D_o K^2 \quad \propto \quad K^2 C^0 \qquad 2.98$$

where D_o is the zero concentration translational diffusion coefficient and a slower long time portion of form, $\exp - \Gamma_2 t$ where

$$\Gamma_2 \quad = (K^2 D_r D_o)^{\frac{1}{2}} \quad \propto \quad KC^{-1} \qquad 2.102$$

Although the EC experimental autocorrelation functions agree qualitatively with this prediction of long time exponential behaviour with increasing slope at low times, the concentration dependence of these slopes is not in line with the DE theory. The long time slope of logarithmic correlation functions for $C > C_r$ vary as $\sim K^2 C^0$ (see Figs 5.32 (b)); despite the experimental scatter, the data are of sufficient accuracy to definitely preclude KC^{-1} behaviour. The intermediate time slope, corresponding to D_m, varies as $K^2 C^{-2}$ for $C > C_r$ (see Figs 5.37 and 5.38) and is also inconsistent with the DE model, although it does tend towards C^0 behaviour at lower concentrations.

Doi [84] and Doi and Edwards [4] also analysed the concentration dependence of the zero shear rate viscosity η_o for

rigid rods. They predicted that ,

$$\eta = \eta_s(1 + C L^3) \qquad C < C^* \qquad 5.18$$

$$\eta \quad \eta_s(1 + (C L^3)^3 \qquad C > C^* \qquad 5.19$$

where η_s is the solvent viscosity. Experimentally the concentration exponent changed from $\simeq 1$ below C_r to a constant value of about 2 above C_r. Again the concentration dependence is weaker than that predicted by the DE theory.

For the dynamic Kerr effect and viscosity, therefore , a semi-quantitative understanding of the experimental results for ethyl cellulose can be obtained in terms of the rigid rod theory. However, the PCS results are in direct conflict with the expectations for such molecules in the semi-dilute regime and it is not possible even semi-quantitatively to reconcile the rotational and translational dynamics of ethyl cellulose in terms of the Doi-Edwards model.

Edward and Evans [19] extended the rigid rod translational dynamics to much higher concentrations towards the critical concentration of the isotropic nematic transition, C^{**}. As seen in section 2.6.2 they predicted a diffusion coefficient - concentration relationship of the form $D \propto C^{1.5}$ for $C^* << C \sim C^{**}$ and the cessation of mobility, $D \rightarrow 0$, at a sufficiently large concentration, corresponding to the onset of a glass-type transition. It is unlikely that the concentrations used in the present studies were sufficiently high to lead to such dramatic decreases in the chain mobility. Although the distinction between the chain diffusion coefficient D_m and the co-operative term D_ℓ essentially disappeared at the highest concentrations studied, there was mo evidence of the behaviour predicted by Edwards and Evans.

Jamieson et al [100] have studied the dynamics in concentrated solution of a very flexible polymer, polystyrene, and a rigid polymer, xanthan gum (a polysaccharide) by PCS. The intensity autocorrelation function, $g^{(2)}$, observed by Jamieson et al for xanthan were similar to those observed in the present work for ethyl cellulose, in that they were also non-exponential overall, but consisted of distinct exponential regions over several decades of time. They analysed their data in terms of a bimodal decay of the type used here, and

their results are illustrated in Fig 5.38 below. They observed $\zeta_m = -2$ for their long time slope, which compares well with the value of -2 for Γ_m ($\simeq D_m$) in this work. They also observed a faster initial region, characterised by Γ_i, which, unlike $\Gamma_i(D_i)$ in the present work, was independent of concentration in the $C^{-2}\Gamma_2$ region and then decreased at lower concentraions. They did not observe the equivalent of the long time Γ_ℓ (D_ℓ) of this work. They interpreted the concentration exponent of Γ_2, $\zeta_c = -2$, to be consistent with the DE theory [4]. However this interpretation is not C^{-2} but C^{-1} (see section 2.6.3). So in both their case and ours there is qualitative disagreement between the experimental observations and the DE theoretical predictions.

A two exponential decay was also observed in their study of polystyrene, which they interpreted in terms of the model of Reihanian and Jamieson (RJ) |52| see section 2.6.3. This model can be applied to the present ethyl cellulose data by identifying Γ_m with Γ_1 and Γ_ℓ with Γ_2 in equations 2.96 and 2.97 which may be rearranged to give,

$$\Gamma_m = 1/\tau_r + (D_c + D_t)K^2 \qquad 5.20$$

$$\frac{1}{\Gamma_\ell} = \frac{1}{D_t}\frac{1}{K^2} + \frac{D_c + D_t}{D_t}\tau_r \qquad 5.21$$

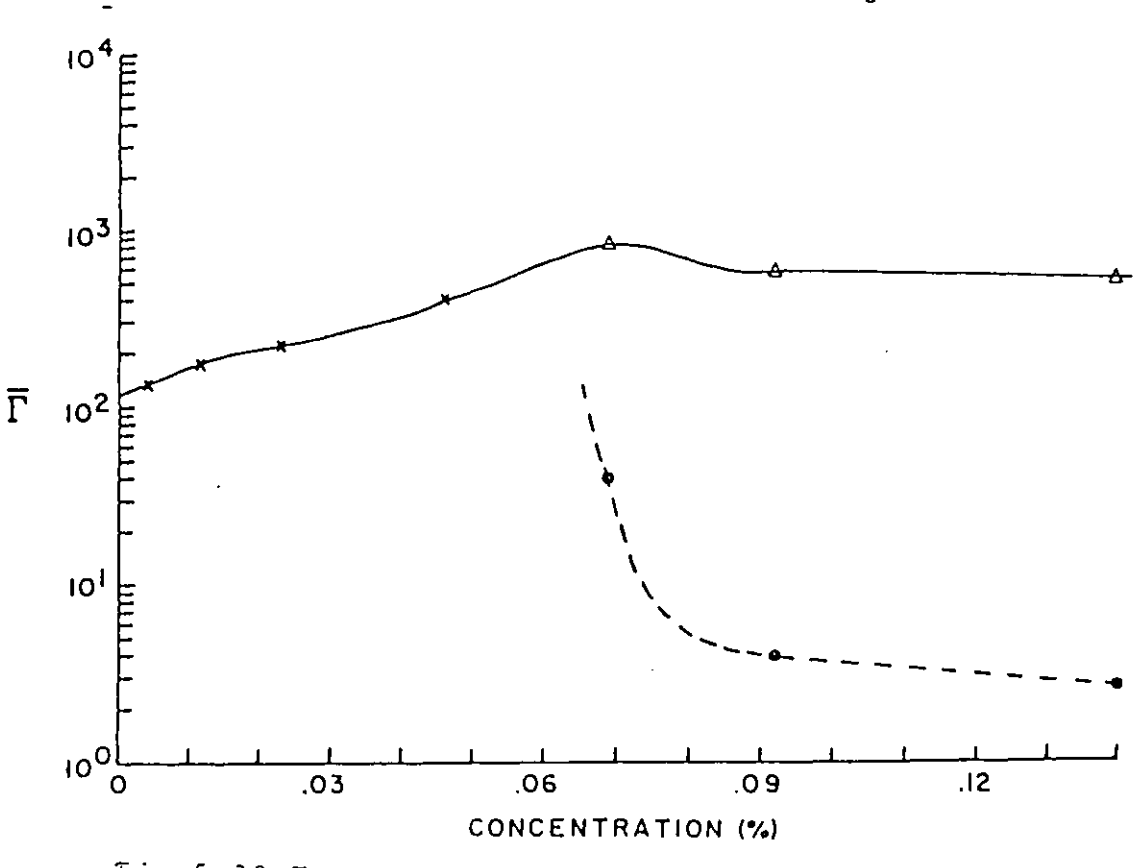

Fig 5.38 The concentration dependence of Γ for Xanthan gum

Fig 5.39 (a),(b) show plots of Γ_m versus K^2 and Γ_ℓ^{-1} versus K^{-2} for the 44 kg m^{-3} solution of ethyl cellulose. As predicted by eqns 5.20 and 5.21 these plots are indeed linear within the data scatter. However, the essentially zero intercept of Fig 5.39 (a) leads to a very high value for the entanglement relaxation time τ_r. As well as being physically unrealistic, it is incompatible with the value extracted from Fig 5.39 (b), even allowing for the large uncertainties in the exact values of the slope and intercept (see Table 5. 24). Hence this theory of the PCS behaviour of semi-dilute solutions of very flexible macromolecules is not quantitatively compatible with the data obtained for the stiff chain ethyl cellulose.

Table 5.24 Reihanian and Jamieson parameters for 44kg m^{-3} ethyl cellulose at 298 K

From Γ_m(Fig 5. (a))	τ_r/μs	$D_c + D_t \times 10^{-13} m^2 s^{-1}$
	∞	12

From Γ_ℓ(Fig 5. (b) Line	τ/ms	$D_t \times 10^{-14} m^2 s^{-1}$	$D_c \times 10^{-14} m^2 s^{-1}$
a	0.0	5.4	6.8
b	8.4	7.0	5.0
c	17.0	8.0	4.0

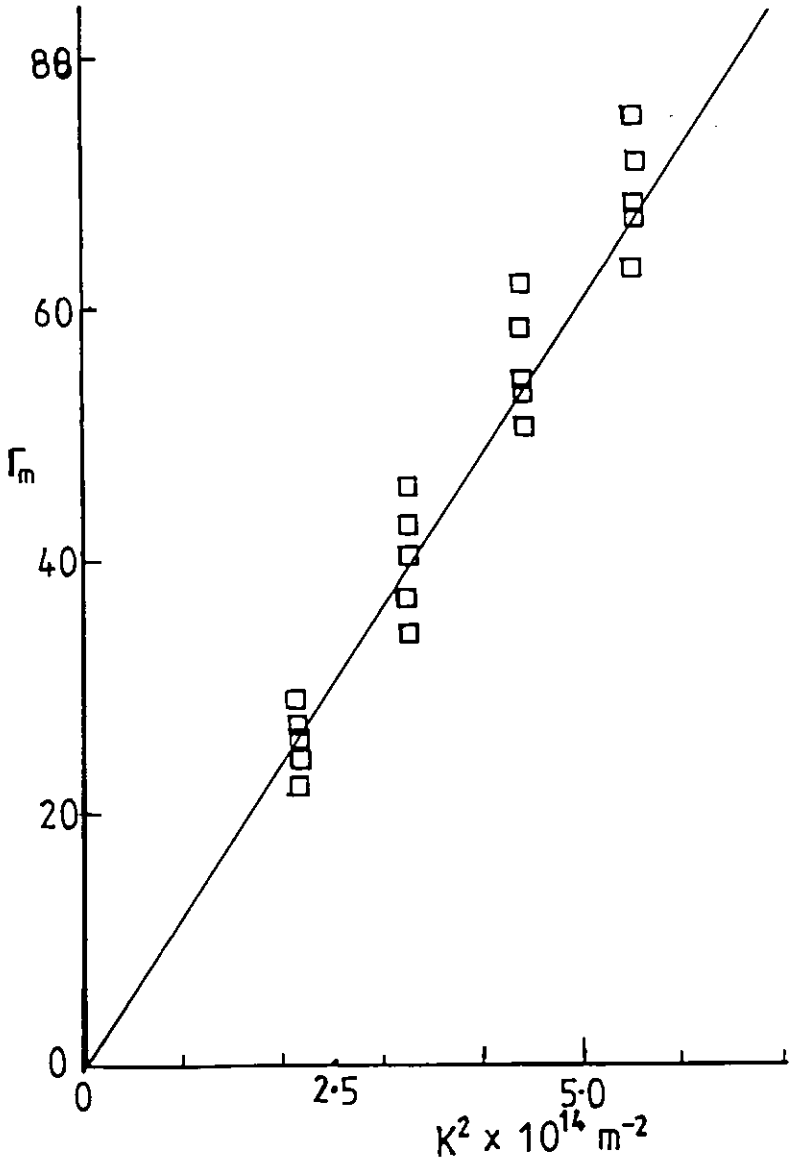

Fig 5.39(a) A plot of Γ_m versus K^2 (eqn 5.20)

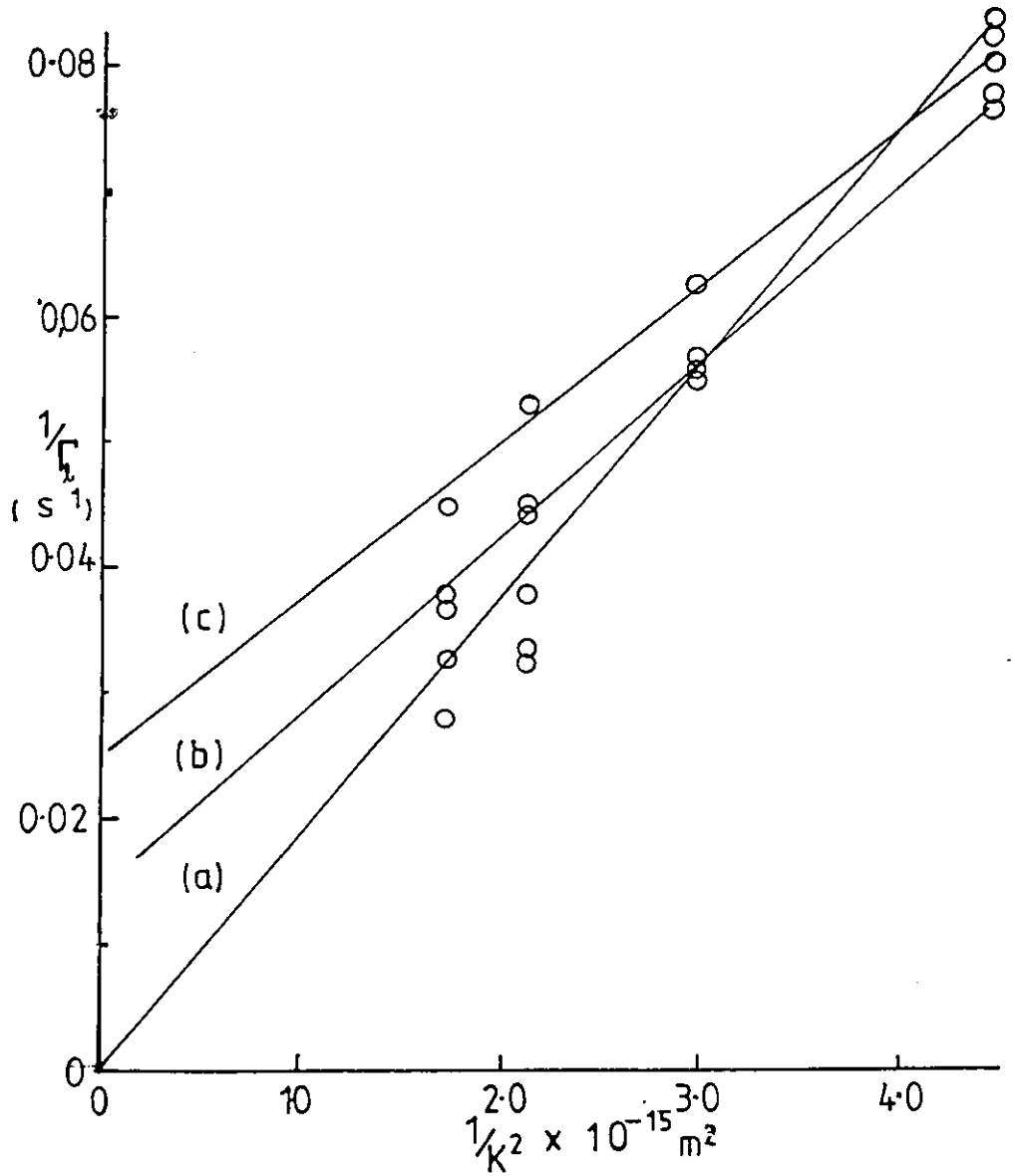

Fig 5.39(b) A plot of I/Γ_l versus I/K^2 (eqn. 5.21)

Section Two

Equilibrium Properties

The concentration dependence of those properties of the molecules which characterise their interaction with an electric field, including the Kerr constant, the permanent dipole moment and the induced dipole moment were studied where possible. These properties are referred to as 'electrical properties' in this work.

For the polymer solutions the relative contributions of the permanent and induced dipole moments were measured using the reversing pulse technique, to give the ratio P/Q using equation 2.59. The values were used in equation 2.47, 2.44 and 2.46 to evaluate dipole moments and polarisability anisotropies. The assumption has been made here that these equations, derived for dilute solutions of rigid molecules, may be applied unmodified to the systems studied. The presence of molecular flexibility and molecular interactions and hence presumably of considerable internal field effects, in the present experiments will mean that only effective values of the dipole moment and polarisability are obtained in this way, through changes in the relative contributions of permanent and induced effects as concentration is increased should be revealed.

5.6 Solvents and standards.

Firstly the Kerr constant of some solvents (toluene and carbon tetrachloride) and of standards used to characterise the time constant of the detection circuit (nitrobenzene and a 10% solution of nitrobenzene in toluene) were measured and compared with literature values. The field dependence of the birefringence signals, plotted in Fig 5.40, was used to evaluate the Kerr constants. The values given in Table 5.25 are in reasonable agreement with the literature values after corrections have been made for the wavelength difference. The Kerr constant B has been observed to be strongly wavelength dependent [112], and the results here correlate well with $B \propto \lambda^{-1}$.

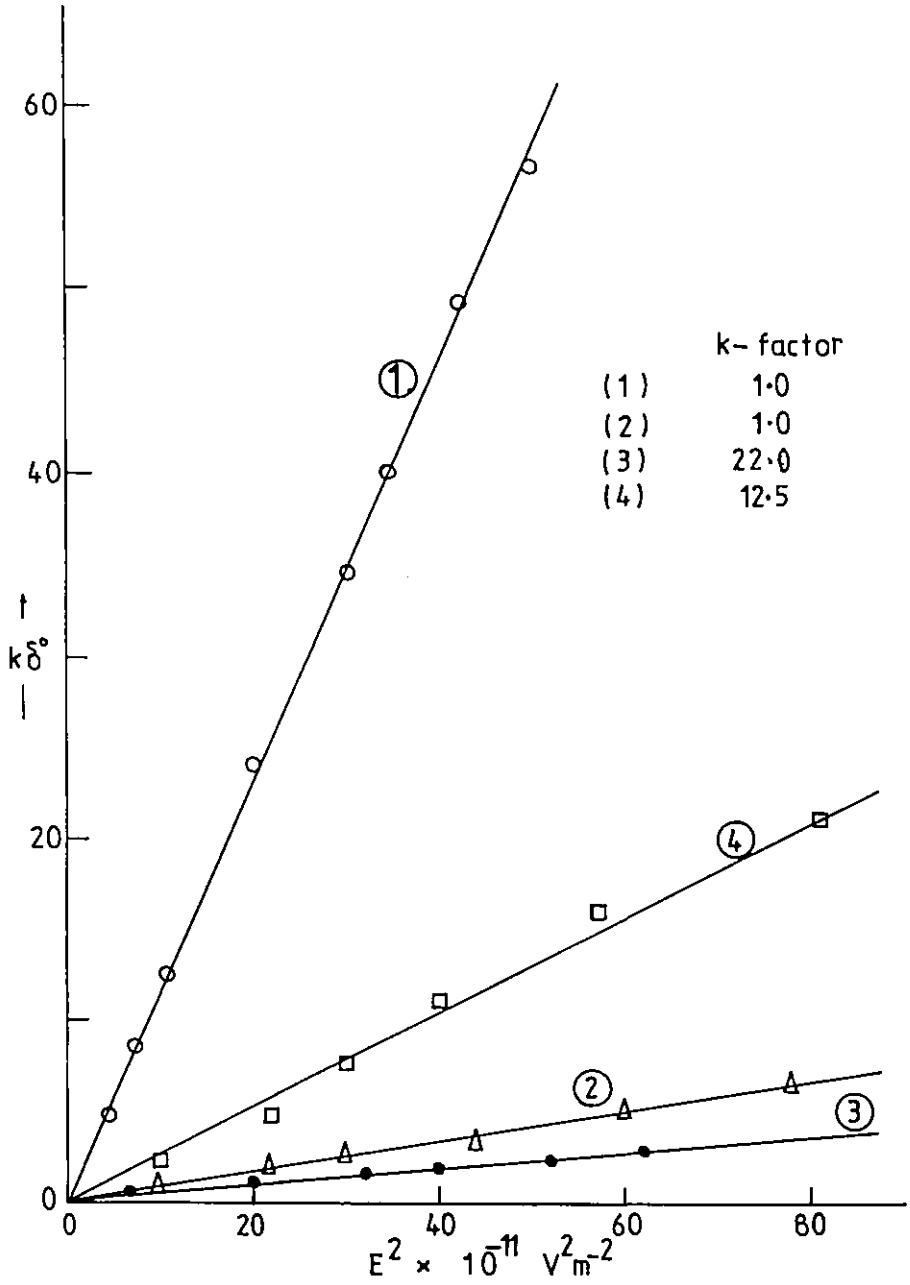

Fig 5·40 The field dependence of the birefringence of the solvents toluene (□), carbontetrachloride (●), nitrobenzene(10%) in toluene, Δ, and standard compound nitrobenzene (○).

Table 5.25 The Kerr constants of solvents

Solvent	This work $B \times 10^{13}$ $V^{-2}m$ at λ = 441.6nm	Reference [73] $B \times 10^{13} V^{-2}m$ at λ=589 nm	Values corrected to λ=441.6 nm using $B\lambda$=a constant.
Nitrobenzene	64	46	61
Toluene	0.12	0.087	0.12
Carbon tetrachloride	0.011	0.009	0.012
10% Nitrobenzene in toluene	0.46	-	-

5.7 Poly-γ-benzyl-L-glutamate, PBLG

Fig 5.41 shows plots of the phase retardation δ against the square of the field strength for various concentrations of PBLG I in chloroform-formamide solution. The plots are linear at low values of the field strength but show increasing curvature at high fields, well known for macromolecules in solution [93]. As will be shown later, the observed retardation is due to a combination of the permanent molecular dipole moment and the anisotropy of molecular polarisability. As the concentration decreases, higher fields are required to reach saturation and at a fixed value of the field, the retardation increases with increasing concentration. For example the 10 kg m^{-3} concentration under an applied field of 100 kV m^{-1} gave a retardation of about 120^{o} while 5.0 kg m^{-3} and 2.0 kg m^{-3} under the same conditions had retardations of 40^{o} and 7^{o} respectively.

The solution Kerr comstants, B at low field strengths are plotted as a function of concentration in the insert Fig 5.41 The plot shows that the Kerr constant increased non-linearly with concentration ($B \propto C^2$). This is suggestive of some cooperative effect for this semi-rigid system by which the extent of orientation for a given field gradient is enhanced by the close proximity of the partially aligned rigid molecules.

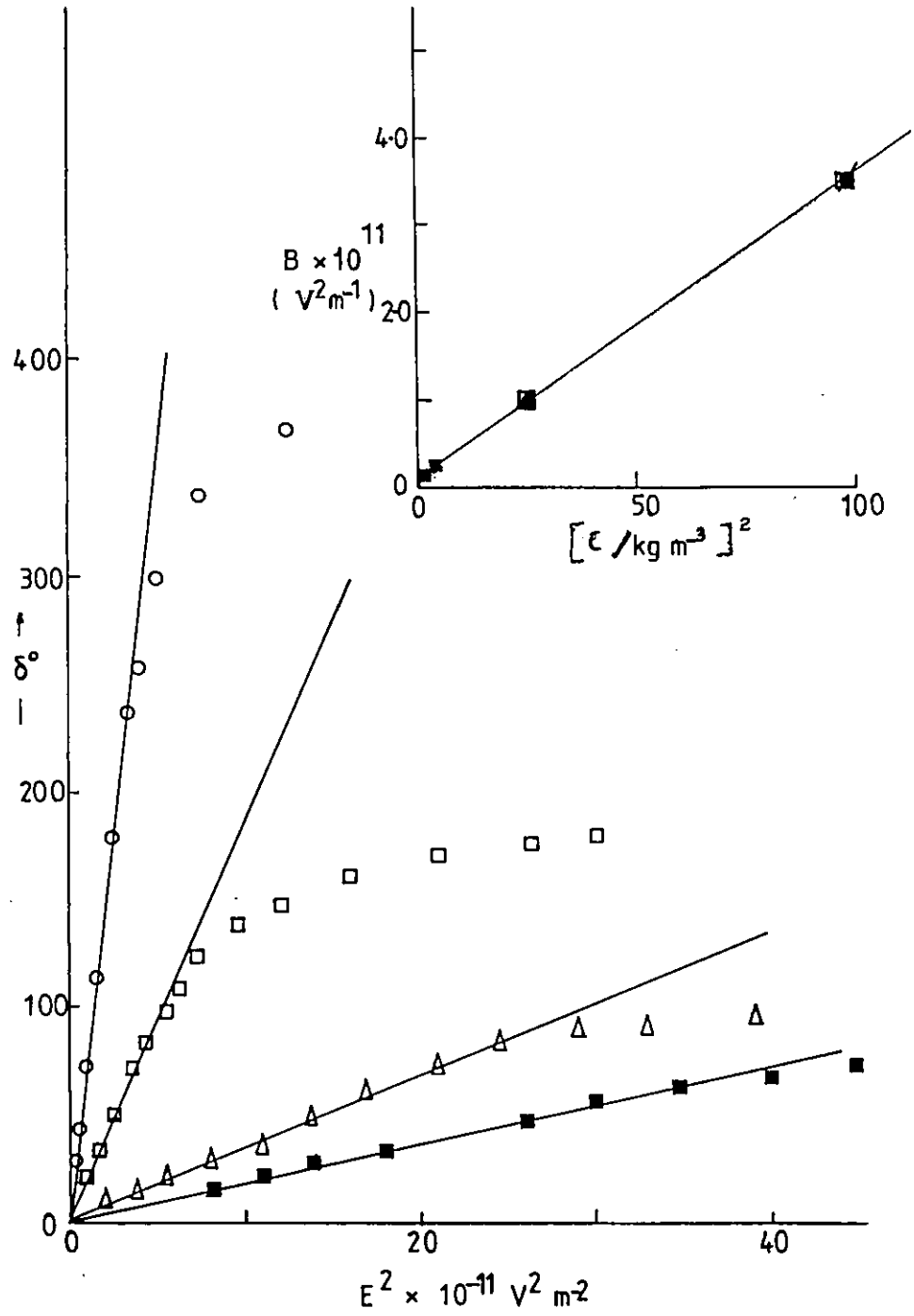

Fig 5·41 The field dependence of the retardation, δ°, for PBLG I of concentrations, 10 kg m^{-3} (○), 5·0 kg m^{-3} (□), 2·0 kg m^{-3} (Δ), and 0·8 kg m^{-3} (■).

The insert is the concentration dependence of the Kerr constants.

The orientation mechanism and the dipole moment

The reversing pulse unit was employed to determine the relative contributions of the permanent and the induced dipole moments to the orientation process for PBLG. The values of the permanent dipole and the polarisability anisotropy are shown in Table 5.26

Table 5.26 Electrical parameters μ, $\alpha_1 - \alpha_2$ for PBLG I at different concentrations in mixed C-F solvent at 298 K

Concentration C/ kg m^{-3}	r = P/Q (rev. pulse)	Apparent dipole $\mu_\beta \times 10^{27}$ Cm	Apparent dipole $\mu_{\gamma\beta} \times 10^{27}$ Cm	Apparent $(\alpha_1 - \alpha_2) \times 10^{33}$ Fm^2	r= P/Q (areas method)
0.8	0.47	3.5	3.4	6.0	1.72
1.0	0.45	3.9	3.5	6.5	1.80
2.0	0.40	4.8	4.2	10.9	1.50
5.0	0.31	8.2	6.2	30.6	1.47
10.0	0.29	14.2	9.6	60.2	1.61

The ratio r of the permanent dipole to the induced dipole term shows both orientation mechanisms to be significant. This ratio decreases with increasing concentration. r may also be determined from the ratio of areas above the rise to that below the decay transient, (see eqn 2.70). The values obtained by this alternative procedure are significantly greater than the reversing pulse values, indicating that the simple dilute solution equations do not transfer directly to concentrated solutions.

As the orientation is due to both induced and permanent dipole moments, it was thought appropriate to use the full orientation factor equations 2.47 and 2.44 - 2.45. The dipole moment evaluated using the full expression is designated $\mu_{\gamma,\beta}$ while the one evaluated assuming that the induced dipole term is negligible is designated μ_β. Table 5.2 shows that the error incurred by neglecting the the induced contribution is small for low concentrations($\sim$10% at C<2.0 kg m^{-3}) but

increases considerably with concentration reaching 50% by $C>5.0$ kg m^{-3}.

The concentration dependence of the apparent dipole moment in Fig 5.4 2 (a) shows that the apparent dipole moment varies linearly with concentration over the range studied and yields a zero concentration value of $2.9 \pm 0.3 \times 10^{-27}$C m, inclusion or neglect of induced effects having little effect on this infinite dilution value. For a sample of the same molecular weight ($M_w = 2.1 \times 10^5$) Watanabe et al[94] have reported an approximate value of $11 - 16.3 \times 10^{-27}$C m using the Kerr effect for concentration 1.85 kg m^{-3} in ethylene dichloride (EDC) in which PBLG is known to be strongly aggregated [72, 32]. Other workers obtained a value of 9.7×10^{-27}C m for 1.0 kg m^{-3} EDC solution of a slightly higher molecular weight PBLG ($M_w=3.15 \times 10^5$) using Kerr effect methods. Values of 6.0×10^{-27} and 9.2×10^{-27} Cm were derived by Pyżuk and Krupkowski [88] for PBLG ($M_w = 1.8 \times 10^5$) in dioxane and EDC respectively (noted that μ was independent of C in the region 0.4 to 1.5 kg m^{-3} covered). With the average monomer dipole momemt μ_o of about 1.15×10^{-29}C m determined by Wada [23] using dielectric methods in EDC, a total dipole moment for PBLG I of 11.0×10^{-27}C m would be expected, a value about four times the present value. This probably reflects differences in the extent of aggregation at finite concentrations in the various solvents involved.

The apparent polarisability anisotropy is linearly dependent on concentration, (see Fig 5.4 2(b)), extrapolating essentially to zero at infinite dilution. This suggests that isolated PBLG molecules are oriented in an electric field by virture of the permanent dipole moment with essentially no induced effects. As the polymer concentration increases, the polarisability of the system increases due to interactions between the molecules and the orientation process becomes more complex.

5.8 Poly(n-butylisocyanate),PBIC

An investigation of the field strength dependence of the birefringence was conducted on various concentrations of PBIC =29 in carbon tetrachloride and the measured retardation, δ as a function of the applied field strength is shown in

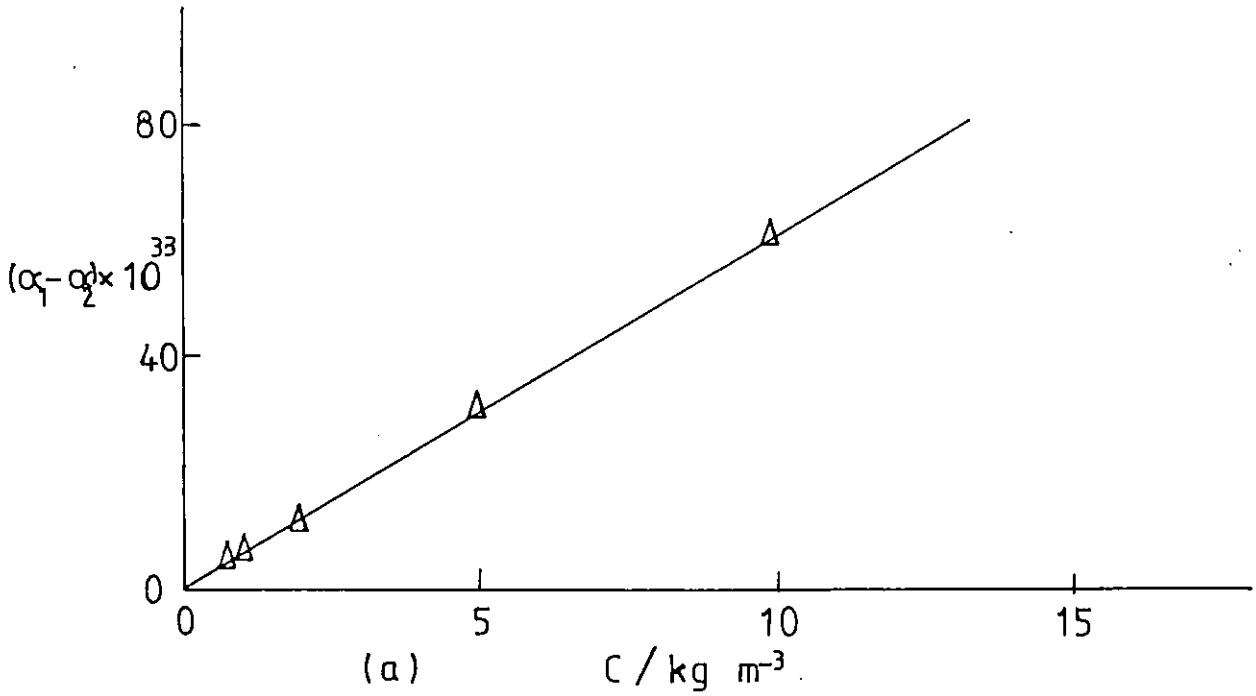

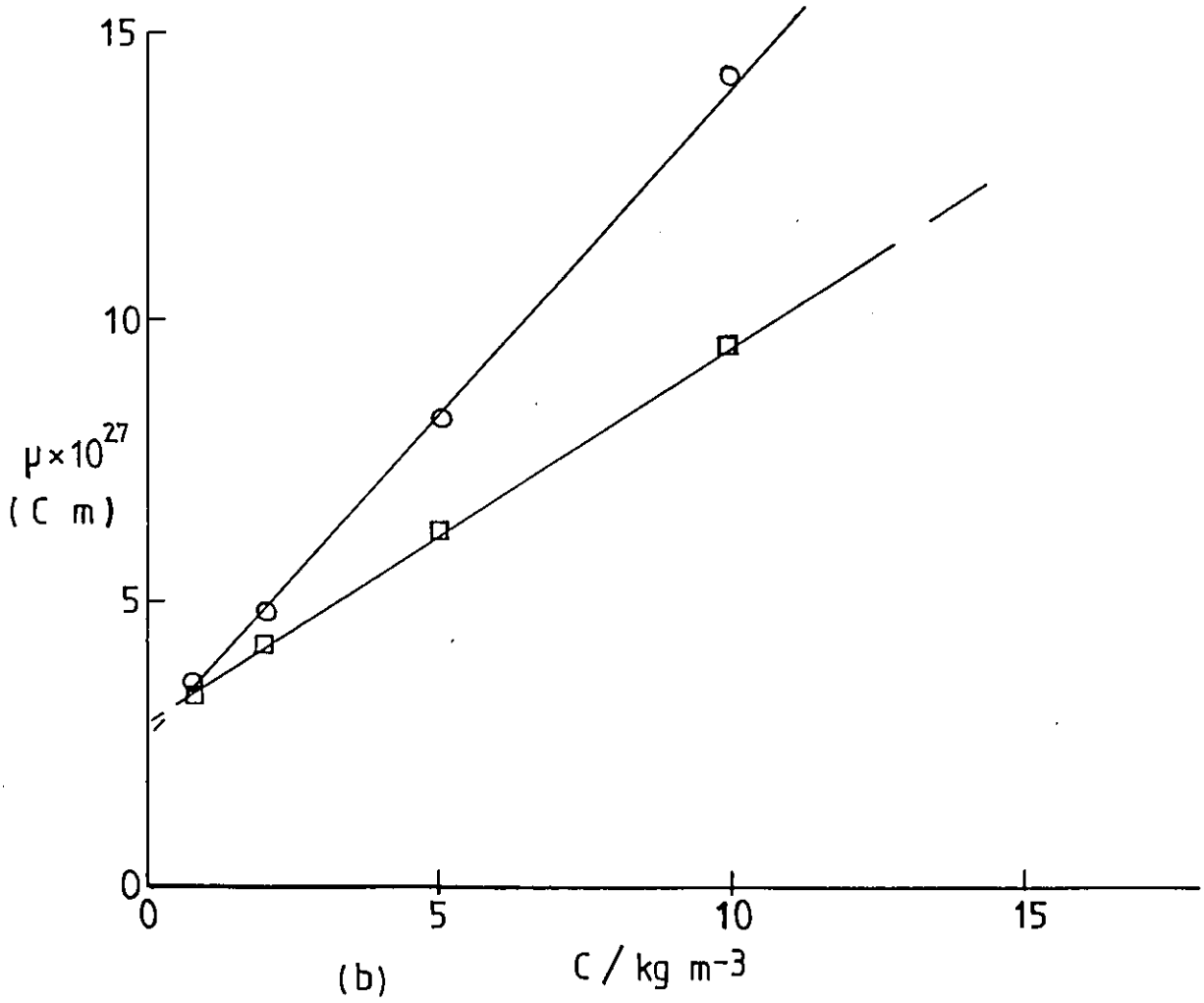

Fig 5·42 (a) Concentration dependence of the induced polarisability anisotropy, $(\alpha_1 - \alpha_2)$(Δ) and (b) the dipole moments, μ_{β} (O); $\mu_{\beta,\alpha}$ (□). for PBLG I

Fig 5.43. For all concentrations, the variation of optical retardation with values of the square of the applied field is linear at low values of the applied field, but significant curvature is observed at higher fields.

The Kerr constants calculated from the initial linear portions are given in Table 5.2 (a) and the variation of the Kerr constant with concentration is shown as an insert in Fig 5.43. Below the critical concentration determined in the dynamic studies, C_r= 0.9 kg m^{-3}, the Kerr constant is approximately linearly dependent on concentration but with increasing concentration, large deviations from linearity are observed. However, in contrast to PBLG, the slope of the B - c curve decreases rather than increases with concentration.

The orientation mechanism and electrical properties

The ratio, r = P/Q ,was measured using the reversing pulse unit for a 1.07 kg m^{-3} solution of PBIC =29 at various field strengths. The results in Table 5.27 show that r increases with field strength, reaching essentially a steady value at higher fields.

Table 5.27 (a) The field dependence of ratio, r, of 1.07 kg m^{-3} PBIC #29 in carbon tetrachloride at 293 K

Applied field gradent,E/kV m^{-1}	90	120	130	165	170	180	200
Ratio,r = P/Q	0.56	0.61	0.68	0.72	0.72	0.73	0.72

Table 5.27 (b) The field dependence of ratio,r, at two concentrations for PBIC # 21 in CCl_4 at 294 K

Field,E/kV m^{-1} / Conc./kg m^{-3}	70	110	130	170	200
0.73	0.35	0.43	0.45	0.50	0.52
1.40	0.31	0.37	0.45	0.44	0.45

This PBIC #29 is unfractionated and a wide range of molecular species are present whose permanent dipoles require varing

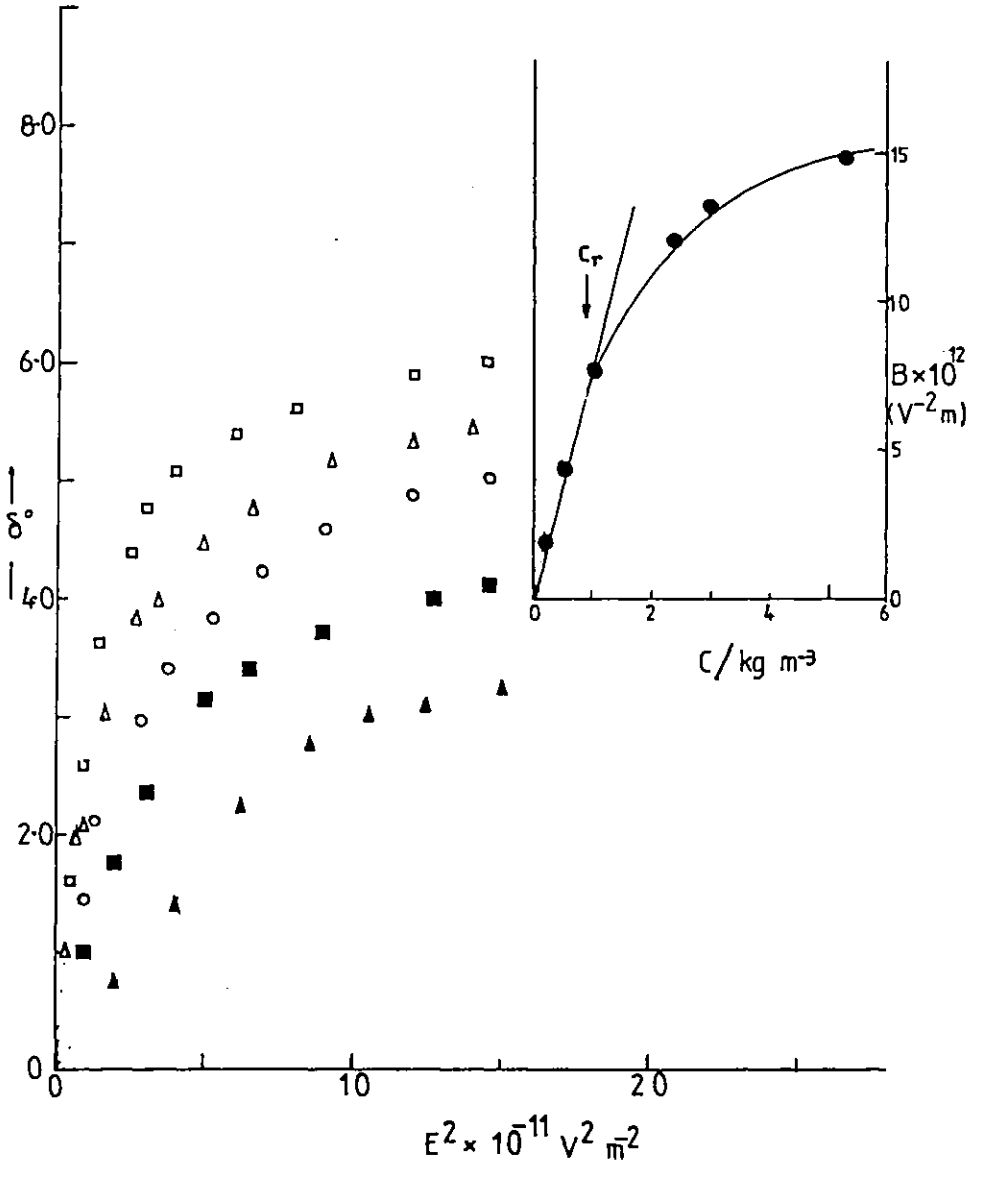

Fig 5·43 The field strength dependence of the retardation, δ, for 5·3 kg m^{-3} (□), 2·67 kg m^{-3} (Δ), 1·07 kg m^{-3} (○), 0·53 kg m^{-3} (■), and 0·27 kg m^{-3} (▲) for PBIC # 29 .

The insert is the Kerr constant, B, (●) of PBIC # 29 in CCl_4 at 20 °C as function of concentration.

field strengths to align them. The value of r = 0.72 shows that the orientation mechanism at the field levels investigated involves both induced and permanent dipole moments. The value of the applied field for which r reaches its steady value is still well within the Kerr law region and all subsequent measurements were made in this plateau region.

Similar measurements on two concentrations for the lower molecular weight PBIC #21 in Table 5.27 (b) also show that the ratio, r, increases with field strength, reaching a steady value at a slightly lower value of the field ($\sim$ 260 V) than for PBIC #29. This suggests that the effect is not associated with polydispersity but with the effect of the field on the interacting molecular system.

Table 5.28 (a) shows the apparent permanent dipole moments $\mu_{\beta,\gamma}$ and μ_{β} calculated using eqns 3.35 and 3.37 respectively. The ratio, r, was found to be 0.72, independent of concentration. This value was used to calculate the apparent electric polarisability anisotropy $\alpha_1 - \alpha_2$ using eqns 2.45 and 3.35. Both the apparent dipole moments and polarisabilities are significantly concentration dependent, and are found to increase with increasing concentration. Table 5.28 (b) shows the equivalent properties evaluated for the fractionated sample PBIC # 21. The error resulting from neglecting the induced contributions in evaluating μ_{β} again increase with concentration, ranging from < 1% for lowest molecular weight sample at low concentrations to 27% for the higher molecular weight sample at high concentrations.

Fig 5.44 illustrates the linear concentration dependence of the apparent dipole moment $\mu_{\beta,\gamma}$ and the apparent polarisability anisotropy, $\alpha_1 - \alpha_2$. Extapolation of the data to zero concentration yields for PBIC #29 of $4.2 \pm 0.3 \times 10^{-27}$ Cm and μ for PBIC #21 of $3.4 \pm 0.5 \times 10^{-27}$ £ m . The zero concentration electric polarisability anisotropies were 0 for PBIC #21 (as for PBLG) and 0.4×10^{-32} F m^2 for PBIC #29. The zero concentration dipole moment for PBIC #21 compares well with the infinite dilute dipole moment of 3.87×10^{-27} C m determined using dielectric relaxation technique [24]. Jennings and Brown [36] obtained a dipole moments in the range 3.4 to 4.08×10^{-27} C m for the same PBIC #21 in benzene,

depending on the value they took for the solute volume. A value of 3.83×10^{-27} C m has also been reported by Beevers et al [27] in carbon tetrachloride.

For perfect rod macromolecules, the ratio of the rod lengths should be equal to the ratio of the dipole moments. The ratio of zero concentration dipole moments for PBIC #29 and PBIC #21 is 1.24. For the two samples the ratio of the weight average molecular weight is 4.8 and of the number average molecular weights is 1.1. The ratio of the number average molecular weights is in better agreement with the the dipole moment ratio, than the weight average ratio. Similar observations based on relaxation times for this system have been made by Jennings and Brown.

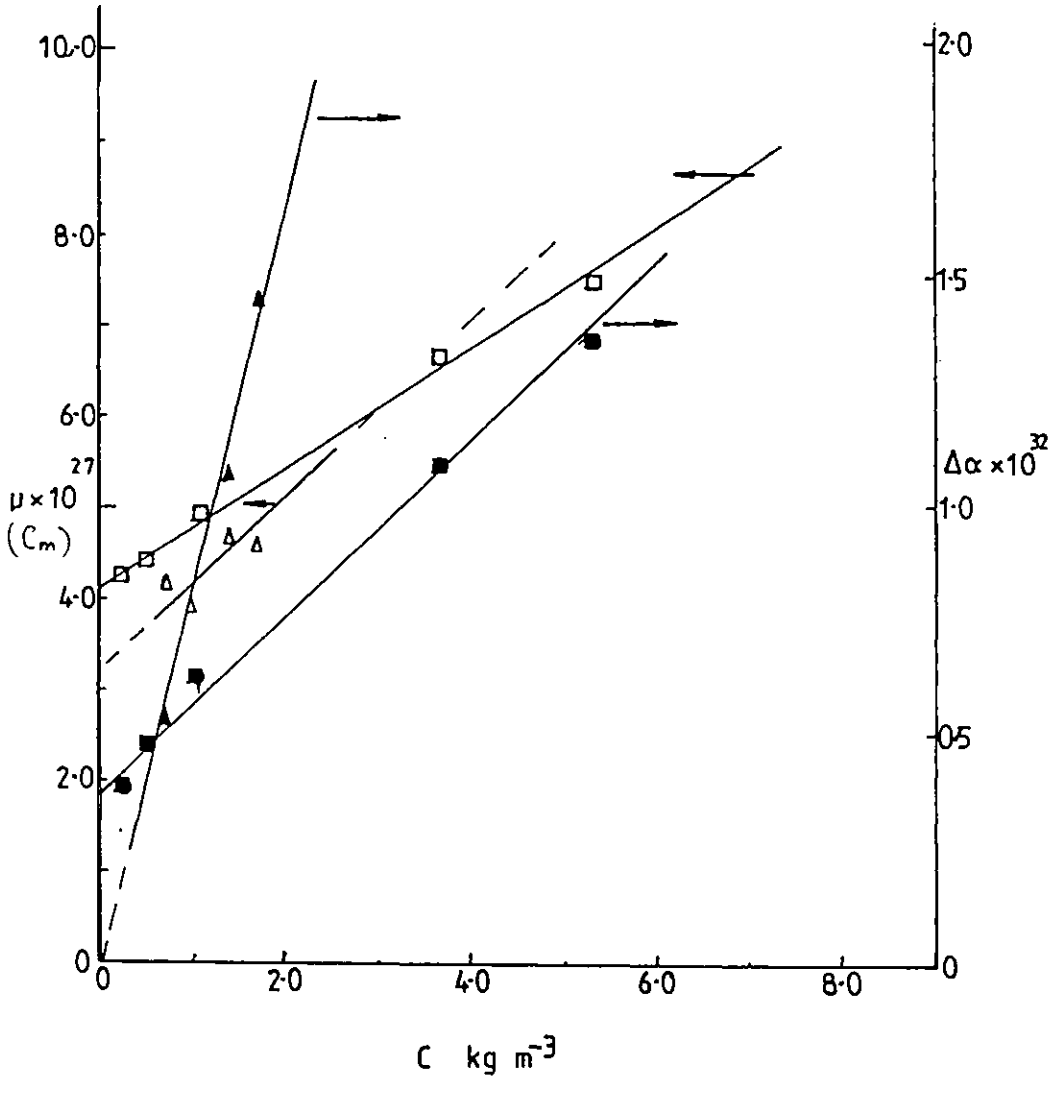

Fig 5·44 Concentration dependence of the apparent dipole moment, μ_{app}, for PBIC #21 (Δ), PBIC #29 (□) and the polarisability anisotropies, $\Delta\alpha$, for PBIC #21 (▲), PBIC #29 (■).

Table 5.28 (a) PBIC #29 electrical properties

(μ, $\Delta\alpha = \alpha_1 - \alpha_2$ and B)

Concentration, C kg m^{-3}	r = P/Q	Apparent $\mu_\beta \times 10^{27}$ C m	Apparent $\mu_{\beta,\gamma} \times 10^{-27} \times 10^{27}$ Cm	Apparent $\alpha_1 - \alpha_2$ $\times 10^{32} Fm^2$	Kerr constants $B \times 10^{12} V^{-2} m$
0.27	0.72	1.9	4.27	0.39	1.9
0.53	0.71	3.29	4.35	0.47	4.3
C_r = 0.9					
1.07	0.7	3.72	4.93	0.6	7.6
3.67	0.72	5.01	6.63	1.09	12.9
5.34	0.73	5.6	7.43	1.36	14.8

Table 5.28 (b) PBIC #21 electrical properties

($\mu, \Delta\alpha = \alpha_1 - \alpha_2$ and B)

Concentration, C/ kg m^{-3}	r = P/Q	Apparent $\mu_\beta \times 10^{27}$ C m	Apparent $\mu_{\beta,\gamma} \times 10^{27}$ C m	Apparent $\Delta\alpha = \alpha_1 - \alpha_2$ $\times 10^{32} Fm^2$	Kerr constants $B \times 10^{12} V^{-12} m$
0.73	0.45	4.43	4.14	0.94	2.1
1.0	0.6	3.4	3.87	0.62	2.4
1.4	0.45	4.66	4.66	1.07	2.7
1.73	0.36	5.63	4.53	1.45	3.2

5.9 Flexible macromolecules.

For poly(2-methyl-pentene -1 sulphone) and the polypropylene glycols/oxides, only the Kerr constants are considered. These molecules produce relatively small optical retardations and require fields in excess of those available from the reversing pulse unit to achieve sufficient orientation. Hence the mechanism of orientation, and the chain electrical properties could not be evaluated by this technique.

5.9.1 Poly(2-methyl pentene-1 sulphone) PMPS

Because of the low birefringence produced by this macromolecule it was necessary to explicitly subtract the retardation due to the solvent and the cell windows from the solution value. The cell strain birefringence, δ_o was evaluated using eqns 3.5 and 3.13. The optical retardation due to the solute as a function of applied field is shown in Fig 5.45; the plots exhibit curvature even at low field strengths.Evaluation of the limiting initial slopes of these curves obviously involves large uncertainties. The Kerr constants evaluated from these slopes are given in Table 5. 2 9 . A more accurate study of the birefringence at low fields would be necessary in order to comment on the concentration dependence of the Kerr constants.

5.9.2 Polypropylene glycols,PPG/oxides

Despite having a dipole component along the chain backbone, the low molecular weight glycols produce low birefringence effects. The temperature of the liquid polymer was lowered in order to obtain sufficient birefringence to obtain accurate results with the available electric fields. Because of the low birefringence exhibited even at temperatures as low as 223 K it was necessary to subtract the cell window birefringence from the measured birefringence in all the cases. The field dependence of the retardation δ of liquid PPG 2257 and was studied at four temperatures and the results are shown in Fig 5.46(a). The $\delta - E^2$ relationship shows that the Kerr law is obeyed in the range studied, and the Kerr constants decreased with increasing temperature. The Kerr constants of the four PPG samples and one 50 v/v% solution of PPG 2257 in toluene were measured at 223 K. The results displayed in Fig 5.46(b) again show a linear $\delta - E^2$ relationship in all cases. The Kerr constants evaluated are plotted as a function of molecular

Table 5.29 The Kerr constants, B, based on the limiting slopes for PMPS at various concentrations and temperature 290 K

Concentration C/ kg m^{-3}	3.2	5.5	12.7	20
B x $10^{-14} V^2 m^{-1}$	5.3	8.5	15.8	32.7

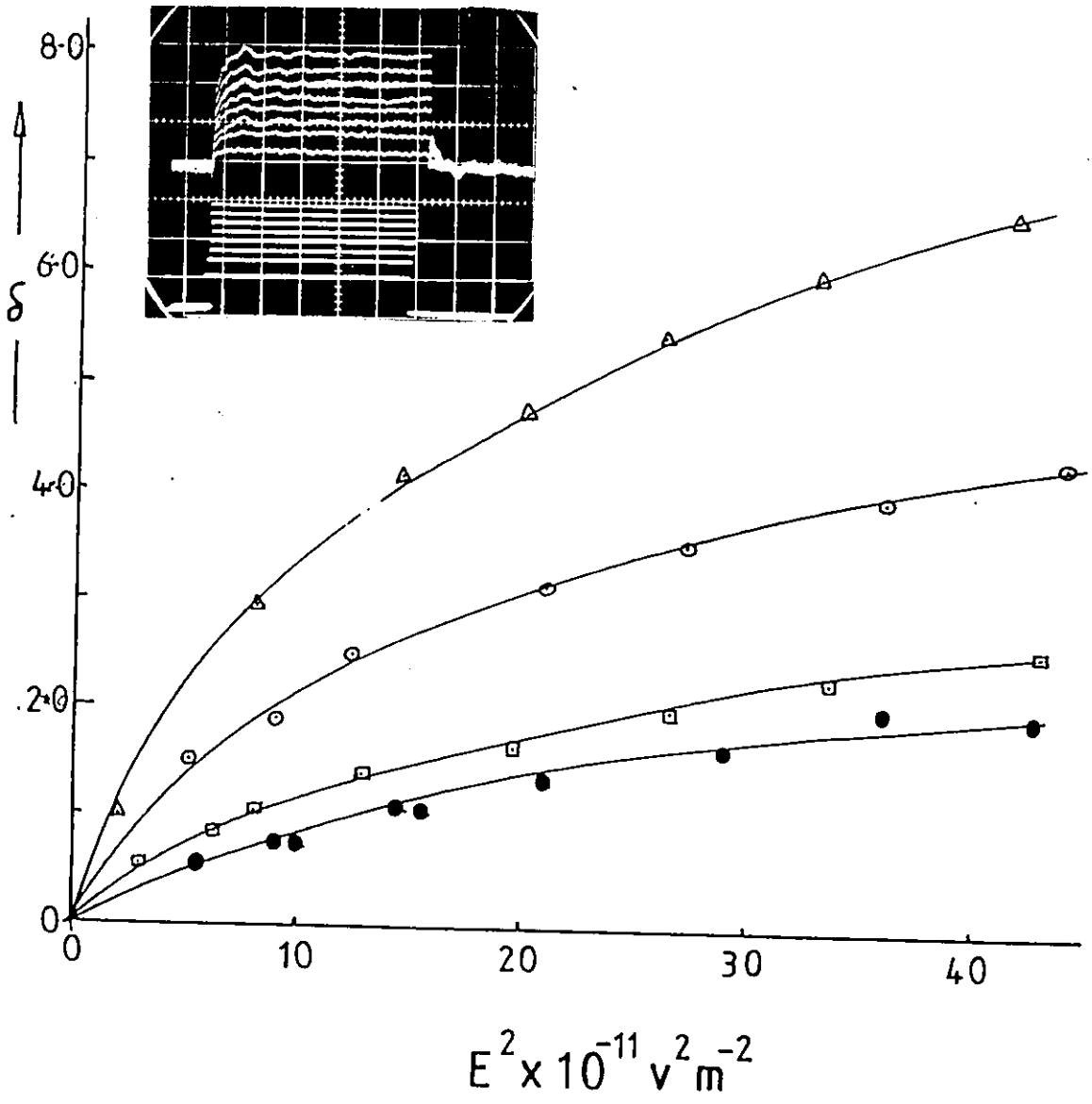

Fig 5.45 Field dependence of the birefringence of PMPS, for 3.2 kg m^{-3}(●), 5.5 kg m^{-3}(□), 12.7 kg m^{-3}(○) and 20 kg m^{-3}(Δ). Insert : The oscillogram shows the birefringence at various fields for 5.5 kg m^{-3} solution.

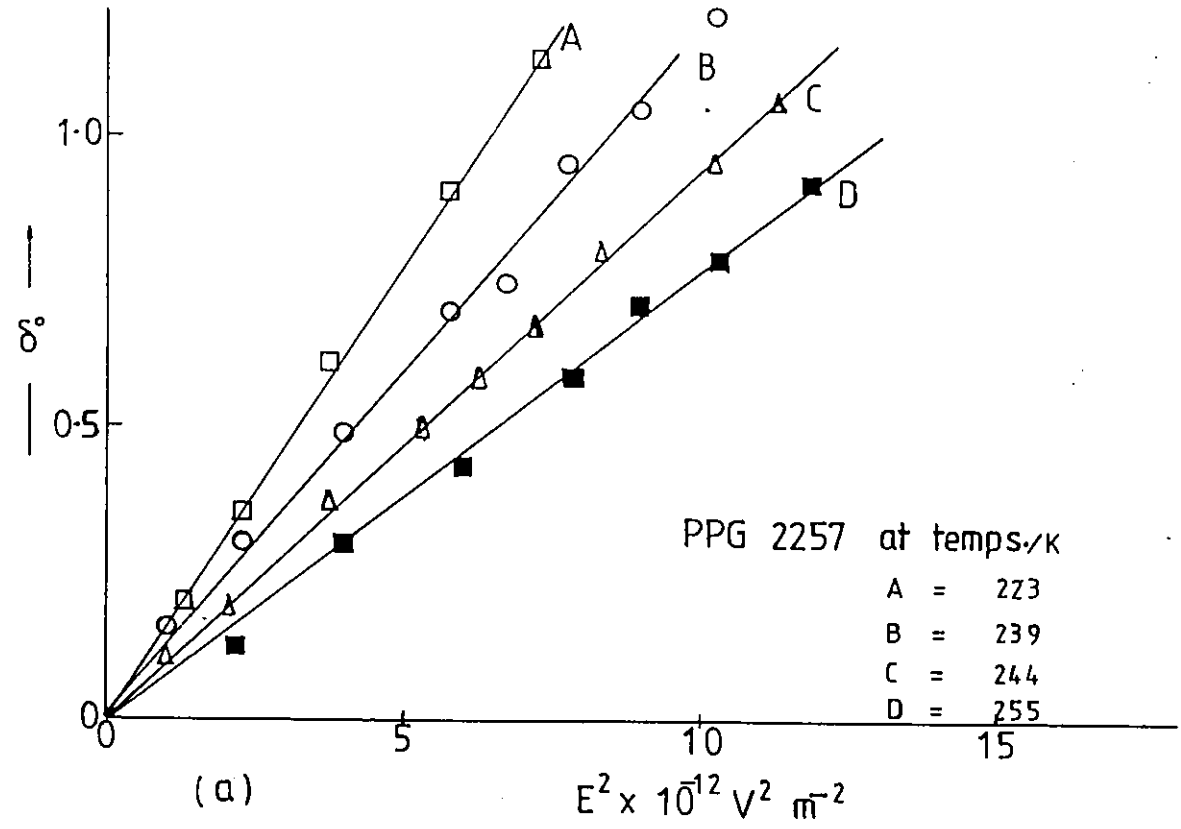

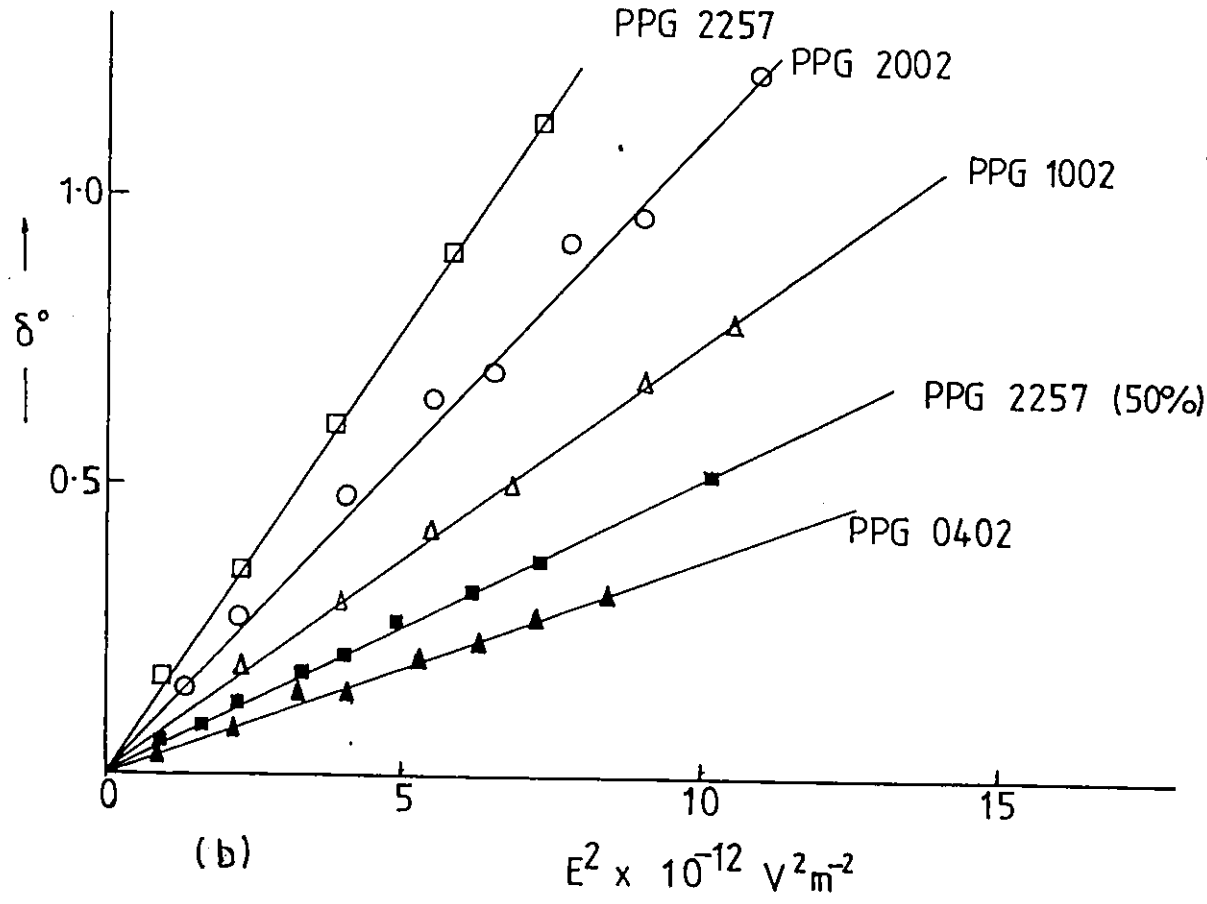

Fig 5·46 The field dependence of the retardation, δ° for Polypropylene glycol (a) PPG 2257 at different temperatures, (K). (b) different molecular weights and diluted sample at 223 K.

weight.

The Kerr constant (4.2×10^{-15} $V^{-2}m$) measured on the sample PPG 1002 ($\bar{M}$ = 1000) at 441.6 nm and 223 K is comparable with a value of 3.1×10^{-15} $V^{-2}m$ measured by Beevers et al [29] on a sample of molecular weight 1025 at 226 K and 633.nm. The Kerr constant of 8.9×10^{-15} V^{-2} m for sample PPG 2257 decreased to 2.9×10^{-15} V^{-2} m when diluted to 50 v/v% using toluene. As the Kerr constant is a direct function of the dipole moments and polarisabilities of the polymer constituent bonds and of the chain geometric parameters, such a reduction may reflect a considerable conformational change on mixing the polymer and the solvent toluene. On the other hand the reduct ion by more than a factor of two may simply be due to changes in the polymer-polymer interactions and their replacement by polymer-solvent interactions. It is nevertheless interesting that the Kerr law behaviour is observed for this solution in which the dynamics are significantly different from those for the undiluted polymer.

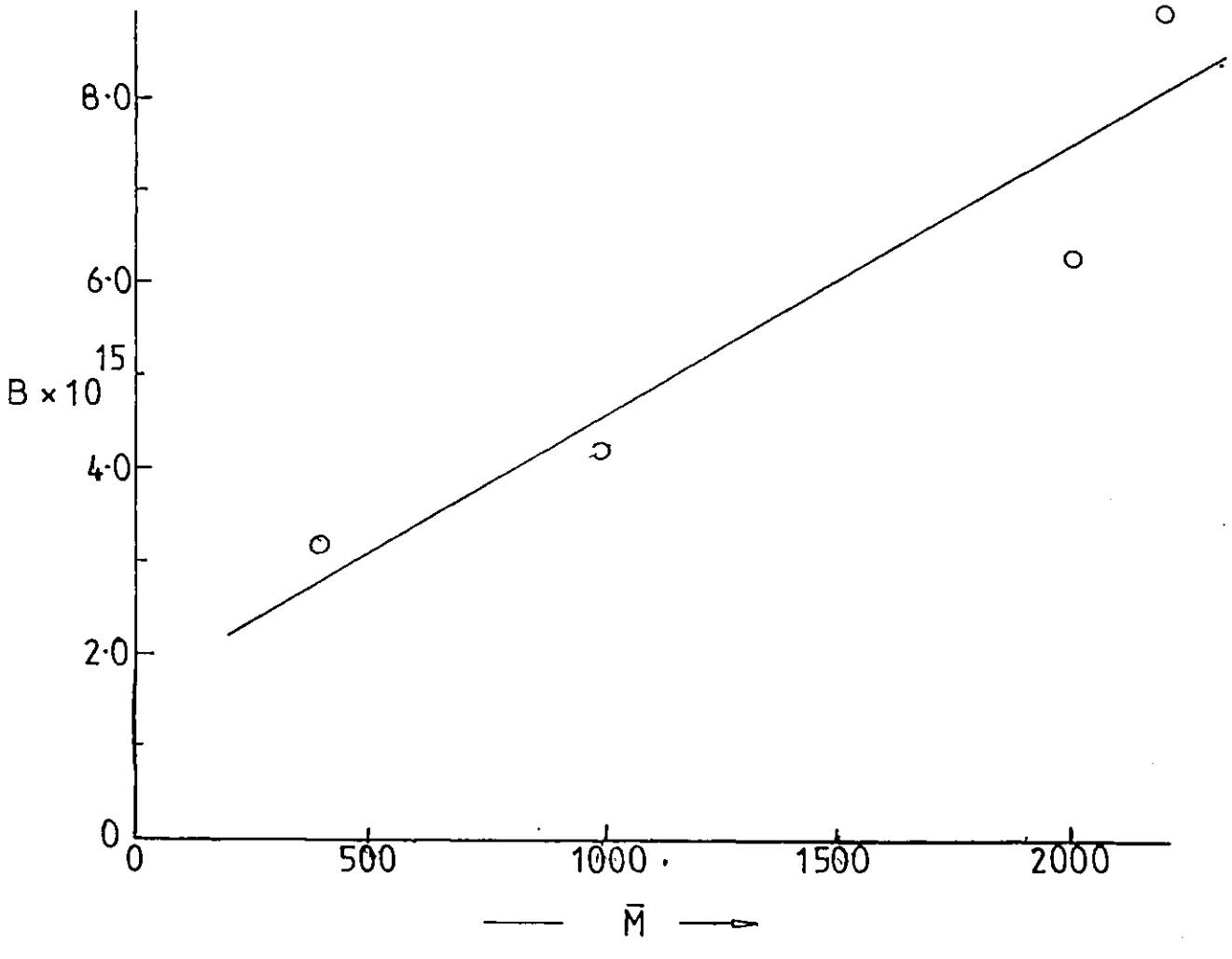

Fig 5.47 *Molecular weight dependence of Kerr constant of Polypropylene glycol at 223 K.*

Table 5.30 Polypropylene glycol Kerr constant variation with molecular weight and temperature.

Sample	B x 10^{15} V^2m^{-1}	PPG 2257	
PPG 0402	3.2	Temperature /K	B x 10^{15} V^2m^{-1}
PPG 1002	4.2	233	8.9
PPG 2002	6.3	239	6.6
PPG 2257	8.9	244	5.2
PPG 2257 (50%)	2.9	255	4.2

Fig 5.48 shows representative $\delta - E^2$ plots for two concentrations of the high molecular weight polypropylene oxides, PPO S3.3 and PPO S4.4. The plots are linear for all concentrations at low field gradients but considerable departure from the Kerr law occurs at higher fields. This contrasts with the liquid glycols where the Kerr law was observed even at higher field gradients. The insert shows the concentration dependence of the Kerr constants for both samples is linear. The zero concentration Kerr constant, $B_{c=0}$ are 4.0×10^{-14} $V^{-2}m$ and 3.0×10^{-14} $V^{-2}m$ for the samples. These values are in the ratio 1.3 as against their molecular weight ratio of 2.0. These zero concentration Kerr constants are about 5 times greater than the Kerr constant of the highest molecular liquid glycol PPG 2257 at even lower temperature.

5.10 Ethyl cellulose

Fig 5.49 shows a representative plot of the retardation, δ against the field strength for some concentrations of ethyl cellulose in toluene. This plot also contains the solvent retardation at various field strengths. The solvent obeyed the Kerr law throughout the field strength range used and has a Kerr constant B = $1,26 \times 10^{-14}$ $V^{-2}m$. The ethyl cellulose solutions deviate from the Kerr law at field strengths, E^2 greater than 1.0×10^{11} V^2m^{-2}. The deviations are similar to those observed in the cases of PBLG and PBIC. The concentration dependence of the Kerr constants is again linear over the range studied, with a zero concentration Kerr constants $B_{c=0}$ of 5.4×10^{-14} $V^{-2}m$. and specific Kerr constant K_{sp},(B/c) of 3.6×10^{-15} V^{-2} kg^{-1} m^4. (see insert Fig 5.49)

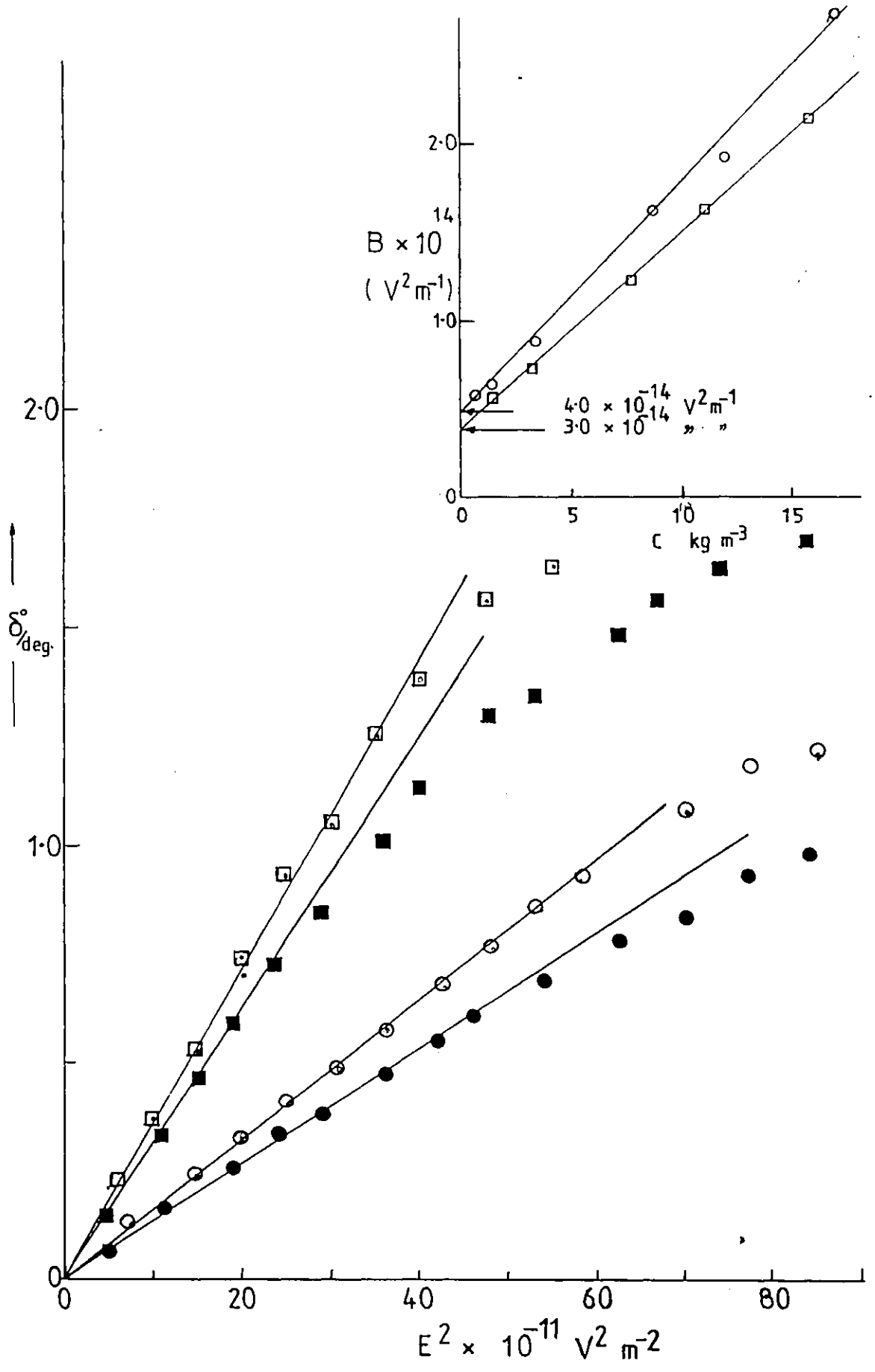

Fig 5·48 The field dependence of the retardation, δ°, for PPO typified by two concentrations each from samples S3·3 , 3·2 kg m^{-3}(●), 11·1 kg m^{-3} (■) and S4·4 , 3·4 kg m^{-3}(○), 12·0 kg m^{-3}(□).

Insert — Concentration dependence of the Kerr constants.

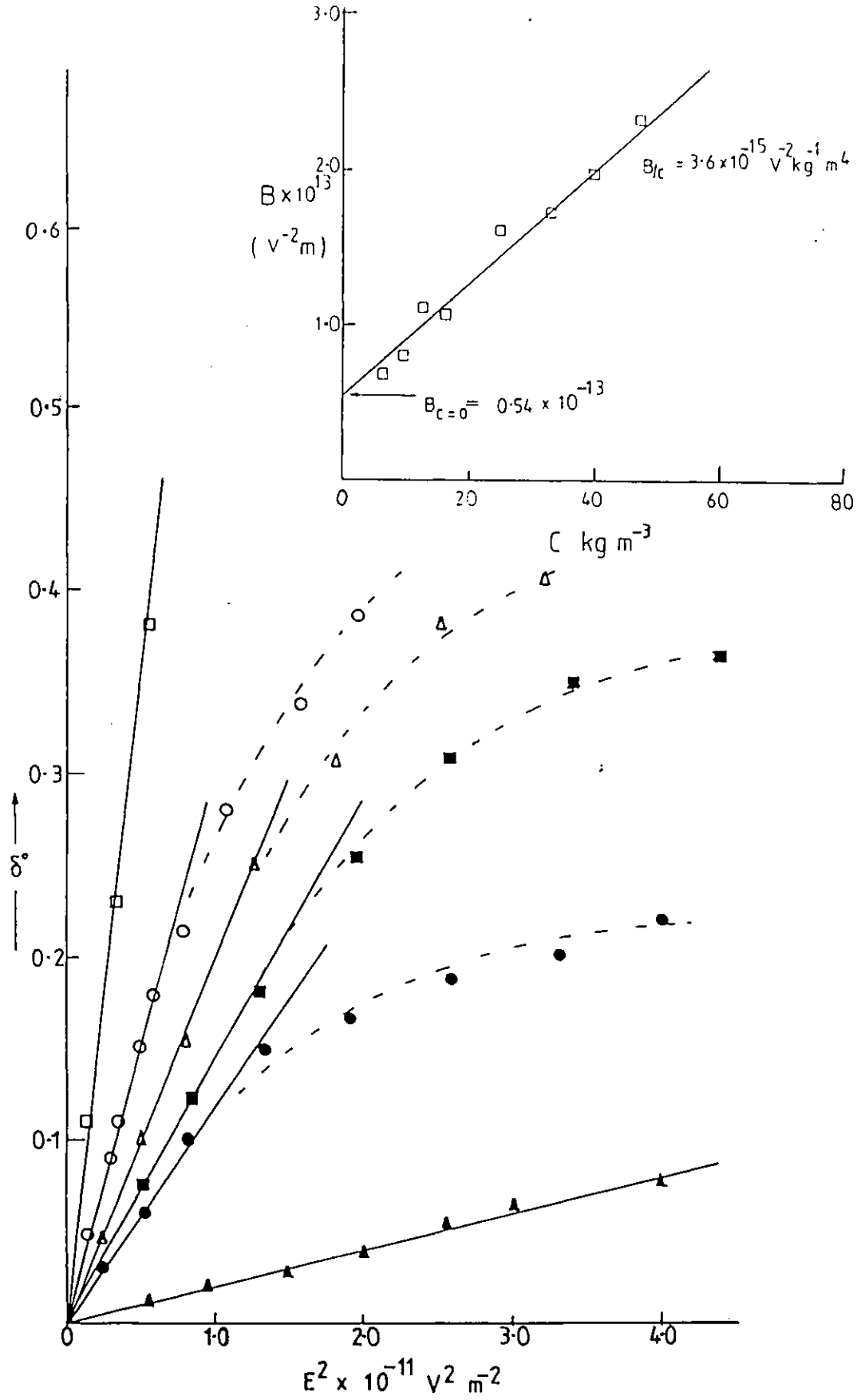

Fig 5·49 The field dependence of the retardation, δ° for ethyl cellulose at concentrations, 6·6 kg m^{-3}(●), 9·9 kg m^{-3} (■), 16·6 kg m^{-3}(Δ), 40·0 kg m^{-3}(○), 57·2 kg m^{-3}(□) and the solvent toluene (▲)

Chapter Six

COMPARISON OF SYSTEMS STUDIED AND CONCLUSIONS

In this Chapter the different systems studied are compared with each other and an attempt is made to rationalise their contrasting behaviour. One of the objectives of this work has been to observe the effect of chain flexibility on the dynamics of polymers in solution. This factor has manifested itself in a variety of ways in the results obtained and a number of quantitative measures of chain flexibility can be defined. The parameters associated with these criteria for assessing flexibility are summarised for different systems in Table 6.1.

Table 6.1 Criteria for assessing chain flexibility and the calculated parameters for the systems studied.

Criteria / Systems	C_r/C^*_{rr}	τ_e/τ_B	$\ell_q \times 10^{-9}$ (.m)	$L/\ell_q = n_p$	$\ell_q/\ell_o = n_s$	ζ_c & ζ_m
PBLG III	6.1	1.25	27.8	1.8	185	
PBLG II	10.8	1.0	39.8	2.2	265	
PBLG I	13.6	0.5	60.6	2.4	404	see
PBIC #21	>35(est. 150)	1.5	-	-	-	
PBIC #29	209	0.06	131.3	5.9	1094	Table
PBIC CN-1	220	0.023	265.9	5.9	2216	
PMPS	7143	0.018	55.4	19.2	112.5	6.3
PPO	$>4.5\times10^6$	$\sim 8\times10^{-5}$	-	-	-	
EC	50	2.1	16.1	3.4	31.3	

The first measure of flexibility (A) is the ratio of the observed critical concentration C_r, assumed to characterise molecular overlap, to that calculated on the basis of a rigid chain using equation 5.5, C^*_{rr}. This ratio is expected to be unity for rigid molecules and to increase with increasing chain flexibility. On this basis the order of decreasing rigidity is:

PBLG III > PBLG II > PBLG I > EC > PBIC #21 > PBIC #29 > PBIC CN-1 > PMPS > PPO

The PBLG samples are seen to deviate from rigid rod behaviour only slightly, confirming the ability of the Broersma equation to interpret the dilute solution Kerr relaxation times discussed in section 5.1. As expected for these weakly bending rods, C_r/C^*_{rr} increases slightly with molecular weight. A similar situation is observed for PBIC which, for the molecular weights studied, is significantly less rigid than the particular PBLG samples studied. It will be seen shortly that this in part simply reflects the higher chain lengths of the PBIC molecules. Ethyl cellulose, despite being an extended chain rather than a helical molecule, is only slightly less stiff than PBLG on this criterion. By contrast PMPS is considerably more flexible although it must still be considered a stiff coil in comparison to PPO, which has a C_r/C^*_{rr} value 10^6 times that of the lowest molecular weight PBLG.

Another quite different criterion of flexibility (B) is the ratio of the infinite dilution experimental relaxation time ascribed to whole molecule rotation, τ_ℓ, to that calculated using Broersma's equation 2.6 assuming rigid rod behaviour (see Table 6.1). This ratio is expected to decrease from unity as molecular flexibility increases. The ranking of of the chain stiffness on this basis is:

EC > PBIC #21 > PBLG III > PBLG II > PBLG I > PBIC #29 PBIC CN-1 > PMPS > PPO.

This order is essentially the same as that based on criterion A, except that EC and the lowest molecular weight PBIC #21 are displaced to the head of the order. Again for both the PBLG and PBIC series there is the expected increase in flexibility with chain length. The characterisation of EC as an

extended rigid chain, PMPS as a rigid coil and PPO as a very flexible coil is confirmed . The agreement of those two criteria based on dilute solution and concentrated solution behaviour is encouraging.

A third measure of chain flexibilty (C) can be based on the length ℓ_q, extracted from the experimental C_r values using equation 5.8, which has been interpreted here as a measure of the chain persistence length (see section 5.2.5). The ratio of the contour length L to ℓ_q, should give the number of persistence segments, n_p, in the chain, which will increase with decreasing chain stiffness. Although the physical basis of this criterion is similar to criterion A, the value of n_p does help to give a more absolute measure of chain stiffness.. The order based on n_p is ,

PBLG III > PBLG II > PBLG I > EC > PBIC #29 ~ PBIC CN-1 > PMPS

which is in line with the previous conclusions. The small number of persistence segments in the PBLG and EC samples is partucularly striking. The number of momomer units per segment n_s, = ℓ_q/ℓ_o, gives an additional interesting piece of information (see Table 6.1). This reveals that the intrinsic flexibility of the chains based on n_s is;

PBIC > PBLG > PMPS > EC

and that the order of chain flexibility observed for the actual samples used is in part a reflection of the fact that the EC sample is a very short chain (n=107), as are the PBLG samples (n= 340 - 960) in comparison to PBIC (n= 1.3×10^3 - 1.3×10^4) and PMPS (n=2160).

Other criteria of flexibility can be based on the concentration and molecular weight dependence of the measured relaxation times. The predictions of the exponents ζ_c and ζ_m for theoretical models based on rigid rods and random coils are summarised in Table 6.2. Although the precise values of ζ_m and ζ_c vary with both concentration and the nature of the solvent, the models predict a general increase in the value as the molecules become more rigid. On this basis the order of chain stiffness suggested by the results of this work is;

$(\zeta_c)_{C<C_r}$ (D);

Table 6.2 Theoretical predictions for concentration and molecular weight dependence of relaxation times

$$\tau \propto C^{\zeta_c} M^{\zeta_m}$$

Molecular type	Dilute solution	Semi-dilute
Flexible random coil)	Rouse [3] $\zeta_m=2$ Zimm [11] $\zeta_m=1.5$	Doi-Edwards-de Gennes (GDE) τ_d: $\zeta_m=2$, $\zeta_c=2\alpha+\beta$, $\alpha=\frac{3}{5}\rightarrow\zeta_c=1.2$ τ_{re} $\zeta_m=2$, $\zeta_c=2\alpha+\beta$, $\alpha=\frac{3}{4}\rightarrow\zeta_c=1.5$ $\beta \sim 0$
Semi-flexible	Hearst [15] $\zeta=1.5$ Hearst & Stockmayer [110] $\zeta_m=2$	Schaefer et al [97] $\zeta_c = 2\alpha$ (assumed) C ↓ Good solvent $\alpha=0.75\rightarrow\zeta_c=1.5$ Marginal solvent $\alpha=0.5\rightarrow\zeta_c=1.0$ θ-solvent $\alpha=1.0\rightarrow\zeta_c=2.0$ Concentrated solution $\alpha=0$ $\rightarrow\zeta_c=0$
Rigid rod	Broersma [14] $\zeta_c=3$	Doi - Edwards (DE) [4] τ_K $\zeta_m = 7$, $\zeta_c = 2$ Γ(PCS) $\zeta_c = -1.0$

EC > PBIC #21 > PBLG II ∿ PBLG III ∿ PBLG I ∿ PBIC CN-1

PBIC #29 ∿ PMPS > PPO(?)

$(\zeta_c)_{C>C_r}$ (E);

EC > (PBIC #21 ?) > PBLG III ∿ PBLG II ∿ PBLG I > PPO

> PBIC #29 ∿ PMPS ∿ PBIC CN-1

$(\zeta_m)_{C<C_r}$ (F);

PBLG > PBIC

$(\zeta_m)_{C>C_r}$ (G);

PBLG > PPG > PBIC > PPO

M↑

In general, these rankings agree with those given by criteria A - C. This comparison shows that, while the extent to which a polymer can be considered to be 'rigid' depends to some degree on the nature of the particular property under consideration, the range of criteria considered here are in broad agreement in the order in which they rank chain flexibility and can in some cases be used as a quantitative measure of this characteristic. In particular the role of increasing molecular weight in increasing chain flexibility has been quantified in the cases of PBLG, PBIC, and PPO/PPG.

We now turn to a quantitative comparison of the experimental concentration and molecular weight exponents with those predicted by various models. The experimental values of ζ_c and ζ_m are summarised in Table 6.3 for all the systems studied. These are to be compared with the theoretical values of Table 6.2, about which a few words of explanation are relevant. The values for ideal rigid rods and ideal flexible chains are predicted by the Doi and Edwards (DE) [4] and de Gennes - Doi -Edwards (GDE) [17, 96] models respectively. τ_K is the Kerr relaxation time for a rigid rod, τ_{re} is the tube renewal time in the GDE reptation model and τ_d is the characteristic time for faster chain wriggling motion within such a tube . For semi-flexible chains it has been assumed that

(i) τ_{re} depends on a_c, the mean distance between chain contacts in the same way as for flexible chains (GDE) and rigid rods (DE):

$$\tau_{re} \propto a_c^{-2}$$

(ii) a_c depends on concentration in the same way predicted by Schaefer et al [97] i.e.

$$a_c \propto C^{-\alpha}$$

where α varies from 0.75, through 0.5 to 1.0 as concentration increases and the system passes from semi-dilute good to semi-dilute medium to semi-dilute theta conditions, as described in section 2.3.2.

$$\text{Hence} \quad \tau_{re} \propto C^{2\alpha}, \quad \zeta_c = 2\alpha$$

giving the range of ζ_c values quoted in Fig 6.2.

Each of the systems can be examined in turn in the light

Table 6.3 Summary of results of this work

Systems		Concentration ζ_c		Molecular weight ζ_m	
		$C < C_r$	$C > C_r$	$C < C_r$	$C > C_r$
PBLG (I,II,III), all τ's		0.25±0.05	1.3±0.1	2.2±0.2	3.5±0.8
PBIC #21	τ_ℓ	0.47±0.07	-		
	τ_p	0.37±0.14	-		
PBIC #29	τ_ℓ	0.10±0.06	0.63±0.05	1.5±0.3	1.5±0.3
	τ_p	0.20	0.11		
PBIC CN-1	τ_ℓ	0.28±0.12	0.50±0.10		
	τ_p	0.26±0.07	0.26±0.07		
PMPS	τ_{pl}	∿0	-		
	τ_e & τ_ℓ	0.12	0.6 ±0.07		
	τ_{in}	0.47±0.07	0.41±0.07		
PPG	τ(primary)	-	-		1.25±0.2
	τ(secondary	-	-		1.95±0.2
PPO	τ_{p2}	-	∿ 0.0		∿0.0
	τ_ℓ & τ_{pl}	-	1.0±0.1		1.3 ± 0.1
EC (Kerr effect)		0.75±0.05	1.75±0.2		
(PCS)	D_m	∿0.0	-2.0	-	-
	D_ℓ	-	∿ 0.0	-	-

of these predictions. The most rigid system studied, on the basis of the previous discussion , was ethyl cellulose. The value of ζ_c ($C>C_r$) for EC was the highest value observed in this work and is close to the DE rigid rod prediction. This is further evidence that in dynamic terms EC is the most rigid of the molecules studied. An alternative explanation for ζ_c is in terms of the GDE semi-flexible model for good to theta solvent conditions. The PCS behaviour of D_m, $\propto C^{-2}$, also agrees with the GDE prediction for single chain diffusion in semi-dilute theta conditions. Unfortunately no experimental ζ_m values are available to distinguish between these alternative explanations.

For PBLG, the dilute solution value of ζ_m (2.2 ± 0.2) is significamtly lower than the Broersma's prediction of 3, suggesting some deviation from rigid rod behaviour . For $C>C_r$ ζ_m (3.5 ± 0.8) is much lower than the DE rigid rod value. Again flexibility of the helix is undoubtedly one source of this discrepancy. Another is probably that the DE theory neglects long range interactions such as dipolar and dispersion interactions, which will be quite significant for polar molecules like PBLG. Deviations from the model which assumes molecules only interact on contact would be expected, independent of any flexibility considerations. The value of ζ_c ($C>C_r$) is also significantly less than the DE value of 2. Infact ζ_c and ζ_m for PBLG are reasonably consistent with the GDE semi-flexible model for τ_{re} in good - medium solvent conditions; such an interpretation is consistent with the previous conclusions on the flexibility of PBLG.

In the case of τ_ℓ for PBIC the dilute solution value of ζ_m (1.5) is much less than the Broersma rigid rod value of 3 and much more consistent with either the Zimm random coil or the Hearst 'worm-like' chain predictions, suggesting a significantly more flexible helical chain than that observed for the PBLG samples. Again in contrast to PBLG, ζ_m hardly changes in increasing concentration above C_r, being far less than both the DE prediction of 7 and the PBLG value of 3.5 ± 0.8. It is even lower than that predicted by the reptation model for either τ_d or τ_{re}. However, as noted ealier, since ζ_m is based only on two points, no definite conclusions should be drawn from this. Nevertheless the concentration exponent for $C>C_r$

confirms this general view, being far lower than the DE prediction and almost one half of those observed in the case of PBLG. This again suggests that the PBIC samples studied are considerably more flexible. Infact the values of ζ_c and ζ_m for PBIC at $C>C_r$ are not explicable by any of the existing models for rigid, semi-flexible or flexible molecules and are both much lower than all the predicted values. The τ_p expoment of ζ_c is less than that associated with τ_ℓ, thus suggesting that this τ_p is not associated with movement of the whole chain but a portion of chain as described earlier.

For PMPS, the $(\zeta_c)_{C>C_r}$ for τ_ℓ compares well with the values obtained for PBIC and is again far less than that expected for rigid rods (DE). It is also less than the GDE predictions for both flexible and semi-flexible chains. So here again we have exponents which are not explained by the present models. A much weaker concentration dependence appears to pertain for very flexible molecules than predicted by theory.

PPG gave two types of relaxation processes. The exponent ζ_m (=1.25±0.2) associated with the primary process is very low in comparison with the GDE predictions for either τ_{re} or τ_d. This suggests that the process is not associated with motion of the whole molecule, as discussed in section 5.4. The secondary process exponent ζ_m (=1.95±0.2) is in good agreement with the GDE τ_d prediction and lower than that expected for τ_{re}. This is rather surprising if τ_ℓ is indeed associated with whole molecule rotation as τ_{re} represents such motion in the reptation model and is expected to scale as M^3 even for flexible chains. Since these PPG molecules are expected to be relatively stiff (see ealier), ζ_m might be expected to be, if anything, greater than 3.

PPO, which on all the criteria is the most flexible of all the systems studied, has a concentration exponent $(\zeta_c)_{C>C_r}$ which is reasonably consistent with GDE semi-flexible model for τ_{re} in marginal solvent conditions. However, the molecular weight exponent $(\zeta_m)_{C>C_r}$ of $\sim$1.3 ± 0.1 is extremely low compared with the value of 3 expected for this model. The value of $(\zeta_c)_{C>C_r}$ is considerably greater than those observed in PBIC and PMPS, suggesting that deviations from the GDE predictions (in the cases of PBIC and PMPS) cannot be entirely due to flexibility considerations.

In conclusion, therefore, this work has systematically investigated the dynamics of polymers of varying flexibility in both dilute and semi-dilute conditions. It has provided quantitative measures of the effects of concentration and molecular weight on the chain dynamics for molecules ranging from essentially rigid rods to very flexible coils. Several complementary criteria for assessing chain flexibility have been proposed and shown to lead to consistent, and in some cases quantitative, conclusions regarding changes in chain stiffness with chain structure and molecular weight. The results have also been compared with available theories for rigid rod and flexible systems and with a modified theory for semi-flexible chains developed in this work. Although the experimental results can be understood in a semi-quantitative way using these models, a full quantitative theoretical explanation of the observations is not possible at the present stage of their development. In particular the much weaker concentration and and molecular weight dependences observed for the relaxation times of the more flexible molecules compared with theoretical predictions requires further investigations.

The work has suggested a number of areas which might profitably be examined in more detail in the future. The field strength dependence of the distorted birefringence transients may offer at high fields for the helical molecules PBLG and PBIC should be further investigated. Such peculiar transients may offer more information on the possible distortion of helical polymers in solution by large electric fields. It is also suggested that the studies be extended to other molecular weights of ethyl cellulose (and its derivatives) in order to investigate the molecular weight dependence , and hence distinguish between the rigid rod and semi-flexible chain interpretations of the dynamics of this molecule. Molecular weight studies should also be extended to PPO and PMPS. In most cases, particularly, PBIC and PMPS, it would be useful to carry out studies at even higher concentrations, to see if the experimental values of ζ_c do increase towards the theoretical predictions before the liquid crystalline transition region is reached. It was shown in this work that for ethyl cellulose , PCS provided useful complementary information to the Kerr effect studies in concentrated solution. The extension

of the PCS experiments to the other molecules in the present work would be extremely useful. On the theoretical side, the present experiments suggest that existing theories of the dynamics of concentrated polymer solutions based on idealised molecular models require some modifications if they are to explain the range or behaviour observed in practice for molecules of different conformational types.

REFERENCES

1. Fredericq, E. & Houssier, C.,"Electric Dichroism and Electri Birefringence," Clarendon Press Oxford(1973).
2. North, A.M., Essay in Chemistry Vol. 4 pp. 1 Academic Press London, New York,(1972).
3. Rouse,P.E. , J. Chem. Phys. 21 603 (1950)
4. Doi, M.& Edwards, S.F.,J. Chem. Soc. Farad. II 74 560, 918 (1978).
5. Freed K,& Edwards, S.F.,J. Chem. Phys. 61 3626 (1974) ibid 62 4032 (1875)
6. de Gennes, P.G.,Phys. 3 37 (1967)
7. Adam, M. & Delsanti, M.,Macromolecules, 10 1229 (1977)
8. Araki,K.,Togawa,S.,Miyama,T., and Imamura, Y., Makromol. Chem. 181 1967 (1980)
9. Peterson, J.M., & Fixman, M., J. Chem. Phy. 39 2516 (1963)
10. Bueche,A.M.,J. Chem. Phys. 22 603(1951).
11. Zimm, B.H. ,J. Chem. Phys. 24 269 (1956).
12. Kirkwood, A.J., and Auer, ,J. Chem. Phys. 19 281 (1957).
13. Riseman,J. & Kirkwood, A.J., J.Chem. Phys. 18 512 (1960)
14. Broersma, S., J. Chem. Phys. 32 1626(1960).
15. Hearst, J.E., J. Chem. Phys. 38 1628 (1963).
16. de Gennes, P.G., J. Chem. Phys. 55 572(1971).
17. de Gennes, P.G., "Scalling Concepts in Polymer Physics"; Cornell University Press: Ithaca, N.Y.,(1979)
18. de Gennes, P.G., Macromolecules, 9 591,594 (1975)
19. Edwards,S.F., & Evans, K.E., J. Chem. Soc. Farad. Trans. II 77 (1981).
20. Yamakawa, H. J.,J. Chem. Phys. 43 1334 (1965).
21. Block, H.,Hayes, E.F. & North, A. M.,Trans. Farad. Soc. 66 1095 (1970).
22. Marchal, E. and Marchal ,J. Chim. Phys. 64 1607 (1967).
23. Wada, A. Bull. Chem, Soc. Jap. 33 822 (1960).
24. Bur,J.A& Roberts,D., J. Chem. Phys. 51 406 (1969).
25. Yu, H.,Bur,J. & Fetters,L.J.,J.Chem. Phys. 44 2568 (1966).
26. Tsvetkov, V.N.,Riumtsev,E.I., Aliev, F.M. & Shitennikova, Europ. Polym. J. 10 55(1974).
27. Beevers,M.S., Garrington,D.C. & Williams, G., Polymer 18 540(1977).
28. Baur, M.E. & Stockmayer, W.H.,J. Chem. Phys. 43 4319(1965).

29. Beveers, M.S.,Elliot,D.A. & Williams, G., Polymer, 21 13(1980).
30. Stockmayer,W.H., Pure Appl. Chem. 15 539 (1967).
31. Davis, M., Williams, G. & Loveluck, Z., Electro-Chem. * 64 575 (1960).
32. Tsuji, K & Watanabe,H.,J. Coll. Inter. Sc. 62 102 (1977).
33. Stoylov, S & Sokrov, S., J. Coll. Inter. Sc. 27 542 (1968).
34. Ullman, R., J. Chem. Phys. 56 1869 (1972).
35. Powers,J.C. & Peticoles, W.L., Biopolymers 9 195 (1970)
36. Jennings, . & Brown, , Europ. Poly. J. 7 805 (1971).
37. (a) Isles, M. & Jennings, B.R.,"The British polymer J." March 34 (1976).
37. Tsvetkov, V.N., Vysokomol.Soed. Ser. A 9 2132 (1968).
38. Gupta, A.K. & Marchal, E.,Biopolymers 13 1293 (1975).
39. Champion,J.V.,Meeten, G.H., & Southwell, G.W., Polymer 17 651 (1976).
40. Allerhand, A. & Oldfield, E., Biochem. 12 3428 (1973).
41. Chien,M., Samulski, E.T. & Wade, G., Macromolecules 6 638 (1973).
42. Bailey, R.T, North, A.M., & Pethrick, R.A.,"Molecular motion in high Polymers" Clarendon Press Oxford(1981).
43. Adam, M. & Delsanti,M., J. Phys(Paris) 37 1045 (1976).
44. de Gennes,P.G., Macromolecules 9 587 (1976).
45. Pecora, R., J. Chem. Phys. 40 1604 (1964).
46. Kupral, R.,Ng,D. & Whittington, S.G., J. Chem. Phys. 64 539 (1976).
47. Akcasu, Z. & Higgins, J.S., J. Poly. Phys. Poly. Phys. Ed, 15 1745(1977).
48. Adam, M. & Delsanti, M.,J. Phy. letters, 38 1 (1977).
49. Letherby, M.R., Ph.D Thesis, University of London,(1980).
50. Broachard, F. & de Geanes, P.G., Macromolecules 10 1157 (1977).
51. Reihanian,H. & Jamieson, A.M., Macromolecules 12 684 (1979).
52. Le Fevre - Le Fevre,"Techniques of Organic chemistry" (ed. A. Weissberger) 3rd. ed. vol.1 pt.3 Interscience New York 1960).
53. Tsvetkov, V.N., Vysokomol. Soedin. A 16 24 (1974).
54. Rjumtsev,E.I., Shtennikova.I.N., Peker, T.V., and Tsvetkov, N.V., Europ. Poly. J. 9 1 (1973)
55. O'Konski,C.& Zimm, B.H., Science III 113 (1950)
56. Yoshioka, K. & O'Konski, C.T., Biopolymers 4 499 (1966).

57. O'Konski, C.T., "Molecular electro-optics" Dekker New York, (1976).
58. Flory, P.J., "Statistical Mechanics of Chain molecules" Interscience Publishers, New York, London, Sydney, Toronto, (1965).
59. Stuart, H.A. & Peterlin, A., J.Poly. Sci. 5 551 (1950).
60. Peterlin, A. & Stuart, H.A., "Hand-un Jahr buch de Chemischen Physik " 8 1B Becker & Erler Leipzig (1943)
61. O'Konski, C.T. , Yoshioka, K. & Orttung, W.H., J. Phys. Chem. 63 1558 (1959).
62. Matsumoto, M. ,Watanabe, H. & Yoshioka, K., J. Phy. Chem. 74 2282 (1970).
63. Dows, D., J. Chem. Phys. 41 2656 (1964).
64. Nagai, K. & Ishikawa, J., J. Chem. Phys. 43 4508 (1965). (a) Nagai, K. , J. Chem. Phys. 40 2818 (1964).
65. Perrin, F., J. Phys. Radium, 5 497 (1934).
66. Benoit, H. , Ann. Phys. 6 561 (1951).
67. Tinoco, I Jr. & Yamaoka, K., J. Phy. Chem. 63 423 (1959).
68. Yoshioka, & Watanabe, H., Nippon Kagaku Zasshi 84 626 (1963).
69. Benoit H.,J. Chim. Phys. 47 719 (1950).
70. Williams, G. & Watts, D.C., Trans. Farad. Soc. 67 1323 (1971).
71. Orttung, W.H. & Meyers, , J. Phy. Chem. 67 1905 (1963).
72. Doty, J.H., Bradbury, & Holtzer, A.M., J. Am. Chem. Soc. 78 947 (1956).
73. Mouton, H., "International Critical Tables" 7 110 (1930)
74. Brandrup, J., Immergat, E.H., "Polymer Handbook", 2nd.
74. Ed. John Wiley & Sons New York (1978).
75. Delaney, D. & Krause, S., Macromolecules 9 455 (1976).
76. Marquire, J.F., McTaque, J.P., & Rondelez, F., Phy. Review Letters, 45 1892 (1980).
77. North, A.M., Chem. Soc. Review 1 49 (1972).
78. Ivin, K.J., Ende, H.A., & Meyeroff, G., Polymer 3 129 (1962).
79. Bates, I.W., Biggins, J., & Ivin, K.J., Makromol. Chem. 87 180 (1965).
80. Beevers, M,S., Crossley, J., Garrington, D.C., Williams, G., Symp. Farad. Soc. Chem. Soc. Ed. 11 38 (1976).
81. Graessley, W.W., Advances in Polymer Science 16 (1974).
82. Simha, R. & Zakin, J.L. , J. Chem. Phys. 33 1791 (1960).

83. Cornet, C.F., Polymer 6 373(1965).
84. Doi, M., J. Phys. (Paris) 36 607 (1975).
85. Stockmayer, W.H. & Baur, M.E.,J.Am. Chem. Soc. 86 3485 (1964).
86. Tinoco, I. Jr., J.Am. Chem. Soc. 79 4336 (1957).
87. North, A.M. & Phillips,P.J., Chem. Comm. 1340 (1968).
88. Pyzuk,W. and Krupkowski, T.,Makromol. Chem. 178 817 (1977)
89. Watanabe,H., Yoshioka, K. & Wada, A., Biopolymers 2 91 (1964).
90. Beevers, M.S., Crossley, J , Garrington, D.C., & Williams, G., J. Chem. Soc. Farad. II 72 1482 (1976).
91. (a) Beevers,M.S., Crossley,J. Garrington, D.C & Williams G. J.Chem. Soc. Farad. Soc. II 73 458 (1977).
91. Crossley, J. & Williams G.,J.Chem. Soc. Farad.II 1 1989 (1977).
92. Wallach,M.L.,and Benoit, H., J. Poly. Sc. 57 41 (1962)
93. Watanabe, H.,Nippon Kagaku Zasshi 85 403 (1964).
94. Maconnachie, A., and Richards, R. W., Polymer 19 739 (1978)
95. Ryumtsev,Y.I., Aliev, F.M., Ysokomol. Soyedin 17 3078 (1975).
96. Doi, M. & Edwards, S.F., J. Chem. Soc. Farad. II 74 1789, 1802, and 1818 (1978).
97. Schaefer, D.W., Joanny, J.F., and Pincus,P., Macromolecules 13 1280(1980).
98. Powers, J.C.Jr, , Procs. Am. Chem. Soc. Symp. ed. Johnson J.F. pp 365 Pleum New York. (1970).
99. Lee, W.,Schmitz,K.,Lin,S.,Schurr,J., Biopolymers 16 583('77)
100. Jamieson,A.M, Reihanian,H.,Southwick, J.G.,Yu,T.L.,and Blackwell,J., Ferroelectrics 30 267 (1980).
101. MacIntyre, D., Gornick, F.,"Light scattering from dilute polymer solutions" Gordon and Breach, New York (1964)
102. Cummis, H.Z., and Pike, E.R., Photon correlation and light Beating spectroscopy " Plenum Press New York, (1974).
103. Berne,B.J and Pecora, R., " Dynamic light scattering" (Wiley Interscience,) Chapters,5,7,8 (1976).
104. Pusey,P.N.,Vaugham, J.M., Williams, G. , J. Chem. Soc. Farad. Trans. II 70 1696 (1974).
105. Luzzati,V.,Cesari, M., Spach, G., Mason, F., and Vincent J.M., J. Mol. Biology 3 566 (1961)

106. Higgins, J.,'Treatise on materials Science & Technology' 15 381 (1979) Ed. Kostorz, G. Academic Press New York London.Toronto and Sydney

107. Kirste, R., Kruse, W., Schelten, J., Makromol. Chem. 162 299 (1973)

108. Lieser, G., Fischer, E., Ibel, K., J. Poly. Sci. Polym. Lett. Ed. 13 39 (1975)

109. Farnoux, B.,Daoud, M.,Decker,D.,Jannink,G.,Ober,R., J. Phy. (Paris) 36 L - 35 (1975)

110. Hearst, J.E., and Stockmayer, W.H., J. Chem. Phy. 37 1425 (1962)

111. Szczepanski, R., and Maitland, G.C., Proc. 182nd. Am. Chem. Soc. National meeting, New York, Aug. (1981)

112. O'Konski, C.T., 'Encyclopedia of Polymer Science and Technology' 9 551 (ed. N. Bikales) Wiley, New York.

113. Schaefer, J., 'Midl. Macromol. Monogr.' 4(Mol. Basis Transitions Relaxation) pp 103 - 15 (1978)

114. Allerhand, A., & Oldfield, E., Biochem. 12 3428 (1973)

115. Chien, M., Samulski, E.T., & Wade, C.G., Macromolecules 6 638 (1973)

116. Heitz, F., Macromolecules 10 1289 (1977)

117. Fawcett, A. H., Heatley, F., Ivin, K.I., Stewart, C.D., & Watt, P., Macromolecules 10 765 (1977); Heatley, F., Nucl. Magn. Reson. 8 266 (1979)

118 Mourou,G.,& Malley, M.M., Opt. Commun. 13 412 (1975)